UNIVERSITY OF CALIFORNIA, IRVINE

Analysis of the Effects of Midlatitude Deep Convection on the Composition and Chemistry of the Upper Troposphere/Lower Stratosphere Using Aircraft Data Collected During the Deep Convective Clouds and Chemistry (DC3) Field Campaign

DISSERTATION

Submitted in partial satisfaction of the requirements for the degree of

DOCTOR OF PHILOSOPHY

In Chemistry

By

Jason R. Schroeder

Dissertation Committee:
Professor Donald R. Blake, Chair
Professor Barbara J. Finlayson-Pitts
Professor Sergey X. Nizkorodov

2015

TABLE OF CONTENTS

LIST OF FIGURES

LIST OF TABLES

Curriculum Vitae

Jason Robert Schroeder

Department of Chemistry
University of California, Irvine
529 Rowland Hall
Irvine, CA 92697
Phone: 262-930-2440
Email: schroedj@uci.edu

Education

B.Sc., Chemistry, University of Wisconsin-La Crosse, 2005-2009. Mentor: Dr. Keith Beyer.
Ph.D. Analytical Chemistry, University of California-Irvine, 2010 – 2015. Advisor: Dr. Donald Blake

Affiliations

Member, American Geophysical Union (AGU)

Awards

UW La Crosse Undergraduate Research Grant – 2008
UW La Crosse travel grant to attend the National Conference for Undergraduate Research – 2009
Excellence in TAing award (for first year TAs) – 2010
NASA Group Achievement Award for SEAC4RS – 2012
UC Irvine Associated Graduate Students Travel Award Grant to attend the American Geophysical Union Fall Meeting - 2013

Teaching Experience

Teaching Assistant
University of California-Irvine, Department of Chemistry

- General Chemistry (4 quarters)
  Supervisors: Dr. Donald Blake, Dr. Craig Murray, and Dr. Ramesh Arasasingham
  - Lead discussion sections with a focus on engaging students, proctored exams, and helped prepare lecture material for the lecturing professors.
- General Chemistry Lab (3 quarters)
  Supervisor: Dr. Kim Edwards
  - Prepared lab equipment for students, supervised and assisted students in lab, and helped design and test new experiments to be integrated into the course.
- Advanced Analytical Chemistry (Instrumental Analysis, 2 quarters)
  Supervisors: Dr. Barbara Finlayson-Pitts and Dr. Niehue Ge
  - Prepared lab equipment and resolved instrument issues before supervising lab sections. Advised and assisted students in their lab work, with a

particular emphasis on good lab procedure and producing high-quality scientific writing. Also helped design new experiments for integration into future classes.

- Physical Chemistry (Quantum Mechanics, 1 quarter)
  Supervisor: Dr. Peter Rentzepis
  - Lead discussion sections, helped write exams and quizzes, proctored and graded exams, and helped prepare lecture material for the lecturing professor.

Research Experience

Undergraduate Research Assistant, University of Wisconsin-La Crosse.

- 9/2007-6/2008, Mentor: Dr. Curtis Czerwinski. Work included synthesis of organometallic compounds and ^{1}H NMR analysis to determine haptotropic rearrangement rate constants.
- 6/2008-1/2010, Mentor: Dr. Keith Beyer. Work included preparation and analysis of ternary aqueous samples by differential scanning calorimetry and FTIR. From these experiments, ternary phase diagrams were constructed and compared to predicted melting points in the atmospheric inorganic model. The last few months were spent constructing and testing a custom-designed humidity-controlled thermogravimetric analyzer.

Graduate Research Assistant, University of California-Irvine

- 5/2010 – present, Mentors: Dr. Donald Blake and Dr. Sherwood Rowland (now deceased). Work included involvement with measurement of VOCs during field campaigns, and quantitative analysis of the impact of deep convective storms on chemistry and composition of the upper troposphere/lower stratosphere region. I also installed and integrated a new instrument (a reduced gas analyzer) into the lab's routine sample analysis procedure, further enhancing our analytical capabilities.

Field Experience, associated with University of California, Irvine

- 6/2010-present, UCI global monitoring of VOCs by flask measurement
- 6/2010-7/2010, performed laboratory analysis on whole air samples collected during the CALNEX field project
- 5/2012-6/2012, collected whole air samples aboard the NASA DC-8 during the deep convective clouds and chemistry (DC3) experiment, and aided in VOC analysis at our UCI laboratory.
- 1/2013, collected ground-based whole air samples in California's central valley for the DISCOVER-AQ field campaign, in coordination with overflies by the NASA DC-8.
- 8/2013-9/2014, collected whole air samples aboard the NASA DC-8 during

the Studies of Emissions and Atmospheric Composition, Clouds and Climate Coupling by Regional Surveys (SEAC4RS) experiment, and aided in VOC analysis at our UCI laboratory.

- 7/2014-9/2014, collected samples using an automated whole air sampler aboard the NSF/NCAR C-130 and helped coordinate and perform mobile van and stationary ground site sampling during the Front Range Air Pollution and Photochemistry Experiment (FRAPPE), and aided in VOC analysis at our UCI laboratory. Also set up and maintained flask sampling equipment at two ground sites and organized mobile van sampling in association with the Colorado phase of the NASA DISCOVER-AQ field campaign.

Publications and Presentations

Publications:

Beyer, K. D., Schroeder, J., and B. Palet (2010), Solid/Liquid Phase Diagram of the Ammonium Sulfate/Malonic Acid/Water System, *J. Phys. Chem. A, 114* (12), 4282-4288

Beyer, K. D., Schroeder, J. R., and C. S. Pearson (2011), Solid/Liquid phase diagram of the ammonium sulfate/maleic acid/water system, *J. Phys. Chem. A, 115* (47), 13842-13851

Czerwinski, C. J., Guzei, I. A., Riggle, K. M., Schroeder, J. R., and L. C. Spencer (2011), Haptotropic rearrangement in tricarbonylchromium complexes of 2-aminobiphenyl and 4-aminobiphenyl, *Dalton Trans., 40* (37), 9439-9446

Schroeder, J. R., Pearson, C. S., and K. D. Beyer (2012), Solid/Liquid phase diagram of the ammonium sulfate/malic acid/water system, *J. Phys. Chem. A, 116* (1), 415-422

Beyer, K. D., Schroeder, J. R., and J. A. Kissinger (2014), Temperature-Dependent Deliquescence Relative Humidities and Water Activities Using Humidity Controlled Thermogravimetric Analysis with Application to Malonic Acid, *J. Phys. Chem. A, 118* (13), 2488-2497

Schroeder, J. R., Pan, L. L., Ryerson, T., Diskin, G., Hair, J., Meinardi, S., Simpson, I., Barletta, B., Blake, N. J., Blake, D. R. (2014), Evidence of Mixing Between Polluted Convective Outflow and Stratospheric Air in the Upper Troposphere during DC3, *J. Geophys. Res. Atm.,* doi:10.1002/2014JD022109.

Conference presentations:

Jason R. Schroeder and Keith D. Beyer, "Experimental determination of the ammonium sulfate/maleic acid/water ternary phase diagram", AGU Joint Assembly, Toronto, May 2008

Jason R. Schroeder and Keith D. Beyer, "Experimental determination of the ammonium sulfate/malonic acid/water ternary liquid/solid phase diagram," National Conference for Undergraduate Research, La Crosse, May 2009

Simpson, I. J., Marrero, J., Blake, N. J., Barletta, B., Hartt, G., Meinardi, S., Schroeder, J., Apel, E. C., Hornbrook, R. S., Blake, D. R. (2013), VOC signatures from North American oil and gas sources. Abstract A52B-03 presented at 2013 Fall Meeting, AGU, San Francisco, Calif., 9-13 Dec 2013.

Blake, N. J., Hartt, G., Barletta, B., Simpson, I. J., Schroeder, J. R., Hung, Y. H., Marrero, J., Hirsch, C., Meinardi, S., Blake, D. R., Apel, E. C. Hornbrook, R. S., Campos, T. L., Emmons, L. K. (2013), VOC source and inflow characterization during the DC3 experiment, Abstract A53C-0185 Presented at 2013 Fall Meeting, AGU, San Francisco, Calif., 9-13 Dec 2013.

Schroeder, J., Cooper, O. R., Ryerson, T. B., Diskin, G., Meinardi, S., Blake, D. R. (2013), In Situ Measurement of Stratosperic Intrusions in the Free Troposphere and Boundary Layer During the DC3 Field Campaign, Abstract A41B-0038 presented at 2013 Fall Meeting, AGU, San Francisco, Calif., 9-13 Dec 2013.

Schroeder, J. R., Pan, L., Ryerson, T., Diskin, G., Huey, G., Marrero, J., Hartt, G., Blake, N., Meinardi, S., Barletta, B., Simpson, I., Blake, D. R. (2014), Vertical Redistribution of Halogenated VOCs by Midlatitude Convective Storms During the DC3 Field Campaign, Abstract A23L-3431 Presented at 2014 Fall Meeting, AGU, San Francisco, Calif., 15-19 Dec 2014.

Blake, N. J., Schroeder, J., Barletta, B., Meinardi, S., Blake, D. R., Schauffler, S. Lueb, R., Campos, T., Flocke, F. Atlas, E., Townsend-Small, A., Botner, C., Jimenez, K., Petron, G., Kofler, J., Bon, D., Results from Whole Air Samples (AWAS): NCAR C-130 and Ground Sampling in Support of FRAPPE and DISCOVER-AQ, Presented at the FRAPPE/DISCOVER-AQ Science Team Meeting, Boulder, CO, 3-8 May 2015

References **References available upon request**

ABSTRACT OF THE DISSERTATION

Analysis of the Effects of Midlatitude Deep Convection on the Composition and Chemistry of the Upper Troposphere/Lower Stratosphere using Airborne Measurements of VOCs and other Trace Gases

By
Jason R. Schroeder
Doctor of Philosophy in Chemistry
University of California, Irvine, 2015
Professor Donald R. Blake, Chair

Measurements of trace gases were taken onboard the NASA DC-8 during the Deep Convective Clouds and Chemistry (DC3) field project with the goal of understanding the role that midlatitude deep convection plays in altering the vertical distribution of atmospherically-relevant species. Measurements of VOCs were obtained via UC Irvine's whole air sampler (WAS) instrument, while measurements of CH_4, O_3, NO_x, N_2O, water vapor, CO, and meteorological variables were performed by a variety of other instruments operated by collaborators onboard the DC-8.

Using known VOC atmospheric lifetimes and measured VOC mixing ratios in the planetary boundary layer (PBL), a tracer for rapid vertical lofting of air from the PBL to the upper troposphere/lower stratosphere region (UT/LS) by convection was created. In this study, it was found that light hydrocarbons associated with oil and natural gas (O&NG) and vehicular sources were widespread throughout the PBL of the DC3 study regions. In the UT/LS, enhanced levels of these light hydrocarbons were strongly correlated with water vapor, indicating a convective source. On the other hand, decreases in the measured mixing ratios of CFCs, HCFCs, and other long-lived halocarbons (LLHCs) in the UT were used as tracers for stratosphere-to-troposphere transport (STT). These two sets of tracers were used to divide the DC3 WAS merge into many subsets of data corresponding to: the PBL, convective outflow in the UT, convective

outflow in the LS (i.e. overshooting tops), STT-influenced air in the troposphere, background UT air, and background LS air.

Using these derived subsets of data, interactions and mixing between stratospheric intrusions and tropospheric air masses was investigated. A large number of stratospherically-influenced samples were found to have reduced levels of O_3 and elevated levels of CO (both relative to background stratospheric air); indicative of mixing with anthropogenically-influenced air. Using *n*-butane and propane as tracers of anthropogenically-influenced air, it is shown that this type of mixing was present both at low altitudes and in the UT. At low altitudes, this mixing resulted in O_3 enhancements consistent with those reported at surface sites during deep stratospheric intrusions, while in the UT, two case studies were performed to identify the process by which this mixing occurs. In the first case study, stratospheric air was found to be mixed with aged outflow from a convective storm, while in the second case study, stratospheric air was found to have mixed with outflow from an active storm occurring in the vicinity of a stratospheric intrusion. From these analyses, it was concluded that deep convective events may facilitate the mixing between stratospheric air and polluted boundary layer air in the UT. Throughout the entire DC3 study region, this mixing was found to be prevalent: 72% of all samples that involve stratosphere-troposphere mixing show influence of polluted air. Applying a simple chemical kinetics analysis to these data, it is shown that the instantaneous production of OH in these mixed stratospheric-polluted air masses was 11 ± 8 ($\pm 1\sigma$) times higher than that of stratospheric air, and 4.2 ± 1.8 times higher than that of background upper tropospheric air, which could result in a quick, high magnitude pulse of O_3 production and reduced lifetimes of OH-controlled species in the UT.

These derived subsets of data were used to investigate the effects of deep convection on mixing ratios of organic chlorine and organic bromine in the UT and LS over the DC3 study region. In the LS, it was found that mixing ratios of organic chlorine in overshooting tops were higher than mixing ratios of organic chlorine in the background LS by an average of 217 ± 179 pptv (6.3 ± 5.2% enhancement), while the total organic bromine mixing ratio in overshooting tops was higher than that of the background LS by an average of 2.8 ± 3.2 pptv (17.4 ± 19.9% enhancement). In both cases, short-lived halocarbons made up a large portion of this enhancement. In the UT, convection was found to play a much more complicated role on the organic halogen content of the region. Model back trajectories and analysis of the chemical composition of the background UT revealed that long-range transport of outflow from East Asia and from the central Pacific affected the background UT of the DC3 study region to varying degrees on different days. When the background UT was affected by East Asian outflow, mixing ratios of organic chlorine in convective outflow were lower than those of the local background UT by up to 150 ± 115 pptv (3.7 ± 2.9% enhancement). On the other hand, when the background UT was affected by clean outflow from the central Pacific, mixing ratios of organic chlorine in convective outflow were higher than the local background UT by up to 115 ± 98 pptv (3.2 ± 2.6% enhancement). Mixing ratios of organic bromine in the background UT were unaffected by these long-range transport processes. However, mixing ratios of organic bromine in convective outflow were highly variable and were affected by the transport of brominated very short-lived halocarbons (VSLH) from the Gulf of Mexico to the surface of the DC3 study region. When organic bromine enhancements in convective outflow were calculated on a flight-by-flight basis, organic bromine mixing ratios in convective outflow were higher than those in the background UT by an average of 1.7 ± 1.6 pptv (8.5 ± 8.1%). Based on these results, it is speculated that

deep convection may play an indirect role in climate change by introducing pulses of short-lived halocarbons into the UT/LS, which in turn result in relatively quick (on the order of a few months) pulses of O_3 loss in the region.

1. Introduction

1.1 The Upper Troposphere/Lower Stratosphere Region

The upper troposphere and lower stratosphere (UT/LS) region is an important part of Earth's atmosphere, particularly with respect to climate change. The radiative forcing (RF) of a given greenhouse gas (GHG) varies with altitude, with the highest gradient located in the UT/LS region for many GHGs (Forster and Thompson, 2010). However, understanding the processes that affect and alter the composition and chemistry of the UT/LS region is complicated, as this region is quite sensitive to changes. This highly dynamic region of the atmosphere is affected by deep convection, breaking gravity waves, and large-scale circulation processes in both the troposphere and stratosphere (Konopka and Pan, 2012; Montzka et al., 2010; Pan, 2004). Of these processes, deep convection is thought to be one of the most important, but one of the least understood. Thus, understanding and quantifying the effect of the UT/LS region on climate change hinges on an accurate quantification of the role that deep convection plays in controlling the composition and chemistry of the UT/LS.

For some time, it has been known that the RF of different GHGs varies with altitude (Clough and Iacono, 1995; Clough et al., 1992). This is primarily due to the temperature profiles of the troposphere and stratosphere, and the availability of outgoing long-wave radiation at a given altitude. In high-opacity regions of Earth's outgoing longwave radiation spectrum, where strong GHGs like carbon dioxide (CO_2) and water vapor (H_2O) absorb and attenuate a large fraction of outgoing radiation, there is little transmission of radiation from Earth's surface to higher altitudes in the atmosphere (Hartmann et al., 2013). Therefore, at high altitudes, most of the upwelling radiation that is received was emitted by molecules that were located well above Earth's surface. This is especially important in the stratosphere, where the air temperature

increases with altitude. In the stratosphere, outgoing longwave radiation originating from the much-colder tropopause region is absorbed while higher energy radiation is emitted (due to the higher temperatures of molecules in the stratosphere), resulting in a net cooling effect for strongly-absorbing GHG species located in the stratosphere (Forster and Thompson, 2010). The magnitude of this stratospheric cooling effect varies between GHGs and is a function of altitude (and therefore, temperature) in the stratosphere. On the other hand, weakly absorbing GHG species (i.e. those that absorb in the "atmospheric window" region of the outgoing longwave spectrum) such as ozone (O_3) experience little attenuation of outgoing longwave radiation, and therefore are still exposed to radiation originating from the surface even at higher altitudes. Thus, weakly absorbing gases have a warming effect that is maximized near the tropopause, where the temperature contrast with Earth's surface is greatest. Because of these non-linear relationships between RF and altitude, understanding the vertical distributions of GHGs and the processes that control those distributions - especially in the UT/LS - is crucial to better understand climate change.

There are three primary processes that regulate the distribution of gases in the UT/LS: deep convection, gravity waves, and large-scale circulation processes. Deep convective thunderstorms can have a widespread impact on the composition of the UT/LS by rapidly lofting of air from the planetary boundary layer (PBL) to higher altitudes. The vertical redistribution of airmasses by convective storms was theoretically recognized by Chatfield and Crutzen (1984), and field observations of the redistribution of reactive chemical species by convective storms, including nitric oxide (NO), carbon monoxide (CO), O_3, and volatile organic compounds (VOCs) soon followed (Dickerson, 1987; Pickering, 1996; Ridley et al., 1997). Gravity waves can create large periodic fluctuations in the vertical distributions of gases in the atmosphere.

When generated in the troposphere, gravity waves are created by frontal systems or by airflow over mountains and can have periods on the order of hours to days (Langford et al., 1996b). Breaking gravity waves can create cross-tropopause fluxes, which are especially important for species like O_3 where only 10% of the total atmospheric column is contained within the troposphere (Lamarque et al., 1996). Airmasses can be transported to and through the UT/LS by slow, large-scale processes such as the Brewer-Dobson circulation pattern (Brewer, 1949; Dobson, 1956). In this circulation pattern, large-scale, slow, vertical ascent across the tropopause takes place in the tropics, while large-scale, slow, vertical descent across the tropopause takes place at midlatitudes. Of these three main processes, large-scale circulation and stationary gravity waves (i.e. those formed by mountains) are well-understood while fast, dynamic processes like deep convection and its associated stratosphere-troposphere exchange (due to breaking gravity waves) are not well-understood, owing to the sporadic nature of these events (Homeyer et al., 2014b; Konopka and Pan, 2012; Montzka et al., 2010; Pan, 2004; Pan et al., 2010). Thus, understanding the role of deep convection on UT/LS composition and chemistry is crucial to understanding the vertical distribution of GHGs and other important trace species.

With this and other problems in mind, the Deep Convective Clouds and Chemistry (DC3) field campaign was designed. DC3 was a collaborative, multi-agency, multi-platform campaign whose primary objective was to study the chemical transport processes associated with deep convection over the central US. A detailed overview of the scientific objectives of DC3 is presented in section 1.4, and a description of the technical aspects of DC3 is presented in chapter 2. For further information about the entire DC3 project, readers are encouraged to read Barth et al. (2014).

1.1 Trace gases in the Troposphere and Stratosphere

The majority of Earth's atmosphere is composed of nitrogen (~78% by volume) and oxygen (~21% by volume), with argon, carbon dioxide, and water vapor comprising ~1%. However, it is the trace species, which account for less than 0.002% of gases by volume, that play the largest role in governing the chemical processes that control the atmosphere. In the troposphere, the composition of these trace species can have great variation even on small horizontal scales based on proximity to emission sources and variations in chemical kinetics. The vertical distribution of highly-reactive trace species (i.e. short-lived species) tends to be heavily weighted towards the surface, with the highest mixing ratios being contained within the PBL. On local and regional scales, these vertical distributions can be perturbed by dynamic processes such as convection. Chemical species with low reactivity (and therefore long atmospheric lifetimes) tend to be more evenly distributed in the tropospheric column and thus may be relatively unaffected by convection. The stratosphere tends to be well-mixed and relatively homogeneous on a horizontal scale because the time required for an airmass at the surface to be vertically transported to the stratosphere can be in excess of one year (Ko and Poulet, 2002). By this time, highly-reactive chemical species will have been removed while only long-lived chemical species remain. In the absence of fast, dynamic vertical transport processes (i.e. deep convection) there is very little short-term variation in stratospheric composition. In the presence of deep convection, however, there can be substantial short-term variation in stratospheric composition, with the largest variations occurring in the lowermost stratosphere.

1.2.1 Methane

Methane (CH_4) is the second most abundant carbon-containing gas in Earth's atmosphere, after CO_2. CH_4 is also an important greenhouse gas and has a global warming

potential (GWP) that is significantly higher than CO_2 – higher by a factor of 86 over a period of 20 years, and higher by a factor of 34 over 100 years (Hartmann et al., 2013). Like CO_2, CH_4 is relatively unreactive and has a long atmospheric lifetime of about 10 years. Mixing ratios of methane steadily increased throughout the 20th century, and current Northern Hemisphere mixing ratios are about 1.83 ppmv - although the rate of increase has significantly declined in recent years (Simpson et al., 2006, 2012). CH_4 has both anthropogenic and natural sources: approximately 60% of global emissions are due to human activities such as natural gas extraction and processing, waste treatment and storage, and dairy farms, while the remaining global emissions originate from biogenic sources such as wetlands and oceans (Simpson et al., 2012).

The primary sink for CH_4 in the atmosphere is by reaction with the hydroxyl radical (OH) (Atkinson et al., 2006):

$$CH_4 + OH \xrightarrow{k_1} CH_3 + H_2O \quad (1.1)$$

$$CH_3 + O_2 + M \xrightarrow{k_2} CH_3O_2 + M \quad (1.2)$$

OH is primarily produced by the reaction of water vapor with electronically-excited atomic oxygen [$O(^1D)$], which is produced by the photolysis of O_3 (Finlayson-Pitts and Pitts, 2000; Levy, 1971). The photochemical reactions that produce OH from O_3 are shown below:

$$O_3 + h\nu \xrightarrow{k_3} O_2 + O(^1D) \quad h\nu < 400 \text{ nm} \quad (1.3)$$

$$O(^1D) + M \xrightarrow{k_4} O(^3P) + M \quad (1.4)$$

$$O(^3P) + O_2 + M \xrightarrow{k_5} O_3 \quad (1.5)$$

$$O(^1D) + H_2O \xrightarrow{k_6} 2OH \quad (1.6)$$

Upon absorption of ultraviolet light, O_3 molecules dissociate into molecular oxygen and electronically-excited atomic oxygen [$O(^1D)$] (1.3). Electronically-excited oxygen atoms can then relax to their ground state [$O(^3P)$] upon collision with spectator molecules (M) (1.4).

Ground-state atomic oxygen can then react with molecular oxygen to re-form O_3 (1.5) in a null cycle. In the presence of water vapor, however, excited-state atomic oxygen can also react to produce two OH radicals (1.6).

In polluted regions of the troposphere, the peroxy radical formed by reaction (1.2) will react with nitric oxide (NO) and lead to the formation of $O(^3P)$, which ultimately leads to the formation of O_3:

$$CH_3O_2 + NO \xrightarrow{k_7} CH_3O + NO_2 \quad (1.7)$$

$$CH_3O + O_2 \xrightarrow{k_8} HCHO + HO_2 \quad (1.8)$$

$$HCHO + O_2 + h\nu \xrightarrow{k_9} 2HO_2 + CO \quad (1.9)$$

$$HO_2 + NO \xrightarrow{k_{10}} OH + NO_2 \quad (1.10)$$

$$NO_2 + h\nu \xrightarrow{k_{11}} NO + O(^3P) \qquad h\nu < 320 \text{ nm} \quad (1.11)$$

For every molecule of CH_4 that reacts via reaction (1.1), up to four molecules of O_3 can potentially be formed (one from the NO_2 molecule produced in (1.7), and up to three from the HO_2 radicals formed in reactions (1.8) and (1.9) that may subsequently go on to form NO_2 by reaction (1.10)), and three molecules of OH can potentially be formed, for a net gain of two OH molecules. Thus, the photochemical reaction of methane with OH has the potential to both produce O_3 *and* enhance the oxidizing capacity of an airmass if adequate amounts of nitrogen oxides (NO_x = NO + NO_2) are present. In clean regions, the peroxy radical formed by reaction (1.2) will undergo a different set of reactions, where it can react with HO_2 to form a hydroperoxide (1.12), or react with another peroxy radical to form two alkoxy radicals (1.13) or formaldehyde (HCHO) and methanol (CH_3OH) (1.14):

$$CH_3O_2 + HO_2 \xrightarrow{k_{12}} CH_3OOH + O_2 \quad (1.12)$$

$$CH_3O_2 + CH_3O_2 \xrightarrow{k_{13}} 2CH_3O + O_2 \quad (1.13)$$

$$CH_3O_2 + CH_3O_2 \xrightarrow{k_{14}} CH_3OH + HCHO + O_2 \quad (1.14)$$

There is also a temperature (and pressure) dependence that must be accounted for in these reactions. If the rate of a reaction is proportional to the product of the concentrations of the reactants (and first order for each reactant), then we expect a decrease in the rate constant just from decreasing temperature and pressure alone – for example 1.83 ppmv of CH_4 gives a concentration of ~$4.5x10^{13}$ molecules/cm^3 at 298 K and 1 atm, but gives a concentration of $2.44x10^{13}$ molecules/cm^3 at 273 K and 0.5 atm. Aside from that, the rate constant (k) for many reactions can also depend on temperature and pressure. For example, k_1 (reaction 1.1) decreases with decreasing temperature but is unaffected by pressure changes, while k_2 (reaction 1.2) *increases* with decreasing temperature and decreases with decreasing pressure (Atkinson et al., 2006). The result is a non-linear relationship between altitude (and thus temperature and pressure) and rate of reaction. An example is shown below in Figure 1.1, where the term $k_1[OH]$ is calculated (left panel), and the reciprocal of this value (known as the atmospheric lifetime, τ) is calculated over a range of temperatures and OH concentrations. In this case, the overall rate of reaction would be equal to $k_1[OH][CH_4]$.

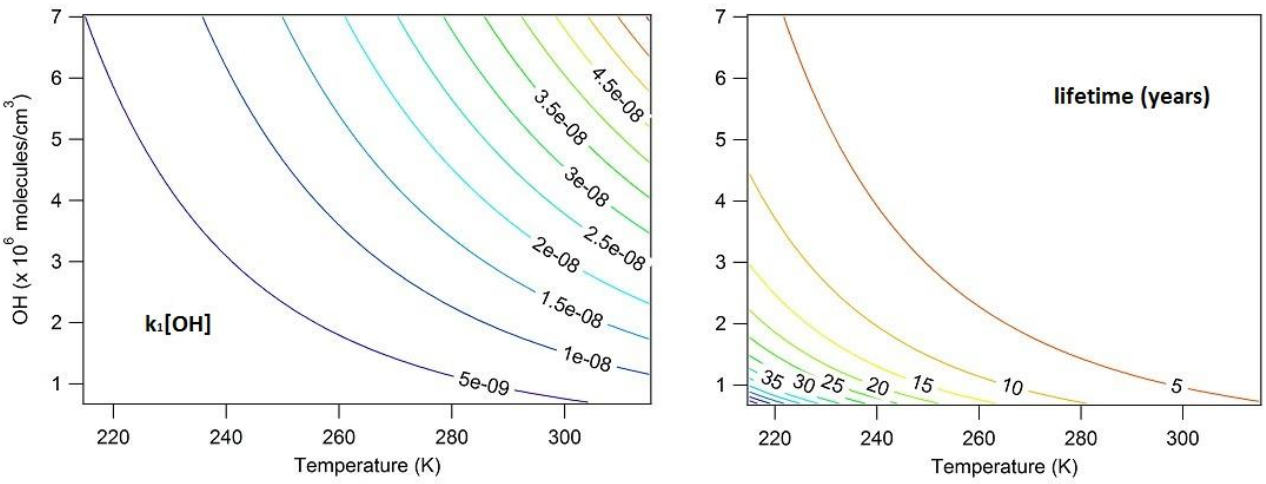

Figure 1.1. Contour plot of the product of $k_1[OH]$ (from reaction 1.1) over a range of temperatures and OH concentrations (left panel, units of s^{-1}). The reciprocal of this value (better known as the atmospheric lifetime of CH_4, and given in units of years) is shown in the right panel.

This OH-initiated destruction of CH_4 (1.1) occurs only in regions where both water vapor and O_3 are present. In the stratosphere, where high levels of O_3 (and thus, high levels of $O(^1D)$) exist, a secondary mechanism of CH_4 destruction becomes important, and helps initiate photochemistry in the stratosphere (Atkinson et al., 2006; Davidson et al., 1977):

$$CH_4 + O(^1D) \xrightarrow{k_{15}} CH_3 + OH \quad (1.15)$$

$$\xrightarrow{k_{16}} CH_3O + H \quad (1.16)$$

$$\xrightarrow{k_{17}} HCHO + H_2 \quad (1.17)$$

In the absence of convection, the UT/LS region has negligible amounts of water vapor, and thus OH-initiated photochemical reactions do not occur at nearly the same rate as in the lower troposphere. The UT/LS also does not have as much O_3 as the stratospheric overworld above it, meaning that reaction (1.15) occurs at a much lower rate in the UT/LS relative to higher in the stratosphere. These facts, coupled with the fact that the lowest temperatures between Earth's surface and the top of the stratosphere are located in the UT/LS, mean that the lifetime of CH_4 in the UT/LS is very long relative to the lower troposphere and stratospheric overworld.

Because CH_4 has a long lifetime, it is well-mixed vertically throughout the troposphere and does not begin to decrease substantially until well above the tropopause. Because of this, it is unlikely that deep convection directly causes significant changes in CH_4 mixing ratios in the UT/LS. However, the water vapor and other trace constituents (such as O_3 and NO_x) that are lofted by deep convection will have an effect on the oxidizing capacity of the UT/LS. Thus, while deep convection may not directly affect CH_4 in the UT/LS, it will indirectly affect it by altering the photochemistry of the region.

1.2.2 Carbon Monoxide

Carbon monoxide (CO) is the third most abundant carbon-containing gas in Earth's atmosphere, after CO_2 and CH_4. CO is produced by the incomplete combustion of hydrocarbons, and has primary emission sources of biomass burning and transportation-related combustion. CO is also produced from the oxidation of atmospheric hydrocarbons (globally, about 55% of CO is produced this way). On a global scale, CH_4 oxidation is the largest source of photochemically-produced CO, but highly-reactive hydrocarbons (discussed in section 1.5) can be the dominant source near strong hydrocarbon sources such as cities, oil fields, and dense forests (Ahmadov et al., 2015; Baker et al., 2008; Blake et al., 1996; Colman et al., 2001; Horowitz, 2003; Simpson et al., 2010).

Unlike CO_2 and CH_4, CO is not a GHG. However, upon oxidation by OH, CO_2 is produced and the potential to form O_3 exists through production of HO_2. Thus, CO can have an indirect effect on climate change by producing CO_2 and O_3, and altering the oxidizing capacity of the atmosphere.

$$CO + OH \xrightarrow{k_{18}} CO_2 + H \quad (1.18)$$

$$H + O_2 \xrightarrow{k_{19}} HO_2 \quad (1.19)$$

Like the reactions listed above for CH_4, these reactions also have temperature and pressure dependencies. However, since k_{18} is significantly higher than k_1 (2×10^{-13} cm^3 $molecules^{-1}$ s^{-1} for k_{18} vs 6.4×10^{-15} cm^3 $molecules^{-1}$ s^{-1} for k_1 - both at 298 K and 1 atm), CO has a relatively short lifetime ($\tau \approx$ 1-2 months). Because of this relatively short lifetime, CO has a strong seasonal and hemispheric gradient (González Abad et al., 2011; Huang et al., 2012). For example, at Barrow, Alaska (71.3N, 156.6W), CO mixing ratios can be as high as 170 ppbv in winter (when heating-related combustion is at its peak and photochemical loss is at its minimum)

while dropping down to 100 ppbv in summer. Contrast this to Cape Grim, Australia (40.7S, 144.7E) where CO mixing ratios peak in winter around 70 ppbv, and are at a minimum in summer around 45 ppbv (Horowitz, 2003).

While its lifetime is not quite short enough to be used as a tracer for short-range transport, CO can still be used as an effective tracer of long-range horizontal and vertical transport. CO has been used as a tracer for polluted airmasses, and provides some information about transport processes and dilution processes. For example, Smyth et al. (1996) used CO to differentiate between different airmasses in the western Pacific, while Hudman et al. (2004) and Nowak et al. (2004) used CO to identify polluted outflow from Asia that had reached the eastern Pacific. These authors were also able to use CO as a tracer of photochemical O_3 production (as in reaction 1.9) to determine how much O_3 in California was attributable to Asian pollution. In the absence of convection, the time required for an airmass at Earth's surface to reach the UT is about 1 month (Apel et al., 2012). For CO, this means there will be a noticeable shape in its vertical profile – CO mixing ratios will be highest near the surface and decrease steadily until reaching the tropopause. At the tropopause there will be a sharp decrease in CO, followed by a continuous decrease with increasing altitude until negligible CO remains in the stratospheric overworld. Because of this, CO can be used as a somewhat-effective tracer for convectively-lofted airmasses, and can be used to differentiate between tropospheric ozone (produced via photochemical reactions) and stratospheric ozone present in the UT/LS (Konopka and Pan, 2012; Pan, 2004).

1.2.3 Nonmethane Hydrocarbons

Nonmethane hydrocarbons (NMHCs) have both biogenic and anthropogenic sources, and are key components of atmospheric chemical cycles. Anthropogenic NMHCs are primarily

emitted by processes such as transportation, industrial use, and domestic use, while biogenic NMHCs are primarily emitted by forests and biomass burning (wildfires). As a class of compounds, NMHCs are very diverse and encompass a range of chemicals with atmospheric lifetimes ranging from less than one hour to multiple months. This means that even though all NMHCs might undergo similar chemical reactions, it is necessary to identify and quantify individual components across many spatial scales if the chemical effects of NMHCs as a class are to be fully understood.

As a class of compounds, all NMHCs can undergo reaction with OH in a manner analogous to that of CH_4, shown in reaction 1.1. This reaction between a hydrocarbon and OH is then followed by a series of reactions analogous to those shown in reactions 1.2 – 1.11 that ultimately produce O_3 and alter the oxidizing capacity of an airmass. The ability of an individual NMHC to produce O_3 is governed by the number of reactive C-H bonds present and its rate of reaction with OH in the presence of NO_x. The term minimum incremental reactivity (MIR, defined as the number of moles of O_3 produced per mole increase of a given NMHC) is often used to describe the potential amount of O_3 that can be produced by a given NMHC. Longer-chained NMHCs tend to have higher MIRs than shorter-chained NMHCs - for example ethane has an MIR of 0.16 while propane has an MIR of 0.44 and *n*-butane has an MIR of 1.23. Individual NMHCs also react with OH at different rates, and thus have different atmospheric lifetimes. Generally, shorter-chained NMHCs like ethane tend to have longer lifetimes, while longer-chained NMHCs and NMHCs with highly reactive double or triple bonds (like isoprene or ethyne) tend to have shorter lifetimes. Thus, the amount of O_3 that can be produced by NMHC photochemistry in a given airmass over a given length of time is dependent on the composition of NMHCs and the availability of OH and NO_x. The atmospheric lifetimes of select NMHCs are

shown in Table 1.1 and were calculated using a temperature of 298 K with a 12-hour average OH concentration of 2 x 10^6 molecules/cm^3.

Table 1.1. Chemical formulas and lifetimes for selected NMHCs.

	Compound	Formula	Lifetime[a]
Alkanes	Ethane	C_2H_6	45 days
	Propane	C_3H_8	10 days
	i-Butane	C_4H_{10}	6 days
	n-Butane	C_4H_{10}	5 days
	i-Pentane	C_5H_{12}	3 days
	n-Pentane	C_5H_{12}	3 days
	n-Hexane	C_6H_{14}	2 days
	n-Heptane	C_7H_{16}	1.5 days
	2,3-Dimethylbutane	C_6H_{14}	2 days
	2-Methylpentane	C_6H_{14}	2 days
Alkenes and Alyknes	Ethene	C_2H_4	1.5 days
	Propene	C_3H_6	11 hours
	Ethyne	C_2H_2	15 days
Aromatics	Benzene	C_6H_6	10 days
	Toluene	C_7H_8	2 days
	Ethylbenzene	C_8H_{10}	2 days
	m + *p*–Xylene	C_8H_{10}	15 hours
	o-Xylene	C_8H_{10}	20 hours
	3-Ethyltoluene	C_8H_{10}	< 1 day
	4-Ethyltoluene	C_8H_{10}	< 1 day
	2-Ethyltoluene	C_8H_{10}	< 1 day
	1,3,5-Trimethylbenzene	C_9H_{12}	5 hours
	1,2,4-Trimethylbenzene	C_9H_{12}	9 hours
	1,2,3-Trimethylbenzene	C_9H_{12}	9 hours
Biogenics	Isoprene	C_5H_8	3 hours
	α-Pinene	$C_{10}H_{16}$	5 hours
	β-Pinene	$C_{10}H_{16}$	4 hours

[a] The lifetimes of NMHCs are controlled by OH concentrations as well as ambient temperature and pressure. In summer, NMHC lifetimes may be shorter than in winter, due to higher OH abundances and higher temperatures. The atmospheric lifetimes of these NMHCs were calculated using kinetics data from Atkinson et al. (2006) and assuming a 12-hour daytime average OH concentration of 2 x 10^6 molecules/cm^3 at a temperature of 298 K.

Short-lived anthropogenic NMHCs are only prevalent in urban areas and downwind regions, while long-lived anthropogenic NMHCs have their highest concentrations near urban areas, but are prevalent even in remote regions of the atmosphere. Thus, short-lived anthropogenic NMHCs will have a highly-variable horizontal distribution, and a vertical distribution that is heavily weighted towards the PBL with negligible presence in the UT and

stratosphere. On the other hand, long-lived anthropogenic NMHCs will have relatively low horizontal variability and tend to be fairly well-mixed throughout the troposphere, with a vertical profile that features the highest amounts in the PBL, moderate amounts in the free troposphere and UT, and low amounts in the stratosphere. On a global scale, biogenic NMHCs such as isoprene and other monoterpenes comprise a large fraction of all reactive carbon compounds (Crutzen et al., 1999; Millet et al., 2008). Because biogenic NMHCs are primarily emitted by trees and biomass burning, their horizontal distribution on local scales tends to be more variable. For example, the air in a heavily-forested region may have quite high amounts of isoprene and monoterpenes (as high as several ppbv), while the air over desert and grassland regions (such as those in the central and southwest US) may have negligible amounts of these compounds. Due to the very short lifetimes of biogenic VOCs, their vertical distributions tend to be heavily weighted towards the PBL with negligible presence in the free troposphere and LS. While short-lived NMHCs may have a negligible presence in the UT/LS under normal atmospheric conditions, the rapid vertical mixing facilitated by deep convection may act to inject these highly-reactive species into the UT/LS, where they may play an important role on the atmospheric chemistry of the region via the photochemical production of O_3 (Apel et al., 2012; Bechara et al., 2010).

Over the central US, oil and natural gas production emits substantial amounts of NMHCs (Ahmadov et al., 2015; Baker et al., 2008; Gilman et al., 2013; Katzenstein et al., 2003; Pétron and Karion, 2014; Pétron et al., 2012). The Denver-Julesberg basin (which includes northeastern Colorado, southeastern Wyoming, western Kansas, and Western Nebraska) has been one of the most rapidly-developing oil and natural gas (O&NG) producing areas in the world. For example, more than 10,000 new wells have opened in Weld county alone (northeast Colorado) since 2005 and top-down estimates of the sum of propane, *n*-butane, *i*-pentane, *n*-pentane, and benzene from

wells in Weld county exceed 25 tons/hour (Pétron and Karion, 2014). Oklahoma has historically been a major extractor of crude oil in the US and currently produces about 180,000 barrels per day (3% of the national total). In recent years, Oklahoma has heavily invested in natural gas extraction, and currently has more than 62,000 natural gas wells which produce 4.3 billion cubic feet of natural gas per day (8% of the national total) (Boyd, 2009). Kansas has followed a similar path to Oklahoma, and currently produces more than 800 million cubic feet of natural gas per day while still producing 128,000 barrels of crude oil per day [*Kansas Geological Survey,* 2015]. As a result, the entire central US region has relatively enhanced levels of O&NG related NMHCs, where even rural areas may have certain NMHCs that are present in levels that are similar to those in polluted urban areas. For example, Katzenstein et al. (2003) saw *n*-butane (emitted from O&NG operations) levels in excess of 400 pptv throughout the majority of the central US and extending into the southeastern US.

1.2.4 Halocarbons

Halocarbons are ubiquitous throughout the atmosphere, and have a wide range of sources, lifetimes, and effects on atmospheric chemistry. Halocarbons are often categorized under different classes that are determined by chemical structure and properties. Chlorofluorocarbons (CFCs) are halocarbons that only contain carbon, chlorine, and fluorine. Hydrochlorofluorocarbons (HCFCs) have hydrogen atoms in addition to carbon, chlorine, and fluorine. Halocarbons containing bromine, chlorine, and fluorine are classified as Halons. Throughout the rest of this work, two additional classes of halocarbons will be used: long-lived halocarbons (LLHC) and very short-lived halocarbons (VSLH). LLHC are defined here as halocarbons that are not classified as CFCs, HCFCs, or halons and have atmospheric lifetimes

greater than six months. VSLH are defined here as halocarbons that are not classified as CFCs, HCFCs, or halons and have atmospheric lifetimes less than six months.

Halocarbons play a diverse role in the chemistry of the atmosphere. One reaction that is common to all halocarbons is the release of halogen atoms upon absorption of high-energy UV light. For example, the photolysis of CCl_3F (known by its refrigerant trade name, CFC-11, and discussed in greater detail below) by short-wave UV light ($\lambda < 230$ nm, which is not normally found in the troposphere) is shown below (Molina and Rowland, 1974):

$$CCl_3F + h\nu \xrightarrow{k_{20}} CCl_2F + Cl \quad (1.20)$$

This production of atomic chlorine is important as it acts to catalytically destroy O_3:

$$Cl + O_3 \xrightarrow{k_{21}} ClO + O_2 \quad (1.21)$$

$$ClO + O \xrightarrow{k_{22}} Cl + O_2 \quad (1.22)$$

This catalytic cycle is terminated by conversion of Cl or ClO to non-radical chlorine reservoirs via reaction with hydrocarbons (RH in reaction 1.23) or NO_2:

$$Cl + RH \xrightarrow{k_{23}} HCl + R \quad (1.23)$$

$$ClO + NO_2 + M \xrightarrow{k_{24}} ClNO_3 + M \quad (1.24)$$

Similar reactions occur for atomic bromine and iodine, as well. However, bromine has, on average, an O_3 destruction efficiency that is 60 times higher than that of chlorine, and iodine is more efficient still (Montzka et al., 2010). The catalytic destruction of O_3 by halogen atoms is especially important in the stratosphere, where high amounts of UV light, O_3, and atomic oxygen are present, while negligible amounts of hydrocarbons and NO_x are present. In the troposphere, atomic halogens can still destroy O_3, but are more likely to be removed by reactions 1.23 and 1.24 before appreciable O_3 loss can occur. It should be noted, however, that tropospheric ozone

depletion events do occur on occasion, and are linked to infrequent events where high levels of BrO are produced from heterogeneous reactions on ice and snow in the arctic (Koo et al., 2012).

The ozone depleting potential (ODP) of a given halocarbon is defined as the cumulative ozone depletion for the same mass pulse emission (same location and time of year) of a given substance versus that of CFC-11 (CCl_3F) (Prather, 1997, 2002; Solomon et al., 1992). For halocarbons that have very long lifetimes (and thus relatively uniform mixing ratios throughout the troposphere), ODP values are independent of location and time of emission. However, for VSLH, ODPs vary greatly with location, time of the year, and the presence or lack of rapid vertical transport processes such as convection. For VSLH destroyed in the lower troposphere, the atomic halogen(s) produced will have little effect on O_3 depletion, while VSLH that are destroyed in the stratosphere will affect O_3 destruction. The time and spatial evolution of ozone depletion is also very different for long-lived versus short-lived substances: the cumulative O_3 loss by a pulse of a long-lived halocarbon like CFC-11 may be spread out over several dozen years and focused in the middle and upper stratosphere, while the cumulative O_3 loss by a pulse of a VSLH may last only a year or less, with most of the O_3 loss occurring near the tropopause. In effect, long-lived halocarbons tend to destroy O_3 in regions of the atmosphere that are important for surface UV radiation (i.e. the middle and upper stratosphere), while short-lived halocarbons tend to destroy O_3 in regions of the atmosphere that are very climate-sensitive, such as the UT/LS. Thus, an in-depth understanding of the emissions and vertical transport of VSLH is required to fully understand O_3 loss processes in our atmosphere and their associated effects on climate.

Aside from destruction of O_3, halogen atoms also can impact the oxidizing capacity of the atmosphere. Atomic halogens are extremely reactive towards VOCs and often have rate

constants that are greater than an order of magnitude larger than those of OH (Atkinson et al., 2006). Atomic halogens (particularly chlorine) are thought to be primarily produced by heterogeneous reactions involving sea salt, and therefore were believed to be of little concern outside of the marine boundary layer. Recent measurements of atomic chlorine precursors in urban mid-continental environments have begun to expand our understanding the potential impact of chlorine to the entire troposphere (Mielke et al., 2011; Thornton et al., 2010). In very remote regions of the atmosphere, such as the UT/LS, an additional mechanism – the production of chlorine from halocarbons - may be an important source of atomic chlorine. In convective conditions, where OH may be produced in the UT/LS and NO_x is produced by lightning, halocarbons may react with OH and undergo chemical reactions that produce atomic chlorine. An example is shown below, where dichloromethane (CH_2Cl_2) is oxidized (Libuda et al., 1990):

$$CH_2Cl_2 + OH \xrightarrow{k_{23}} CHCl_2 + H_2O \quad (1.23)$$

$$CHCl_2 + O_2 \xrightarrow{k_{24}} CHCl_2O_2 \quad (1.24)$$

$$CHCl_2O_2 + NO \xrightarrow{k_{25}} CHCl_2O + NO_2 \quad (1.25)$$

$$CHCl_2O \xrightarrow{k_{26}} COCl_2 + H \quad (\sim 5\%) \quad (1.26)$$

$$CHCl_2O \xrightarrow{k_{27}} CHOCl + Cl \quad (\sim 95\%) \quad (1.27)$$

The ability of atomic halogens to act as potential sources of O_3 (via halogen-VOC-NO_x chemistry similar to the OH-VOC-NO_x chemistry highlighted in sections 1.2.1 and 1.2.3) or sinks of O_3 depends on their surrounding environment. In the lower troposphere, most atomic halogens will react with the abundant VOCs and thus not participate in catalytic O_3 destruction cycles. In the stratospheric overworld, where O_3 and atomic oxygen are very abundant but reactive VOCs are not, halogens tend to act primarily as destroyers of O_3. In the UT/LS, the role of atomic halogens can fall into either category depending on how troposphere-like or stratosphere-like the surrounding airmass is. Because of this dual role that halogen atoms may

play in the UT/LS, it is very important to understand the vertical distributions of halocarbons – particularly VSLH – and the processes that affect them.

1.2.4.1 CFCs

CFCs are man-made compounds that have no natural source, and are incredibly stable in the troposphere where they are unaffected by oxidants like OH. This stability led to their widespread use as solvents, refrigerants, and propellants. In the 1970's, Rowland and Molina showed that CFCs photolytically decompose in the stratosphere to form atomic chlorine, which later goes on to catalytically destroy ozone (i.e. reactions 1.20 – 1.22) (Molina and Rowland, 1974; Stolarski and Cicerone, 1974). This work and the later discovery of the Antarctic ozone hole in 1985 led to an international ban of CFCs under the 1987 Montreal Protocol. Under the Montreal Protocol, CFCs were listed under Group I of Annex A and were slowly phased out until 1996, whereupon their use in developed countries was restricted. Because there is no appreciable source of CFCs throughout the world, CFC mixing ratios are essentially constant throughout the troposphere, and do not begin to decline appreciably until well above the tropopause. Over the past decade, CFC mixing ratios have begun to slowly and steadily decrease by 0.5-1% per year (Montzka et al., 2010). Select CFCs are presented in

Table 1.2.

Table 1.2. classification, chemical formula, and lifetimes of selected halocarbons

	Compound	**formula**	**Lifetime**	**ODP[c]**	**Montreal Protocol Regulation**
CFCs	CFC-11	CCl_3F	45 yr[a]	1	Annex A, Group 1[d]
	CFC-12	CCl_2F_2	100 yr[a]	0.82	Annex A, Group 1[d]
	CFC-113	CCl_2FCClF_2	85 yr[a]	0.85	Annex A, Group 1[d]
	CFC-114	$CClF_2CClF_2$	190 yr[a]	0.58	Annex A, Group 1[d]
Halons	H-1211	$CBrClF_2$	16 yr[a]	7.9	Annex A, Group 2[e]
	H-1301	$CBrF_3$	65 yr[a]	15.9	Annex A, Group 2[e]
	H-2402	$CBrF_2CBrF_2$	20 yr[a]	13.0	Annex A, Group 2[e]
HCFCs	HCFC-22	CHF_2Cl	12 yr[a]	0.04	Annex C[f]
	HCFC-141b	CH_3CClF_2	9 yr[a]	0.12	Annex C[f]
	HCFC-142b	CH_3CClF_2	18 yr[a]	0.06	Annex C[f]
LLHCs	Methyl chloroform	CH_3CCl_3	5 yr[a]	0.16	Annex B[d]
	Carbon tetrachloride	CCl_4	26 yr[a]	0.82	Annex B[d]
	Methyl chloride	CH_3Cl	1 yr[a]	0.02	Unregulated
	Methyl bromide	CH_3Br	0.8 yr[a]	0.66	Annex E[g]
VSLH	Dibromomethane	CH_2Br_2	3-4 mo[b]		Unregulated
	Dichloromethane	CH_2Cl_2	3-5 mo[b]		Unregulated
	Chloroform	$CHCl_3$	3-5 mo[b]	0.01	Unregulated
	Trichloroethene	C_2HCl_3	5 d[b]		Unregulated
	Tetrachloroethene	C_2Cl_4	2-3 mo[b]	0.007	Unregulated
	1,2-Dichloroethane	CH_2ClCH_2Cl	1-2 mo[b]		Unregulated
	Bromodichloromethane	$CHBrCl_2$	2-3 mo[b]		Unregulated
	Dibromochloromethane	$CHBr_2Cl$	2-3 mo[b]		Unregulated
	Bromoform	$CHBr_3$	11 d[b]		Unregulated
	Ethyl Chloride	CH_3CH_2Cl	1 mo[b]		Unregulated
	Methyl Iodide	CH_3I	4 d[b]		Unregulated

[a] photolysis lifetimes are taken from Montzka and Riemann (2010)
[b] Calculated at 298 K using a 12-hour OH concentration of 1 x 10^6 molecules/cm^3 (Atkinson et al., 2008)
[c] taken from WMO/ UNEP(2010). The ODPs of many VSLH are not reported.

[d] Complete phase-out by 1996
[e] Complete phase-out in developed countries by 1994, developing countries by 2010
[f] 90% phase-out by 2015 in developed countries. Complete phase out by 2020 in developed countries, 2030 in developing countries.
[g] complete phase-out by 2005

1.2.4.2 HCFCs

HCFCs were introduced as alternatives to CFCs due to their shorter atmospheric lifetimes, which results in them delivering less chlorine to the stratosphere and thus having a smaller impact on stratospheric O_3 depletion. Because HCFCs contain at least one C-H bond, they are susceptible to reaction with OH in the troposphere, where the chlorine they release will not destroy appreciable amounts of O_3. Under the Montreal Protocol Annex C, HCFCs are mandated to be completely phased out by 2020 in developed countries, and 2030 in developing countries. Current legislation dictates that developed countries must have achieved a 90% reduction from peak levels by 2015. Because of this, HCFCs currently have a negligible source in the US, and only have a small global source that is distributed among developing countries. Global annual mean atmospheric mixing ratios of HCFCs spiked in the 1990's, began to plateau in the early 2000's, and have recently begun increasing again by 2-4% per year (Montzka et al., 2010). Because of the relatively long atmospheric lifetimes of HCFCs and only limited use taking place in developing countries, HCFCs are well-mixed throughout the troposphere, and mixing ratios over the US are essentially stable over short time scales. Like CFCs, the vertical profiles of HCFCs do not feature an appreciable decrease until well above the tropopause. Select HCFCs are presented in Table 1.2, above.

1.2.4.3 Halons

Halons are primarily used as fire suppressing agents, although their use has also been banned under the Montreal protocol where a complete ban (except for essential use applications)

was mandated in developed countries in 1994, and in developing countries in 2010. As a result, global annual means of halons have steadily decreased since the mid-1990's, and are currently decreasing by 0.5-1% per year, with the exception being Halon-1301, which has remained at a stable atmospheric concentration for the past several years (Montzka et al., 2010). Because Halons have relatively long lifetimes, no appreciable source in the troposphere, and a sole sink in the stratosphere, their mixing ratios are relatively constant on both horizontal and vertical scales in the troposphere. Like CFCs and HCFCs, the vertical profiles of halons do not show appreciable decreases until well above the tropopause. Select Halons are presented in Table 1.2, above.

1.2.4.4 LLHC

LLHC have both anthropogenic and biogenic sources, and in some cases are regulated by the Montreal Protocol. Two LLHC: Carbon tetrachloride (CCl_4) and methyl chloroform (CH_3CCl_3) are entirely man-made and have been used as solvents, cleaning agents, and chemical feedstocks for the synthesis of other chemicals such as hydrofluorocarbons and HCFCs. Both were banned under Annex B of the montreal protocol and have global annual means that are currently decreasing (-1% per year for CCl_4, and -17% for CH_3CCl_3) (Mcculloch, 1999; Montzka et al., 2010). Methyl bromide (CH_3Br) has anthropogenic uses as a fumigant and pesticide, and biogenic sources from oceans and biomass burning. Because of its high ODP, the production and use of CH_3Br has been eliminated under the Montreal Protocol Annex E. The global annual mean of CH_3Br is currently decreasing by about 3% per year (Montzka et al., 2010). Methyl Chloride (CH_3Cl) is the most abundant chlorine-containing organic compound in the atmosphere, and is believed to contribute ~16% of the total chlorine from LLHC despite only having one chlorine atom. Although it is not a controlled substance, CH_3Cl has many sources in common

with CH_3Br and its global annual mean is increasing by 0.5-1% per year (Montzka et al., 2010). Select LLHC are presented in Table 1.2, above.

1.2.4.5 VSLH

Of all of the classes of halocarbons, VSLH are perhaps the most dynamic and least understood. VSLH have anthropogenic sources that include solvent use, fumigation, cleaner use, and fossil fuel use, and biogenic sources that include oceans and biomass burning. In general, chlorinated VSLH tend to be mostly anthropogenically-produced, while brominated and iodinated VSLH tend to be biogenically produced. Notable exceptions to this rule are chloroform ($CHCl_3$, 75% biogenic and 25% anthropogenic, globally), dichloromethane (CH_2Cl_2, 25% biogenic and 75% anthropogenic, globally), ethyl chloride (C_2H_5Cl, about 50% biogenic and 50% anthropogenic, globally) and bromoform ($CHBr_3$, 80% biogenic and 20% anthropogenic, globally) (Law and Sturges, 2006).

At present, VSLH are believed to account for ~25% of all bromine and 1-5% of all chlorine in the stratosphere (Montzka et al., 2010). These relative contributions will likely increase in the future as the concentrations of gases that are regulated by the Montreal Protocol continue to decline (Dessens et al., 2009; Hossaini et al., 2012). Once transported to the stratosphere, VSLH affect the natural balance of O_3, with the majority of this effect occurring in the LS where perturbations in ambient O_3 concentrations will have the largest affect on temperature and climate (Hartmann et al., 2013). VSLH may also play an important role in the UT: Previous field studies and model simulations have shown the presence of appreciable amounts of VSLH in the UT (Hossaini et al., 2010; Schauffier et al., 1998, 1999), and recent work has shown that halogen chemistry initiated by VSLH in the upper troposphere can also have an impact on O_3 loss in the region (Saiz-Lopez et al., 2012). In a recent study by Hossaini et

al. (2015), VSLH-driven O_3 loss in the troposphere and stratosphere was found to reduce the radiative forcing of the atmosphere by 0.16 – 0.23 W/m^2 (although it should be noted that the only VSLH considered in this study were $CHBr_3$, CH_2Br_2, $CHCl_3$, CH_2Cl_2 and CH_3I). Based on this, it is essential that we better understand not only the source strength of each VSLH, but also the processes that affect vertical mixing. Although the strength of the Brewer-Dobson circulation is expected to be affected by climate change, this will likely only result in a small change in VSLH loading in the UT/LS due to the short lifetimes of VSLH (Hartmann et al., 2013). Deep convection, however, can facilitate the rapid lofting of VSLH from the PBL to the UT/LS, although the importance of this process in affecting vertical distributions of VSLH is unclear (Law and Sturges, 2006; Montzka et al., 2010; Riese et al., 2012). Select VSLH are presented in Table 1.2, above.

1.2 Stratosphere-Troposphere Exchange, Deep Convection, and the Formation of the Extra-Tropical Transition Layer

The composition of the troposphere and stratosphere are fundamentally different: The troposphere has relatively high levels of water vapor and reactive VOCs, but relatively low levels of O_3, while the stratosphere has very low levels of water vapor and reactive VOCs, but high levels of O_3. Thus, airmass exchange across the tropopause is of great interest. There are two commonly used methods for determining the height of the tropopause. The first method identifies what is called the "thermal tropopause," and uses the WMO definition of the lowest level at which the temperature lapse rate decreases to 2 K/km or less, and the lapse rate averaged between this level and any level within the next 2 km does not exceed 2 K/km (Stohl, 2003). The second method identifies what is called the "dynamic tropopause," and involves calculation of potential vorticity whereby the tropopause height is considered the altitude where the potential

vorticity is equal to 2 pvu (potential vorticity units = 10^{-6} m^2 s^{-1} K kg^{-1}) (Browell, 2003; Stohl, 2003). Through aircraft measurements, it has been shown that using chemical gradients to calculate tropopause heights yields values that are very similar to the calculated thermal tropopause height, and about 1-2 km higher than the 2PVU tropopause height (Konopka and Pan, 2012; Pan, 2004). Because the primary topic of this dissertation is to identify changes in the chemistry and composition of the UT/LS due to convection, the thermal tropopause height will be used as the primary metric for estimating tropopause height.

In the tropics, the tropopause is located at an altitude of 15-18 km, and slopes downwards towards the poles where it may be as low as 6-8 km. stratosphere-troposphere exchange (STE) occurs in two directions: troposphere-to-stratosphere transport (TST) and stratosphere-to-troposphere transport (STT). TST occurs primarily in the tropics, where airmasses rise slowly to the tropical tropopause layer (TTL), and then slowly move poleward and across the tropopause where they enter the midlatitude lower stratosphere. This process may take in excess of one year (Law and Sturges, 2006). STT occurs primarily in the midlatitudes as part of a slow, large-scale descent described by Brewer-Dobson circulation. Rapid STT may also occur on occasion due to tropopause folds, and is described in detail below. Deep convection in both the tropics and midlatitudes frequently allows air from the PBL to reach the UT, and occasionally penetrate into the LS in midlatitude regions via overshooting tops of deep convective storms. As a result of these transport mechanisms, there is a finite tropopause transition layer, called the "extra-tropical tropopause layer (ExTL)" that is 1-3 km thick and centered on the thermal tropopause in midlatitude regions (Hintsa et al., 1998; Homeyer et al., 2014b; Konopka and Pan, 2012; Pan, 2004). A diagram of these mixing processes is presented in Figure 1.2.

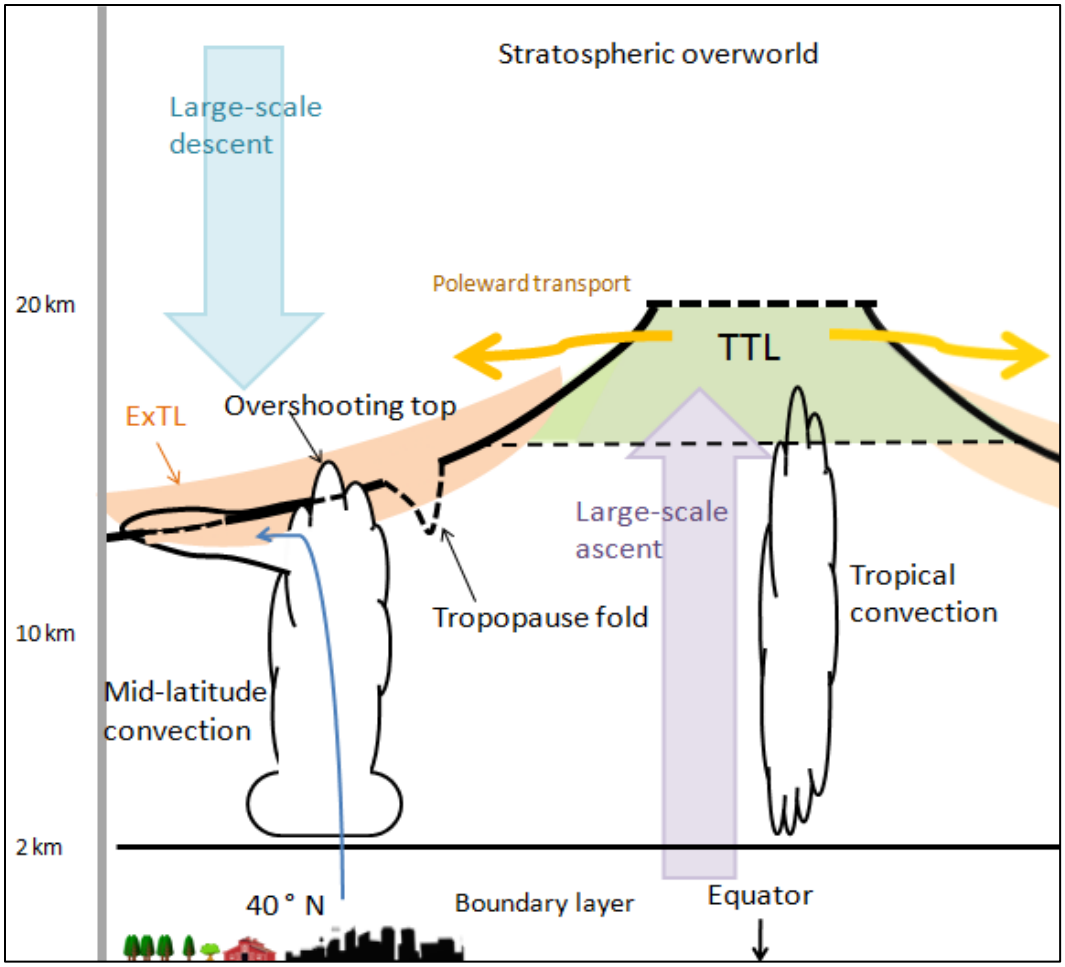

Figure 1.2. Diagram of transport processes that affect the UT/LS. Large scale ascent or airmasses from the PBL to the TTL (green highlighted region) occurs in the tropics (purple arrow), whereupon it moves poleward (golden arrow) into the midlatitude lower stratosphere. Here, large scale descent (blue arrow) eventually pushes it down into the midlatitude troposphere. Two convective storms are shown: in the midlatitudes, the storm is shown penetrating into the stratosphere – rapidly injecting PBL air into the LS – while the tropical convection is shown rapidly lofting PBL air into the TTL. A tropopause fold is shown as a dashed line through the tropopause (thick black line). The ExTL is highlighted as an orange layer that extends 1-2 km above and below the tropopause.

1.3.1 Stratosphere-to-Troposphere Transport

STT commonly occurs at mid- to high latitudes as part of a general large-scale downward mass flux, and its impact on regional and global tropospheric O_3 has been studied (Avery et al., 2010; Büker et al., 2008; Langford et al., 2012; Lin et al., 2012). The average depth to which stratospheric airmasses penetrate into the midlatitude troposphere has a seasonal variation, with the deepest STT events occurring in winter and spring [*Stohl*, 2003]. Midlatitude STT events are

associated with synoptic-scale and mesoscale processes, including the formation of tropopause folds in the vicinity of polar and subtropical jet streams (Langford et al., 1996a; Vaughan et al., 1994), erosion and folding of the tropopause by convective activity near cut-off-lows (Ancellet and Beekmann, 1994; Price and Vaughan, 1993; Sprenger et al., 2007), mesoscale convective systems (Poulida et al., 1996) and isolated convective storms (Cho et al., 2001; Colette and Ancellet, 2006; Pan et al., 2014; Stohl, 2003). From this, it can be inferred that STT in the midlatitudes is sporadic in nature and generally associated with unstable meteorological conditions, often in the immediate vicinity of convection. On a global scale, 30-50% of O_3 in the UT is believed to have originated from the stratosphere, and, through photochemical reactions in the presence of water vapor, is the dominant natural source of OH in the troposphere (i.e. reactions 1.3 – 1.6) (Crutzen et al., 1999; Fusco, 2003). Figure 1.3 shows regions of the UT in the northern hemisphere that are frequently affected by STT.

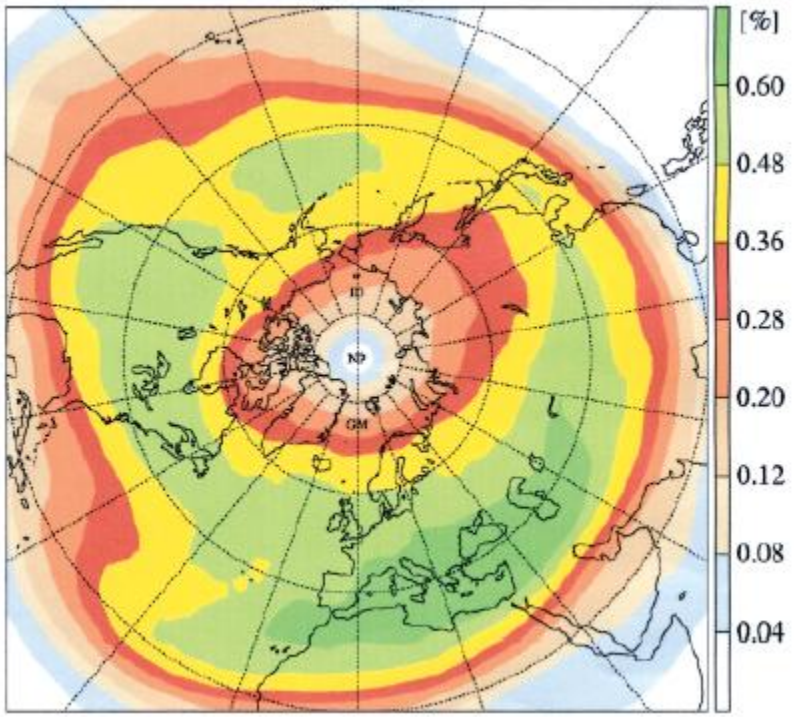

Figure 1.3. Upper-tropospheric "destinations" of shallow stratospheric intrusions averaged over 1979-1993. Values are color-coded by the probability that a given airmass was affected by shallow STT at any time over the previous four days. Adapted from Stohl et al., (2003)

Because they have high concentrations of O_3 and low levels of water vapor and CO, pristine stratospheric intrusions are relatively easy to detect by ground-based lidar and simple *in-situ* surface and airborne-based measurements (Bithell et al., 2000; Browell, 2003; Fenn et al., 1999; Langford et al., 2012; Lin et al., 2012; Vaughan et al., 2001). After mixing with relatively polluted tropospheric air, detection of stratospheric influence becomes more difficult, because O_3 will be diluted and the introduction of water vapor, CO and VOCs effectively acts to mask the stratospheric character (Stohl et al., 2003). The cosmogenic nuclide ^{7}Be has often been used as a tracer for stratospheric air, but its usefulness is questionable as it is estimated that a third of all ^{7}Be originates in the UT, and is removed by deposition onto aerosols and wet scavenging (Dibb et al., 1994; Doering and Akber, 2008; Gerasopoulos et al., 2001; Koch, D., Mann, 1996). Certain anthropogenic halocarbons including long-lived species like CFCs and their replacement HCFCs, are only photochemically destroyed in the stratosphere and (as a result of the Montreal Protocol) currently have minimal surface sources, even on a global scale (see section 1.2.4). As a result, these halocarbons are evenly distributed throughout the troposphere, but relatively depleted in the stratosphere - making them ideal tracers for stratospheric air. Nitrous oxide (N_2O) is also relatively evenly-distributed in the troposphere and solely destroyed in the stratosphere, and has been used as a tracer for stratospheric air (Assonov et al., 2013; Ishijima et al., 2010).

1.3.2 Troposphere-to-Stratosphere Transport

TST occurs primarily via slow ascent in the tropics as part of the Brewer-Dobson circulation. Upon reaching the TTL, airmasses are transported poleward before beginning slow descent into the LS. Since the vertical transport time for surface emissions to reach the TTL is roughly six months and the horizontal transport time from the TTL to the stratosphere is 20-80

days, the flux of short-lived substances into the stratosphere via this pathway is small and highly sensitive to the location and timing of the emission of these substances (Law and Sturges, 2006; Levine et al., 2007; Park et al., 2010). Infrequent deep convection in the tropics provides a fast pathway for surface emissions to reach altitudes as high as 15 km. Liang et al. (2014) showed that convection in the tropics can contribute 8 ppt of total bromine (in the form of VSLH) to the TTL, and Law et al. (2010) estimated that 10-50% of airmasses sampled in the TTL over West Africa during the summer monsoon were affected by local convection.

In the extra-tropics, TST can occur by diabatic ascent and by deep convection that penetrates above the tropopause (Hintsa et al., 1998; Poulida et al., 1996). Because the average circulation pattern in this region is downward, airmasses that cross the tropopause into the LS do not ascend to the stratospheric overworld and instead remain in the LS, generally for long lengths of time (Sprenger et al., 2007; Stohl, 2003). In the extra-tropics, deep convective storms are frequent but sporadic in nature and have peak activity during spring and summer over the continental United States (Carbone et al., 2002). Deep convective storms can rapidly transport air from the PBL to the UT/LS region, with observed transport times ranging from 15-120 minutes (Apel et al., 2012; Aschmann et al., 2009). Several studies have aimed to quantify the transport of water vapor and O_3 into the LS by midlatitude deep convective storms, but none have directly addressed the transport of NMHCs or halocarbons and their potential impacts on chemistry in the region (Hintsa et al., 1998; Homeyer et al., 2014a, 2014b; Peevey et al., 2014; Poulida et al., 1996).

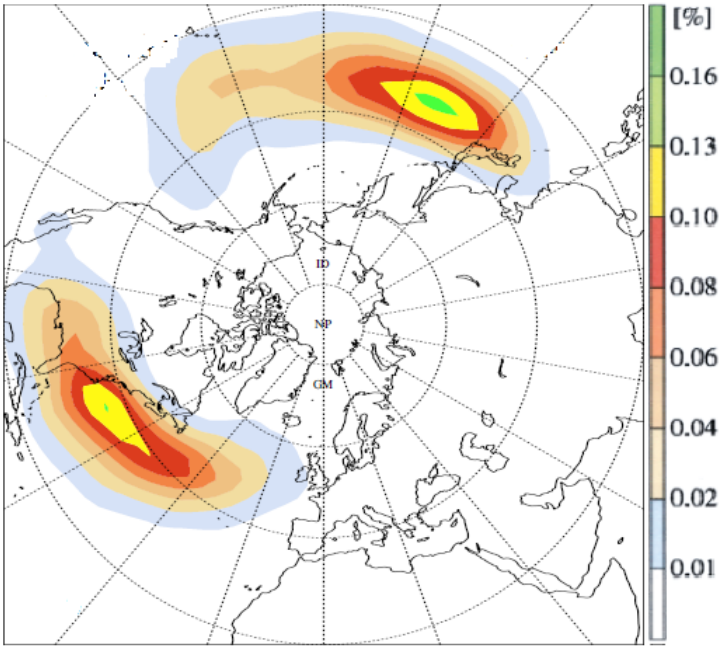

Figure 1. 4. The probability that an airmass from the lower troposphere will be transported upwards into the LS at any time during the next four days. Adapted from Stohl et. al. (2003).

1.4 Objectives and Motivation for This Work

Over the continental US, convection (and associated TST) peaks over summer, while STT has a peak over winter. As a result, the ExTL has a strong tropospheric character during summer and a stratospheric character during winter. In summer, the UT will be heavily influenced by frequent convection, and the LS will be somewhat influenced by convection. In winter, the LS will be strongly stratospheric in character, while the UT will be somewhat stratospheric in character with infrequent convective events lofting air from the lower troposphere. In spring and fall, the UT/LS will be in a state of transition and may have a high amount of variation from day-to-day. Because of this, spring and fall provide excellent opportunities to sample frequent deep convection and the associated TST and STT that come with it, and understand the roles of these processes in controlling the chemistry and composition of the UT/LS.

The DC3 field experiment was based out of Salina, Kansas from May-June 2012, and had two primary scientific objectives: 1) to quantify and characterize the convective transport of fresh emissions and water to the UT/LS within the first few hours of convection, and 2) to quantify the changes in chemistry and composition of the UT/LS that result from this transport (Barth et al., 2014). DC3 aimed to sample convective storms over three regions: Northeast Colorado, Oklahoma, and Northern Alabama. Having three study regions afforded investigators the opportunity to study the effects of convection under different surface emission regimes. Colorado tends to have relatively low NO_x emissions, but high CO and VOC emissions from oil and gas infrastructure. Oklahoma has surface emissions that are similar to Colorado, but with more emissions of biogenic VOCs. Of the three regions, Alabama has the highest emissions of NO_x, CO, anthropogenic VOCs, and biogenic VOCs (Barth et al., 2014). Two airborne scientific platforms were used during DC3: the NASA DC-8 and the NCAR/NSF GV. Two primary types of flight plan were flown: in the first, the two aircraft worked together to sample the inflow and outflow regions of active convective storms (i.e. in the PBL below the storm, and the "anvil" of the storm in the UT/LS), while the second type of flight focused on sampling aged convective outflow in the UT/LS 24-48 after convection had dissipated. A technical overview of DC3 is provided in chapter 2 of this work.

The transport efficiency of chemical species by deep convection is not uniform. For example, water-soluble species such as HCl and HNO_3 may be removed by wet deposition during convection, while relatively insoluble species such as NMHCs may be unaffected (Apel et al., 2012; Riese et al., 2012). Aside from wet-scavenging of soluble species, all chemical species that are not vertically well-mixed within the troposphere will be affected by dilution. For example, in convective outflow, the mixing ratio of long-lived species such as CH_4 will be

relatively unaffected by dilution (since the mixing ratio of CH_4 is relatively constant throughout the troposphere), while mixing ratios of short-lived species like isoprene will be affected by dilution with isoprene-depleted air in the free troposphere. The degree to which both wet-scavenging and dilution occur depends on the residence time of an airmass in a convective storm - a rapidly-lofted airmass may experience less wet-scavenging and dilution than a slowly-lofted airmass. Thus, the mixing ratio of a given species in the convective outflow of a storm will be a function of its mixing ratio in the inflow region of the storm, its solubility, its residence time in the storm, and its atmospheric lifetime. In chapter 3 of this dissertation, tracers are created to identify airmasses affected by STT, PBL air, background UT air, convective outflow in the UT, background LS air, and overshooting tops (i.e. convective outflow above the tropopause) that were sampled during DC3. These data are then used to make inferences about vertical transport times and to investigate dilution of convected airmasses with background air in the free troposphere and UT.

Deep convection is important for the redistribution and production of hydrogen oxides ($HO_x = OH + HO_2$) and HO_x precursors such as formaldehyde (HCHO). The convective redistribution of HO_x precursors to the UT/LS was first theoretically recognized by Chatfield and Crutzen (1984), but early observations of HO_x in the UT over the central pacific sometimes exceeded model predictions by a factor of 2 or more (Jaegle et al., 1997). Later work by Crawford et al. (1999) presented results that supported the hypothesis of HO_x precursors being lofted into the UT over the central pacific by convection, although the levels observed did not close the modeled HO_x disrepency. At the time of this writing, this discrepancy still has not been fully resolved. In chapter 4 of this work, a suite of long-lived halocarbons is used to identify stratospheric intrusions that were sampled during DC3 and provide evidence that stratospheric

intrusions with high levels of O_3 may mix with the high levels of water vapor found in convective outflow to produce OH via the pathway shown in reactions 1.3-1.6.

In section 1.2.4, halocarbons, particularly VSLH, were presented as important gases with respect to O_3 loss in the UT/LS, and deep convection was described as a process that may facilitate the rapid transport of VSLH from the PBL to the UT/LS. The extent to which convection amplifies the VSLH loading in the UT/LS depends on the background composition of the UT/LS and the composition of the convected air. Because chlorinated VSLH tend to be primarily emitted by anthropogenic activity but brominated VSLH tend to be primarily emitted by oceans, continental convection over the central US may transport high amounts of chlorinated VSLH but relatively low amounts of brominated VSLH. Furthermore, the background composition of the UT/LS may vary day-to-day, and may be influenced by long-range transport of airmasses with starkly different chemical compositions (Cooper et al., 2007; Hudman et al., 2004). For example, if the background UT/LS is influenced by long-range transport of air from Asia, it may feature relatively high mixing ratios of chlorinated halocarbons and low mixing ratios of brominated halocarbons, but if it is influenced by long-range transport of air from the central pacific it may feature relatively high mixing ratios of brominated halocarbons and low mixing ratios of chlorinated halocarbons. In chapter 5 of this work, the influence of deep convection and long-range transport on halocarbon mixing ratios in the UT/LS is investigated throughout the DC3 study region.

References

Ahmadov, R., McKeen, S., Trainer, M., Banta, R., Brewer, a., Brown, S., Edwards, P. M., de Gouw, J. a., Frost, G. J., Gilman, J., Helmig, D., Johnson, B., Karion, a., Koss, a., Langford, a., Lerner, B., Olson, J., Oltmans, S., Peischl, J., Pétron, G., Pichugina, Y., Roberts, J. M., Ryerson, T., Schnell, R., Senff, C., Sweeney, C., Thompson, C., Veres, P. R., Warneke, C., Wild, R., Williams, E. J., Yuan, B. and Zamora, R.: Understanding high wintertime ozone pollution events in an oil- and natural gas-producing region of the western US, Atmos. Chem. Phys., 15(1), 411–429, doi:10.5194/acp-15-411-2015, 2015.

Ancellet, G. and Beekmann, M.: Impact of a cutoff low development on downward transport of ozone in the troposphere, J. Geophys. Res., 99, 3451–3468, doi:10.1029/93JD02551, 1994.

Apel, E. C., Olson, J. R., Crawford, J. H., Hornbrook, R. S., Hills, a. J., Cantrell, C. a., Emmons, L. K., Knapp, D. J., Hall, S., Mauldin III, R. L., Weinheimer, a. J., Fried, a., Blake, D. R., Crounse, J. D., Clair, J. M. St., Wennberg, P. O., Diskin, G. S., Fuelberg, H. E., Wisthaler, a., Mikoviny, T., Brune, W. and Riemer, D. D.: Impact of the deep convection of isoprene and other reactive trace species on radicals and ozone in the upper troposphere, Atmos. Chem. Phys., 12(2), 1135–1150, doi:10.5194/acp-12-1135-2012, 2012.

Aschmann, J., Sinnhuber, B. M., Atlas, E. L. and Schauffler, S. M.: Modeling the transport of very short-lived substances into the tropical upper troposphere and lower stratosphere, Atmos. Chem. Phys., 9(5), 18511–18543, doi:10.5194/acpd-9-18511-2009, 2009.

Assonov, S. S., Brenninkmeijer, C. a. M., Schuck, T. and Umezawa, T.: N_2O as a tracer of mixing stratospheric and tropospheric air based on CARIBIC data with applications for CO_2, Atmos. Environ., 79, 769–779, doi:10.1016/j.atmosenv.2013.07.035, 2013.

Atkinson, R., Baulch, D. L., Cox, R. a, Crowley, J. N., Hampson, R. F., Hynes, R. G., Jenkin, M. E., Rossi, M. J. and Troe, J.: Evaluated kinetic and photochemical data for atmospheric chemistry: Volume II – gas phase reactions of organic species, Atmos. Chem. Phys., 6(11), 3625–4055 [online] Available from: http://www.atmos-chem-phys.net/6/3625/2006/, 2006.

Atkinson, R., Baulch, D. L., Cox, R. a., Crowley, J. N., Hampson, R. F., Hynes, R. G., Jenkin, M. E., Rossi, M. J., Troe, J. and Wallington, T. J.: Evaluated kinetic and photochemical data for atmospheric chemistry: Volume IV – gas phase reactions of organic halogen species, Atmos. Chem. Phys., 8, 4141–4496, doi:10.5194/acp-8-4141-2008, 2008.

Avery, M., Twohy, C., MCabe, D., Joiner, J., Severance, K., Atlas, E., Blake, D., Bui, T. P., Crounse, J., Dibb, J., Diskin, G., Lawson, P., McGill, M., Rogers, D., Sachse, G., Scheuer, E., Thompson, A. M., Trepte, C., Wennberg, P. and Ziemke, J.: Convective Distribution of Tropospheric Ozone and Tracers in the Central American ITCZ Region: Evidence from Observations During TC4, J. Geophys. Res., 115, D00J21–, doi:10.1029/2009JD013450, 2010.

Baker, A. K., Beyersdorf, A. J., Doezema, L. a., Katzenstein, A., Meinardi, S., Simpson, I. J., Blake, D. R. and Sherwood Rowland, F.: Measurements of nonmethane hydrocarbons in 28

United States cities, Atmos. Environ., 42(1), 170–182, doi:10.1016/j.atmosenv.2007.09.007, 2008.

Barth, M. C., Cantrell, C. a., Brune, W. H., Rutledge, S. a., Crawford, J. H., Huntrieser, H., Carey, L. D., MacGorman, D., Weisman, M., Pickering, K. E., Bruning, E., Anderson, B., Apel, E., Biggerstaff, M., Campos, T., Campuzano-Jost, P., Cohen, R., Crounse, J., Day, D. a., Diskin, G., Flocke, F., Fried, A., Garland, C., Heikes, B., Honomichl, S., Hornbrook, R., Huey, L. G., Jimenez, J. L., Lang, T., Lichtenstern, M., Mikoviny, T., Nault, B., O'Sullivan, D., Pan, L. L., Peischl, J., Pollack, I., Richter, D., Riemer, D., Ryerson, T., Schlager, H., Clair, J. St., Walega, J., Weibring, P., Weinheimer, A., Wennberg, P., Wisthaler, A., Wooldridge, P. J. and Ziegler, C.: The Deep Convective Clouds and Chemistry (DC3) Field Campaign, Bull. Am. Meteorol. Soc., 141211133556008, doi:10.1175/BAMS-D-13-00290.1, 2014.

Bechara, J., Borbon, a., Jambert, C., Colomb, a. and Perros, P. E.: Evidence of the impact of deep convection on reactive Volatile Organic Compounds in the upper tropical troposphere during the AMMA experiment in West Africa, Atmos. Chem. Phys., 10(21), 10321–10334, doi:10.5194/acp-10-10321-2010, 2010.

Bithell, M., Vaughan, G. and Gray, L. .: Persistence of stratospheric ozone layers in the troposphere, Atmos. Environ., 34(16), 2563–2570, doi:10.1016/S1352-2310(99)00497-5, 2000.

Blake, N. J., Blake, D. R., Sive, B. C., Chen, T.-Y., Rowland, F. S., Collins, J. E., Sachse, G. W. and Anderson, B. E.: Biomass burning emissions and vertical distribution of atmospheric methyl halides and other reduced carbon gases in the South Atlantic region, J. Geophys. Res., 101, 24151, doi:10.1029/96JD00561, 1996.

Boyd, D. T.: Oklahoma Oil and Gas Production : Its Components and Long-Term Outlook., 2009.

Brewer, A. W.: Evidence for a world circulation provided by the measurements of helium and water vapor distribution in the stratosphere, Q. J. R. Meteorol. Soc., 75(326), 351–363, 1949.

Browell, E. V.: Ozone, aerosol, potential vorticity, and trace gas trends observed at high-latitudes over North America from February to May 2000, J. Geophys. Res., 108(D4), 8369, doi:10.1029/2001JD001390, 2003.

Büker, M. L., Hitchman, M. H., Tripoli, G. J., Pierce, R. B., Browell, E. V. and Al-Saadi, J. a.: Long-range convective ozone transport during INTEX, J. Geophys. Res., 113(D14), D14S90, doi:10.1029/2007JD009345, 2008.

Carbone, R. E., Tuttle, J. D., Ahijevych, A. and Trier, S. B.: Inferences of Predictability Associated with Warm Season Precipitation Episodes, J. Atmos. Sci., 59(13), 2033–2056, doi:10.1175/1520-0469, 2002.

Chatfield, R. B. and Crutzen, P. J.: Sulfur dioxide in remote oceanic air: Cloud transport of reactive precursors, J. Geophys. Res. Atmos., 89(D5), 7111–7132, doi:0148-0227/84/004D-0378, 1984.

Cho, J. Y. N., Newell, R. E., Grant, B., Butler, C. F. and Fenn, M. A.: Observation of pollution plume capping by a tropopause fold measurement, Geophys. Res. Lett., 28(17), 3243–3246, doi:10.1029/2001GL012898, 2001.

Clough, S. A. and Iacono, M. J.: Line-by-line calculation of atmospheric fluxes and cooling rates 2 . Application to carbon dioxide , ozone , methane , nitrous oxide and the halocarbons role of the water vapor in the lower troposphere and to provide offsets the cooling not included in ma, J. Geophys. Res., 100(D8), 16519–16535, doi:0148-0227/95/95JD-01386, 1995.

Clough, S. A., Iacono, M. J. and Moncet, J.: Line-by-Line calculations of atmospheric fluxes and cooling rates: Application to water vapor, J. Geophys. Res., 97(D14), 15761–15785, doi:0148-0227/92/92JD-01419, 1992.

Colette, a. and Ancellet, G.: Variability of the tropospheric mixing and of streamer formation and their impact on the lifetime of observed ozone layers, Geophys. Res. Lett., 33(9), L09808, doi:10.1029/2006GL025793, 2006.

Colman, J., Swanson, A., Meinardi, S., Sive B., Blake, D. R. and Rowland, F. S.: Description of the analysis of a wide range of volatile organic compounds in whole air samples collected during PEM-Tropics A and B, Anal. Chem., (73), 3723–3731, 2001.

Cooper, O. R., Trainer, M., Thompson, a. M., Oltmans, S. J., Tarasick, D. W., Witte, J. C., Stohl, a., Eckhardt, S., Lelieveld, J., Newchurch, M. J., Johnson, B. J., Portmann, R. W., Kalnajs, L., Dubey, M. K., Leblanc, T., McDermid, I. S., Forbes, G., Wolfe, D., Carey-Smith, T., Morris, G. a., Lefer, B., Rappenglück, B., Joseph, E., Schmidlin, F., Meagher, J., Fehsenfeld, F. C., Keating, T. J., Van Curen, R. a. and Minschwaner, K.: Evidence for a recurring eastern North America upper tropospheric ozone maximum during summer, J. Geophys. Res., 112(D23), D23304, doi:10.1029/2007JD008710, 2007.

Crawford, J., Davis, D., Olson, J., Chen, G., Liu, S., Gregory, G., Barrick, J., Sachse, G., Sandholm, S., Heikes, B., Singh, H. and Blake, D.: Assessment of upper tropospheric HOx sources over the tropical Pacific based on NASA GTE/PEM data: Net effect on HOx and other photochemical parameters, J. Geophys. Res. Atmos., 104(D13), 16225–16273, 1999.

Crutzen, P. J., Lawrence, M. G. and Paeschl, U.: On the background photochemistry of tropospheric ozone, Tellus A, doi:10.3402/tellusa.v51i1.12310, 1999.

Davidson, J. A., Schiff, H. I., Streit, G. E., McAfee, J. R., Schmeltekopf, A. L. and Howard, C. J.: Temperature dependence of O(1D) rate constants for reactions with N_2O, H_2, CH_4, HCl, and NH_3, J. Chem. Phys., 67, 5021–5025, doi:10.1063/1.434724, 1977.

Dessens, O., Zeng, G., Warwick, N. and Pyle, J.: Short-lived bromine compounds in the lower stratosphere; impact of climate change on ozone, Atmos. Sci. Lett., 10, 249–254, doi:10.1002/asl, 2009.

Dibb, J. E., Meeker, L. D., Finkel, R. C., Southon, J. R., Caffee, M. W. and Barrie, L. A.: Estimation of stratospheric input to the Arctic troposphere : 7Be and 10Be in aerosols at Alert , Canada, J. Geophys. Res., 99, 855–864, doi:0148-0227/94/94JD-00742, 1994.

Dickerson, R. R.: Thunderstorms: An important mechanism in the transport of air pollutants, Science, 235, 460–465, 1987.

Dobson, G. M. B.: Origin and distribution of the polyatomic molecules in the atmosphere, in Proceedings of the Royal Society. Mathematical, physical, and engineering sciences, pp. 187–193., 1956.

Doering, C. and Akber, R.: Beryllium-7 in near-surface air and deposition at Brisbane, Australia., J. Environ. Radioact., 99(3), 461–7, doi:10.1016/j.jenvrad.2007.08.017, 2008.

Fenn, A., Browell, V., Butler, F., Grant, B., Kooi, A., Clayton, B., Gregory, L., Newell, E., Dibb, E., Fuelberg, E., Anderson, E., Bandy, R., Blake, R., Bradshaw, D., Heikes, G., Sachse, W., Sandholm, T., Singh, B., Talbot, W. and Thornton, C.: Ozone and Aerosol distributions and air mass characteristics over the South Pacific during the burning season, J. Geophys. Res., 104(13), 16197–16212, doi:0148-0227/99/1999JD900065, 1999.

Finlayson-Pitts, B. J. and Pitts, J. N.: Chemistry of the Upper and Lower Atmosphere: Theory, Experiments, and Applications, Academic Press, San Diego, California., 2000.

Forster, P. M. and Thompson, D. W. J.: Stratospheric Changes and Climate, in Scientific Assesment of Ozone Depletion: 2010, World Meteorological Organization, Geneva, Switzerland., 2010.

Fusco, A. C.: Analysis of 1970–1995 trends in tropospheric ozone at Northern Hemisphere midlatitudes with the GEOS-CHEM model, J. Geophys. Res., 108(D15), 4449, doi:10.1029/2002JD002742, 2003.

Gerasopoulos, E., Zanis, P., Stohl, A., Zerefos, C. S. and Papastefanou, C.: A climatology of 7 Be at four high-altitude stations at the Alps and the Northern Apennines, Atmos. Chem. Phys. Discuss., 35, 6347–6360, doi:1352-2310/01, 2001.

Gilman, J. B., Lerner, B. M., Kuster, W. C. and de Gouw, J. a: Source signature of volatile organic compounds from oil and natural gas operations in northeastern Colorado., Environ. Sci. Technol., 47(3), 1297–305, doi:10.1021/es304119a, 2013.

González Abad, G., Allen, N. D. C., Bernath, P. F., Boone, C. D., McLeod, S. D., Manney, G. L., Toon, G. C., Carouge, C., Wang, Y., Wu, S., Barkley, M. P., Palmer, P. I., Xiao, Y. and Fu, T. M.: Ethane, ethyne and carbon monoxide concentrations in the upper troposphere and lower

stratosphere from ACE and GEOS-Chem: a comparison study, Atmos. Chem. Phys., 11(18), 9927–9941, doi:10.5194/acp-11-9927-2011, 2011.

Hartmann, D. L., Tank, A. M. G. K., Rusticucci, M., Alexander, L. V., Brönnimann, S., Y. Charabi, F. J., Dentener, E. J., Dlugokencky, D. R., Easterling, A., Kaplan, B. J., Soden, P. W., Wild, M., Horne, P. W. and Zhai, P. M.: Observations: Atmosphere and Surface, in Climate Change 2013: The Physical Science Basis. Contribution of Working Group I to the Fifth Assessment Report of the Intergovernmental Panel on Climate Change, edited by G.-K. Stocker, T.F., D. Qin and V. B. and P. M. M. Plattner, M. Tignor, S.K. Allen, J. Boschung, A. Nauels, Y. Xia, pp. 159–254, Cambridge University Press, Cambridge, UK, and New York, USA., 2013.

Hintsa, E. J., Boering, K. A., Weinstock, E. M., Anderson, J. G., Gary, B. L., Pfister, L., Daube, B. C., Wofsy, S. C., Loewenstein, M., Podolske, J. R., Margitan, J. J. and Bui, T. P.: Troposphere-to-stratosphere transport in the lowermost stratosphere from measurements of H2O, CO2, N2O, and O3, Geophys. Res. Lett., 25(14), 2655–2658, 1998.

Homeyer, C. R., Pan, L. L. and Barth, M. C.: Transport from convective overshooting of the extratropical tropopause and the role of large-scale lower stratosphere stability, J. Geophys. Res. Atmos., 119, 2220–2240, doi:10.1002/2013JD020931, 2014a.

Homeyer, C. R., Pan, L. L., Dorsi, S. W., Avallone, L. M., Weinheimer, A. J., Brien, A. S. O., Digangi, J. P., Zondlo, M. A., Ryerson, T. B., Diskin, G. S. and Campos, T. L.: Convective transport of water vapor into the lower stratosphere observed during double-tropopause events, J. Geophys. Res., 1–18, doi:10.1002/2014JD021485.Received, 2014b.

Horowitz, L. W.: A global simulation of tropospheric ozone and related tracers: Description and evaluation of MOZART, version 2, J. Geophys. Res., 108, doi:10.1029/2002JD002853, 2003.

Hossaini, R., Chipperfield, M. P., Dhomse, S., Ordóñez, C., Saiz-Lopez, a., Abraham, N. L., Archibald, a., Braesicke, P., Telford, P., Warwick, N., Yang, X. and Pyle, J.: Modelling future changes to the stratospheric source gas injection of biogenic bromocarbons, Geophys. Res. Lett., 39, 2–5, doi:10.1029/2012GL053401, 2012.

Hossaini, R., Chipperfield, M. P., Monge-Sanz, B. M., Richards, N. a. D., Atlas, E. and Blake, D. R.: Bromoform and dibromomethane in the tropics: a 3-D model study of chemistry and transport, Atmos. Chem. Phys., 10(2), 719–735, doi:10.5194/acp-10-719-2010, 2010.

Hossaini, R., Chipperfield, M. P., Montzka, S. a, Rap, a, Dhomse, S. and Feng, W.: Efficiency of short-lived halogens at influencing climate through depletion of stratospheric ozone, Nat. Geosci., 8(February), 1–5, doi:10.1038/NGEO2363, 2015.

Huang, L., Fu, R., Jiang, J. H., Wright, J. S. and Luo, M.: Geographic and seasonal distributions of CO transport pathways and their roles in determining CO centers in the upper troposphere, Atmos. Chem. Phys., 12(10), 4683–4698, doi:10.5194/acp-12-4683-2012, 2012.

Hudman, R. C., Jacob, D. J., Cooper, O. R., Evans, M. J., Heald, C. L., Park, R. J., Fehsenfeld, F., Flocke, F., Holloway, J., Hübler, G., Kita, K., Koike, M., Kondo, Y., Neuman, a., Nowak, J., Oltmans, S., Parrish, D., Roberts, J. M. and Ryerson, T.: Ozone production in transpacific Asian pollution plumes and implications for ozone air quality in California, J. Geophys. Res. D Atmos., 109, 1–14, doi:10.1029/2004JD004974, 2004.

Ishijima, K., Patra, P. K., Takigawa, M., Machida, T., Matsueda, H., Sawa, Y., Steele, L. P., Krummel, P. B., Langenfelds, R. L., Aoki, S. and Nakazawa, T.: Stratospheric influence on the seasonal cycle of nitrous oxide in the troposphere as deduced from aircraft observations and model simulations, J. Geophys. Res., 115(D20), D20308, doi:10.1029/2009JD013322, 2010.

Jaegle, L., Jacob, D. J., Wennberg, P. O., Spivakovsky, C. M., Hanisco, T. F., Hintsa, E. J., Fahey, D. W., Keim, E. R., Proffitt, M. H., Atlas, E. L., Flocke, F., Schauffler, S., Mcelroy, C. T., Midwinter, C., Pfister, L. and Wilson, J. C.: Observed OH and HO2 in the upper troposphere suggest a major source from convective injection of peroxides in summer, J. Geophys. Res., 24(24), 3181–3184, 1997.

Katzenstein, A. S., Doezema, L. a, Simpson, I. J., Blake, D. R. and Rowland, F. S.: Extensive regional atmospheric hydrocarbon pollution in the southwestern United States., Proc. Natl. Acad. Sci. U. S. A., 100(21), 11975–9, doi:10.1073/pnas.1635258100, 2003.

Ko, M. K. W. and Poulet, G.: Very Short-Lived Halogen and Sulfur Substances, in Scientific Assesment of Ozone Depletion: 2002., 2002.

Koch, D., Mann, M.: Koch 1996 - Spatial and temporal variability of 7Be surface concentrations.pdf, Tellus, 48B, 387–396, 1996.

Konopka, P. and Pan, L. L.: On the mixing-driven formation of the Extratropical Transition Layer (ExTL), J. Geophys. Res. Atmos., 117(D18), n/a–n/a, doi:10.1029/2012JD017876, 2012.

Koo, J. H., Wang, Y., Kurosu, T. P., Chance, K., Rozanov, a., Richter, a., Oltmans, S. J., Thompson, a. M., Hair, J. W., Fenn, M. a., Weinheimer, a. J., Ryerson, T. B., Solberg, S., Huey, L. G., Liao, J., Dibb, J. E., Neuman, J. a., Nowak, J. B., Pierce, R. B., Natarajan, M. and Al-Saadi, J.: Characteristics of tropospheric ozone depletion events in the Arctic spring: Analysis of the ARCTAS, ARCPAC, and ARCIONS measurements and satellite BrO observations, Atmos. Chem. Phys., 12, 9909–9922, doi:10.5194/acp-12-9909-2012, 2012.

Lamarque, J.-F., Langford, A. O. and Proffitt, M. H.: Cross-tropopause mixing of ozone through gravity wave breaking: Observation and modeling, J. Geophys. Res., 101(D17), 22969–22976, doi:0148-0227/96/96JD-02442, 1996.

Langford, a. O., Brioude, J., Cooper, O. R., Senff, C. J., Alvarez, R. J., Hardesty, R. M., Johnson, B. J. and Oltmans, S. J.: Stratospheric influence on surface ozone in the Los Angeles area during late spring and early summer of 2010, J. Geophys. Res. Atmos., 117(D21), n/a–n/a, doi:10.1029/2011JD016766, 2012.

Langford, A. O., Masterst, C. D., Proffitt, M. H., Hsie, E. and Tuck, A. F.: Ozone measurements in a tropopause with a cut-off low system, Geophys. Res. Lett., 23(18), 2501–2504, doi:0094-8534/96/96GL-02227, 1996a.

Langford, A. O., Proffitt, M. H. and Vanzandt, T. E.: Modulation of tropospheric ozone by a propagating gravity wave, J. Geophys. Res. Atmos., 101(96), 26605–26613, doi:0148-0227/96/96JD-0242, 1996b.

Law, K. S., Fierli, F., Cairo, F., Schlager, H., Bormann, S., Streibel, M., Real, E., Kunkel, D., Schiller, C. and Ravegnani, F.: Air mass origins influencing TTL chemical composition over West Africa during 2006 summer monsoon, Atmos. Chem. Phys., 10(22), 10753–10770, 2010.

Law, K. S. and Sturges, W. T.: Halogenated Very Short-Lived Substances, in Scientific Assesment of Ozone Depletion: 2006, World Meteorological Organization, Geneva, Switzerland., 2006.

Levine, J. G., Braesicke, P., Harris, N. R. P., Savage, N. H. and Pyle, J. a.: Pathways and timescales for troposphere-to-stratosphere transport via the tropical tropopause layer and their relevance for very short lived substances, J. Geophys. Res. Atmos., 112, 1–15, doi:10.1029/2005JD006940, 2007.

Levy, H.: Normal atmosphere: large radical and formaldehyde concentrations predicted., Science (80-.)., 173(3992), 141–143, doi:10.1126/science.173.3992.141, 1971.

Liang, Q., Atlas, E., Blake, D., Dorf, M., Pfeilsticker, K. and Schauffler, S.: Convective transport of very short lived bromocarbons to the stratosphere, Atmos. Chem. Phys., 14(11), 5781–5792, 2014.

Libuda, H. G., Zabel, F., Fink, E. H. and Becker, K. H.: Formyl Chloride - Uv Absorption Cross-Sections and Rate Constants for the Reactions With Cl and Oh, J. Phys. Chem., 94, 5860–5865, doi:10.1021/j100378a047, 1990.

Lin, M., Fiore, A. M., Cooper, O. R., Horowitz, L. W., Langford, A. O., Levy, H., Johnson, B. J., Naik, V., Oltmans, S. J. and Senff, C. J.: Springtime high surface ozone events over the western United States: Quantifying the role of stratospheric intrusions, J. Geophys. Res. Atmos., 117(D21), n/a–n/a, doi:10.1029/2012JD018151, 2012.

Mcculloch, A.: CFC and Halon replacements in the environment, Atmos. Env., 100(July), 1999.

Mielke, L. H., Furgeson, A. and Osthoff, H. D.: Observation of $ClNO_2$ in a mid-continental urban environment., Environ. Sci. Technol., 45, 8889–96, doi:10.1021/es201955u, 2011.

Millet, D. B., Jacob, D. J., Boersma, K. F., Fu, T.-M., Kurosu, T. P., Chance, K., Heald, C. L. and Guenther, A.: Spatial distribution of isoprene emissions from North America derived from formaldehyde column measurements by the OMI satellite sensor, J. Geophys. Res., 113(D2), D02307, doi:10.1029/2007JD008950, 2008.

Molina, M. J. and Rowland, F. S.: Stratospheric sink for chlorofluoromethanes: chlorine atom-catalysed destruction of ozone, Nature, 249, 1974.

Montzka, S. A., Reimann, S., Engel, A., Kruger, K., O'Doherty, S. and Sturges, W. T.: Ozone Depleting Substances (ODSs) and Related Chemicals, in Scientific Assesment of Ozone Depletion: 2010, World Meteorological Organization, Geneva, Switzerland., 2010.

Nowak, J. B., Parrish, D. D., Neuman, J. a., Holloway, J. S., Cooper, O. R., Ryerson, T. B., Nicks, J. K., Flocke, F., Roberts, J. M., Atlas, E., de Gouw, J. a., Donnelly, S., Dunlea, E., Hübler, G., Huey, L. G., Schauffler, S., Tanner, D. J., Warneke, C. and Fehsenfeld, F. C.: Gas-phase chemical characteristics of Asian emission plumes observed during ITCT 2K2 over the eastern North Pacific Ocean, J. Geophys. Res. D Atmos., 109, 1–18, doi:10.1029/2003JD004488, 2004.

Pan, L. L.: Definitions and sharpness of the extratropical tropopause: A trace gas perspective, J. Geophys. Res., 109(D23), D23103, doi:10.1029/2004JD004982, 2004.

Pan, L. L., Bowman, K. P., Atlas, E. L., Wofsy, S. C., Zhang, F., Bresch, J. F., Ridley, B. a., Pittman, J. V., Homeyer, C. R., Romashkin, P. and Cooper, W. a.: The Stratosphere–Troposphere Analyses of Regional Transport 2008 Experiment, Bull. Am. Meteorol. Soc., 91(3), 327–342, doi:10.1175/2009BAMS2865.1, 2010.

Pan, L. L., Homeyer, C. R., Honomichl, S., Ridley, B. A., Weisman, M., Crawford, J. H., Ryerson, T. B., Pollack, I. and Peischl, J.: Thunderstorms enhance tropospheric ozone by wrapping and shedding stratospheric air, J. Geophys. Res., 7785–7790, doi:10.1002/2014GL061921, 2014.

Park, S., Atlas, E. L., Jiménez, R., Daube, B. C., Gottlieb, E. W., Nan, J., Jones, D. B. a, Pfister, L., Conway, T. J., Bui, T. P., Gao, R. S. and Wofsy, S. C.: Vertical transport rates and concentrations of OH and Cl radicals in the tropical tropopause layer from observations of CO2 and halocarbons: Implications for distributions of long-and short-lived chemical species, Atmos. Chem. Phys., 10, 6669–6684, doi:10.5194/acp-10-6669-2010, 2010.

Peevey, T. R., Gille, J. C., Homeyer, C. R. and Manney, G. L.: The double tropopause and its dynamical relationship to the tropopause inversion layer in storm, J. Geophys. Res., 194–212, doi:10.1002/2014JD021808.Received, 2014.

Pétron, G., Frost, G., Miller, B. R., Hirsch, A. I., Montzka, S. a., Karion, A., Trainer, M., Sweeney, C., Andrews, A. E., Miller, L., Kofler, J., Bar-Ilan, A., Dlugokencky, E. J., Patrick, L., Moore, C. T., Ryerson, T. B., Siso, C., Kolodzey, W., Lang, P. M., Conway, T., Novelli, P., Masarie, K., Hall, B., Guenther, D., Kitzis, D., Miller, J., Welsh, D., Wolfe, D., Neff, W. and Tans, P.: Hydrocarbon emissions characterization in the Colorado Front Range: A pilot study, J. Geophys. Res., 117(D4), D04304, doi:10.1029/2011JD016360, 2012.

Pétron, G. and Karion, A.: A new look at methane and nonmethane hydrocarbon emissions from oil and natural gas operations in the Colorado Denver-Julesburg Basin, J. Geophys. Res. Atmos., 119(11), 6836–6852, doi:10.1002/2013JD021272.Received, 2014.

Pickering, K. E.: Convective tarnsport of biomass burning emissions over Brazil during TRACE-A, J. Geophys. Res. Atmos., 101(23), 993–1024, 1996.

Poulida, O., Dickerson, R. R. and Heymsfield, A.: Stratosphere-troposphere exchange in a midlatitude mesoscale convective complet, J. Geophys. Res., 101(95), 6823–6836, doi:doi:10.1029/95JD03523, 1996.

Prather, M. J.: Timescales in atmospheric chemistry : CHBr , the ocean , and ozone depletion potentials, Global Biogeochem. Cycles, 11(3), 393–400, doi:10.1029/97GB01055, 1997.

Prather, M. J.: Lifetimes of atmospheric species: Integrating environmental impacts, Geophys. Res. Lett., 29(22), 2063, doi:10.1029/2002GL016299, 2002.

Price, J. and Vaughan, G.: The potential for stratosphere-troposphere exchange in cut-off-low systems, Q. J. R. Meteorol. Soc., 119(510), 343–365, doi:10.1002/qj.49711951007, 1993.

Ridley, B. A., Walega, J. G., Dye, J. E. and Grahek, F. E.: Distribution of NO, NOx, NOy, and O3 to 12 km altitude during the summer monsoon season over New Mexico, J. Geophys. Res. Atmos., 99, 25519–25534, doi:10.1029/94JD02210, 1997.

Riese, M., Ploeger, F., Rap, a., Vogel, B., Konopka, P., Dameris, M. and Forster, P.: Impact of uncertainties in atmospheric mixing on simulated UTLS composition and related radiative effects, J. Geophys. Res., 117(D16), D16305, doi:10.1029/2012JD017751, 2012.

Saiz-Lopez, a., Lamarque, J. F., Kinnison, D. E., Tilmes, S., Ordóñez, C., Orlando, J. J., Conley, a. J., Plane, J. M. C., Mahajan, a. S., Sousa Santos, G., Atlas, E. L., Blake, D. R., Sander, S. P., Schauffler, S., Thompson, a. M. and Brasseur, G.: Estimating the climate significance of halogen-driven ozone loss in the tropical marine troposphere, Atmos. Chem. Phys., 12, 3939–3949, doi:10.5194/acp-12-3939-2012, 2012.

Schauffier, S. M., Atlas, E. L., Flocke, F., Lueb, R. A., Stroud, V. and Travnicek, W.: Measurements of bromine containing organic compounds at the tropical tropopause,Geophys. Res. Let., 25(3), 317–320, 1998.

Schauffler, S. M., Atlas, E. L., Flocke, F., Lueb, R. A., Stroud, V. and Travnicek, W.: Distributions of brominated organic compounds in the troposphere and lower stratosphere chlorine, J. Geophys. Res., 104, 1999.

Simpson, I. J., Andersen, M. P. S., Meinardi, S., Bruhwiler, L., Blake, N. J., Helmig, D., Rowland, F. S. and Blake, D. R.: Long-term decline of global atmospheric ethane concentrations and implications for methane, Nature, 488(7412), 490–494, doi:10.1038/nature11342, 2012.

Simpson, I. J., Blake, N. J., Barletta, B., Diskin, G. S., Fuelberg, H. E., Gorham, K., Huey, L. G., Meinardi, S., Rowland, F. S., Vay, S. a., Weinheimer, a. J., Yang, M. and Blake, D. R.: Characterization of trace gases measured over Alberta oil sands mining operations: 76 speciated C2–C10 volatile organic compounds (VOCs), CO2, CH4, CO, NO, NO2, NOy, O3, Atmos. Chem. Phys., 10(23), 11931–11954, doi:10.5194/acp-10-11931-2010, 2010.

Simpson, I. J., Rowland, F. S., Meinardi, S. and Blake, D. R.: Influence of biomass burning during recent fluctuations in the slow growth of global tropospheric methane, Geophys. Res. Lett., 33(22), doi:10.1029/2006GL027330, 2006.

Smyth, S., Bradshaw, J., Sandholm, S., Liu, S., McKeen, S., Gregory, G., Anderson, B., Talbot, R., Blake, D., Rowland, F. S., Browell, E., Fenn, M., Merrill, J., Backmeier, S., Sachse, G., Collins, J., Thornton, D., Davis, D. and Singh, H.: Comparison of free tropospheric western Pacific air mass classification schemes for the PEM-West A experiment, J. Geophys. Res., 101, 1743–1762, 1996.

Solomon, S., Mills, M., Heidt, L. E., Pollock, W. H. and Tuck, a. F.: On the evaluation of ozone depletion potentials, J. Geophys. Res., 97(D1), 825, doi:10.1029/91JD02613, 1992.

Sprenger, M., Wernli, H. and Bourqui, M.: Stratosphere–Troposphere Exchange and Its Relation to Potential Vorticity Streamers and Cutoffs near the Extratropical Tropopause, J. Atmos. Sci., 64(5), 1587–1602, doi:10.1175/JAS3911.1, 2007.

Stohl, a.: Stratosphere-troposphere exchange: A review, and what we have learned from STACCATO, J. Geophys. Res., 108(D12), 8516, doi:10.1029/2002JD002490, 2003.

Stohl, A., Wernli, H., James, P., Bourqui, M., Forster, C., Liniger, M. a., Seibert, P. and Sprenger, M.: A New Perspective of Stratosphere–Troposphere Exchange, Bull. Am. Meteorol. Soc., 84(11), 1565–1573, doi:10.1175/BAMS-84-11-1565, 2003.

Stolarski, R. S. and Cicerone, R. J.: Stratospheric chlorine - Possible sink for ozone, Can. J. Chem., 52(8), 1610–1615, doi:10.1139/v74-233, 1974.

Survey, K. G.: State energy production and historical info, [online] Available from: http://www.kgs.ku.edu/PRS/petro/state.html, 2015.

Thornton, J. a, Kercher, J. P., Riedel, T. P., Wagner, N. L., Cozic, J., Holloway, J. S., Dubé, W. P., Wolfe, G. M., Quinn, P. K., Middlebrook, A. M., Alexander, B. and Brown, S. S.: A large atomic chlorine source inferred from mid-continental reactive nitrogen chemistry., Nature, 464(March), 271–274, doi:10.1038/nature08905, 2010.

Vaughan, G., Connor, F. M. O. and Wareing, D. P.: Observations of Streamers in the Troposphere and Stratosphere Using Ozone Lidar,Atmos. Chem. Phys., 295–315, 2001.

Vaughan, G., Price, J. D. and Howells, A.: Transport into the troposphere in a tropopause fold, Q. J. R. Meteorol. Soc., 120(518), 1085–1103, doi:10.1002/qj.49712051814, 1994.

World Meteorological Organization (WMO)/United Nations Environment Programme (UNEP): Scientific Assessment of Ozone Depletion : 2010.

2. Methods

All data presented in this dissertation were collected onboard the NASA DC-8 during the DC3 field campaign, which took place during May-June of 2012 over the central US. Measurements of VOCs were obtained via UC Irvine's whole air sampler (WAS) instrument, while measurements of CH_4, O_3, NO_x, N_2O, water vapor, CO, and meteorological variables were performed by a variety of other instruments operated by collaborators onboard the DC-8. Detailed technical descriptions of study design, sampling protocol, and analytical instrumentation are provided below.

2.1 Study Design

During DC3, the NASA DC-8 flew18 research flights over the central US with a main operations base in Salina, Kansas (UTC – 5:00 hours). Of these 18 flights, 14 had a primary objective of sampling active convective storms in one of the three primary study regions: Northeast Colorado, Oklahoma, and Northern Alabama. The four remaining flights focused on tracking aged outflow from storms that were sampled the previous day. For flights where active convection was sampled, the DC-8 flew "L" shaped patterns at low altitudes in the inflow region of the storm (typically 1-4 km altitude), while a second aircraft, the NCAR/NSF GV, sampled the outflow region at high altitudes. After sampling the inflow region, the DC-8 then spiraled up to 9-12 km and flew passes through the outflow before returning to Salina. An example of this type of flight is shown in Figure 2. 1, where typical DC-8 inflow (top panel) and outflow (bottom panel) sampling patterns are shown. Information about all 18 DC-8 flights, including the date, sampling region, and the primary objective of each flight is presented in table 2.1. A list of all species and variables measured onboard the DC-8 that will be used in later chapters of this work

is presented in section 2.2. Since only data collected onboard the DC-8 was used for analysis in this dissertation, the NCAR/NSF GV will not be discussed.

Model forecasts, radar returns, and satellite images were used to determine the probability of thunderstorms occurring in each sampling region and to predict the location of aged convective outflow in the UT 12-48 hours after active convection. Weather Research and Forecasting (WRF) model simulations were conducted twice a day (00 and 12 UTC) using a 3 km grid spacing to determine the location of active convection (Romine et al., 2013). The FLEXible PARTicle dispersion model (FLEXPART; Stohl et al., 2005) was used to precisely identify the location of the downwind outflow plume 12-48 hours later, and was initialized using the location of convective outflow from active storms that were sampled by the aircraft. FLEXPART was also used to give context on the chemical environment of the UT, including information on the effects of biomass burning and long-range transport. Satellite measurements of NO_2 column densities from once-daily overpasses of the Global Ozone Monitoring Instrument (GOME-2) were used to further corroborate the location of aged convective outflow.

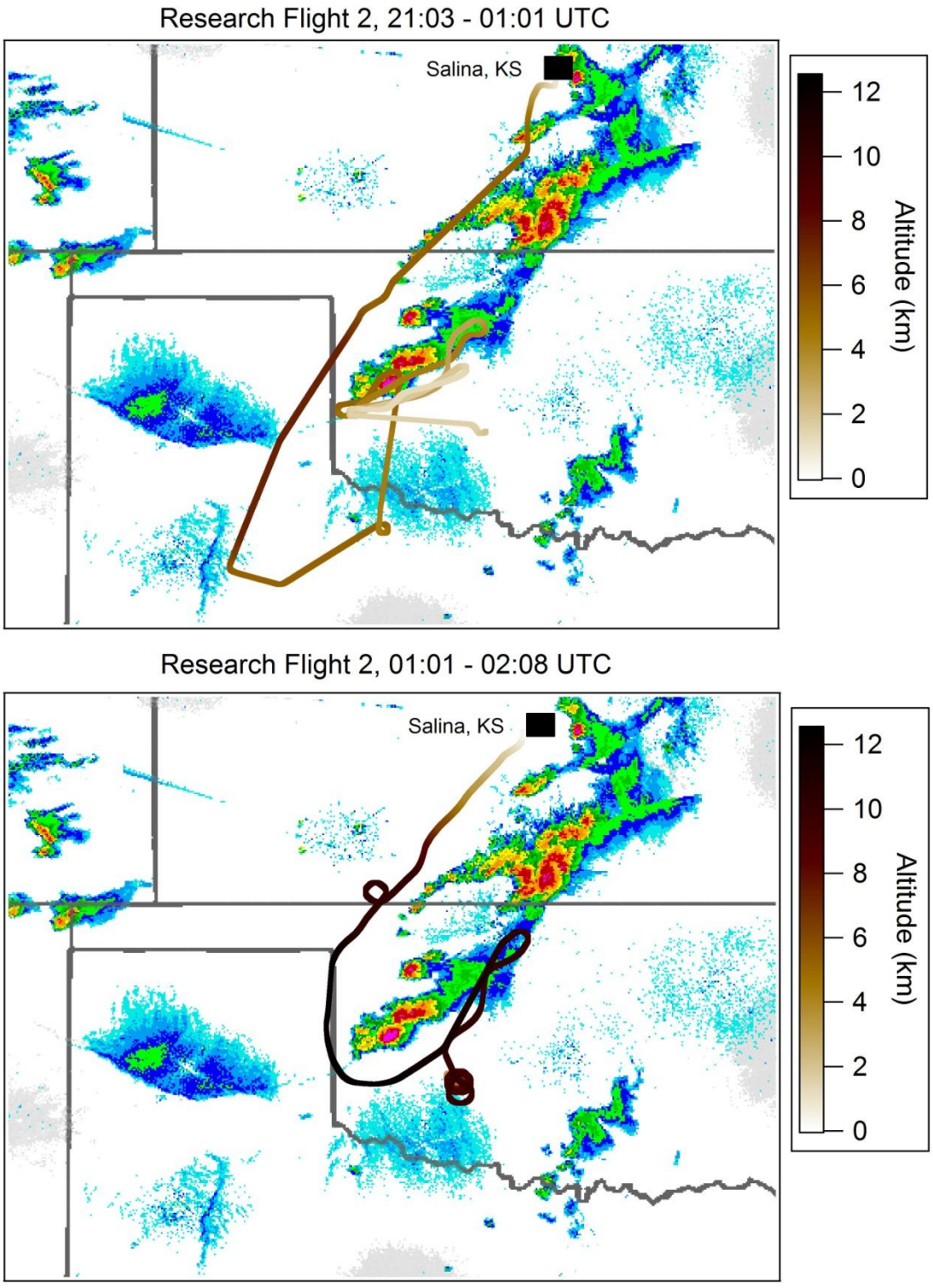

Figure 2. 1. Flight tracks from research flight 2 showing the DC-8 sampling the inflow area at low altitudes (top panel) and the outflow area at high altitudes (bottom panel). A radar image shows the location of the storm that was being sampled during this flight.

Table 2.1. Flight information for all 18 research flights flown by the DC-8 during DC3.

Research Flight	Date (2012), Takeoff Time (UTC)	Region	Primary Objective
1	5/18, 14:04	CO	Active Convection
2	5/19, 16:03	OK/TX	Active Convection
3	5/21, 11:00	AL	Active Convection
4	5/25, 15:11	OK/TX	Active Convection
5	5/26, 14:04	TN	Tracking outflow from RF 4
6	5/29, 14:54	OK	Active Convection
7	5/30, 13:33	VA	Tracking outflow from RF 6
8	6/1, 14:39	CO/TX	Source characterization, active convection
9	6/2, 13:13	CO	Active Convection
10	6/5, 15:00	CO	Active Convection
11	6/6, 14:11	CO	Active Convection
12	6/7, 13:30	MO/AR	Tracking outflow from RF 11
13	6/11, 10:00	AL	Active Convection
14	6/15, 13:00	CO	Active Convection
15	6/16, 16:07	OK/TX	Active Convection
16	6/17, 15:07	AR/LA	Tracking outflow from RF 15
17	6/21, 5:58	OK/MO	Sampling outflow from an overnight storm
18	6/22, 14:54	CO	Active Convection

2.2 Airborne measurements

A variety of chemical species and meteorological variables were measured onboard the DC-8. Species used for data analysis in this work are presented in Table 2.2. Whole air sample collection on board the DC-8 was controlled using a dual-head metal bellows pump (connected in series) attached to a 0.25" forward-facing inlet on the outside of the aircraft. The outlet of the pump was connected to a sampling manifold, allowing air to be drawn from outside the plane and directed towards sampling canisters. Sampling canisters were 2 L stainless steel canisters that were evacuated before use, and manually opened and closed during flight using a metal bellows valve. Sampling canisters were arranged in "snakes" of 24 canisters, where eight canisters were placed in series and were interconnected with two other rows of canisters using

stainless steel flex tubing and ultra-torr unions. When all cans were closed, air was flowed from the pump outlet and through the snake lines before exiting via an exhaust line that vented outside the aircraft. This allowed the sampling manifold to be constantly flushed with fresh air from outside the plane. Sample collection was done by closing this exhaust line and opening a given canister until a final pressure of 35-40 psig was reached. Typically, this took anywhere from 30 seconds to 2 minutes, depending on altitude. In total, 1,795 WAS samples were collected over the 18 research flights, and sample frequency ranged from every 0.5 – 5 min depending flight objectives and the location of the aircraft relative to points of interest. An on-board live feed provided aircraft location, precipitation radar, wind direction, and mixing ratios of NO, CO, and O_3. On a typical 4-7 hour research flight, 70-110 samples were collected. All samples were then shipped back to UC Irvine and analyzed by gas chromatography within one week of collection. Canister preparation procedures and a description of UC Irvine's gas chromatography system are provided in section 2.3.

Mixing ratios of CO, N_2O, O_3, CH_4, and water vapor were measured every second, while O_3 vertical profiles were updated every minute. Carbon monoxide, N_2O, and CH_4 were measured every 1-s by mid-infrared tunable diode laser absorption spectroscopy (DACOM), operated by NASA Langley (Diskin et al., 2002; Sachse and Hill, 1987; Sachse et al., 1991). Water vapor was measured every 1-s by a near-infrared long-path laser hygrometer, also operated by NASA Langley (Diskin et al., 2002; Podolske, 2003). Ozone was measured every 1-s using chemiluminescence, operated by NOAA's Earth System Research Laboratory (Carroll et al., 1992). These 1-s data were useful for identifying the exact times the DC-8 entered or exited a specific airmass – for example locating the exact times when the DC-8 entered or exited convective outflow in the UT. For comparison with WAS data, these 1-s data were averaged

over the filling period of a given WAS canister (the so-called "WAS data merge", accessible at http://www.air.larc.nasa.gov/cgi-bin/ArcView/dc3). Ozone lidar profiles were collected by differential absorption lidar (DIAL), operated by NASA Langley (Browell, 1989; Fenn et al., 1999; Rogers et al., 2009). Lidar profiles were collected every 10-s and averaged over a period of one minute. The "blind spot" for the DIAL instrument (i.e. where the overlap function dictated by the lidar geometry is less than 1) was ± 2.5 km, and vertical profiles extended from near-surface up to 22 km. These lidar profiles were useful for ascertaining locations and shapes of potential stratospheric intrusions.

Table 2.2. List of species used for analysis in this dissertation, and the instruments they were measured with.

Instrument Name	PI, Instution	Species Measured	References
Whole Air Sampler (WAS)	Blake, UC Irvine	VOCs	Colman et al. (2001)
Differential Absorption of CO and Methane (DACOM)	Diskin, NASA	CO, CH_4 N_2O	Sachse et al. (1991); Diskin et al. (2002)
Differential Laser Hygrometer (DLH)	Diskin, NASA	H_2O vapor	Diskin et al. (2002); Podolske (2003)
NO_y and O_3 measuring instrument (NO_yO_3)	Ryerson, NOAA	O_3	Carroll et al. (1992)
Differential Absorption LiDAR (DIAL)	Hair, NASA	O_3 vertical profiles	Browell (1989); Fenn et al. (1999)

A meteorological variable - tropopause height - was also calculated along the DC-8 flight path for each flight. This was done by interpolating the National Centers for Environmental Prediction Global Forecast System (NCEP-GFS) model analysis in space and time and comparing it to aircraft location at a given time. From this, the local thermal tropopause height above (or below) the DC-8 was calculated using the WMO lapse rate definition. The associated uncertainty in calculated tropopause height is proportional to the GFS vertical resolution, and is

generally around ~500 meters (Homeyer et al., 2014). These data were calculated by NCAR, and are also available in the DC3 WAS data merges.

2.3 VOC Measurement

2.3.1 Canister Preparation

Prior to use during DC3, canisters were conditioned to ensure analytical precision. In the first stage of the conditioning process, all canisters were pressurized to 35 psig using ambient air and then flushed. This process was repeated ten times for each canister to ensure that any impurities or adsorbed species were removed. Next, the canisters were baked at 150 °C under humidified, ambient air conditions. This creates an oxide layer on the interior surface of each canister, which prevents surface adsorption of gases. After baking, canisters were pressurized with air that was collected at White Mountain Research Station (WMRS, altitude 10,200 feet), a remote, atmospherically-clean location in the eastern Sierra Nevada Mountains. After two minutes, cans were vented then re-pressurized. This process was repeated 15 times, and after the last pressurization the canisters were pumped down to 10^{-2} torr. Next, canisters were flushed with ultra-high-purity helium that had been further purified by flowing through stainless steel tubing filled with glass beads that was submerged in liquid nitrogen. After flushing with helium, canisters were again pumped down to 10^{-2} torr. All canisters were then sealed for two weeks, after which they were checked for leaks. Finally, 17 torr of water vapor was added to each canister to quench active surface sites.

Sensitivity tests have been conducted to assess the long-term stability of VOCs housed in these canisters (Sive, 1998). These tests showed that, following these pre-conditioning procedures, VOC mixing ratios are stable over a period of two weeks. Over a two month period, small growths of ethene, ethyne, propene, benzene, and toluene were observed, and small losses

of heavy hydrocarbons (i.e. C_8 and higher alkanes, terpenes, etc.) were observed. Growth rates generally were between 0.1-0.2 pptv/day, and loss rates were of a similar magnitude. To minimize these internal growth and losses, all samples collected during DC3 were analyzed within one week of collection.

2.3.2 VOC Analysis

VOCs were analyzed by gas chromatography in the Rowland-Blake group laboratory. Pressurized samples were introduced into a manifold which contained a 2 L "excess volume" stainless steel canister (same size and construction as the sampling canisters) via an ultra-torr union. The sampling canister was used to pressurize the excess volume canister to 900.0 torr. Following pressurization, the sampling canister was closed and removed from the manifold. Next, an aliquot of sample was pulled from the excess volume can through a 5 cm^3 pre-concentration loop immersed in liquid nitrogen by use of a downstream pump. This loop consisted of 0.25" stainless steel tubing packed with glass beads. During DC3, samples were flowed through this pre-concentration loop until the pressure in the manifold (upstream from the loop) reached 100.0 torr. This corresponded to a 2033 cm^3 sample aliquot (at STP) that was flowed through this pre-concentration loop. While flowing through this pre-concentration loop, VOCs with boiling points significantly higher than that of liquid nitrogen (77 K) readily condense on the glass beads while gases with boiling points that are near or lower than that of liquid nitrogen are effectively removed. After this pre-concentration process, the loop was closed from the manifold and downstream pump, and a hot water bath was introduced to re-volatilize the sample. Next, a helium carrier gas was flowed through the loop and carried towards the gas chromatographs (GCs). Upstream from the GCs, a splitter box divided the sample into five streams which were sent to five different column/detector combinations housed among three

Hewlett-Packard 6890 GCs. The first GC housed a J&W Scientific DC-5ms column coupled to a quadrupole mass spectrometer detector (MSD) and a RESTEK-1701/DC-5 column coupled with an electron capture detector (ECD). A second GC housed a RESTEK-1701 column connected to a second ECD and a J&W PLOT/J&W DB-1 column connected to a flame ionization detector (FID). The final GC housed a J&W DB-1 column connected to a second FID, and a Cyclodex column connected to a third FID. FIDs allowed for the detection of hydrocarbon compounds, while ECDs allowed detection of halocarbons and alkyl nitrates. The MSD allowed detection of a subset of hydrocarbons, halocarbons, and alkyl nitrates and allowed for identification of potentially unknown compounds. Signal output from the ECDs and FIDs were sent to a PC running Chromeleon software, and the MSD signal output was sent to a second PC running Hewlett-Packard Chemstation. A brief summary of these column/detector combinations is provided in Table 2.3, and a visual schematic of this setup is shown in Figure 2.2. A list of all VOCs measured during DC3 is provided in Table 2.4.

Working standards were run after every eighth sample. Working standards were contained in 34 L pressurized pontoons, and were analyzed in the same manner as sample canisters (i.e. via the excess volume canister). In addition, separate standards were analyzed once daily for comparison to the working standard. Standard preparation occurred in-house, and was done by pressurizing pontoons with air collected at WMRS. This ensured that levels of permanent gases like nitrogen and oxygen were identical between standards and samples, and that CH_4, CO, and CO_2 mixing ratios in standards were similar to those measured in samples. This similarity in composition ensured consistent behavior between samples and standards in our analytical systems. Small aliquots of high-concentration synthetic standards were used to dope

these standards with VOCs of interest. All whole air standards were previously calibrated using a combination of synthetic standards and previously-calibrated whole air standards.

Instrument response factors for each compound were calculated by taking the ratio of the peak area of a given compound to the known mixing ratio of that compound in the working standard. These response factors were then fit to a polynomial curve relative to the injection time of each working standard. Mixing ratios of compounds in samples were then calculated by comparing the peak area of a given compound (with a given sample injection time) to the calculated polynomial fit for the response factor at that time.

Table 2.3. GC column/detector combinations used for VOC analysis during DC3

GC	Column	Detector	Compound Classes
1	60m J&W DB-5ms	MSD	Hydrocarbons, halocarbons, alkyl nitrates
	30m J&W DB-5 + 5m RESTEK-1701	ECD	Halocarbons, alkyl nitrates
2	60m J&W DB-1	FID	C_3-C_{10} NMHCs
	60m Cyclodex	FID	C_5-C_{10} NMHCs
3	60m Restek-1701	ECD	Halocarbons, alkyl nitrates
	30m J&W PLOT + 5m J&W DB-1	FID	C_2-C_6 NMHCs

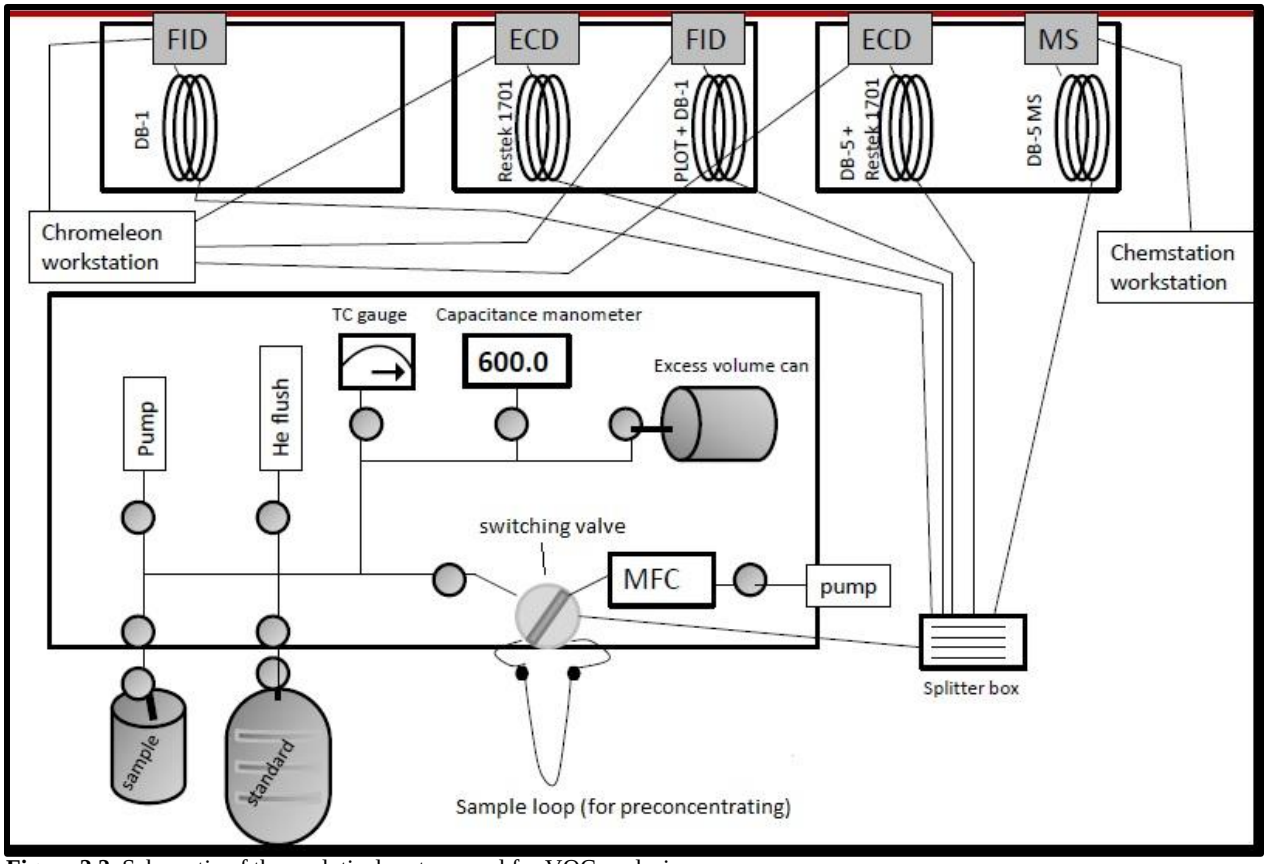

Figure 2.2. Schematic of the analytical system used for VOC analysis

Table 2.4. VOCs measured during DC3 using UC Irvine's analytical system

	Compound	Formula	LOD (pptv)	Precision (%)	Accuracy (%)
Alkanes	Ethane	C_2H_6	3	1	5
	Propane	C_3H_8	3	2	5
	i-Butane	C_4H_{10}	3	3	5
	n-Butane	C_4H_{10}	3	3	5
	i-Pentane	C_5H_{12}	3	3	5
	n-Pentane	C_5H_{12}	3	3	5
	n-Hexane	C_6H_{14}	3	3	5
	n-Heptane	C_7H_{16}	3	3	5
	2,3-Dimethylbutane	C_6H_{14}	3	3	5
	2-Methylpentane	C_6H_{14}	3	3	5
Alkenes and Alyknes	Ethene	C_2H_4	3	3	5
	Propene	C_3H_6	3	3	5
	Ethyne	C_2H_2	3	3	5
Aromatics	Benzene	C_6H_6	3	3	5
	Toluene	C_7H_8	3	3	5
	Ethylbenzene	C_8H_{10}	3	3	5
	m + *p*–Xylene	C_8H_{10}	3	3	5
	o-Xylene	C_8H_{10}	3	3	5
	3-Ethyltoluene	C_8H_{10}	3	3	5
	4-Ethyltoluene	C_8H_{10}	3	3	5
	2-Ethyltoluene	C_8H_{10}	3	3	5
	1,3,5-Trimethylbenzene	C_9H_{12}	3	3	5
	1,2,4-Trimethylbenzene	C_9H_{12}	3	3	5

Table 2.5. Continued.

	Compound	Formula	LOD (pptv)	Precision (%)	Accuracy (%)
Aromatics	1,2,3-Trimethylbenzene	C_9H_{12}	3	3	5
Biogenics	Isoprene	C_5H_8	3	3	5
	α-Pinene	$C_{10}H_{16}$	3	3	5
	β-Pinene	$C_{10}H_{16}$	3	3	5
CFCs	CFC-11	CCl_3F	10	1	3
	CFC-12	CCl_2F_2	10	1	3
	CFC-113	CCl_2FCClF_2	5	1	3
	CFC-114	$CClF_2CClF_2$	1	1	5
Halons	H-1211	$CBrClF_2$	0.1	1	5
	H-1301	$CBrF_3$	0.1	10	5
	H-2402	$CBrF_2CBrF_2$	0.01	1	5
HCFCs	HCFC-22	CHF_2Cl	2	5	5
	HCFC-141b	CH_3CClF_2	0.5	3	10
	HCFC-142b	CH_2CClF_2	0.5	3	10
LLHCs	Methyl chloroform	CH_3CCl_3	0.1	5	5
	Carbon tetrachloride	CCl_4	1	5	5
	Methyl chloride	CH_3Cl	50	5	10
	Methyl bromide	CH_3Br	0.5	5	10
VSLHs	Dibromomethane	CH_2Br_2	0.01	5	20
	Dichloromethane	CH_2Cl_2	1	5	10
	Chloroform	$CHCl_3$	0.1	5	10
	Trichloroethene	C_2HCl_3	0.01	5	10
	Tetrachloroethene	C_2Cl_4	0.01	5	10
	1,2-Dichloroethane	CH_2ClCH_2Cl	0.1	5	10
	Bromodichloromethane	$CHBrCl_2$	0.01	10	50
	Dibromochloromethane	$CHBr_2Cl$	0.01	5	50
	Bromoform	$CHBr_3$	0.01	10	20
	Methyl Iodide	CH_3I	0.005	5	10
Alkyl Nitrates	Methyl nitrate	CH_3ONO_2	0.02	5	10
	Ethyl nitrate	$C_2H_5ONO_2$	0.02	5	10
	i-propyl nitrate	$C_3H_7ONO_2$	0.02	5	10
	n-propyl nitrate	$C_3H_7ONO_2$	0.02	5	10
	2-butyl nitrate	$C_4H_9ONO_2$	0.02	5	10
	2-pentyl nitrate	$C_5H_{11}ONO_2$	0.02	5	10
	3-pentyl nitrate	$C_5H_{11}ONO_2$	0.02	5	10
	3-methyl 2-butyl nitrate	$C_5H_{11}ONO_2$	0.02	5	10

References

Browell, E. V.: Differential absorption lidar sensing of ozone, Proc. IEEE, 77(3), 419–432, doi:10.1109/5.24128, 1989.

Carroll, M. A., Ridley, B. A., Montzka, D. D., Hubler, G., Walega, J. G. and Norton, R. B.: Measurements of Nitric Oxide and Nitrogen Dioxide During the Mauna Loa Observatory, J. Geophys. Res. Atmos., 97(D10), 10361–10374, 1992.

Colman, J., Swanson, A., Meinardi, S., Sive B., Blake, D. R. and Rowland, F. S.: Description of the analysis of a wide range of volatile organic compounds in whole air samples collected during PEM-Tropics A and B, Anal. Chem., (73), 3723–3731, 2001.

Diskin, G. S., Podolske, J. R., Sachse, G. W. and Slate, T. A.: Open-Path Airborne Tunable Diode Laser Hygrometer, in Proceedings of the Society for Photo-Optical Instrumentation Engineers (SPIE), vol. 4817, edited by A. Fried, pp. 196–204., 2002.

Fenn, A., Browell, V., Butler, F., Grant, B., Kooi, A., Clayton, B., Gregory, L., Newell, E., Dibb, E., Fuelberg, E., Anderson, E., Bandy, R., Blake, R., Bradshaw, D., Heikes, G., Sachse, W., Sandholm, T., Singh, B., Talbot, W. and Thornton, C.: Ozone and Aerosol distributions and air mass characteristics over the South Pacific during the burning season, J. Geophys. Res., 104(13), 16197–16212, doi:0148-0227/99/1999JD900065, 1999.

Homeyer, C. R., Pan, L. L. and Barth, M. C.: Transport from convective overshooting of the extratropical tropopause and the role of large-scale lower stratosphere stability, J. Geophys. Res. Atmos., 119, 2220–2240, doi:10.1002/2013JD020931, 2014.

Podolske, J. R.: Calibration and data retrieval algorithms for the NASA Langley/Ames Diode Laser Hygrometer for the NASA Transport and Chemical Evolution Over the Pacific (TRACE-P) mission, J. Geophys. Res., 108(D20), 8792, doi:10.1029/2002JD003156, 2003.

Rogers, R. R., Hair, J. W., Hostetler, C. A., Ferrare, R. A., Obland, M. D., Cook, A. L., Harper, D. B. and Burton, S. P.: NASA LaRC airborne high spectral resolution lidar aerosol measurements during MILAGRO : observations and validation, Atmos. Chem. Phys., 9, 4811–4826, 2009.

Romine, G. S., Schwartz, C. S., Snyder, C., Anderson, J. L. and Weisman, M. L.: Model Bias in a Continuously Cycled Assimilation System and Is Influence on Convective-Permitting Forecasts, Mon. Weather Rev., 141(4), doi:10.1175/MWR-D-12-00112.1, 2013.

Sachse, G. W., Collins, J. E., Hill, G. F., Wade, L. O., Burney, L. G. and Ritter, J. A.: Airborne tunable diode laser sensor for high-precision concentration and flux measurements of carbon monoxide and methane, in Proceedings of the Society for Photo-Optical Instrumentation Engineers (SPIE), vol. 1433, edited by H. I. Schiff, pp. 157–166., 1991.

Sachse, G. W. and Hill, G. F.: Fast-Response, High-Precision Carbon Monoxide Sensor Using a Tunable Diode Laser Absorption Technique, J. Geophys. Res. Atmos., 92(6), 2071–2081, doi:10.1029/JD092iD02p02071, 1987.

Sive, B. C.: Atmospheric Nonmethane Hydrocarbons: Analytical Methods and Estimated Hydroxyl Radical Concentrations, University of California, Irvine., 1998.

Stohl, A., Forster, C., Frank, A., Seibert, P. and Wotawa, G.: Technical note: The lagrangian particle dispersion model FLEXPART version 6.2, Atmos. Chem. Phys., 5, 2461–2474, doi:10.5194/acp-5-2461-2005, 2005.

3. Development of Chemical Tracers for Convection and STT over the DC3 Study Region

Using known VOC atmospheric lifetimes and measured VOC mixing ratios in the PBL, a tracer for rapid vertical lofting of air from the PBL to the UT/LS by convection was created. In this study, it was found that light hydrocarbons associated with O&NG and vehicular sources were widespread throughout the PBL of the DC3 study regions. In the UT/LS, enhanced levels of these light hydrocarbons were strongly correlated with water vapor, indicating a convective source. On the other hand, decreases in the measured mixing ratios of CFCs, HCFCs, and LLHCs in the UT were used as tracers for STT. These two sets of tracers were used to divide the DC3 WAS merge into many subsets of data corresponding to: the PBL, convective outflow in the UT, convective outflow in the LS (i.e. overshooting tops), STT-influenced air in the troposphere, background UT air, and background LS air. In this section, descriptions and statistical justifications for the use of these tracers are presented, and dilution factors for the rapid vertical lofting of air from the PBL to the UT by deep convection are calculated. Readers are referred to Figure 3.10 at the end of this chapter for a visual representation of the hierarchy of filters used to partition the WAS data merge into sub-sets of data.

3.1. Development of a Tracer for Stratospherically-Influenced Air over the DC3 Study Region

As discussed in Chapter 1 of this work, STT can affect the composition of the troposphere, particularly the UT, and is often associated with deep convection. Thus, development of a tracer for stratospheric influence is necessary for understanding the effects of convection on the composition and chemistry of the UT/LS. Furthermore, development of this

tracer can be used to serve two purposes: to identify STT in the troposphere, and to detect background air in the LS (that is, air in the LS that has little to no influence from TST). To determine which air masses had stratospheric influence, a tracer with a distinct tropospheric vs. stratospheric profile must be used, ideally with little to no altitudinal variation within the troposphere. To accomplish this, an ensemble of eight long-lived halocarbons was used. These halocarbons are listed in Table 3.1.

Table 3.1. Gases used as tracers for stratospheric air. Min, max, average, and 25th percentile values are from the entire DC3 dataset.

Gas	Formula	Lifetime[a] (years)	Measurement Precision (%)	Min (pptv)	Max (pptv)	Avg (pptv)	25th percentile value (pptv)
CFC-11	CCl_3F	45	1	209	250	240.8	239
CFC-12	CCl_2F_2	100	1	238	557	541.3	538
CFC-113	CCl_2FCClF_2	85	1	58.7	81.3	70.3	67.5
H-1211	$CBrClF_2$	16	1	3.31	4.90	4.23	4.17
HCFC-22	CHF_2Cl	11.9	1	216.4	278.9	247.7	242.3
HCFC-141b	CH_3CCl_2F	9.2	5	17.3	31.1	23.6	22.4
HCFC-142b	CH_2CClF_2	17.2	3	19.7	26.5	22.6	22.1
Carbon Tetrachloride	CCl_4	26	3	73.5	97.5	91.7	90.9

As described in Chapter 1 of this dissertation, these long-lived halocarbons have minimal emissions on a global scale, near-zero emissions in the US, and are essentially inert with respect to gas-phase oxidation by OH. The exceptions to this are the HCFCs, which do react with OH. However, the rate at which HCFCs react with OH is significantly slower than the rate at which they photolyze, meaning that they still have a very pronounced gradient across the tropopause. Essentially, photolysis by UV light is the primary sink for all eight of these compounds, and is strongest in the stratosphere and negligible in the troposphere. Furthermore, all eight have sufficiently long atmospheric lifetimes that they are globally well-mixed and have very little variation in tropospheric mixing ratios (Forster and Thompson, 2010; Law and Sturges, 2006; Montzka et al., 2010).

A simple quantitative analysis was used to differentiate "stratospherically-influenced" (abbreviated SI throughout the rest of this thesis) samples from the rest of the WAS merge. To be

labeled as an SI sample, certain criteria had to be met: If, in a given sample, the mixing ratios of at least seven of the eight gases listed in Table 3.1 were in their respective lowest quartile from the entire DC3 data set, that sample was labeled as "SI." In this case, SI samples could be samples collected in the stratosphere, in fresh stratospheric intrusions in the troposphere, or in air masses where a detectable amount stratospheric air has mixed with tropospheric air. Histograms showing the distribution of mixing ratios for each of these eight gases are shown in Figure 3.1, where the lowest quartile cutoff value is indicated with a dashed black line. Of the 1,795 whole air samples collected during DC3, only 96 met these criteria. These samples were collected on 13 of the 18 research flights, which are listed in Table 3.2.

Table 3.2. Flights in which stratospherically-influenced (SI) samples were collected.

Research Flight	Date, Takeoff Time (UTC)	Primary Objective of Flight	Number of SI samples collected
1	5/18, 19:04	Active Convection	18
2	5/19, 16:03	Active Convection	17
3	5/21, 16:00	Active Convection	12
4	5/25, 20:11	Active Convection	3
5	5/26, 19:04	Tracking aged outflow	4
6	5/29, 19:54	Active Convection	3
7	5/30, 18:33	Tracking aged outflow	7
11	6/6, 18:11	Active Convection	2
13	6/11, 16:03	Active Convection	5
14	6/15, 18:32	Active Convection	6
15	6/16, 20:07	Active Convection	3
16	6/17, 19:07	Tracking aged outflow	8
18	6/22, 19:54	Active Convection, Biomass Burning	8

To assess the sensitivity of this result to the criteria selected (that is, the number of SI samples detected by the method described above), the percentile used as a cutoff was allowed to vary. For example if, instead of requiring at least seven gases to have mixing ratios in their lowest 25%, we require at least seven gases to have mixing ratios in their lowest 30%, 194 SI samples are identified. Following this method, the cutoff percentile was allowed to vary by steps of 5% over the range 10-50%, and the number of SI samples identified at each step was counted. These results are shown in Figure 3.2, and suggest that using 25% as a cutoff was the best way to maximize the number of SI samples identified while still remaining fairly conservative - using a cutoff larger than 25% leads to a marked increase in the number of SI samples identified and in the slope of each line segment.

Instrumental drift during the sample analysis stage could potentially produce a false-positive, as a low bias could be applied across all measured compounds in a given sample. To check for this, N_2O, which was measured by another instrument aboard the DC-8 (DOAS-DACOM), was used. Like the gases used in Table 3.1, N_2O also has a primary sink of UV photolysis in the stratosphere, and can be used to identify some stratospheric airmasses (Assonov et al., 2013; Ishijima et al., 2010). Due to instrumental errors, N_2O measurements were not collected for flights 1, 6, and 13-18, and thus N_2O could not be used as a tracer alongside the gases listed in Table 3.1. However, of the SI samples where N_2O data are available, 84% have an N_2O mixing ratio in its lowest quartile from among all DC3 measurements. It should be noted that the average N_2O mixing ratio ($\pm 1\sigma$) from the DC3 WAS merge was 325.3 ± 1.7 pptv, while the lowest quartile threshold was 324.8 pptv.

This SI dataset was further partitioned into two subsets: one corresponding to SI air in the stratosphere (as opposed to overshooting tops or TST-influenced air in the stratosphere), which

will be later used to establish a stratospheric background composition, and one corresponding to stratospherically-influenced air in the troposphere from STT. This was done by comparing the altitude of a given SI sample to the calculated local thermal tropopause height (described in Chapter 2). Since the uncertainty in the calculated tropopause height is ± 500 meters, SI samples collected more than 500 meters above the tropopause were labeled as "Background-LS,", and SI samples collected more than 500 meters below the thermal tropopause were labeled as "STT." These abbreviations for these data sets will be used during the rest of this dissertation.

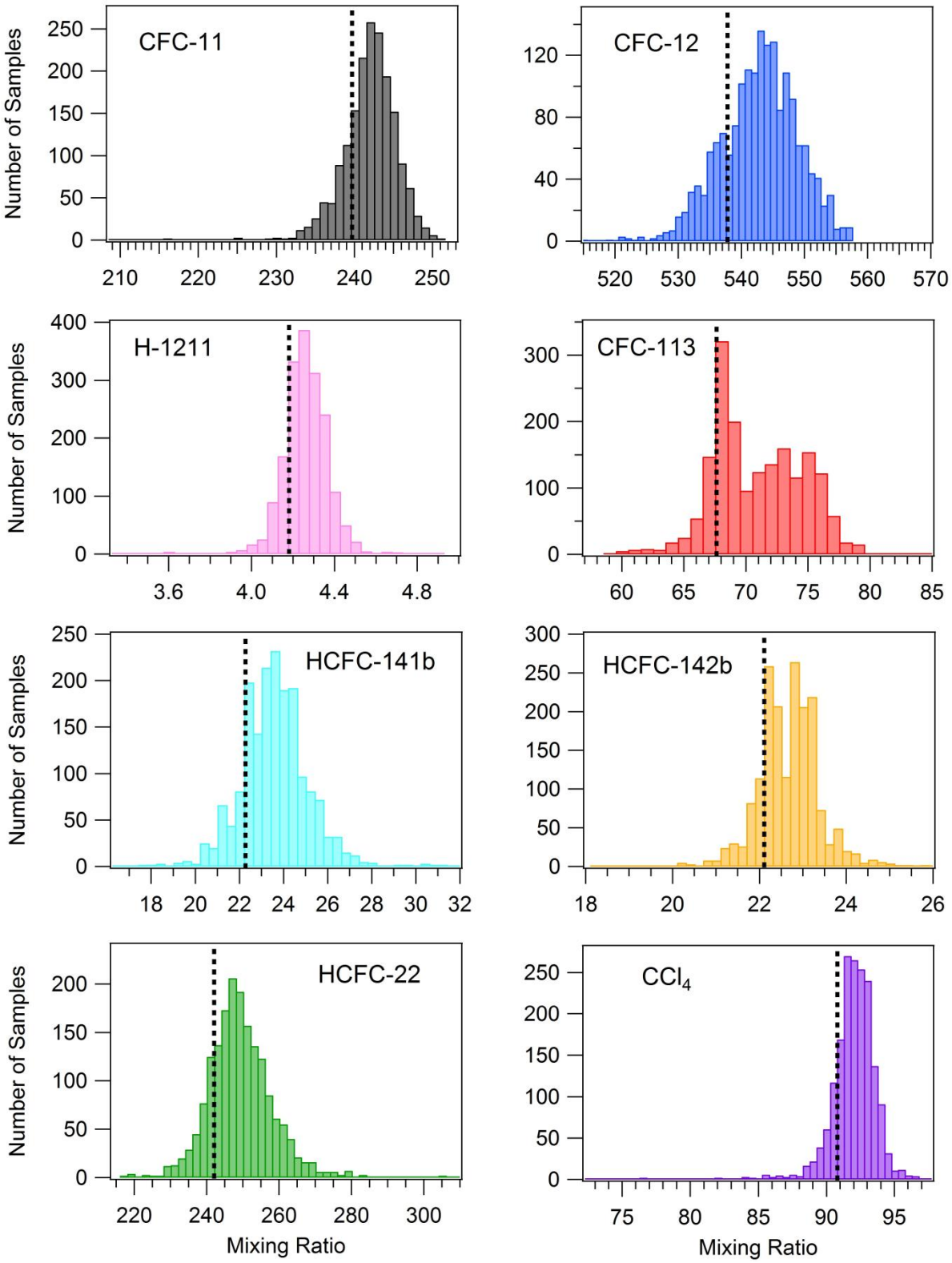

Figure 3.1. Histograms showing the distribution of mixing ratios for the eight long-lived halocarbons chosen as tracers for stratospheric influence. In each panel, the dashed black line represents the 25th percentile mixing ratio for that gas.

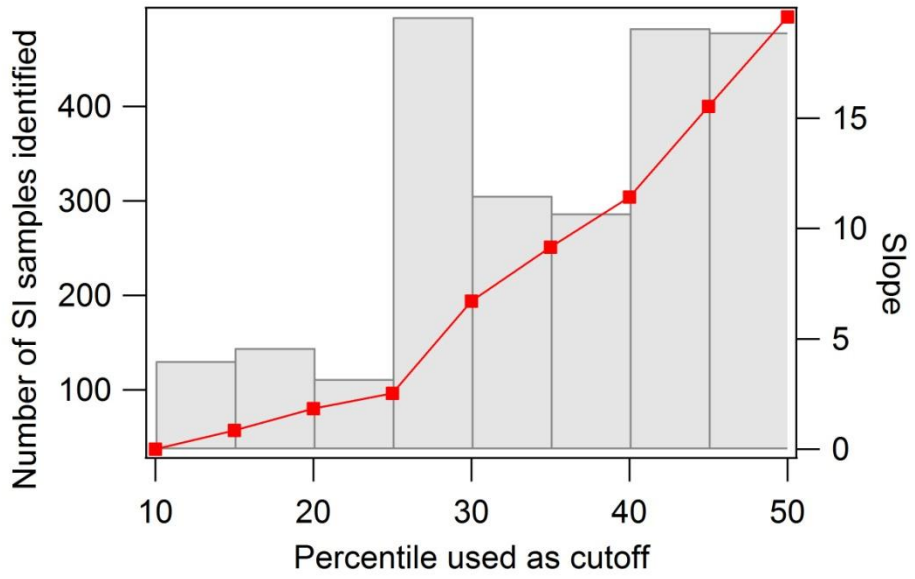

Figure 3.2. Variance in the number of SI samples identified by chosen cutoff percentiles (red squares). The slope of each line segment was calculated and is plotted as gray bars.

3.2. Distribution of VOCs in the PBL of the DC3 Study Region

In order to develop a tracer for the rapid lofting of air from the PBL to the UT/LS by deep convection, the composition of the PBL throughout the DC3 study region must be known. During the summer months, the PBL starts off as a very shallow layer during the morning hours before expanding to depths of 2-3 km (above ground level – AGL) during the day with a peak in the mid-afternoon. As surface temperatures cool down in the late afternoon and evening, the PBL begins to collapse and returns to being a shallow layer after sunset. Since most flights during DC3 focused on sampling the low-altitude inflow region of convection during the mid-to-late afternoon, an upper limit of 2 km (AGL) was chosen to represent PBL depth during DC3. This upper limit was applied to all WAS data, and allowed for isolation of PBL samples from the WAS data merge (Bechara et al., 2010; Bertram et al., 2007). From this PBL subset of data, samples collected in the three primary regions of study (Colorado, Oklahoma, and northern Alabama) were flagged and separated for further analysis. Figure 3.3 shows all PBL samples

collected during DC3, and shows the latitude and longitude bounds used to flag PBL samples collected in the three primary study regions.

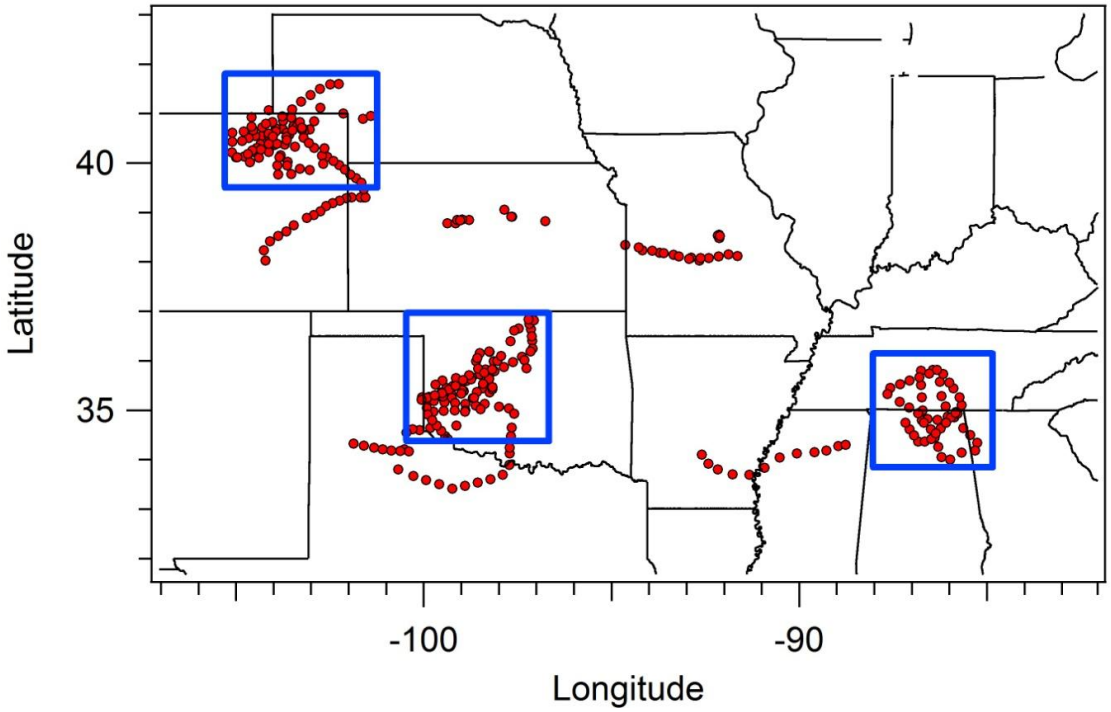

Figure 3.3. All WAS samples collected below 2 km (above ground level) during DC3. Blue boxes indicate the bounds used to identify the three primary study regions.

With PBL samples from each primary study region flagged, the mean, standard deviation, maximum, and minimum mixing ratios of different trace gases were calculated in each primary study region. These values are presented in Table 3.3. In general, Oklahoma had the highest average values of short-chained NMHCs (likely due to O&NG emissions) while northern Alabama had the lowest. It should be noted, however, that while Colorado had lower average values of short-chained NMHCs than Oklahoma, it had max values and relative standard deviations that are higher than Oklahoma, which indicates that the PBL airmasses sampled over Colorado were relatively less homogeneous than Oklahoma. Ratios of *i*-pentane/*n*-pentane for Colorado and Oklahoma (0.95 ± 0.014 and 0.86 ± 0.011, respectively) suggest O&NG as a primary source of short-chained NMHCs in those regions (Gilman et al., 2013; Pétron et al.,

2012). In northern Alabama, this ratio (1.6 ± 0.11) was closer to that of vehicle exhaust (~2), which suggests a strong vehicular source of NMHCs mixed with O&NG emissions from upwind areas (Russo et al., 2010; Ryerson, 2003). This was further corroborated by examining correlations between short-lived NMHCs and CO. For example, northern Alabama had an *n*-butane/CO ratio of 2.3 ± 0.15 and moderate degree of correlation between the two species (r^2 =0.60), while Colorado and Oklahoma had ratios of 22.1 ± 5.5 and 10.5 ± 4.5, respectively, and showed no statistical correlation between the two gases ($r^2 < 0.15$ in both cases). Because NMHCs produced by vehicular emissions will be co-emitted with CO, this ratio should be lower in areas where vehicles are the primary NMHC source, and higher in areas where O&NG operations are the primary NMHC source (and should have little to no correlation) (Simpson et al., 2013). Northern Alabama also had substantially higher mixing ratios of biogenics, particularly isoprene, which had an average value of 270 pptv and a max value of nearly 2 ppbv, while Oklahoma and Colorado had relatively low levels of these gases.

In general, halocarbons did not vary significantly between regions, with a few notable exceptions. For example, C_2Cl_4, which has an industrial source, is highest in northern Alabama, while $CHBr_3$ and CH_3I - which have oceanic and agricultural sources - were lowest in Colorado and highest in Oklahoma (Montzka et al., 2010). Even though average values of most halocarbons do not vary between regions, maximum values of VSLH did show some variation, which suggests the presence of isolated and unevenly-distributed point sources. For example, a maximum mixing ratio of CH_2Cl_2 of 95.2 pptv was measured in Colorado, even though the average for this region is not statistically higher than that of Oklahoma and Alabama.

Table 3.3. Mixing ratio statistics of different trace gases in the PBL of each of the three primary study regions. "LOD" signifies a value that is below the limit of detection for that compound. All gases are measured in pptv unless otherwise noted.

	Colorado				Oklahoma				Northern Alabama			
Compound	avg	st. dev	min	max	avg	st. dev	min	max	avg	st. dev	min	max
Methane (ppbv)	1860	18	1833	1931	1881	33	1821	1959	1890	20	1858	1935
O_3 (ppbv)	54.7	10.9	33.9	76.3	53.1	10.5	31.7	78.7	52.8	14.9	29.9	74.4
CO (ppbv)	115	12	95	154	127	20	92	160	133	16	110	161
Ethane	2806	2186	711	12102	4510	3095	1203	15495	1496	139	1242	1851
Propane	1498	1567	205	8209	2645	2228	305	11440	452	79	326	661
i-Butane	206	256	11	1513	370	279	42	1419	61	23	29	122
n-Butane	534	682	50	3834	937	831	63	4421	119	37	66	252
i-Pentane	160	210	10	1230	262	207	22	1105	68	33	30	224
n-Pentane	157	218	9	1297	268	240	14	1170	45	18	21	112
Hexane	40	60	LOD	384	78	72	3	337	13	7	4	38
Heptane	11	15	LOD	96	24	22	LOD	107	5	4	LOD	20
2,3-Dimethylbutane	4	5	LOD	30	8	20	LOD	144	LOD	n/a	LOD	7
2-Methylpentane	21	33	LOD	214	38	35	LOD	174	7	4	LOD	25
Ethene	50	39	11	205	56	27	7	134	48	23	9	103
Propene	11	22	LOD	181	8	9	LOD	37	4	4	LOD	18
Ethyne	125	53	60	334	146	52	52	257	161	47	98	313
Benzene	28	19	8	104	36	16	11	99	24	6	15	41
Toluene	13	26	LOD	133	18	13	LOD	69	12	10	LOD	50
Ethylbenzene	LOD	n/a	LOD	21	LOD	n/a	LOD	13	LOD	n/a	LOD	32
m+ *p*-Xylene	LOD	n/a	LOD	42	LOD	n/a	LOD	15	LOD	n/a	LOD	84
o-Xylene	LOD	n/a	LOD	16	LOD	n/a	LOD	6	LOD	n/a	LOD	14
3-Ethyltoluene	LOD	n/a	LOD	17	LOD	n/a	LOD	5	LOD	n/a	LOD	11
4-Ethyltoluene	LOD	n/a	LOD	21	LOD	n/a	LOD	5	LOD	n/a	LOD	15
2-Ethyltoluene	LOD	n/a	LOD	19	LOD	n/a	LOD	4	LOD	n/a	LOD	15
1,3,5-Trimethylbenzene	LOD	n/a	LOD	28	LOD	n/a	LOD	6	LOD	n/a	LOD	20
1,2,4-Trimethylbenzene	LOD	n/a	LOD	44	LOD	n/a	LOD	12	LOD	n/a	LOD	31
1,2,3-Trimethylbenzene	LOD	n/a	LOD	41	LOD	n/a	LOD	13	7	18	LOD	84
Isoprene	11	11	LOD	52	46	80	LOD	420	270	347	LOD	1953
α-Pinene	LOD	n/a	LOD	57	LOD	n/a	LOD	22	14	25	LOD	118
β-Pinene	4	14	LOD	99	44	87	LOD	465	53	105	LOD	596
CFC-11	241	4	231	250	243	3	237	248	244	2	239	247
CFC-12	537	6	525	565	541	6	531	549	540	3	531	546
CFC-113	71.7	3.8	66.4	79.3	70.2	3.6	65.5	78.1	69.4	2.6	65.9	73.7
CFC-114	16.9	0.3	16.4	17.7	17.0	0.4	16.4	17.9	17.3	0.3	16.8	17.9
H-1211	4.2	0.1	4.1	4.5	4.3	0.1	4.0	4.4	4.1	0.1	3.9	4.5
H-1301	3.2	0.1	3.0	3.6	3.7	1.1	3.0	7.2	3.2	0.2	3.0	3.6
H-2402	0.5	0.0	0.5	0.6	0.5	0.0	0.5	0.5	0.5	0.0	0.5	0.5
HCFC-22	250.6	10.2	234.8	304.6	253.5	8.7	238.7	287.1	263.3	16.8	248.8	317.0
HCFC-141b	24.0	1.7	20.6	29.2	23.8	1.5	20.0	26.8	24.3	1.4	22.2	31.0

Table 3.3. Continued.

	Colorado				Oklahoma				Alabama			
Compound	avg	st. dev	min	max	avg	st. dev	min	max	avg	st. dev	min	max
HCFC-142b	22.8	0.6	21.2	24.6	22.7	1.3	21.1	33.2	24.0	6.6	21.2	70.2
CH_3CCl_3	5.9	0.2	5.3	6.3	6.0	0.2	5.6	6.5	6.0	0.2	5.6	6.4
CCl_4	91.8	1.3	88.0	97.5	92.2	1.1	89.0	94.2	92.5	1.0	90.3	95.0
CH_3Cl	629	35	578	699	681	54	611	829	657	53	587	753
CH_3Br	9.2	0.8	7.8	12.2	9.9	0.8	8.7	15.1	10.1	4.3	8.5	37.2
CH_2Br_2	0.73	0.12	0.51	1.12	0.89	0.17	0.56	1.37	0.75	0.10	0.58	1.13
CH_2Cl_2	35.1	8.3	19.2	95.2	30.0	6.1	17.3	44.0	33.2	5.7	23.8	47.2
$CHCl_3$	9.9	1.0	8.0	12.4	10.2	1.5	7.4	15.3	10.3	1.0	8.5	13.5
C_2HCl_3	0.23	0.24	0.00	1.77	0.28	0.12	0.11	0.75	0.33	0.17	0.10	0.96
C_2Cl_4	3.6	2.3	2.0	16.0	3.5	1.0	1.7	7.1	4.9	2.6	2.3	15.4
CH_2ClCH_2Cl	10.7	1.9	6.5	17.0	13.3	8.1	4.9	44.0	12.5	1.4	9.0	15.8
$CHBrCl_2$	0.19	0.07	0.12	0.49	0.24	0.05	0.14	0.41	0.24	0.05	0.19	0.43
$CHBr_2Cl$	0.10	0.04	0.05	0.29	0.16	0.05	0.08	0.38	0.12	0.03	0.08	0.23
$CHBr_3$	0.64	0.54	0.21	3.13	1.48	0.87	0.38	5.59	0.99	0.39	0.31	1.68
CH_3I	0.21	0.11	0.10	0.53	0.49	0.16	0.13	0.84	0.45	0.13	0.17	0.60
Methyl nitrate	2.4	0.8	1.2	6.0	2.4	0.4	1.6	3.4	2.7	0.4	1.7	3.7
Ethyl nitrate	3.2	1.5	1.2	8.4	3.7	1.1	1.4	7.3	2.7	0.4	1.8	3.6
i-Propyl nitrate	11.8	8.9	1.7	41.6	15.3	7.2	3.8	39.3	8.2	1.3	5.9	11.7
n-Propyl nitrate	1.4	1.0	0.2	4.4	1.6	0.7	0.4	4.0	0.8	0.1	0.5	1.2
2-Butyl nitrate	21.8	20.8	1.3	96.5	27.4	17.5	5.9	86.2	8.9	1.6	5.7	13.5
2-Pentyl nitrate	11.0	11.4	0.3	51.4	12.6	9.1	2.1	42.7	3.6	1.1	1.1	6.7
3-Pentyl nitrate	6.3	6.1	0.2	27.2	7.3	4.9	1.3	23.4	2.3	0.6	1.0	4.1
3-Methyl-2-butyl nitrate	6.6	6.4	0.4	28.4	8.3	4.9	1.8	23.9	3.2	1.1	2.0	7.7

Even in areas outside of the three primary study regions, hydrocarbons were abundant. The DC-8 sampled the PBL outside of the three primary study regions for a variety of reasons, including: departing and returning to the operations base in Kansas, sampling a biomass burning event in southern Colorado, sampling O&NG infrastructure near Dallas, and coordinating an inter-comparison with a surface monitoring site in Missouri. During these segments, short-chained hydrocarbons were prevalent. For example, the lowest mixing ratios of both propane and *n*-butane outside of the three primary regions were 455 and 103 pptv, respectively, and were higher than the minimum values measured inside the three primary study regions (205 and 50

pptv, respectively). To examine the spatial distribution of short-chained NMHCs, mixing ratios of both propane and *n*-butane in the PBL across the entire DC3 study region were fit to matrices (500 x 500 points), and are displayed in Figure 3.4. It should be noted that, at similar latitudes, background mixing ratios of propane and *n*-butane in the remote pacific are ~60 pptv and ~15 pptv, respectively (Simpson et al., 2012). This suggests that all airmasses in the PBL of the DC3 study region have been influenced to some extent by anthropogenic activity.

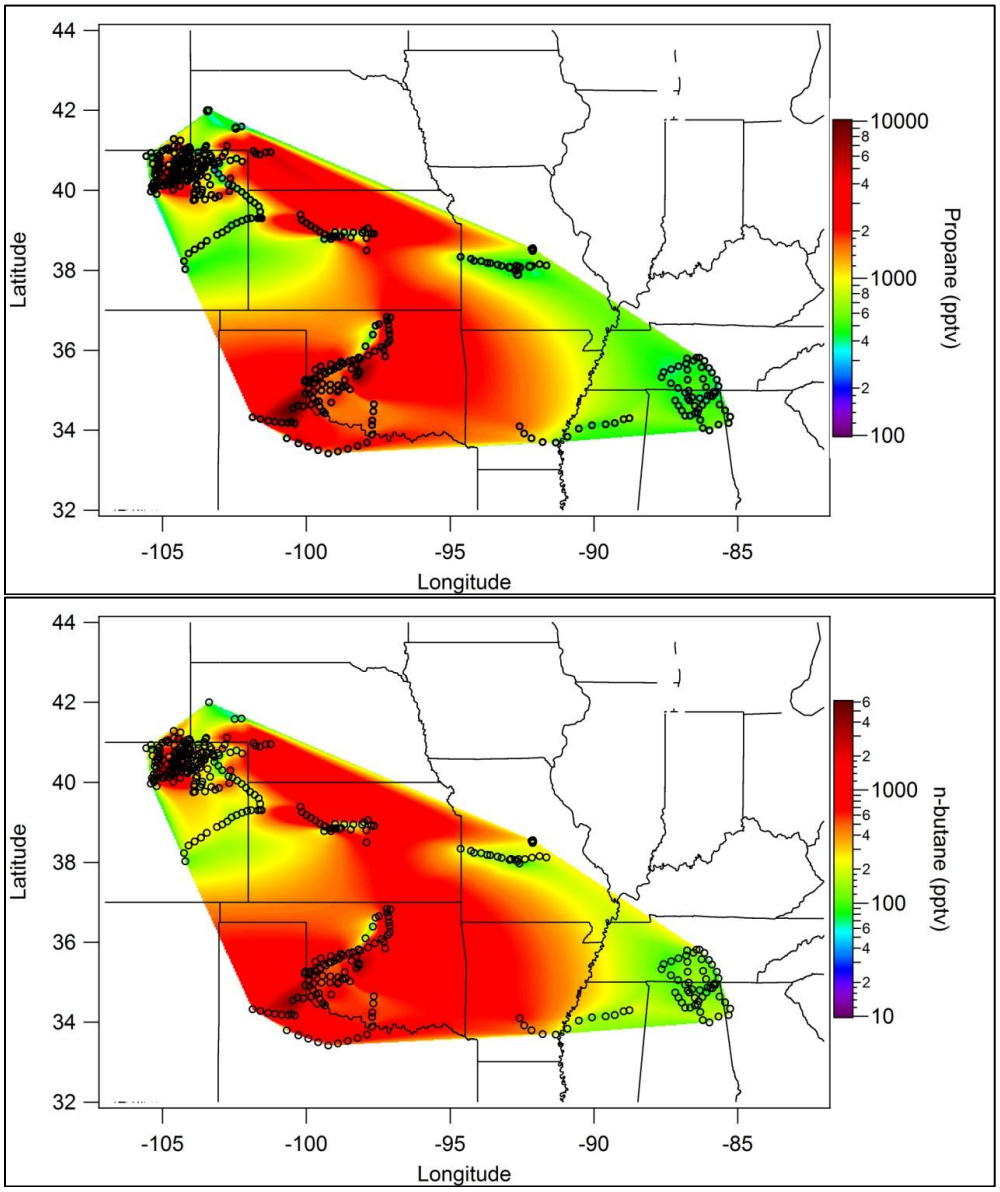

Figure 3.4. Matrix-fitted values of propane (top panel) and *n*-butane (bottom panel) in the PBL over the entire DC3 study region. Mixing ratios in samples (black circles) were fit to 500 x 500 point matrices and are colorized on a logarithmic scale. The lowest mixing ratios of propane and *n*-butane were measured in northern Colorado, and were 205 and 50 pptv, respectively.

3.3. Development of a Tracer for Recently-convected Air in the UT/LS over the DC3 Study Region

To determine whether or not a specific air mass in the UT/LS has been impacted by convective lofting of anthropogenically-influenced air from the PBL, a filter must be applied. An ideal chemical tracer with which to create this filter must have the following characteristics: (1) a significant source that is associated with human activity, (2) widespread distribution over the entire DC3 study region, and (3) a moderate atmospheric lifetime (long enough so we can detect both fresh pollution and pollution that is a few days old, but short enough to still have a strong vertical gradient in the absence of convection). CO (lifetime ~ 2 months) is a useful marker for anthropogenic activity, but its long lifetime leads to an observable seasonal trend even in background UT air, and thus it is not necessarily a good marker of individual convective events (González Abad et al., 2011; Homeyer et al., 2014; Huang et al., 2012). As discussed in section 3.2, light hydrocarbons from O&NG processes were ubiquitous throughout the PBL of the DC3 study region. Of these light hydrocarbons, propane and *n*-butane make ideal choices for anthropogenic filters. With lifetimes of ~11 days and ~5 days respectively, enhancements in propane and *n*-butane will still be measured several days downwind of sources, which results in their widespread distribution in Figure 3.4. Hydrocarbons with shorter lifetimes will tend to be more concentrated around point sources, and less homogeneous throughout the region. Because the average transport time from the PBL to the UT in the absence of convection is ~1-2 months (Apel et al., 2012), both propane and *n*-butane will also have low mixing ratios in the UT in the absence of convection. Thus, if a deep convective storm were to occur anywhere in the DC3 study region, air from the PBL with propane values greater than 205 pptv and *n*-butane levels greater than 50 pptv (the minimum values measured for each gas in the PBL – see section 3.2) would be lofted into the UT/LS, and a strong enhancement in these two gases would be observed

in association with elevated levels of water vapor. This concept is highlighted in Figure 3.5, where at a given altitude in the UT/LS, high propane and *n*-butane mixing ratios are always associated with high levels of water vapor, indicating recent vertical transport by deep convection (Aschmann et al., 2009; Barth et al., 2014; Bechara et al., 2010). For comparison, CO is also shown in Figure 3.5, and many high- altitude samples with low levels of water vapor are shown to have relatively high levels of CO (over 125 ppbv in some cases). This indicates that elevated levels of CO can be present in the UT/LS even in the absence of recent convection, making it a non-ideal tracer for this application. For reference, the lowest CO mixing ratio measured in the PBL over the DC3 study region was 90 ppbv, and the average CO mixing ratio from all PBL samples was 125 ppbv.

Thus, a filter was constructed whereby samples with both a propane mixing ratio exceeding 205 pptv and an *n*-butane mixing ratio exceeding 50 pptv were labeled as anthropogenically influenced. Samples collected in convective outflow were further flagged as those that were anthropogenically-influenced and were collected above 8 km. In total, 421 samples met these criteria to be labeled as convective outflow. Sensitivity tests showed that loosening these requirements (for example, using 160 pptv of propane and 40 pptv of *n*-butane as cutoffs) resulted in large increases in the number of samples that were flagged as "anthropogenically-influenced," while making these requirements more conservative resulted in a small increase in the number of samples that were flagged. In effect, nearly all anthropogenically-influenced samples had propane mixing ratios much greater than 205 pptv and *n*-butane mixing ratios much greater than 50 pptv. In Figure 3.6, altitude profiles of propane and *n*-butane from all DC3 data are shown, and the 421 samples that were flagged as convective outflow are marked with black dots.

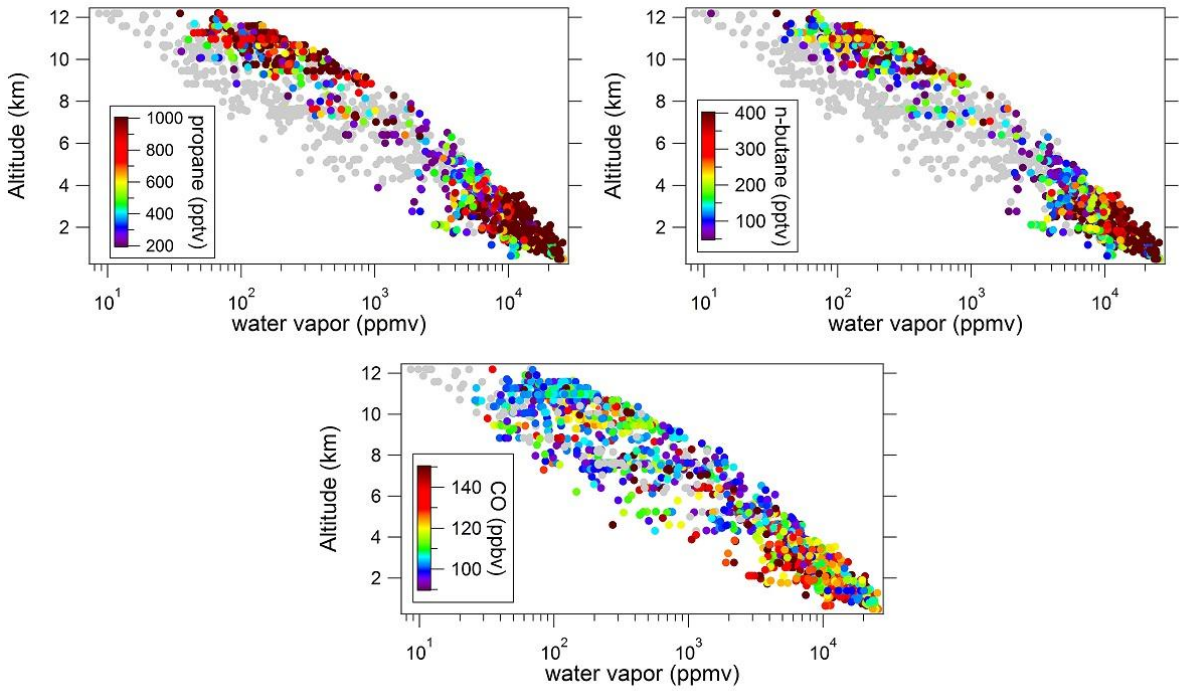

Figure 3.5. Altitude profiles from the DC3 WAS data merge. In the upper left panel, samples are colored by propane mixing ratio, where values below 205 pptv are colored gray. In the upper right panel, samples are colored by *n*-butane mixing ratio, where values below 50 pptv are colored gray. In the bottom panel, samples are colored by CO mixing ratio, where values below 90 ppbv are colored gray.

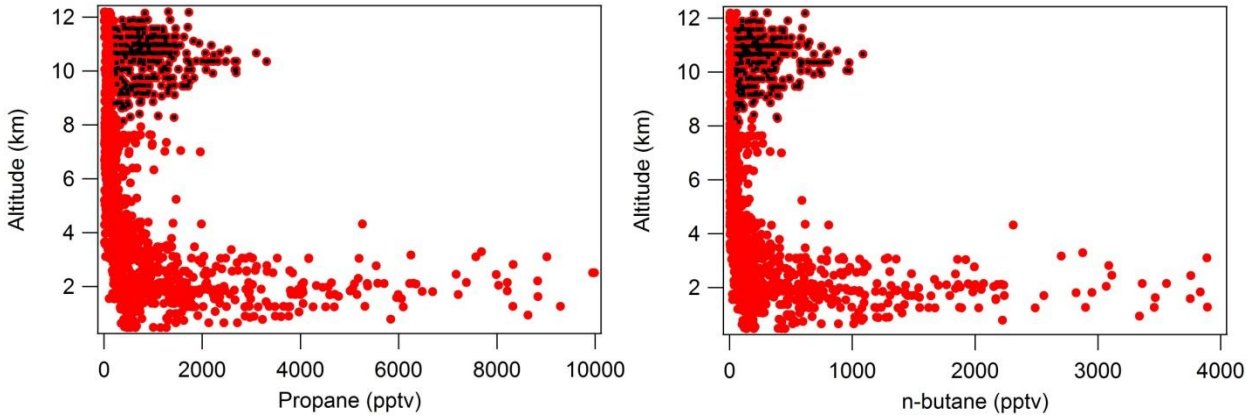

Figure 3.6. Vertical profiles of propane and *n*-butane (red). Samples that were flagged as convective outflow are marked with black dots.

As discussed in Chapter 1 of this dissertation, the radiative and ozone-depleting properties of an airmass can change depending on whether that airmass is above or below the tropopause. For this reason, these convective outflow samples were further partitioned into two

data sets that represent convective outflow that was sampled in the UT and convective outflow that was sampled in the LS. These two data sets are described in sections 3.3.1 and 3.3.2.

3.3.1. Convective Outflow in the UT over the DC3 Study Region

To differentiate between convective outflow samples collected in the UT (i.e. below the tropopause) from those collected in the LS (i.e. above the tropopause), the location of each sample relative to the local tropopause height was used as a filter. As discussed in chapter 2 of this work, tropopause heights were calculated by interpolating the GFS modeled thermal tropopause height in space and time relative to the position of the DC-8 at a given time. Because the uncertainty in the calculated tropopause height is ± 500 meters, convective outflow samples that were located more than 500 meters below the tropopause height were flagged as "UT convective outflow samples." Of the original 421 samples that met the criteria to be labeled as convective outflow, 413 were located in the UT. This subset of data will hereafter be referred to as "Outflow-UT." A histogram showing the number of Outflow-UT samples collected during each flight is shown in Figure 3.7, and a table showing the average, standard deviation, minimum, and maximum mixing ratios of measured trace gases is shown in Table 3.4.

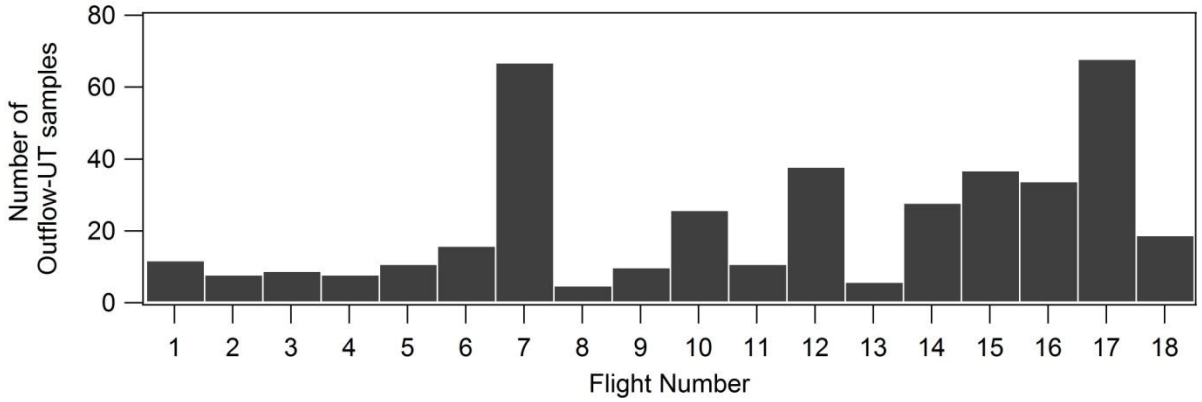

Figure 3.7. Histogram showing the number of Outflow-UT samples collected during each research flight.

Table 3.4. Trace gas mixing ratio averages, standard deviations, minimum values, and maximum values for all samples collected in convective outflow in the UT. All mixing ratios are pptv unless otherwise noted.

Compound	avg	st. dev	min	max
Methane (ppbv)	1847	15	1808	1893
O_3 (ppbv)	84	20	49	167
CO (ppbv)	109	17	76	284
Ethane	2109	790	488	5444
Propane	951	512	207	3307
i-Butane	110	66	19	394
n-Butane	274	177	50	1086
i-Pentane	62	50	3	323
n-Pentane	63	50	5	292
Hexane	14	15	LOD	107
Heptane	4	6	LOD	79
2,3-Dimethylbutane	LOD	n/a	LOD	24
2-Methylpentane	6	8	LOD	44
Ethene	30	147	LOD	1932
Propene	6	47	LOD	634
Ethyne	129	59	66	700
Benzene	21	26	LOD	289
Toluene	4	15	LOD	168
Ethylbenzene	LOD	n/a	LOD	21
m+ *p*-Xylene	LOD	n/a	LOD	30
o-Xylene	LOD	n/a	LOD	11
3-Ethyltoluene	LOD	n/a	LOD	8
4-Ethyltoluene	LOD	n/a	LOD	5
2-Ethyltoluene	LOD	n/a	LOD	5
1,3,5-Trimethylbenzene	LOD	n/a	LOD	19
1,2,4-Trimethylbenzene	LOD	n/a	LOD	19
1,2,3-Trimethylbenzene	LOD	n/a	LOD	17
Isoprene	LOD	n/a	LOD	23
α-Pinene	LOD	n/a	LOD	22
β-Pinene	LOD	n/a	LOD	41
CFC-11	240	3	229	249
CFC-12	542	7	526	559
CFC-113	70.2	4.1	58.7	78.7
CFC-114	17.0	0.3	16.3	17.8
H-1211	4.2	0.1	4.1	4.5
H-1301	3.2	0.1	2.9	4.4
H-2402	0.5	0.0	0.5	0.6
HCFC-22	248.6	6.5	231.0	269.0
HCFC-141b	23.2	1.6	21.4	26.4
HCFC-142b	22.4	1.2	20.9	24.4

Table 3.4. Continued.

Compound	avg	st. dev	min	max
CH_3CCl_3	5.8	0.2	5.3	6.4
CCl_4	91.8	1.4	87.0	96.0
CH_3Cl	674	46	601	1226
CH_3Br	9.2	2.9	7.6	66.6
CH_2Br_2	0.78	0.16	0.41	1.69
CH_2Cl_2	32.9	4.4	20.1	64.0
$CHCl_3$	9.5	1.1	6.9	17.6
C_2HCl_3	0.13	0.12	0.00	0.67
C_2Cl_4	2.6	0.6	1.3	5.8
CH_2ClCH_2Cl	10.9	2.7	3.9	30.5
$CHBrCl_2$	0.20	0.05	0.11	0.43
$CHBr_2Cl$	0.11	0.06	0.03	0.95
$CHBr_3$	0.91	0.73	0.02	4.07
CH_3I	0.14	0.13	LOD	1.10
Methyl nitrate	2.2	0.7	1.0	8.1
Ethyl nitrate	2.5	0.7	1.0	5.4
i-Propyl nitrate	8.8	4.2	1.3	26.3
n-Propyl nitrate	0.7	0.5	LOD	2.4
2-Butyl nitrate	11.0	9.1	0.1	59.4
2-Pentyl nitrate	3.4	3.7	LOD	16.9
3-Pentyl nitrate	2.4	2.3	LOD	10.4
3-Methyl-2-butyl nitrate	2.4	2.4	LOD	11.2

While the Outflow-UT dataset might be useful for evaluating the overall effects of convection on the composition of the UT, it is not useful making comparisons to the composition of the PBL. Even though active convection was only sampled in the three primary study regions, convective outflow could extend hundreds of miles downwind from the core of a storm. This is particularly relevant for flights where the primary objective was to sample aged outflow from a storm that occurred the previous day. For example, in research flight 5 the DC-8 sampled a storm over central Oklahoma, and in research flight 6 the DC-8 sampled the aged outflow from that storm 24 hours later, which was then located over Virginia. At this point, the aged outflow would have mixed with background UT air, and will appear significantly different in composition from both its location of origin (i.e. the PBL in Oklahoma) and the PBL directly beneath it.

Furthermore, the histogram presented in Figure 3.7 suggests that the Outflow-UT data might be unequally weighted towards aged outflow (i.e. the high number of Outflow-UT samples collected during research flights 7, 12, and 16), which will have a different composition than fresh outflow. Because of this, the Outflow-UT data cannot be directly compared to the PBL data provided in Table 3.3.

In order to compare convective outflow composition to PBL composition and calculate dilution factors for the rapid vertical transport of air by convection, the Outflow-UT dataset was further partitioned. To calculate dilution factors, convective outflow from an active storm must be directly compared to air sampled in the PBL below the same storm. To accomplish this, the Outflow-UT dataset was further partitioned so that samples collected during active convection (i.e. Outflow-UT samples collected during research flights 1, 2, 3, 4, 6, 9, 10, 11, 13, 14, 15, and 18) were separated from aged convective outflow samples (i.e. Outflow-UT samples collected during research flights 5, 7, 12, and 16). These subsets are hereafter referred to as Active-Outflow-UT and Aged-Outflow-UT, respectively.

3.3.2. Convective Outflow in the LS

Convective outflow that was sampled in the LS was separated from the convective outflow dataset by comparing sample altitude to the local tropopause height. Convective outflow samples in the LS were defined as convective outflow samples that were collected above the local thermal tropopause, and are hereafter referred to as "Outflow-LS." In total, five samples met these criteria. These samples were collected from 500 meters above the tropopause (the uncertainty in the calculated tropopause height) up to 1.1 km above the tropopause, and were collected during research flights 2 (three samples), 3 (one sample), and 7 (one sample). The

average, standard deviation, minimum, and maximum mixing ratios for the Outflow-LS dataset are provided in Table 3.5.

Table 3.5. Trace gas mixing ratio averages, standard deviations, minimum values, and maximum values for all samples collected in convective outflow in the LS. All mixing ratios are pptv unless otherwise noted.

Compound	avg	st. dev	min	max
Methane (ppbv)	1841	45	1799	1889
O_3 (ppbv)	161	78	78	230
CO (ppbv)	98	24	76	123
Ethane	2448	1141	820	3259
Propane	1210	698	206	1706
i-Butane	157	96	46	238
n-Butane	384	258	51	594
i-Pentane	93	85	9	168
n-Pentane	92	82	13	164
Hexane	31	20	8	44
Heptane	10	5	4	13
2,3-Dimethylbutane	LOD	n/a	LOD	4
2-Methylpentane	18	1	17	19
Ethene	38	16	19	48
Propene	11		11	11
Ethyne	121	35	74	158
Benzene	19	11	6	26
Toluene	9	2	7	10
Ethylbenzene	LOD	n/a	LOD	LOD
m+ *p*-Xylene	LOD	n/a	LOD	LOD
o-Xylene	LOD	n/a	LOD	LOD
3-Ethyltoluene	LOD	n/a	LOD	LOD
4-Ethyltoluene	LOD	n/a	LOD	LOD
2-Ethyltoluene	LOD	n/a	LOD	LOD
1,3,5-Trimethylbenzene	LOD	n/a	LOD	LOD
1,2,4-Trimethylbenzene	LOD	n/a	LOD	LOD
1,2,3-Trimethylbenzene	LOD	n/a	LOD	LOD
Isoprene	17	1	LOD	18
α-Pinene	LOD	n/a	LOD	LOD
β-Pinene	LOD	n/a	LOD	LOD
CFC-11	233	6	224	238
CFC-12	529	6	520	532
CFC-113	66.2	1.8	63.6	67.4
CFC-114	16.7	0.4	16.4	17.1
H-1211	3.9	0.1	3.7	4.0
H-1301	3.6	0.7	2.9	4.3

Table 3.5. Continued.

Compound	avg	st. dev	min	max
H-2402	0.5	0.0	0.5	0.5
HCFC-22	235.3	4.6	229.5	239.8
HCFC-141b	21.8	0.9	21.1	23.0
HCFC-142b	21.5	0.3	21.1	21.8
CH_3CCl_3	5.9	0.1	5.8	6.0
CCl_4	87.6	2.8	83.6	89.9
CH_3Cl	618	22	597	643
CH_3Br	8.6	0.4	8.2	9.0
CH_2Br_2	0.56	0.22	0.27	0.77
CH_2Cl_2	27.6	7.9	19.0	35.4
$CHCl_3$	7.9	2.3	5.9	10.6
C_2HCl_3	0.17	0.20	LOD	0.37
C_2Cl_4	2.3	1.4	0.9	3.7
CH_2ClCH_2Cl	6.73	4.66	2.18	11.96
$CHBrCl_2$	0.17	0.08	0.08	0.24
$CHBr_2Cl$	0.07	0.04	0.03	0.11
$CHBr_3$	0.38	0.31	LOD	0.65
CH_3I	0.17	0.16	0.03	0.35
Methyl nitrate	1.6	0.7	1.0	2.4
Ethyl nitrate	1.9	1.6	0.3	3.5
i-Propyl nitrate	7.2	6.4	0.8	12.8
n-Propyl nitrate	0.7	0.7	0.1	1.3
2-Butyl nitrate	13.0	10.9	0.4	19.5
2-Pentyl nitrate	7.6	0.2	7.5	7.8
3-Pentyl nitrate	4.6	0.2	4.5	4.7
3-Methyl-2-butyl nitrate	5.8	0.3	5.5	6.0

In general, the Outflow-LS dataset has average NMHC mixing ratios that are higher than those the Outflow-UT dataset. This is an unexpected result, as convective outflow above the tropopause would have been diluted with not only clean air from the UT, but also very clean air from the LS, while convective outflow below the tropopause would only be diluted with clean air from the UT. Two factors may contribute to this result: 1) the statistically-small Outflow-LS dataset is biased towards active convection (only one sample was collected in aged outflow), while the Outflow-UT dataset is biased towards aged outflow, and 2) the Outflow-LS dataset is

biased towards fresh outflow collected during research flight 2 (3/5 of Outflow-LS samples were collected then), which occurred over the NMHC-rich Oklahoma region. It should be noted that combustion tracers, such as CO and ethyne, are lower in the Outflow-LS dataset, which also reflects these geographic biases. On the other hand, the average O_3 mixing ratio in the Outflow-LS dataset is significantly higher than the Outflow-UT dataset (92% higher). This is due to dilution of convective outflow with O_3-rich air from the LS.

3.4. Composition of the Background UT and LS

In order to fully quantify the effects of convection on the composition of the UT/LS, it is necessary to quantify the background composition of the UT/LS. Background UT samples were separated from the WAS merge by identifying samples that were collected between 8 km and the local tropopause height that were neither influenced by convective outflow or STT. 196 samples met these criteria, and will be referred to as the Background-UT dataset throughout the rest of this dissertation. These Background-UT samples were collected on every flight except research flight 17. A histogram showing the distribution of these Background-UT samples among the 18 research flights is shown in Figure 3.8, and the average, standard deviation, minimum, and maximum mixing ratios for the Background-UT dataset are shown in Table 3.6. Background LS samples were separated from the WAS merge by identifying samples that were collected above the local tropopause, met the criteria to be labeled as "SI", and had no influence from convective outflow. 11 samples met these criteria, and will be referred to as the Background-LS dataset throughout the rest of this dissertation. These Background-LS samples were collected on three flights: research flight 2 (three samples), research flight 3 (seven samples), and research flight 7

(one sample). The average, standard deviation, minimum, and maximum mixing ratios for the Background-LS dataset are shown in

Table 3.7. It should be noted that these three flights are the same flights in which convective outflow was sampled in the LS as well.

Table 3.6. Trace gas mixing ratio averages, standard deviations, minimum values, and maximum values for all Background-UT samples. All mixing ratios are pptv unless otherwise noted.

Compound	avg	st. dev	min	max
Methane (ppbv)	1829	15	1786	1868
O_3 (ppbv)	88	25	40	160
CO (ppbv)	99	19	57	188
Ethane	771	183	316	1334
Propane	112	59	8	297
i-Butane	10	8	LOD	40
n-Butane	18	13	LOD	49
i-Pentane	4	4	LOD	17
n-Pentane	4	4	LOD	18
Hexane	LOD	n/a	LOD	9
Heptane	LOD	n/a	LOD	13
2,3-Dimethylbutane	LOD	n/a	LOD	LOD
2-Methylpentane	LOD	n/a	LOD	LOD
Ethene	9	25	LOD	294
Propene	LOD	n/a	LOD	21
Ethyne	137	79	35	686
Benzene	11	13	LOD	104
Toluene	LOD	n/a	LOD	18
Ethylbenzene	LOD	n/a	LOD	LOD
m+ *p*-Xylene	LOD	n/a	LOD	LOD
o-Xylene	LOD	n/a	LOD	LOD
3-Ethyltoluene	LOD	n/a	LOD	LOD
4-Ethyltoluene	LOD	n/a	LOD	LOD
2-Ethyltoluene	LOD	n/a	LOD	LOD
1,3,5-Trimethylbenzene	LOD	n/a	LOD	LOD
1,2,4-Trimethylbenzene	LOD	n/a	LOD	LOD
1,2,3-Trimethylbenzene	LOD	n/a	LOD	LOD
Isoprene	LOD	n/a	LOD	LOD
α-Pinene	LOD	n/a	LOD	12

β-Pinene	LOD	n/a	LOD	90
CFC-11	241	3	228	258
CFC-12	543	6	525	575
CFC-113	70.3	3.4	63.7	77.5
CFC-114	17.0	0.3	16.3	18.0
H-1211	4.3	0.1	4.0	4.5

Table 3.7. Continued.

Compound	avg	st. dev	min	max
H-1301	3.2	0.1	2.4	3.7
H-2402	0.5	0.0	0.5	0.5
HCFC-22	242.7	6.4	227.0	261.6
HCFC-141b	22.7	1.2	18.5	26.9
HCFC-142b	22.3	0.6	20.8	24.1
CH_3CCl_3	5.8	0.2	4.9	7.0
CCl_4	91.0	1.8	84.4	98.4
CH_3Cl	666	56	574	1137
CH_3Br	8.8	0.8	7.2	14.9
CH_2Br_2	0.60	0.18	0.04	0.93
CH_2Cl_2	33.7	8.5	8.6	69.7
$CHCl_3$	9.1	1.8	2.1	16.1
C_2HCl_3	0.1	0.1	LOD	0.4
C_2Cl_4	2.0	0.7	0.1	4.0
CH_2ClCH_2Cl	10.42	5.20	0.17	31.70
$CHBrCl_2$	0.15	0.04	0.04	0.28
$CHBr_2Cl$	0.07	0.04	LOD	0.26
$CHBr_3$	0.38	0.40	LOD	2.92
CH_3I	0.05	0.06	LOD	0.44
Methyl nitrate	2.0	1.0	0.4	7.3
Ethyl nitrate	1.2	0.5	0.1	2.9
i-Propyl nitrate	2.1	1.6	0.1	14.6
n-Propyl nitrate	0.2	0.1	LOD	0.8
2-Butyl nitrate	1.1	1.3	LOD	7.9
2-Pentyl nitrate	0.3	0.4	LOD	2.1
3-Pentyl nitrate	0.2	0.3	LOD	1.9
3-Methyl-2-butyl nitrate	0.2	0.3	LOD	1.7

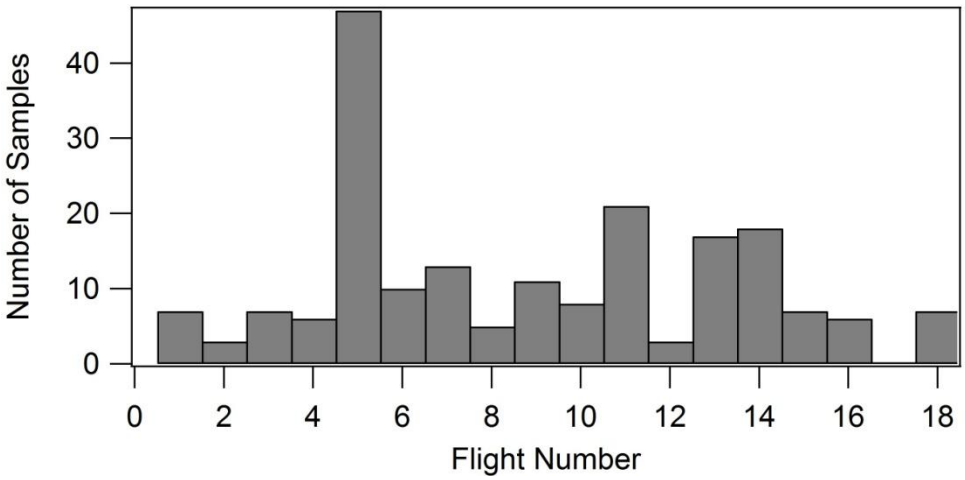

Figure 3.8. Histogram showing the distribution of Background-UT samples among the 18 research flights.

Table 3.7. Trace gas mixing ratio averages, standard deviations, minimum values, and maximum values for all Background-LS data. All mixing ratios are pptv unless otherwise noted.

Compound	avg	st. dev	min	max
Methane (ppbv)	1753	32	1703	1791
O_3 (ppbv)	337	71	231	432
CO (ppbv)	46	14	23	69
Ethane	334	149	115	582
Propane	28	21	LOD	67
i-Butane	LOD	n/a	LOD	5
n-Butane	LOD	n/a	LOD	7
i-Pentane	LOD	n/a	LOD	LOD
n-Pentane	LOD	n/a	LOD	LOD
Hexane	LOD	n/a	LOD	LOD
Heptane	LOD	n/a	LOD	LOD
2,3-Dimethylbutane	LOD	n/a	LOD	LOD
2-Methylpentane	LOD	n/a	LOD	LOD
Ethene	4.8	8.3	LOD	21
Propene	LOD	n/a	LOD	LOD
Ethyne	39	20	9	70
Benzene	LOD	n/a	LOD	LOD
Toluene	LOD	n/a	LOD	LOD
Ethylbenzene	LOD	n/a	LOD	LOD
m+ *p*-Xylene	LOD	n/a	LOD	LOD
o-Xylene	LOD	n/a	LOD	LOD
3-Ethyltoluene	LOD	n/a	LOD	LOD
4-Ethyltoluene	LOD	n/a	LOD	LOD
2-Ethyltoluene	LOD	n/a	LOD	LOD
1,3,5-Trimethylbenzene	LOD	n/a	LOD	LOD

Table 3.7. Continued.

Compound	avg	st. dev	min	max
1,2,4-Trimethylbenzene	LOD	n/a	LOD	LOD
1,2,3-Trimethylbenzene	LOD	n/a	LOD	LOD
Isoprene	LOD	n/a	LOD	LOD
α-Pinene	LOD	n/a	LOD	LOD
β-Pinene	LOD	n/a	LOD	LOD
CFC-11	222	7	209	232
CFC-12	517	8	508	532
CFC-113	63.8	1.9	59.4	66.5
CFC-114	16.3	0.3	15.9	16.7
H-1211	3.7	0.2	3.3	4.0
H-1301	3.0	0.2	2.5	3.3
H-2402	0.5	0.0	0.4	0.5
HCFC-22	221.3	6.1	216.4	235.0
HCFC-141b	19.2	1.3	17.3	20.8
HCFC-142b	20.5	0.6	19.7	21.5
CH_3CCl_3	5.5	0.4	4.5	6.0
CCl_4	82.5	3.5	73.5	86.3
CH_3Cl	568	34	509	633
CH_3Br	7.6	0.6	6.6	8.4
CH_2Br_2	0.22	0.15	0.05	0.61
CH_2Cl_2	13.3	5.8	4.9	21.0
$CHCl_3$	4.5	1.8	1.8	7.1
C_2HCl_3	LOD	n/a	LOD	LOD
C_2Cl_4	0.4	0.3	0.1	0.8
CH_2ClCH_2Cl	1.24	1.23	0.16	4.07
$CHBrCl_2$	0.05	0.03	0.02	0.11
$CHBr_2Cl$	0.03	0.01	0.02	0.05
$CHBr_3$	0.06	0.05	LOD	0.18
CH_3I	0.02	0.01	0.01	0.03
Methyl nitrate	0.5	0.2	0.2	0.9
Ethyl nitrate	0.2	0.1	0.1	0.5
i-Propyl nitrate	0.3	0.2	0.1	1.0
n-Propyl nitrate	0.03	0.08	LOD	0.03
2-Butyl nitrate	0.1	0.1	LOD	0.11
2-Pentyl nitrate	0.03	0.1	LOD	0.2
3-Pentyl nitrate	0.03	0.1	LOD	0.2
3-Methyl-2-butyl nitrate	LOD	n/a	LOD	LOD

When comparing the Outflow-UT dataset to the Background-UT dataset, gases with relatively short lifetimes are enhanced in the Outflow-UT dataset. Short-chained hydrocarbons associated with O&NG emissions were enhanced by a factor of 5-12, while long-chained hydrocarbons and other short-lived NMHCs – which were below our limit of detection in the UT background – were present in detectable amounts. These short-lived NMHCs tended to have greater variability in the outflow than longer-lived NMHCs, likely due to their highly-variable distribution in the PBL of the study region. When comparing the Outflow-LS dataset to the Background-LS dataset, nearly all gases are enhanced in the Outflow-LS dataset, with O_3 being the sole exception that is higher in the Background-LS dataset. When comparing the Background-UT dataset to the Background-LS dataset, nearly all gases are enhanced in the Background-UT dataset, with O_3 again being the sole exception. These results match theoretically expected results that predict enhancements in trace gases in convective outflow relative to background levels, and lower trace gas mixing ratios in the LS than in the UT.

3.5. Calculation of Dilution Factors

To obtain a quantitative understanding of vertical transport of trace gases from the PBL to the UT by deep convection, the fractional changes of selected VOCs were calculated. In effect, the fractional change (*f*) represents the fraction of PBL air that is present in convective outflow, and was calculated using equation 3.1 (Bertram et al., 2007):

$$f_i = \frac{(\bar{x}_{i,Active-Outflow-UT} - \bar{x}_{i,Backround-UT})}{(\bar{x}_{i,PBL} - \bar{x}_{i,Background-UT})} \qquad (3.1)$$

In this equation, $\bar{x}_i$ indicates the mean value of a given VOC in a given dataset (i.e. Active-Outflow-UT, Background-UT, or PBL) during a given research flight (*i*). In this way, the fractional change of each chosen VOC can be calculated for each relevant research flight. Eight

relevant VOCs were chosen for this analysis (lifetime given in parenthesis): $CHCl_3$ (~160 days), CH_2Cl_2 (~140 days), CO (~60 days), ethane (45 days), propane (11 days), benzene (10 days), *i*-butane (5.5 days), and *n*-butane (5 days). These VOCs were chosen for two reasons: 1) they have very low Henry's law constants and thus will not be removed by wet deposition or rain-out during the transport process, and 2) they have ideal atmospheric lifetimes for this work. Gases with longer lifetimes (such as methane) will not have a significant vertical profile, and thus will likely only be marginally affected by dilution. Gases with very short lifetimes (such as isoprene) have sporadic surface sources and are not evenly-distributed horizontally in the boundary layer. This means that the distribution of these short-lived gases will be very non-homogeneous in convective outflow, leading to unacceptably large uncertainties in the calculated fractional change. Fractional changes for these eight VOCs were calculated during research flights where sampling active convection was the primary goal (i.e. research flights 1, 2, 3, 4, 6, 8, 9, 10, 11, 13, 14, 15, and 18). For flights where statistically inadequate sampling of the outflow, UT background, or PBL (i.e. $n < 3$ for any of the preceding data sets – which occurred during research flights 8 and 15), fractional changes were not calculated.

From these per-flight fractional changes, the overall mean fractional change for all active convection during DC3 was calculated by averaging the fractional changes for each VOC over the entire range of research flights. This is presented in

Figure **3.9**, where the average fractional change of each VOC during the entire DC3 field campaign is plotted against the atmospheric lifetime (in days) for that VOC. In general, the uncertainty in the average fractional change decreases with increasing VOC lifetime. This is because shorter-lived VOCs tend to be less evenly distributed in the PBL, which introduces higher uncertainties to the mean PBL and mean convective outflow values. Two notable

exceptions are CH_2Cl_2 and $CHCl_3$, which have the longest atmospheric lifetimes of the eight chosen VOCs, but the highest calculated uncertainty in their fractional changes. The cause for this uncertainty in halocarbon mixing ratios in the UT is thoroughly investigated in Chapter 5 of this dissertation. The two VOCs with the smallest uncertainty in f were ethane and CO. Using ethane as a tracer for dilution during active convection, we report a fractional change of 0.64 ± 0.21, while using CO yields a fractional change of 0.60 ± 0.15. These ranges fall within the ranges reported in the literature. Bechara et al. (2010) measured the fraction of boundary layer air contained in convective outflow in West Africa to be 0.40 ± 0.15, while Cohan et al. (1999) measured this fraction to be 0.32 – 0.64 over the tropical West Pacific. The discrepancy between our measured value and literature values is likely due to the latitudes at which storms were sampled. In the midlatitudes, where DC3 took place, the tropopause height is generally ~12 km, and the majority of convective outflow during DC3 was sampled around ~10 km. Over West Africa and the West Pacific, the tropopause height is much higher, and Bechara et al. (2010) typically sampled convective outflow around ~12 km. Typically, midlatitude convective storms also have faster updraft velocities than tropical convective storms (Barth et al., 2014). Thus, it can be inferred that the vertical transport time in midlatitude convective storms may be shorter than that in tropical convective storms, resulting in less dilution via mixing with background air from the free troposphere. Because most DC3 storms were sampled around sunset and negligible photochemistry happens in the dark centers of convective storms, a photochemical clock (that is, a model that looks at the time-dependant relationship between two sets of gases – usually a reactant/product pair or two reactants with dissimilar lifetimes) cannot be used to estimate vertical transport times. Since there were only 5 outflow samples collected above the tropopause (over three flights), a similar analysis for the Outflow-LS dataset cannot be performed.

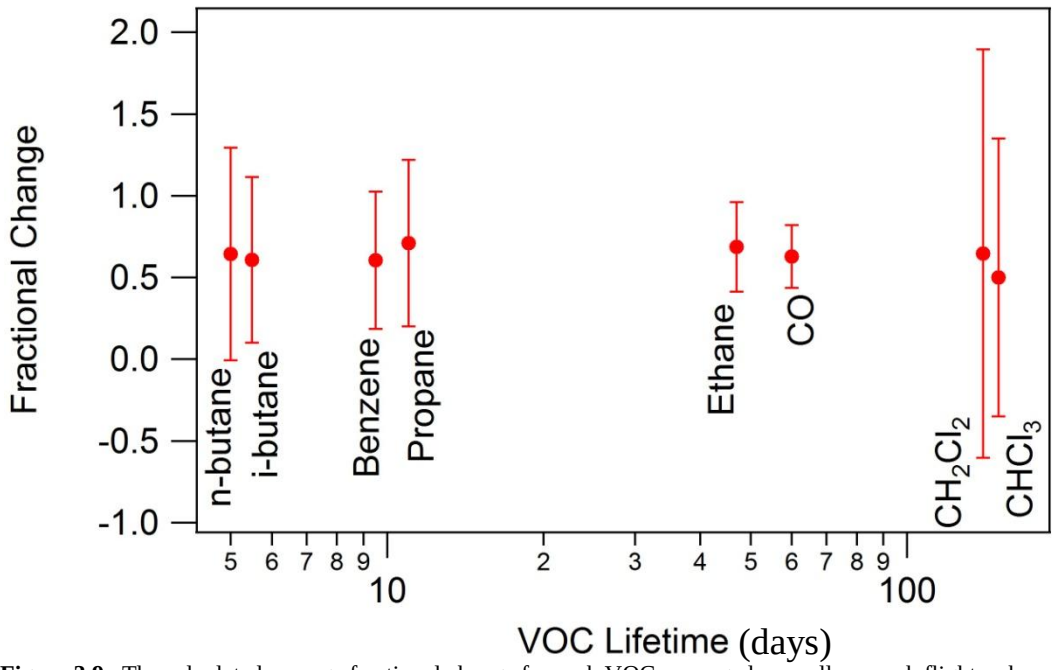

Figure 3.9. The calculated average fractional change for each VOC, averaged over all research flights where active convection was adequately sampled during DC3. This is plotted versus the atmospheric lifetime of each VOC (given in days), which are given in Chapter 1 of this dissertation.

3.5. Summary

The WAS data merge from the DC3 field project was divided into several subsets of data. Stratospherically-influened (SI) samples were identified using a suite of long-lived halocarbons, which are listed in Table 3.1. This SI subset of data was used to identify background LS samples and samples in the troposphere that were affected by recent STT. Samples collected below 2 km were identified as PBL samples. Throughout the PBL, short-chained hydrocarbons such as propane and *n*-butane were ubiquitous. These two short-chained hydrocarbons were then used as tracers for convective outflow in the UT/LS. This convective outflow dataset was divided further using the tropopause as a filter, and two datasets pertaining to outflow in the LS and outflow in the UT were created. From the Outflow-UT dataset, two more subsets of data were created, which include fresh outflow (the Active-Outflow-UT dataset) and aged outflow (the Aged-Outflow-UT dataset). Background UT air was defined as any air sampled between 8 km and the

tropopause that was unaffected by convection or STT. This hierarchy of datasets is shown in Figure 3.10. It should be noted that the SI dataset is not completely unique – SI samples may be present in the Outflow-LS dataset (i.e. outflow that has mixed with stratospheric air above the tropopause), the Outflow-UT dataset (i.e. convective outflow that has mixed with a stratospheric intrusion in the UT), and in the PBL dataset. Lastly, the Active-Outflow-UT, Background-UT, and PBL datasets were used to calculate the fraction of PBL air that is present in the outflow of active storms. In this work, eight different VOCs were evaluated as tracers for this type of dilution, and it was found that ethane and CO resulted in the lowest uncertainties. Using ethane as a tracer, we calculated the fraction (f) of PBL air in active outflow to be 0.64 ± 0.21, while using CO as a tracer yielded an f of 0.60 ± 0.15.

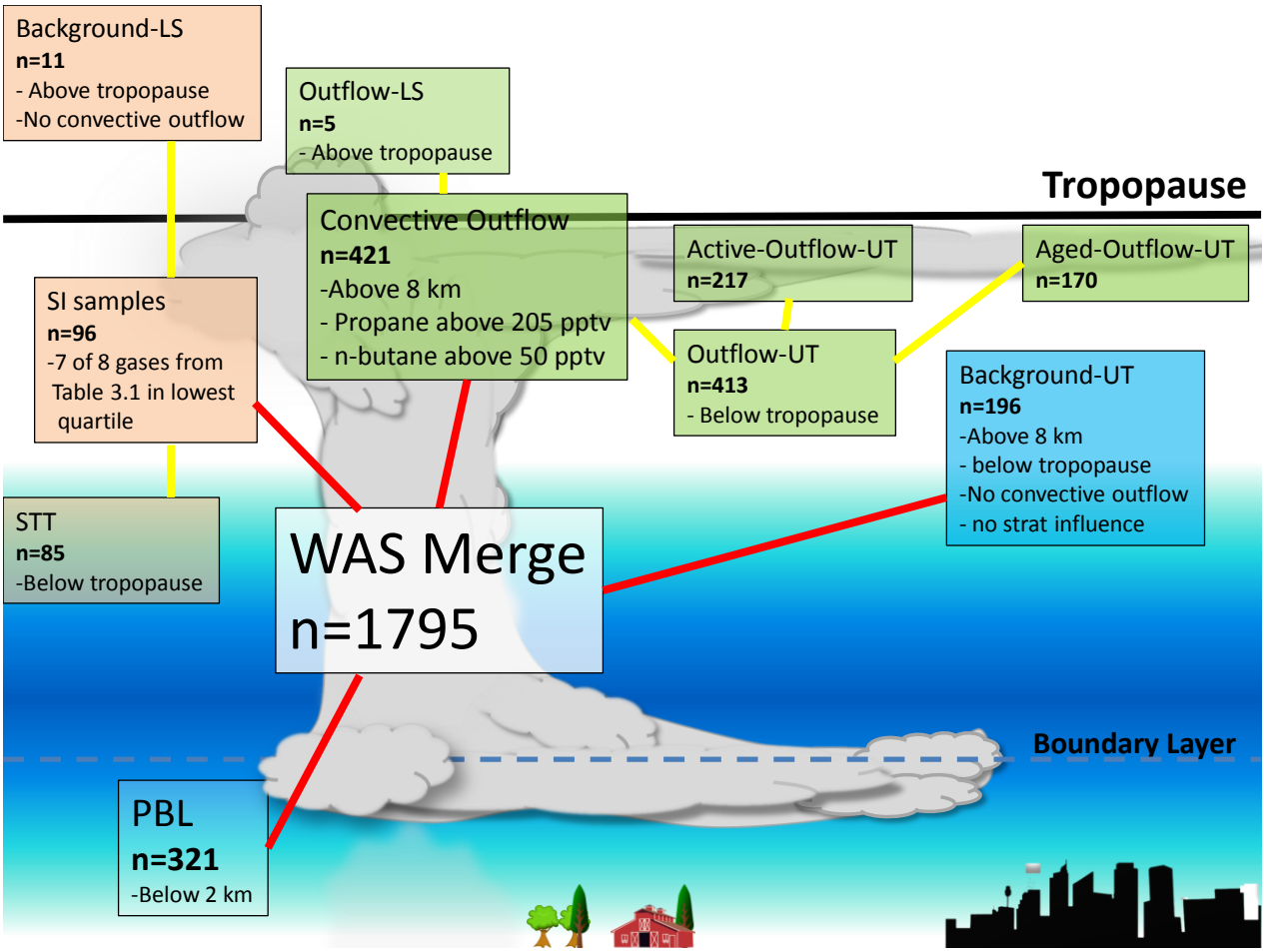

Figure 3.10. A diagram of a convective storm cloud, overlain with the datasets that were described in this chapter and descriptions of the filters used to create each dataset. Red lines indicate primary divisions from the WAS data merge, and yellow lines indicate secondary divisions into smaller datasets.

References

Apel, E. C., Olson, J. R., Crawford, J. H., Hornbrook, R. S., Hills, a. J., Cantrell, C. a., Emmons, L. K., Knapp, D. J., Hall, S., Mauldin III, R. L., Weinheimer, a. J., Fried, a., Blake, D. R., Crounse, J. D., Clair, J. M. St., Wennberg, P. O., Diskin, G. S., Fuelberg, H. E., Wisthaler, a., Mikoviny, T., Brune, W. and Riemer, D. D.: Impact of the deep convection of isoprene and other reactive trace species on radicals and ozone in the upper troposphere, Atmos. Chem. Phys., 12(2), 1135–1150, doi:10.5194/acp-12-1135-2012, 2012.

Aschmann, J., Sinnhuber, B. M., Atlas, E. L. and Schauffler, S. M.: Modeling the transport of very short-lived substances into the tropical upper troposphere and lower stratosphere, Atmos. Chem. Phys., 9(5), 18511–18543, doi:10.5194/acpd-9-18511-2009, 2009.

Assonov, S. S., Brenninkmeijer, C. a. M., Schuck, T. and Umezawa, T.: N2O as a tracer of mixing stratospheric and tropospheric air based on CARIBIC data with applications for CO2, Atmos. Environ., 79, 769–779, doi:10.1016/j.atmosenv.2013.07.035, 2013.

Barth, M. C., Cantrell, C. a., Brune, W. H., Rutledge, S. a., Crawford, J. H., Huntrieser, H., Carey, L. D., MacGorman, D., Weisman, M., Pickering, K. E., Bruning, E., Anderson, B., Apel, E., Biggerstaff, M., Campos, T., Campuzano-Jost, P., Cohen, R., Crounse, J., Day, D. a., Diskin, G., Flocke, F., Fried, A., Garland, C., Heikes, B., Honomichl, S., Hornbrook, R., Huey, L. G., Jimenez, J. L., Lang, T., Lichtenstern, M., Mikoviny, T., Nault, B., O'Sullivan, D., Pan, L. L., Peischl, J., Pollack, I., Richter, D., Riemer, D., Ryerson, T., Schlager, H., Clair, J. St., Walega, J., Weibring, P., Weinheimer, A., Wennberg, P., Wisthaler, A., Wooldridge, P. J. and Ziegler, C.: The Deep Convective Clouds and Chemistry (DC3) Field Campaign, Bull. Am. Meteorol. Soc., 141211133556008, doi:10.1175/BAMS-D-13-00290.1, 2014.

Bechara, J., Borbon, a., Jambert, C., Colomb, a. and Perros, P. E.: Evidence of the impact of deep convection on reactive Volatile Organic Compounds in the upper tropical troposphere during the AMMA experiment in West Africa, Atmos. Chem. Phys., 10(21), 10321–10334, doi:10.5194/acp-10-10321-2010, 2010.

Bertram, T. H., Perring, A. E., Wooldridge, P. J., Crounse, J. D., Kwan, A. J., Wennberg, P. O., Scheuer, E., Dibb, J., Avery, M., Sachse, G., Vay, S. a, Crawford, J. H., McNaughton, C. S., Clarke, A., Pickering, K. E., Fuelberg, H., Huey, G., Blake, D. R., Singh, H. B., Hall, S. R., Shetter, R. E., Fried, A., Heikes, B. G. and Cohen, R. C.: Direct measurements of the convective recycling of the upper troposphere., Science, 315(5813), 816–20, doi:10.1126/science.1134548, 2007.

Cohan, D. S., Schultz, M. G., Jacob, D. J., Heies, B. G. and Blake, D. R.: Convective injection and photochemical decay of peroxides in teh tropical upper troposphere: Methyl iodide as a tracer of marine convection., J. Geophys. Res. Atmos., (104),1184-1199, 1999.

Forster, P. M. and Thompson, D. W. J.: Stratospheric Changes and Climate, in Scientific Assesment of Ozone Depletion: 2010, World Meteorological Organization, Geneva, Switzerland., 2010.

Gilman, J. B., Lerner, B. M., Kuster, W. C. and de Gouw, J. a: Source signature of volatile organic compounds from oil and natural gas operations in northeastern Colorado., Environ. Sci. Technol., 47(3), 1297–305, doi:10.1021/es304119a, 2013.

González Abad, G., Allen, N. D. C., Bernath, P. F., Boone, C. D., McLeod, S. D., Manney, G. L., Toon, G. C., Carouge, C., Wang, Y., Wu, S., Barkley, M. P., Palmer, P. I., Xiao, Y. and Fu, T. M.: Ethane, ethyne and carbon monoxide concentrations in the upper troposphere and lower stratosphere from ACE and GEOS-Chem: a comparison study, Atmos. Chem. Phys., 11(18), 9927–9941, doi:10.5194/acp-11-9927-2011, 2011.

Homeyer, C. R., Pan, L. L., Dorsi, S. W., Avallone, L. M., Weinheimer, A. J., Brien, A. S. O., Digangi, J. P., Zondlo, M. A., Ryerson, T. B., Diskin, G. S. and Campos, T. L.: Convective transport of water vapor into the lower stratosphere observed during double-tropopause events, , 1–18, doi:10.1002/2014JD021485.Received, 2014.

Huang, L., Fu, R., Jiang, J. H., Wright, J. S. and Luo, M.: Geographic and seasonal distributions of CO transport pathways and their roles in determining CO centers in the upper troposphere, Atmos. Chem. Phys., 12(10), 4683–4698, doi:10.5194/acp-12-4683-2012, 2012.

Ishijima, K., Patra, P. K., Takigawa, M., Machida, T., Matsueda, H., Sawa, Y., Steele, L. P., Krummel, P. B., Langenfelds, R. L., Aoki, S. and Nakazawa, T.: Stratospheric influence on the seasonal cycle of nitrous oxide in the troposphere as deduced from aircraft observations and model simulations, J. Geophys. Res., 115(D20), D20308, doi:10.1029/2009JD013322, 2010.

Law, K. S. and Sturges, W. T.: Halogenated Very Short-Lived Substances, in Scientific Assesment of Ozone Depletion: 2006, World Meteorological Organization, Geneva, Switzerland., 2006.

Montzka, S. A., Reimann, S., Engel, A., Kruger, K., O'Doherty, S. and Sturges, W. T.: Ozone Depleting Substances (ODSs) and Related Chemicals, in Scientific Assesment of Ozone Depletion: 2010, World Meteorological Organization, Geneva, Switzerland., 2010.

Pétron, G., Frost, G., Miller, B. R., Hirsch, A. I., Montzka, S. a., Karion, A., Trainer, M., Sweeney, C., Andrews, A. E., Miller, L., Kofler, J., Bar-Ilan, A., Dlugokencky, E. J., Patrick, L., Moore, C. T., Ryerson, T. B., Siso, C., Kolodzey, W., Lang, P. M., Conway, T., Novelli, P., Masarie, K., Hall, B., Guenther, D., Kitzis, D., Miller, J., Welsh, D., Wolfe, D., Neff, W. and Tans, P.: Hydrocarbon emissions characterization in the Colorado Front Range: A pilot study, J. Geophys. Res., 117(D4), D04304, doi:10.1029/2011JD016360, 2012.

Russo, R. S., Zhou, Y., White, M. L., Mao, H., Talbot, R. and Sive, B. C.: Multi-year (2004-2008) record of nonmethane hydrocarbons and halocarbons in New England: Seasonal variations

and regional sources, Atmos. Chem. Phys., 10, 4909–4929, doi:10.5194/acp-10-4909-2010, 2010.

Ryerson, T. B.: on tropospheric ozone formation in Houston, Texas, J. Geophys. Res., 108(x), 1–24, doi:10.1029/2002JD003070, 2003.

Simpson, I. J., Andersen, M. P. S., Meinardi, S., Bruhwiler, L., Blake, N. J., Helmig, D., Rowland, F. S. and Blake, D. R.: Long-term decline of global atmospheric ethane concentrations and implications for methane, Nature, 488(7412), 490–494, doi:10.1038/nature11342, 2012.

Simpson, I. J., Marrero, J. E., Batterman, S., Meinardi, S., Barletta, B. and Blake, D. R.: Air quality in the Industrial Heartland of Alberta, Canada and potential impacts on human health, Atmos. Environ., 81, 702–709, doi:10.1016/j.atmosenv.2013.09.017, 2013.

4. Evidence of Mixing Between Polluted Convective Outflow and Stratospheric Air in the Upper Troposphere during DC3

Note: Portions of this chapter are adapted from the following paper: Schroeder, J. R., L. L. Pan, T. Ryerson, G. Diskin, J. Hair, S. Meinardi, I. Simpson, B. Barletta, N. Blake, and D. R. Blake (2014), Evidence of mixing between polluted convective outflow and stratospheric air in the upper troposphere during DC3, *J. Geophys. Res. Atmos.*, 119(19), 11477–11491, doi: 10.1002/2014JD022109.

The WAS data merge and its derived subsets of data (described in Chapter 3) were used to investigate interactions and mixing between stratospheric intrusions and tropospheric air mases. A large number of stratospherically-influenced samples were found to have reduced levels of O_3 and elevated levels of CO (both relative to background stratospheric air); indicative of mixing with anthropogenically-influenced air. Using *n*-butane and propane as tracers of anthropogenically-influenced air, it is shown that this type of mixing was present both at low altitudes and in the upper troposphere (UT). At low altitudes, this mixing resulted in O_3 enhancements consistent with those reported at surface sites during deep stratospheric intrusions, while in the UT, two case studies were performed to identify the process by which this mixing occurs. In the first case study, stratospheric air was found to be mixed with aged outflow from a convective storm, while in the second case study, stratospheric air was found to have mixed with outflow from an active storm occurring in the vicinity of a stratospheric intrusion. From these analyses, it was concluded that deep convective events may facilitate the mixing between stratospheric air and polluted boundary layer air in the UT. Throughout the entire DC3 study region, this mixing was found to be prevalent: 72% of all samples that involve stratosphere-troposphere mixing show influence of polluted air. Applying a simple chemical kinetics analysis to these data, it is shown that the instantaneous production of OH in these mixed stratospheric-polluted air masses was 11 ± 8 times higher than that of stratospheric air, and 4.2 ± 1.8 times higher than that of background upper tropospheric air.

4.1 Spatial Distribution of Tropospheric Samples Influenced by STT

The spatial distribution of tropospheric samples that were influenced by STT was investigated using the STT dataset (see Chapter 3 for description). During DC3, active convective storms were only sampled in three primary study regions where ground imaging was available (Chapter 2). As a result, sample locations were biased towards these three regions, and this bias is also reflected in the geographic distribution of STT samples, as seen in Figure 4.1. Of the 85 STT samples, 40 were collected in the first three research flights, and the majority of low-altitude STT samples were collected near the CO/WY/NE border. These trends were expected, as previous modeling and field work suggest that STT over the US peaks in spring and grows weaker into summer, with most deep STT events occurring over the western US (Kuang et al., 2012; Langford et al., 2012; Lefohn et al., 2011; Lin et al., 2012; Stohl et al., 2003).

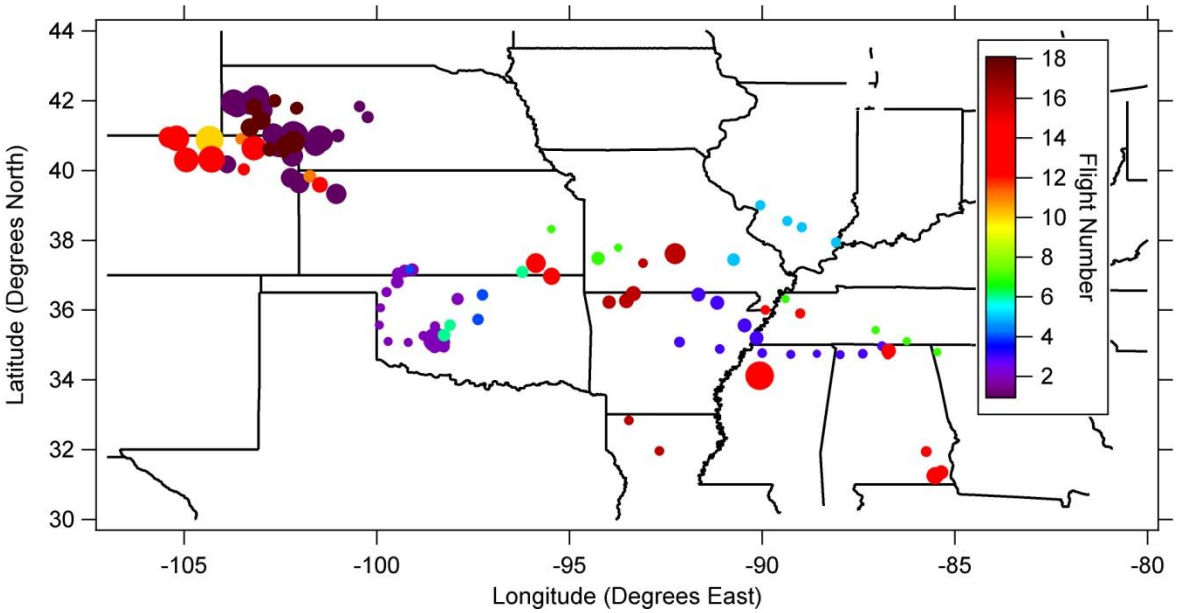

Figure 4.1. Location of WAS samples determined to have stratospheric influence. Samples are colorized by flight number, and sized by altitude with the largest dots being closest to ground level. Sample altitudes ranged from 0.8 km to 12.5 km. The three primary areas of study are circled.

During deep STT events, O_3 levels at the surface may exceed national ambient air quality standards set by the US EPA. To investigate the resulting O_3 enhancements caused by STT, the

SI dataset was compared to a modified version of the WAS merge, which was created by removing all SI samples from the WAS data merge. O_3 values in these non-SI samples were fit to a line using a least squares linear regression (with altitude as the independent variable), and the 95% confidence interval for this line was calculated. It is important to note that, in this analysis, non-SI samples could include both polluted and non-polluted tropospheric air, and therefore represents the regional troposphere as a whole rather than a true "background" (that is, the background defined here is not a true global background). At each altitude in which an SI sample was collected, the percent enhancement of O_3 (that is, enhancement in O_3 in SI samples relative to the non-SI tropospheric O_3 background) was calculated. Figure 4. 2 shows the percent enhancement of O_3 for each SI sample. As expected, O_3 enhancements are largest at high altitudes where the DC-8 would have flown through fresh, undiluted stratospheric intrusions, or in the stratosphere itself. At low altitudes, modest enhancements were still observed. For example, the lowest-altitude SI sample (819 meters above ground level) had an O_3 mixing ratio of 70 ppbv - an enhancement of 29 ± 11% over modeled tropospheric levels. This falls within the range observed by Langford (2012) - who observed a 23% O_3 enhancement at surface sites in southern California during a deep stratospheric intrusion - and Lin (2012) who observed surface O_3 levels of 60-75 ppbv across the western US during deep stratospheric intrusions. This sample, however, shows significant tropospheric character as evidenced by its CO mixing ratio of 130 ppbv. In fact, the majority of SI samples with modest O_3 enhancements (< 30% above background) have CO mixing ratios greater than 100 ppbv.

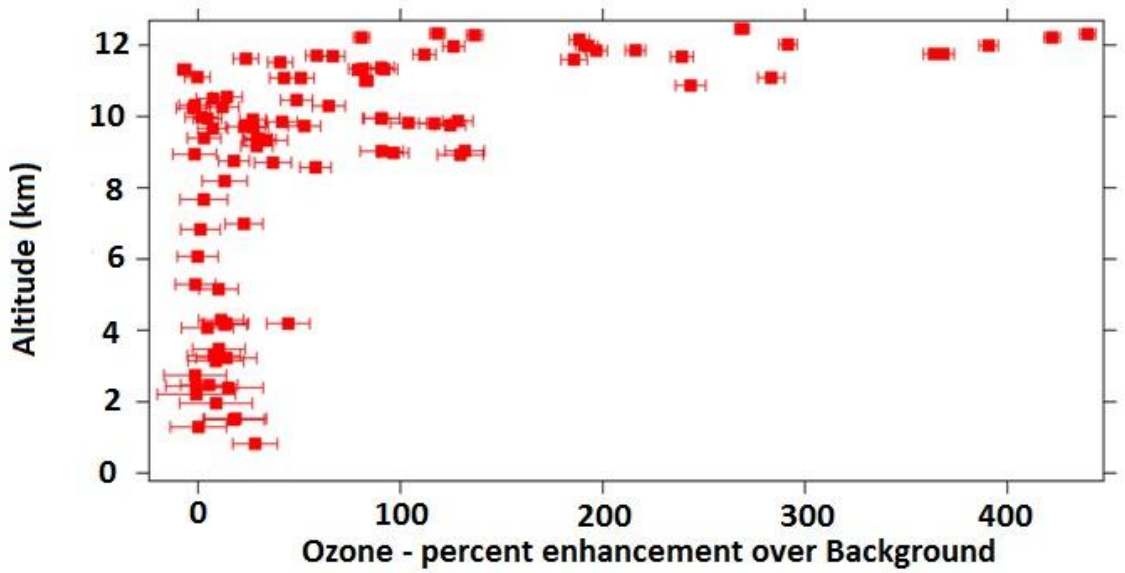

Figure 4. 2. Percent enhancement of O_3 in SI samples compared to the modeled background.

4.2. O_3 vs. CO Tracer Space, and its Implications on Stratosphere-Troposphere Mixing

A plot of O_3 vs CO for the WAS data merge shows two distinct branches: a positive slope indicating photochemical production of O_3 (that is, of tropospheric origin), and a negative slope indicating stratospheric origin (Figure 4.3). The area where these two lines intersect may be the result of mixing between tropospheric and stratospheric air. Here, this mixing was observed at many altitudes – both near and well below the tropopause. Pan (2004) showed that the extra-tropical tropopause is best represented as a layer, rather than a surface. This layer can be as much as 3 km thick, and is centered on the thermal tropopause. In this work, the thermal tropopause is used as the upper boundary of the troposphere (described in Chapter 2). When the SI samples are highlighted in this tracer space (red dots in Figure 4.3), it can be seen that some samples that are well within the tropospheric branch have stratospheric influence. These SI samples would go un-detected by conventional analysis, as O_3 has either been significantly diluted or chemically removed, and polluted air has masked the pristine stratospheric nature. However, these well-

mixed samples may be important from a local chemistry standpoint, as will be described in section 4.6.

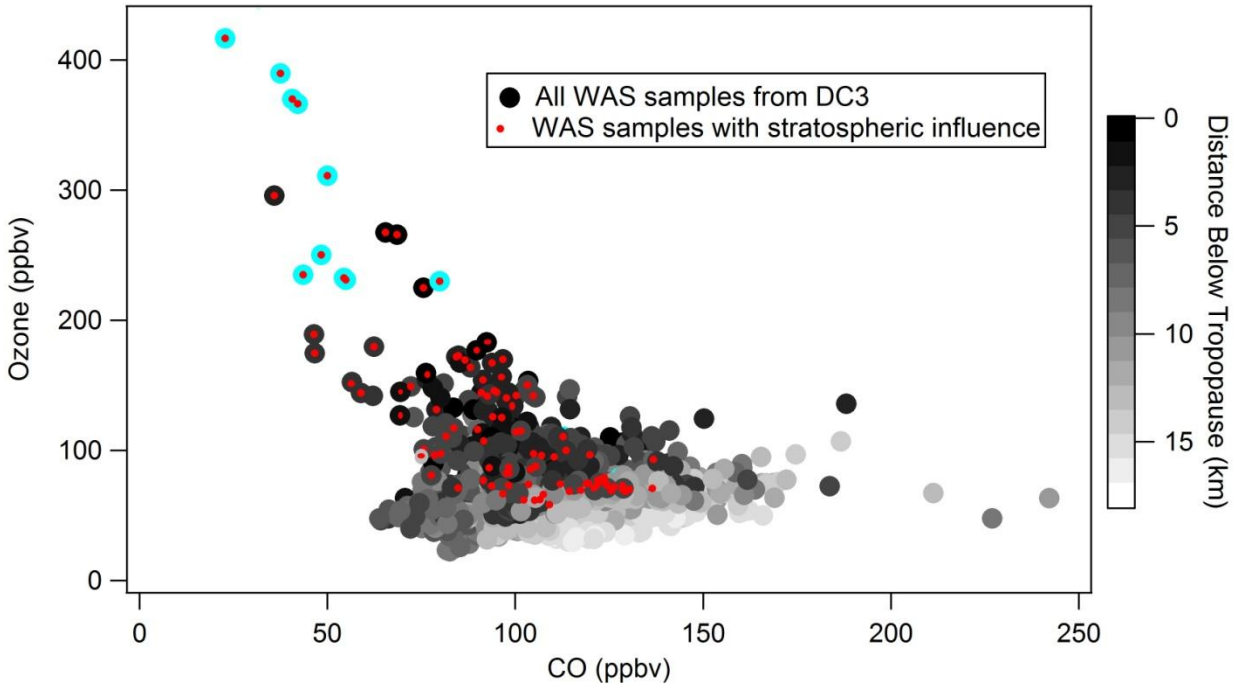

Figure 4.3. O_3 vs CO for the WAS data merge. Samples that met the criteria to be labeled as SI samples are indicated by red dots. All samples are colored by distance below the thermal tropopause, and cyan samples were collected above the thermal tropopause.

In the lower troposphere, this mixing likely occurred when deep stratospheric intrusions mixed with polluted air in the PBL, as has been described elsewhere (Langford et al., 2012; Lin et al., 2012). In the upper troposphere, this mixing likely occurred when polluted air was lofted to the UT by deep convection in the vicinity of a stratospheric intrusion. In the following sections, we focus our attention on this mixing in the UT and aim to do the following: Show evidence of a specific case where polluted convective outflow mixed with stratospheric air, determine a timescale for this mixing during DC3 (did it occur while storms were active, or after they had dissipated?), and assess the extent of this mixing during DC3 and potential impacts on chemistry of the UT.

4.3 Case study: Evidence of Stratospheric Air Mixing with Aged, Polluted Convective Outflow

During DC3 research flight 16 (June 17 2012), the DC-8 had a primary objective of tracking down and probing aged outflow from a storm that had occurred the previous day over Oklahoma. The DC-8 altitude profile (colorized by the measured 1 Hz O_3 mixing ratio) for this flight is shown in Figure 4.4. While flying at altitudes between 8-12 km over the target area, the DC-8 regularly encountered air with elevated propane and *n*-butane values (i.e. over 205 pptv and 50 pptv, respectively), indicative of convective outflow (i.e. the Outflow-UT dataset described in Chapter 3). In Figure 4.4, propane mixing ratios are indicated by red bars and a dashed red line represents the chosen cutoff of 205 pptv, while *n*-butane mixing ratios are omitted for the sake of clarity. At 21:00 and 21:30 UTC air with elevated propane and O_3 levels was encountered. In these patches of high O_3, four SI samples were identified. The entire flight took place below the thermal tropopause (thick black line in Figure 4.4), suggesting that at some

point in the previous 24 hours, stratospheric air had entered the troposphere and mixed with this outflow.

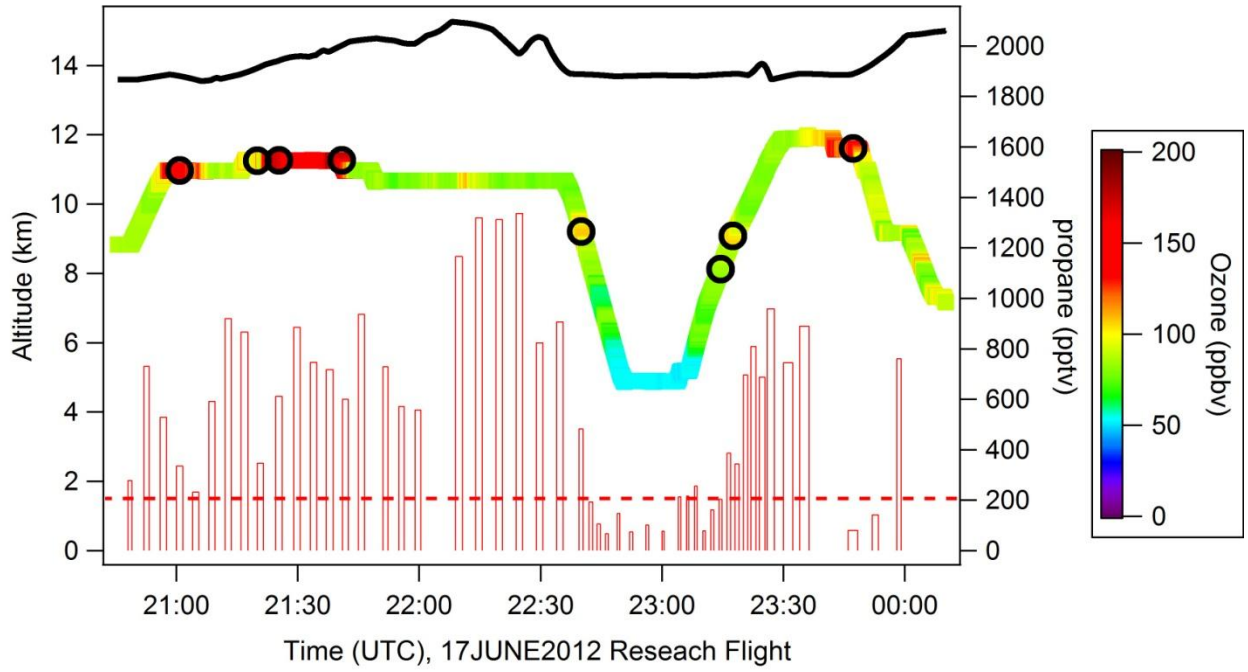

Figure 4.4. The DC-8 altitude profile for DC3 research flight 16. The flight path is colored by 1-s O_3 measurements, and SI samples are marked with circles. WAS propane mixing ratios (right axis) are shown as red bars, and are used to indicate the presence of convective outflow. A dashed red line marks the propane cutoff value of 205 pptv described in section 4.3. The entire flight took place below the thermal tropopause, which is indicated by a thick black line.

To determine when this mixing took place, we looked at the origin of this convective outflow. Back trajectory analyses were performed using the NOAA HYSPLIT model. Although these trajectories do not accurately reproduce convective motion, they do identify the location of convective systems responsible for the observed outflow. These analyses show that the aged convective outflow sampled during research flight 16 originated from a convective storm near the Texas/Oklahoma border that had occurred the previous day (research flight 15; June 16, 2012). During research flight 15, the DC-8 sampled the inflow and outflow regions of this storm. The inflow air contained high levels of propane, *n*-butane, and other hydrocarbons associated with the widespread regional oil and natural gas extraction activities. While sampling

the outflow from the active storm on June 16, three SI samples were detected at altitudes of 11 - 11.5 km. Of these three SI samples, two had evidence of mixing with polluted convective outflow – elevated levels of not only propane and *n*-butane, but other short-lived hydrocarbons associated with oil and natural gas extraction including *n*-heptane (lifetime ~ 1.7 days) and ethene (lifetime ~ 1.4 days). This supports a hypothesis that mixing with stratospheric air may occur as a convective storm is developing. However, since only three SI samples were collected during research flight 15, it is difficult to draw any firm conclusions about the dynamics of mixing near an active storm. For a more detailed perspective on the dynamics of this mixing, we examined a flight where a higher number of SI samples were collected near an active storm.

4.4 Case Study: Evidence of Stratospheric Air Mixing With Outflow from an Active Storm

To more thoroughly evaluate the mixing dynamics near active storms, more SI samples are needed in the vicinity of a storm. Research flight 2 (May 19, 2012) had a primary objective of probing the inflow and outflow regions of an isolated, active convective storm over Oklahoma. During this flight, 17 SI samples were collected. The DC-8 flew L-shaped patterns in the low-altitude inflow region of the storm – which was characterized by elevated levels of hydrocarbons and biogenic emissions like isoprene - then spiraled up to an altitude of 12 km to probe the outflow of this storm. The altitude profile for this flight is shown in Figure 4. 5. The track of the spiral-up and outflow pass segments are shown in Figure 4.6.

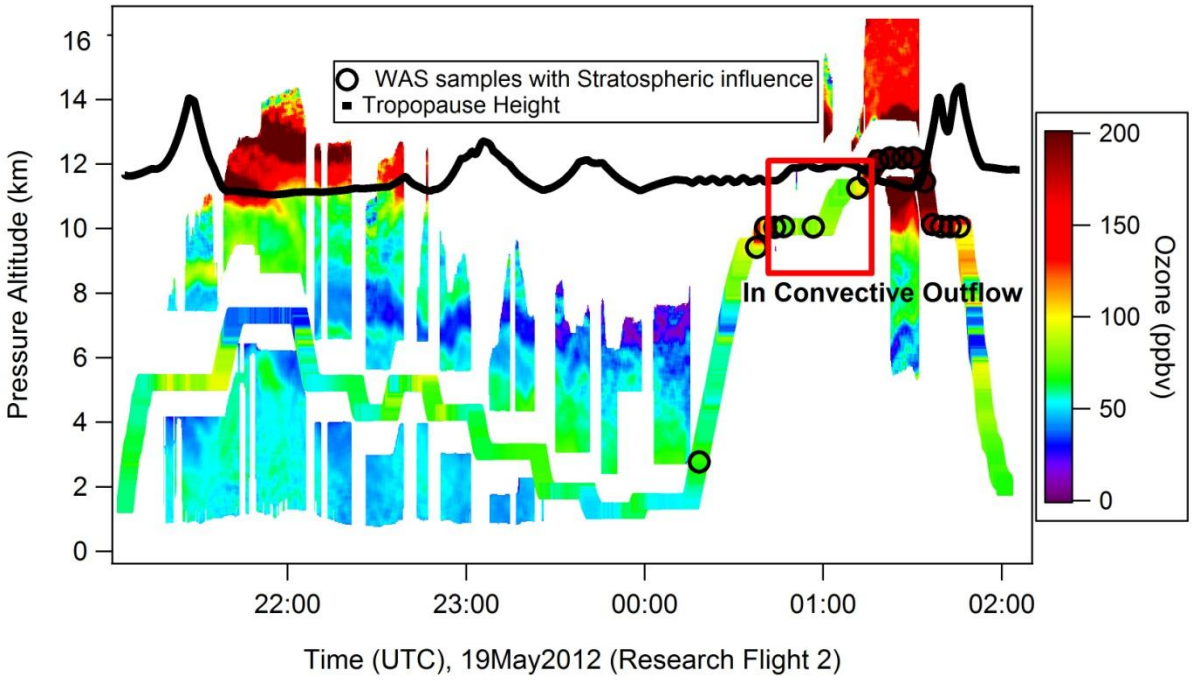

Figure 4. 5. The DC-8 altitude profile for DC3 research flight 2. The altitude profile (flight track) is colored by 1-s O_3 measurements, and SI samples are indicated by circles. The DC-8 also carried an O_3 lidar, the profile of which is shown above and below the altitude profile and colorized on the same scale. The thermal tropopause is represented as a thick black line. The period when the DC-8 passed through the outflow region of the storm is indicated by a red rectangle.

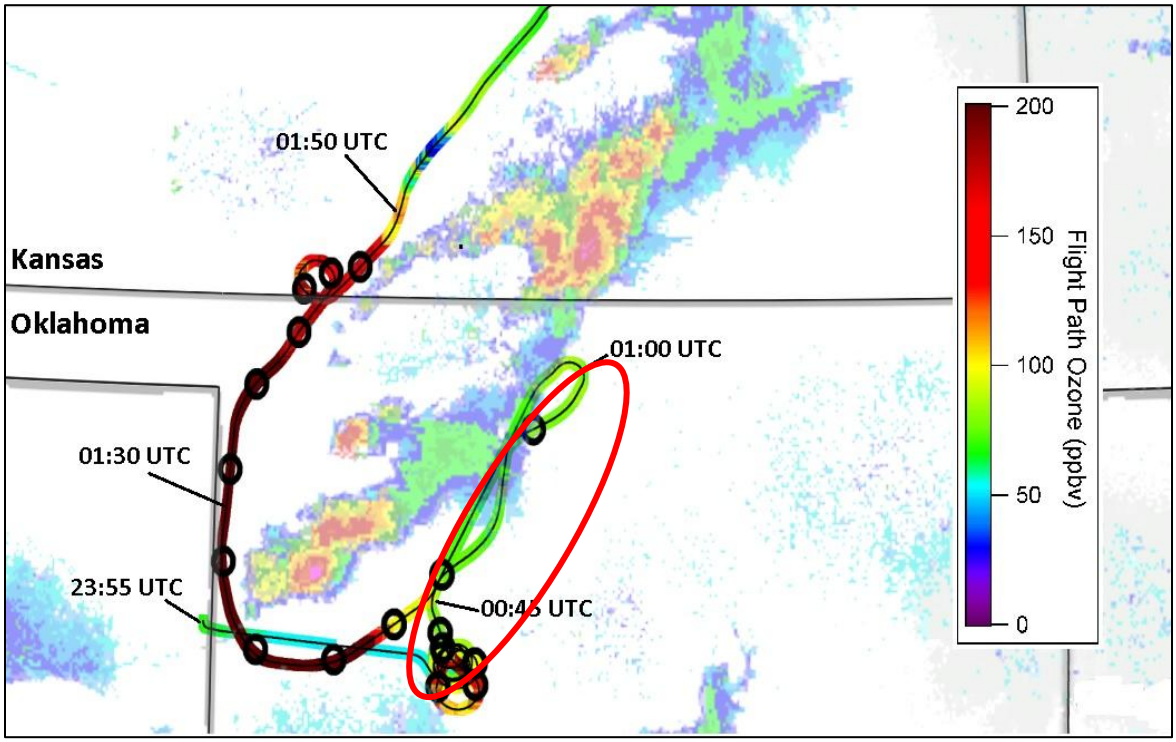

Figure 4.6. The DC-8 flight track for the spiral-up and outflow segments of DC3 research flight 2 (flight path begins at 23:55 UTC in the bottom left corner, and ends at 02:00 UTC at the top of the image). The flight path is colorized by 1-s O_3 measurements, and SI samples are indicated by black circles. A NEXRAD radar image from 01:05 UTC is overlain, showing the weather pattern probed by the DC-8. The portion of the flight where the DC-8 flew through convective outflow is circled in red.

Before entering the convective outflow at about 00:45 UTC (end of the upward spiral segment), an air mass with strong stratospheric character was observed (O_3 levels above 100 ppbv, large decreases in mixing ratios of long-lived halocarbons and N_2O, low water vapor content, very low levels of hydrocarbons), and three SI samples were identified. These SI samples were located about 1.3 km below the thermal tropopause. Then, from 00:43 – 01:16 UTC the DC-8 flew two passes through convective outflow from this active storm (red rectangle in Figure 4.5; red oval in Figure 4.6). During both of these outflow passes, the DC-8 remained below the thermal tropopause. The outflow was marked by large enhancements in both short-lived and long-lived hydrocarbons. For example, long-lived species like ethane (lifetime ~ 47 days) were enhanced by several hundred percent over background UT mixing ratios at the same time that very-short-lived species (like isoprene, which has an average atmospheric lifetime of ~ 3 hours and is below our 3 pptv detection limit in background UT air masses) were observed in detectable amounts. Upon entering the convective outflow, O_3 levels decreased, water vapor increased, and hydrocarbon levels increased, effectively masking any obvious stratospheric character that may be mixed in. However, four SI samples were identified in the outflow, indicating that stratospheric air had indeed mixed with the outflow.

After leaving the convective outflow, the DC-8 ascended to 12 km, flew around the south end of the convective cell, and returned to Salina along the backside of the storm front. Upon ascending, the DC-8 briefly crossed the thermal tropopause and sampled stratospheric air around 01:20 UTC. Four SI samples were collected during this flight segment. After spending several minutes above the tropopause, the DC-8 then descended below the tropopause, but the same strong stratospheric character remained, and 5 SI samples were identified. Lidar O_3 profiles from

this backside segment show an air mass with a strong stratospheric character reaching down to 10 km (Figure 4.5). A dip in the thermal tropopause height, from 12 km to 11 km, was also observed in this region. From this, it is apparent that stratospheric air had penetrated below the tropopause on the backside of the storm front, and this stratospheric air had mixed, in varying degrees, with the outflow on the east side of the storm. This information, combined with the *in situ* evidence regarding the SI samples, shows that the polluted boundary layer air encountered in this convective outflow was rapidly mixed with stratospheric air upon being lofted to the UT. In this case, mixing was likely facilitated by the strong northwesterly winds observed in the UT behind the storm front. A 3-D representation of this event is provided in Figure 4.7. On the right side of this figure, the DC-8 is sampling the convective outflow, and encountering relatively low O_3 values while high O_3 values are contained in the stratosphere above the DC-8, as indicated by the Lidar profile. Upon rounding the bottom of the storm, the DC-8 encounters SI samples, and a decreasing tropopause height. On the backside of the storm (near-side of Figure 4.7), several SI samples are detected along with high in-situ values of O_3. The Lidar profile during this segment shows high O_3 values above the DC-8, and a narrow band of high O_3 below the DC-8, indicating that the DC-8 was above the local tropopause during this segment.

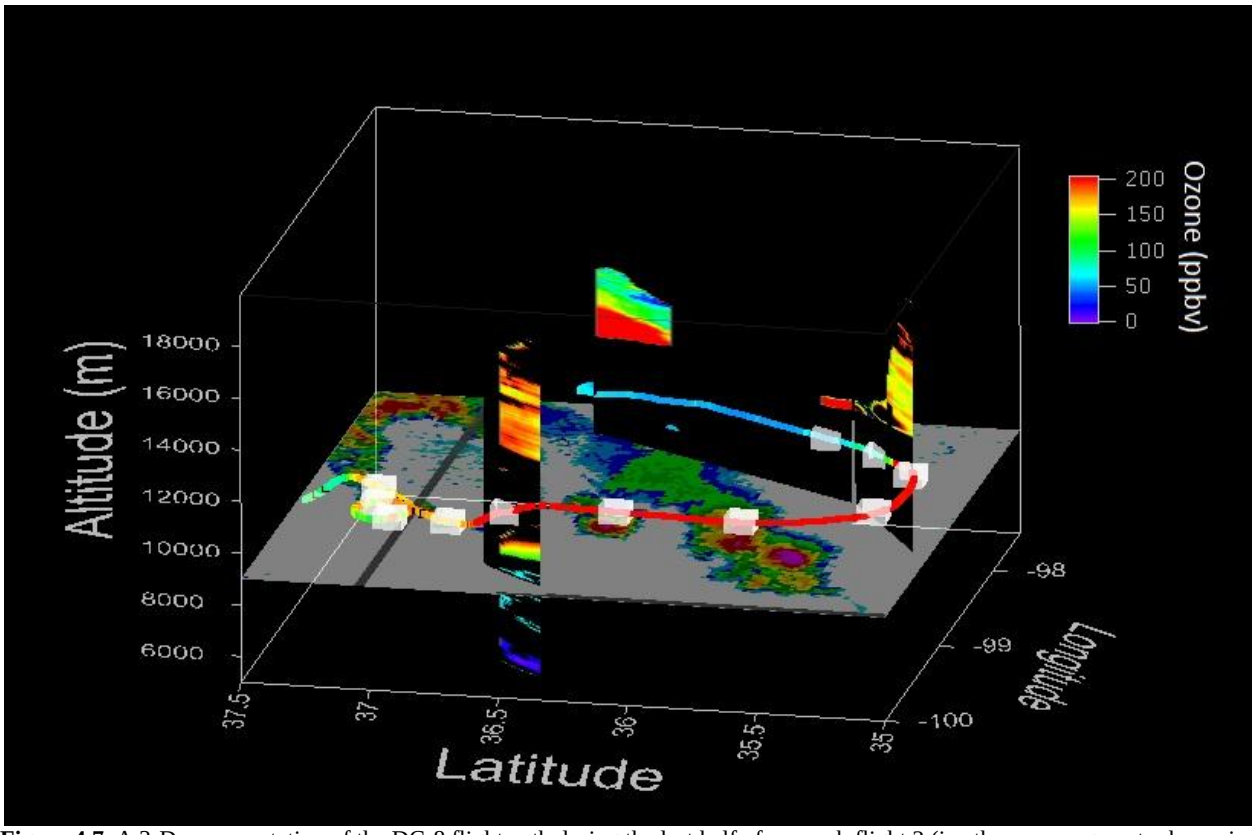

Figure 4.7. A 3-D representation of the DC-8 flight path during the last half of research flight 2 (i.e. the same segments shown in Figure 4.5 and Figure 4.6). Lidar profiles of O_3 are shown where available. The NEXRAD radar image shown in Figure 4.6 is depicted here as a surface at 9500 meters, for visibility purposes. Both the DC-8 flight path and the Lidar O_3 profiles are colored by O_3 values, and SI samples are marked as white boxes along the flight path.

4.5 Evidence of Wide-scale Mixing of Stratospheric Air with Convective Outflow

To assess the overall impact of mixing between polluted convective outflow and stratospheric air, overlap region between the SI and outflow-UT datasets was investigated. That is, all SI samples that had propane values over 205 pptv and *n*-butane values over 50 pptv were considered for this analysis. Ozone was used as an approximate indicator for the level of dilution of a stratospheric air mass. SI samples with high O_3 values were either collected in the stratosphere or were fresh, recent stratospheric intrusions. SI samples with reduced O_3 values (i.e. below 150 ppbv) are the result of dilution of a stratospheric air mass – either by mixing with clean background air in the FT, mixing with boundary layer air that has been convectively lofted into the FT, or direct mixing with boundary layer air during a deep stratospheric intrusion. It

should be noted that O_3 levels are not constant within the stratosphere, and are subject to variation by altitude, geographic location, and seasonal changes (Stohl et al., 2003; Zeng et al., 2010). Because of this, we make no attempt to quantify the amount of dilution observed here.

Figure 4.8 shows the tropopause-relative altitude profile for O_3 in all SI samples collected during DC3. Based on their propane and *n*-butane mixing ratios, samples were binned as having relatively recent anthropogenic influence (i.e. propane > 205 pptv, *n*-butane > 50 pptv) or not. As expected, SI samples with the highest O_3 values are located near the tropopause and show no recent anthropogenic influence, as they consist mostly of undiluted stratospheric air. By contrast, most SI samples collected below the tropopause had elevated propane and *n*-butane levels, implying that the SI samples had mixed with polluted boundary layer air to some extent. Based on all SI samples with O_3 values below 150 ppbv, 72% met our criteria to be labeled as anthropogenically-influenced. Even in the UT, most SI samples that have experienced significant mixing with tropospheric air (O_3 < 150 ppbv) have done so by mixing with polluted air rather than clean free tropospheric air. This result suggests that over central US in late spring the primary mixing mechanism for storm-associated stratospheric intrusions is the mixing with convective outflow that has recently been lifted out of the polluted boundary layer.

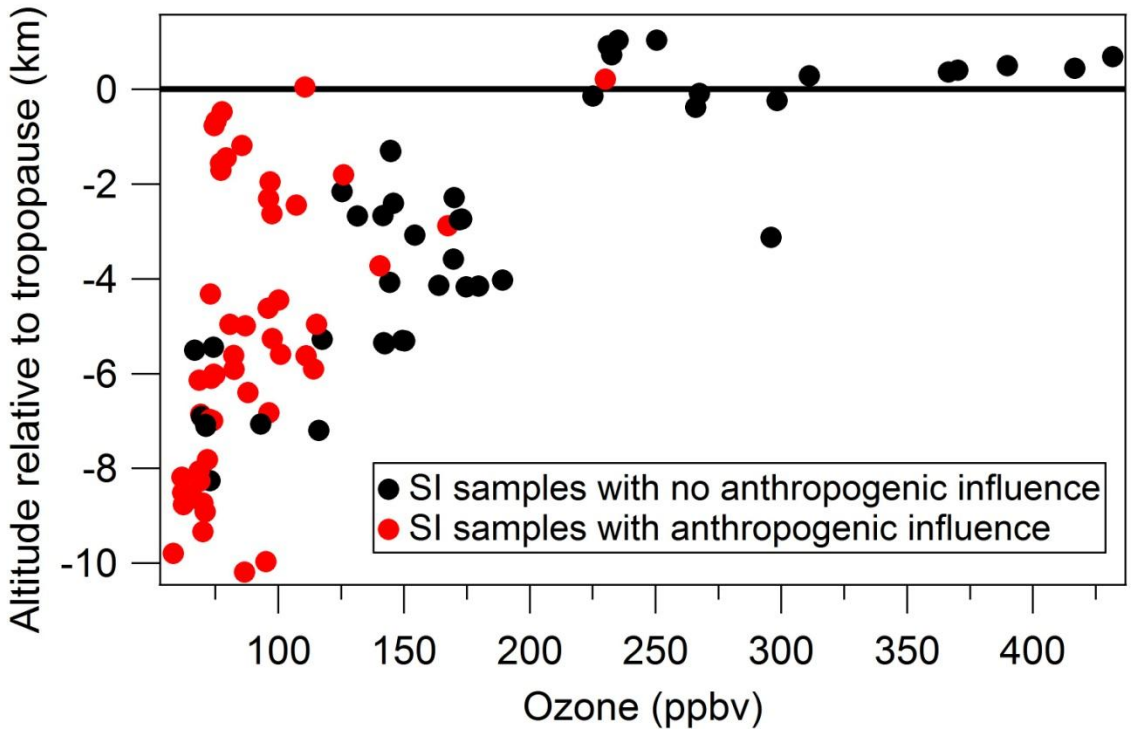

Figure 4.8. All SI samples from DC3. Black circles indicate samples that did not meet our criteria to be labeled "anthropogenically-influenced", and red circles indicate samples that did meet these criteria. Altitudes are listed relative to the tropopause height calculated for each sample, where positive altitudes were collected above the tropopause and negative altitudes were collected below the tropopause.

4.6 Effects on OH production

With moist air from convective outflow mixing with the high-O_3 air of stratospheric intrusions, the oxidizing capacity of convective outflow – and the regional upper troposphere – may be altered via an increased production of OH radicals. The mechanism by which OH radicals are produced by O_3 and water vapor is described in Chapter 1 (section 1.2.1), and referenced here. Assuming steady-state conditions for $O(^1D)$ and $k_4 >> k_6$, the instantaneous production of OH (P_{OH}) can be calculated by equation 4.1 (Crutzen et al., 1999; Fusco, 2003):

$$P_{OH} = \frac{2k_3k_6}{k_4[M]}[O_3][H_2O] \qquad (4.1)$$

When comparing the relative OH productivity of two air masses, equation 4.1 can be further simplified into equation 4.2 under the assumption that both air masses have identical temperature and pressure conditions:

$$\frac{P_{OH,1}}{P_{OH,2}} = \frac{[H_2O]_1[O_3]_1}{[H_2O]_2[O_3]_2} \qquad (4.2)$$

Table 4.1 shows relevant chemical data used for calculating this ratio, and includes the mean and 95% confidence interval for both H_2O and O_3. SI samples collected at altitudes above 8 km with O_3 values above 200 ppbv and no anthropogenic influence (as per the propane and *n*-butane filter described in Chapter 3) were labeled as fresh stratospheric intrusions. These were compared to a modified version of the Background-UT dataset where all SI samples were removed. Mixed stratospheric/convective outflow samples were identified as SI samples collected above 8 km with detectable anthropogenic influence (i.e. propane > 205 pptv and *n*-butane > 50 pptv).

Using equation 4.2, P_{OH} for mixed stratospheric/convective outflow was calculated to be higher than P_{OH} for fresh stratospheric intrusions by a factor of 11 ± 8. The high uncertainty is due to the low levels of water vapor present in stratospheric air and the wide range of O_3 values allowed to be classified as "fresh stratospheric intrusions" – a difference of even a few ppb of O_3 and water vapor between samples results in a high uncertainty in the mean value. Comparing mixed stratospheric/convective outflow to background UT air, this factor was calculated to be 4.2 ± 1.8. These results are summarized in Table 4.1.

Table 4.1. Chemical data for different air masses in the UT and their calculated instantaneous OH production. Here, "mixed" refers to airmasses where stratospheric air has mixed with convective outflow. Error bars represent 1σ.

Air mass	H_2O (ppb)	O_3 (ppb)	$\frac{P_{OH,mixed}}{P_{OH,air\ mass}}$
Fresh stratospheric intrusion	13,000 ± 8300	333 ± 128	11 ± 8
Background UT	138,000 ± 39,000	82 ± 18	4.2 ± 1.8
Mixed stratospheric/convective outflow	371,000 ± 64,080	125 ± 50	1

If our hypothesis from section 4.5 is true – that storm-associated stratospheric intrusions often mix with convective outflow – then this could be a potentially large source of OH radicals in the UT over the central US and affect chemistry in the UT, particularly in areas where deep convection is frequent. In the presence of this type of mixing, the lifetimes of OH-controlled VOCs would be shorter than currently predicted. This could alter the radiative forcing of the UT by reducing the lifetimes of radiatively-important gases like CH_4 and ethane, while cirrus cloud formation may be altered due to the enhanced production of secondary VOCs and their associated changes in gas/particle partitioning (Riese et al., 2012). Recent studies by Pan et al. (2014) and Homeyer et al. (2011) have also investigated this relationship between convection and stratospheric intrusions, but focused on the meteorological aspects rather than chemistry. At this point, however, there is still no consensus as to how frequent these mixing events are, nor whether or not we can say with certainty that these results hold true on a global scale over a period of a whole year. Further work must be done to assess the validity of this study.

4.7 Conclusions

The SI and Convective outflow datasets were used to investigate the mixing between stratospheric intrusions and convection in the UT. O_3 levels in SI samples indicated that, below the tropopause, stratospheric air had been mixed with tropospheric air on a number of occasions.

Many of these samples with mixed stratospheric-tropospheric character had elevated levels of CO – indicative of anthropogenic influence. These mixed samples were identified in both the PBL and the UT. During DC3, rapid vertical transport of polluted air occurred via deep convective lofting of air from the PBL to the UT. This polluted convective outflow was detected during active storms, where it remained in the UT and was transported downwind for several days. To investigate the process by which stratospheric air mixes with convectively-lofted polluted air, a case study was performed: Using the Convective outflow dataset and back trajectories, aged, polluted convective outflow (lofted to the UT one day prior to sampling) was identified as having been sampled during research flight 16. Embedded within this outflow were six samples that had both anthropogenic and stratospheric influence. A case study performed on a flight where an active storm was sampled (research flight 2) also shows evidence of this type of mixing. During this flight, a large stratospheric intrusion was identified behind a storm front passing over Oklahoma. While probing the outflow from this storm, five samples were collected that met our criteria to be labeled as stratospherically-influenced. These results indicate that active convection may act to facilitate the mixing between stratospheric and polluted air in the UT, although we do not attempt to draw any conclusions about the meteorological relationship between co-located stratospheric intrusions and deep convective storms and the frequency by which this type of mixing occurs. Since the DC-8 primarily sampled convective outflow below the tropopause, and nearly all SI samples with detectable anthropogenic influence were collected below the tropopause, we can not speculate about the presence of this type of mixing in the lowermost stratosphere.

Of all SI samples collected during DC3, 72% showed detectable anthropogenic influence. In the UT, the majority of SI samples that had experienced some degree of mixing with

tropospheric air had done so by mixing with polluted convective outflow. Relative to tropospheric air, stratospheric air has very high O_3 levels, while, relative to stratospheric air, tropospheric air has very high levels of water vapor. Thus, mixing between the two is expected to lead to an enhanced instantaneous production of OH relative to un-mixed stratospheric or tropospheric air. Indeed, based on O_3 and water vapor mixing ratios measured during DC3, air masses that had both stratospheric and anthropogenic influence was calculated to have an instantaneous production of OH that is 11 ± 8 times higher than undiluted stratospheric intrusions, and 4.2 ± 1.8 times higher than background tropospheric air. This process creates a unique chemical environment where boundary layer pollution that is convectively lofted in the upper troposphere may experience higher-than-expected loss rates of OH-controlled trace gases. Although the work presented here may help lay the groundwork for understanding this type of mixing, future measurements and modeling studies must be done to assess the regional, global, and temporal trends of this type of mixing, and any potential impacts on tropospheric chemistry.

Although the observations made here were not extensive enough to allow for an estimate of O_3 flux from the stratosphere via this pathway, this pathway may be significant because hundreds of deep convective storms occur over the continental US every year. The topic of upper tropospheric O_3 enhancements over North America has been the focus of many studies, and the general consensus in recent years has been that the chemical production of O_3 from lightning-NO_x (LNO_x) is the main cause (Cooper et al., 2006, 2007, 2009). Taking the work presented here into consideration, this notion may need to be edited to include the introduction of stratospheric airmasses into the UT and the potential for enhanced production of OH when convective outflow is mixed with stratospheric air. Under these enhanced-OH conditions, the OH-VOC-LNO_x chemistry will be altered in a way where the timescale for O_3 production in convective outflow

may be shortened. In effect, mixing ratios of VOCs and LNO_x would be highest shortly after convection, as would P_{OH}, which would result in a "pulse" of O_3 production that is both shorter and greater in magnitude than a similar convective event where mixing between convective outflow and stratospheric air did not take place. This would have important implications on the distribution of O_3 in the UT/LS (via both cross-tropopause transport and photochemical production) and the lifetimes of OH-controlled GHGs such as CH_4 and ethane.

4.8 References

Cooper, O. R., Eckhardt, S., Crawford, J. H., Brown, C. C., Cohen, R. C., Bertram, T. H., Wooldridge, P., Perring, a, Brune, W. H., Ren, X., Brunner, D. and Baughcum, S. L.: Summertime buildup and decay of lightning NO x and aged thunderstorm outflow above North America, J. Geophys. Res., 114(D1), 1–18, doi:10.1029/2008JD010293, 2009.

Cooper, O. R., Stohl, a, Trainer, M., Thompson, a M., Witte, J. C., Oltmans, S. J., Morris, G., Pickering, K. E., Crawford, J. H., Chen, G., Cohen, R. C., Bertram, T. H., Wooldridge, P., Perring, a, Brune, W. H., Merrill, J., Moody, J. L., Tarasick, D., Nedelec, P., Forbes, G., Newchurch, M. J., Schmidlin, F. J., Johnson, B. J., Turquety, S., Baughcum, S. L., Ren, X., Fehsenfeld, F. C., Meagher, J. F., Spichtinger, N., Brown, C. C., McKeen, S. a, McDermid, I. S. and Leblanc, T.: Large upper tropospheric ozone enhancements above midlatitude North America during summer: In situ evidence from the IONS and MOZAIC ozone measurement network, J. Geophys. Res., 111(D24), 1–19, doi:10.1029/2006JD007306, 2006.

Cooper, O. R., Trainer, M., Thompson, a. M., Oltmans, S. J., Tarasick, D. W., Witte, J. C., Stohl, a., Eckhardt, S., Lelieveld, J., Newchurch, M. J., Johnson, B. J., Portmann, R. W., Kalnajs, L., Dubey, M. K., Leblanc, T., McDermid, I. S., Forbes, G., Wolfe, D., Carey-Smith, T., Morris, G. a., Lefer, B., Rappenglück, B., Joseph, E., Schmidlin, F., Meagher, J., Fehsenfeld, F. C., Keating, T. J., Van Curen, R. a. and Minschwaner, K.: Evidence for a recurring eastern North America upper tropospheric ozone maximum during summer, J. Geophys. Res., 112(D23), D23304, doi:10.1029/2007JD008710, 2007.

Crutzen, P. J., Lawrence, M. G. and Paeschl, U.: On the background photochemistry of tropospheric ozone, Tellus A, doi:10.3402/tellusa.v51i1.12310, 1999.

Fusco, A. C.: Analysis of 1970–1995 trends in tropospheric ozone at Northern Hemisphere midlatitudes with the GEOS-CHEM model, J. Geophys. Res., 108(D15), 4449, doi:10.1029/2002JD002742, 2003.

Homeyer, C. R., Bowman, K. P., Pan, L. L., Zondlo, M. a. and Bresch, J. F.: Convective injection into stratospheric intrusions, J. Geophys. Res., 116(D23), D23304, doi:10.1029/2011JD016724, 2011.

Kuang, S., Newchurch, M. J., Burris, J., Wang, L., Knupp, K. and Huang, G.: Stratosphere-to-troposphere transport revealed by ground-based lidar and ozonesonde at a midlatitude site, J. Geophys. Res. Atmos., 117(D18), 125-139, doi:10.1029/2012JD017695, 2012.

Langford, a. O., Brioude, J., Cooper, O. R., Senff, C. J., Alvarez, R. J., Hardesty, R. M., Johnson, B. J. and Oltmans, S. J.: Stratospheric influence on surface ozone in the Los Angeles area during late spring and early summer of 2010, J. Geophys. Res. Atmos., 117(D21), 1130-1145, doi:10.1029/2011JD016766, 2012.

Lefohn, A. S., Wernli, H., Shadwick, D., Limbach, S., Oltmans, S. J. and Shapiro, M.: The importance of stratospheric–tropospheric transport in affecting surface ozone concentrations in

the western and northern tier of the United States, Atmos. Environ., 45(28), 4845–4857, doi:10.1016/j.atmosenv.2011.06.014, 2011.

Lin, M., Fiore, A. M., Cooper, O. R., Horowitz, L. W., Langford, A. O., Levy, H., Johnson, B. J., Naik, V., Oltmans, S. J. and Senff, C. J.: Springtime high surface ozone events over the western United States: Quantifying the role of stratospheric intrusions, J. Geophys. Res. Atmos., 117(D21), n/a–n/a, doi:10.1029/2012JD018151, 2012.

Pan, L. L.: Definitions and sharpness of the extratropical tropopause: A trace gas perspective, J. Geophys. Res., 109(D23), D23103, doi:10.1029/2004JD004982, 2004.

Pan, L. L., Homeyer, C. R., Honomichl, S., Ridley, B. A., Weisman, M., Crawford, J. H., Ryerson, T. B., Pollack, I. and Peischl, J.: Thunderstorms enhance tropospheric ozone by wrapping and shedding stratospheric air, J. Geophys. Res., 7785–7790, doi:10.1002/2014GL061921, 2014.

Riese, M., Ploeger, F., Rap, a., Vogel, B., Konopka, P., Dameris, M. and Forster, P.: Impact of uncertainties in atmospheric mixing on simulated UTLS composition and related radiative effects, J. Geophys. Res., 117(D16), D16305, doi:10.1029/2012JD017751, 2012.

Stohl, A., Wernli, H., James, P., Bourqui, M., Forster, C., Liniger, M. a., Seibert, P. and Sprenger, M.: A New Perspective of Stratosphere–Troposphere Exchange, Bull. Am. Meteorol. Soc., 84(11), 1565–1573, doi:10.1175/BAMS-84-11-1565, 2003.

Zeng, G., Morgenstern, O., Braesicke, P. and Pyle, J. a.: Impact of stratospheric ozone recovery on tropospheric ozone and its budget, Geophys. Res. Lett., 37(9), doi:10.1029/2010GL042812, 2010.

5. Vertical Redistribution of Halogenated VOCs by Midlatitude Convective Storms during the DC3 Field Campaign

The WAS data merge and its derived subsets of data (see Chapter 3) were used to investigate the effects of deep convection on mixing ratios of organic chlorine and organic bromine in the UT and LS over the DC3 study region. In the LS, it was found that mixing ratios of organic chlorine in overshooting tops were higher than mixing ratios of organic chlorine in the background LS by an average of 217 ± 179 pptv (6.3 ± 5.2% enhancement, ± 1σ uncertainty). Of all the classes of halocarbons described in this work, mixing ratios of VSLH organic chlorine (enhanced by 76 ± 42 pptv), LLHC organic chlorine (enhanced by 65 ± 69 pptv), and CFC organic chlorine (enhanced by 56 ± 78 pptv) were most enhanced in overshooting tops relative to the background LS. The total organic bromine mixing ratio in overshooting tops was higher than that of the background LS by an average of 2.8 ± 3.2 pptv ((17.4 ± 19.9% enhancement), ± 1σ uncertainty), with VSLH organic bromine (enhanced by 1.3 ± 1.9 pptv) contributing the most to this enhancement, and halons and LLHC contributing less to this enhancement (organic bromine from both halons and LLHC were enhanced by 0.8 ± 1.2 pptv in overshooting tops).

In the UT, convection was found to play a much more complicated role on the organic halogen content of the region. Organic chlorine mixing ratios in the background UT and organic bromine mixing ratios in convective outflow were both found to have very large ranges of mixing ratios, leading to relatively large uncertainties when calculating enhancements from convective outflow (i.e. the average value in convective outflow minus the average value in the background UT). Model back trajectories and analysis of the chemical composition of the background UT revealed that long-range transport of outflow from East Asia and from the central Pacific affected the background UT of the DC3 study region to varying degrees on

different days. When the background UT was affected by East Asian outflow, mixing ratios of organic chlorine in local convective outflow from storms over the central US were lower than those of the local background UT by up to 150 ± 115 pptv (VSLH organic chorine was lower by up to 24 ± 20 pptv, and LLHC organic chlorine was lower by 73 ± 23 pptv). On the other hand, when the background UT was affected by clean outflow from the central Pacific, mixing ratios of organic chlorine in convective outflow were higher than the local background UT by up to 115 ± 98 pptv (VSLH organic chlorine was higher by up to 22 ± 21 pptv, and LLHC organic chlorine was higher by up to 34 ± 22 pptv). Mixing ratios of organic bromine in the background UT were unaffected by these long-range transport processes. However, mixing ratios of organic bromine in convective outflow were highly variable and were affected by the transport of brominated VSLH from the Gulf of Mexico to the surface of the DC3 study region. When organic bromine enhancements in convective outflow were calculated on a flight-by-flight basis, organic bromine mixing ratios in convective outflow were higher than those in the background UT by an average of 1.7 ± 1.6 pptv (range -0.3 to 6.0 pptv), VSLH organic bromine was higher by an average of 1.3 ± 1.5 pptv (range -0.3 to 6.0 pptv), and LLHC organic bromine was higher by an average of 0.5 ± 0.5 pptv (range -0.1 to 2.0 pptv).

5.1. Organic Halogens in the UT/LS

The total mixing ratio of a given organic halogen in a given sample was calculated using equation 5.1, where C_i is the mixing ratio of VOC i, and N_i is the number of atoms of X (X= chlorine or bromine) in VOC i:

$$Total\ Organic\ X = \sum_i C_i N_i \tag{5.1}$$

For example, CFC-11 (CCl_3F) contains 3 chlorine atoms, and at a mixing ratio of 250 pptv would contribute 750 pptv of organic chlorine, while methyl bromide (CH_3Br) contains one

bromine atom, and at a mixing ratio of 8 pptv would contribute 8 pptv of organic bromine. The organic halogen contribution from different classes of halocarbon (i.e. CFCs, HCFCs, VSLH, etc.) was also calculated using equations 5.2 – 5.6:

$$Total\ X\ from\ CFCs = \sum_{j} C_j N_j \tag{5.2}$$

In equation 5.2, C_j is the mixing ratio of CFC *j*, and N_j is the number of X atoms in CFC *j*.

$$Total\ X\ from\ HCFCs = \sum_{k} C_k N_k \tag{5.3}$$

In equation 5.3, C_k is the mixing ratio of HCFC *k*, and N_k is the number of X atoms in HCFC *k*.

$$Total\ X\ from\ Halons = \sum_{l} C_l N_l \tag{5.4}$$

In equation 5.4, C_l is the mixing ratio of Halon *l*, and N_l is the number of X atoms in Halon *l*.

$$Total\ X\ from\ LLHCs = \sum_{m} C_m N_m \tag{5.5}$$

In equation 5.5, C_m is the mixing ratio of LLHC *m*, and N_m is the number of X atoms in LLHC *m*.

$$Total\ X\ from\ VSLH = \sum_{n} C_n n \tag{5.6}$$

In equation 5.6, C_n is the mixing ratio of LLHC *n*, and N_n is the number of X atoms in LLHC *n*.

Because convection that penetrates into the LS is a somewhat rare event and was sampled to a much lesser extent during DC3, the effects of convection on the organic halogen content of the UT and in the LS are considered separately in this work. To determine the difference in organic halogen mixing ratios (and the species that contribute most to these differences) between convective outflow in the UT and background UT air, the Outflow-UT dataset was compared to the Background-UT dataset, with SI samples having been removed from both datasets (see Chapter 3 for descriptions of these datasets). To determine the difference in organic halogen mixing ratios between overshooting tops and background LS air, the Outflow-LS dataset was compared to the Background-LS dataset. The following two sections will focus on the effects of convection on local mixing ratios of organic chlorine and organic bromine, respectively.

5.2. Organic Chlorine in the UT/LS

As described in Chapter 1, atomic chlorine plays an important role in catalyzing O_3 destruction (Molina and Rowland, 1974; Stolarski and Cicerone, 1974). This catalytic destruction occurs primarily in the stratosphere, where sinks of atomic chlorine are weaker than in the troposphere, but can also occur in the UT (Hossaini et al., 2015; Saiz-Lopez et al., 2012). All classes of halocarbon discussed in Chapter 1 (CFCs, HCFCs, Halons, LLHC, VSLH) contribute to the organic chlorine content of an airmass. In general, chlorinated VOCs tend to have anthropogenic sources, with only a few VSLH having significant natural sources (Montzka et al., 2010). Because DC3 focused on continental convection and the convective outflow sampled during DC3 showed anthropogenic influence (see Chapter 3), we expect convection to enhance mixing ratios of organic chlorine in the UT/LS. Of all of the classes of halocarbon considered here, UT/LS mixing ratios of chlorinated VSLH are expected to be most affected by the presence of convection because of their short lifetimes. Furthermore, CFCs, HCFCs, halons, and many LLHCs (CH_3Cl being the notable exception that is not regulated) have been completely banned or have heavily-restricted use, meaning mixing ratios of these compounds in the UT are expected to be relatively unchanged by deep convection, and mixing ratios of these compounds in the LS are expected to be only modestly enhanced (relative to VSLH) by deep convection. This section will be partitioned into two subsections that focus on the effects of convection on the organic chlorine content of the UT and LS, respectively.

5.2.1. The Effects of Deep Convection on Organic Chlorine in the LS

Using equations 5.1-5.6, the total organic chlorine content and organic chlorine contributions from different halocarbon classes were calculated for each sample in the Outflow-LS and Background-LS dataset. These calculated values are shown in Table 5.1, and are visually

represented in Figure 5.1. Mixing ratios of total organic chlorine calculated here in both the background LS (3431 ± 95 pptv) and in overshooting tops (3648 ± 86 pptv) are higher than the tropospheric background organic chlorine mixing ratio of ~3350 pptv reported in the 2010 Scientific Assessment of Ozone Depletion (Montzka et al., 2010). It should be noted that the estimates used in Montzka et al. (2010) do not include organic chlorine contributions from CFC-114 or halons, include an estimate of 550 pptv of organic chlorine from CH_3Cl (which is lower than the 666 pptv measured in the background UT and lower than the 568 pptv measured in the background LS), and include a constant estimate of 80 pptv of organic chlorine from VSLH. The values presented here suggest that estimates of organic chlorine in the troposphere may be underestimated by a significant amount, and, as a result, the modeled amount of organic chlorine transported to the stratosphere will be underestimated as well, as mixing ratios of organic chlorine in the stratosphere are controlled by input from the troposphere.

Table 5.1. Calculated values for total organic chlorine, and the organic chlorine contribution from different classes of halocarbons in the Outflow-LS and Background-LS datasets. All values listed have units of pptv. The average outflow enhancements over background were calculated by subtracting the average value from the Background-LS dataset from the average value from the Outflow-LS dataset. The maximum enhancement was calculated by subtracting the minimum value from the Background-LS dataset from the maximum value from the Outflow-LS dataset (i.e. Outflow-LS max – Background-LS min), and the minimum enhancement was calculated by subtracting the maximum value from the Background-LS dataset from the minimum value from the Outflow-LS dataset (i.e. Outflow-LS min – Background-LS max).

		Total organic chlorine	**CFCs**	**HCFCs**	**Halons**	**LLHCs**	**VSLH**
Outflow-LS	Average	3648	2274	297	3.9	979	95
	max	3736	2307	307	4.0	1011	143
	min	3533	2232	284	3.7	949	64
	St. dev.	86	38	8	0.1	22	33
Background-LS	Average	3431	2218	280	3.5	914	19
	max	3536	2262	298	3.9	996	34
	min	3317	2161	271	3.3	816	18
	St. dev.	95	34	8	0.2	47	9
Outflow enhancement over background	Average	217	56	17	0.5	65	76
	max	419	146	36	0.7	195	125
	min	-3	-30	-14	-0.2	-47	30
	St.dev	179	78	16	0.3	69	42

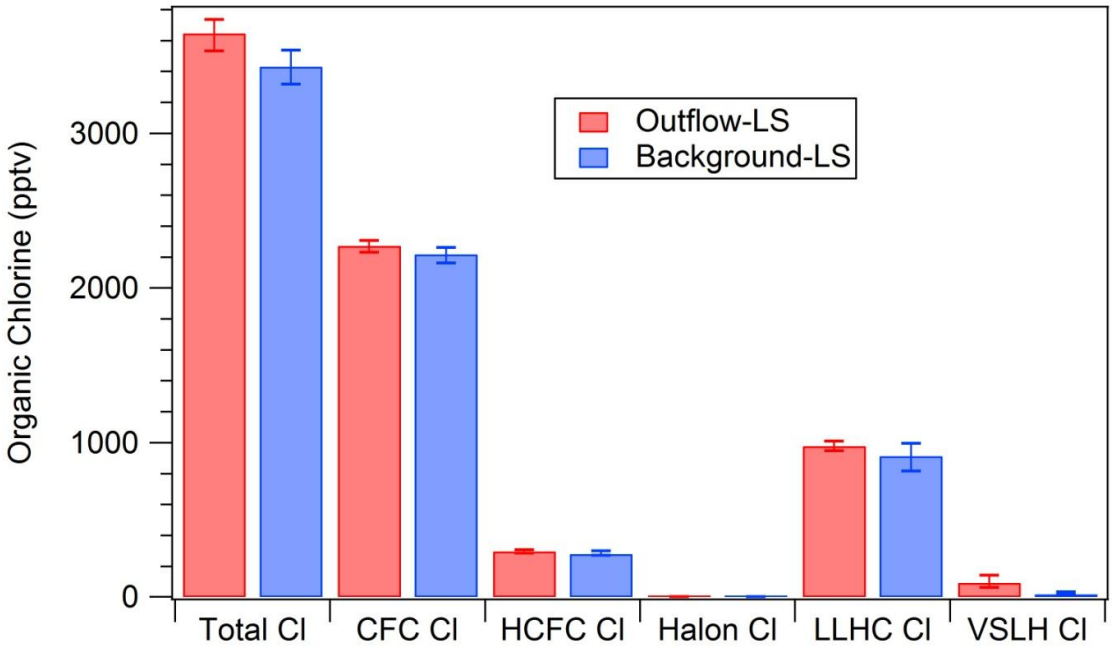

Figure 5.1. A visual representation of the average, maximum, and minimum values of organic chlorine from different classes of halocarbons. Error bars are asymmetric and cover the range of calculated values (i.e. error bars represent the max and min values shown in Table 5.1).

Mixing ratios of total organic chlorine in the Outflow-LS dataset are higher than those in the Background-LS dataset by an average of 217 ± 179 pptv (± 1σ). Of all the classes of halocarbon considered here, mixing ratios of VSLH organic chlorine (enhanced by 76 ± 42 pptv), LLHC organic chlorine (enhanced by 65 ± 69 pptv), and CFC organic chlorine (enhanced by 56 ± 78 pptv) contribute the most to this enhancement over the background LS (that is, the enhancement of overshooting tops relative to the background LS). Because the standard deviations are quite large (larger than the average enhancement in some cases), the range of enhancements should also be considered. The maximum enhancement for a given species (i.e. total chlorine, chlorine from CFCs, etc.) was calculated by subtracting the minimum value from the Background-LS dataset from the maximum value from the Outflow-LS dataset, and is shown in Figure 5.2. The minimum enhancement was calculated by subtracting the maximum value

from the Background-LS dataset from the minimum value from the Outflow-LS dataset. A negative value for the minimum suggests the presence of at least one sample in the Background-LS dataset that yielded a higher value than the minimum value in the Outflow-LS dataset. These large ranges may suggest some limitations of the filtering process described in Chapter 3 – that perhaps using a set of hydrocarbons as tracers for convection is not an ideal tracer for convection above the tropopause. That is, some samples that were flagged as "Background-LS" could actually be from convective outflow, but may not have been flagged as convective outflow due to high dilution of hydrocarbons. Because both the Outflow-LS and Background-LS datasets are quite small (N=5 and N=11, respectively), this cannot be remedied by creating a new tracer for convection above the tropopause.

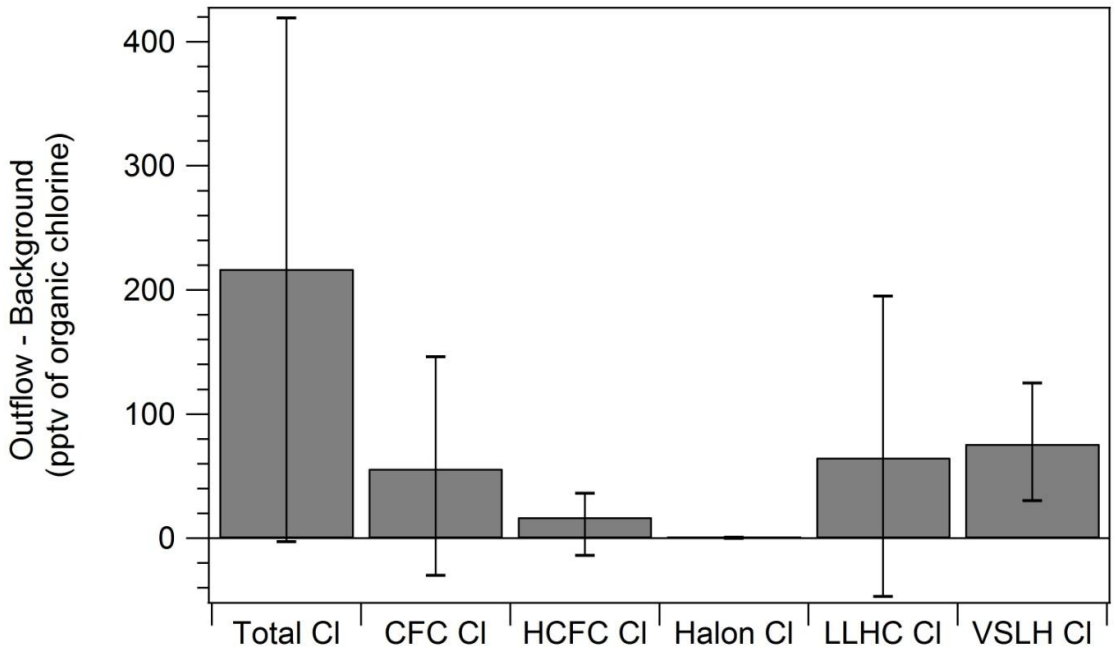

Figure 5.2. A visual representation of the average enhancement of organic chlorine in the Outflow-LS dataset relative to the Background-LS dataset. Error bars are asymmetric and represent the calculated range of enhancements (i.e. the min and max enhancements calculated in Table 5.1).

While the majority of organic chlorine is contained in CFCs, VSLH and LLHC were most enhanced in the LS in the presence of convection (organic chlorine from VSLH enhanced by 76 ± 42 pptv, organic chlorine from LLHC enhanced by 65 ± 69 pptv, and organic chlorine from CFCs enhanced by 56 ± 78 pptv). VSLH lofted into the LS by deep convection contribute the largest enhancement to organic chlorine in the LS, and, as a group, have the smallest relative range of enhancement values (i.e. the error bars in Figure 5.2 are the smallest for VSLH, relative to the average value). During previous airborne studies conducted in the tropical UT, such as PEM-West A and B, TC4, Pre-AVE, and CR-AVE, the lower limit for organic chlorine entering the LS in the form of VSLH via slow, poleward transport from the TTL (described in Chapter 1) was estimated to be 55 pptv (38-80 pptv range) (Laube et al., 2008; Law and Sturges, 2006; Schauffler et al., 1999). This number is significantly higher than the 19 pptv (18-34 pptv range) of VSLH organic chlorine that was observed in the background LS during DC3. Since the mixing ratio of VSLH organic chlorine in the Background-UT dataset was 124 pptv (range 76-246 pptv), this suggests that the background LS air that was sampled during DC3 may have been diluted with air from the middle and/or upper stratosphere. This is further corroborated by the fact that very long-lived compounds like CFCs and CCl_4 are also largely enhanced in the Outflow-LS dataset relative to the Background-LS dataset.

In Figure 5.3, the average organic chlorine enhancement in overshooting tops (enhancement relative to the background LS) from individual halocarbons is shown. Mixing ratios of CFC-11 and CFC-12 were enhanced by an average of 11 and 12 pptv respectively (resulting in the 33 and 24 pptv of organic chlorine shown in Figure 5.3), while mixing ratios of CFC-113 and CFC-114 were only marginally enhanced. This is a result of the higher mixing

ratios of CFC-11 and CFC-12 that are present in the troposphere (~240 and 540 pptv, respectively) – for example, if mixing ratios of CFC-11 in the LS were 10% lower than in the troposphere, that would result in a larger reduction in organic chlorine than a 10% reduction in CFC-114, which has a tropospheric mixing ratio of ~17 pptv. Also of note are HCFC-22 and CCl_4, which were enhanced by 14 and 5 pptv, respectively (resulting in the 14 and 20 pptv of organic chlorine shown). The large enhancements in organic chlorine from these long-lived halocarbons (lifetimes of 12 and 25 years, respectively) are also due to their relatively high abundances in the troposphere (~240 and 90 pptv, respectively). HCFCs and LLHCs with lower tropospheric abundances were not as greatly enhanced in overshooting tops. Of the shorter-lived halocarbons, CH_3Cl and CH_2Cl_2 produced large enhancements in organic chlorine: mixing ratios of CH_3Cl were enhanced by 50 pptv in overshooting tops, while mixing ratios of CH_2Cl_2 were enhanced by 14.5 pptv in overshooting tops (resulting in the 50 and 29 pptv of organic chlorine shown). This is due to the relatively short lifetimes of these compounds (lifetimes 12 months and 4 months, respectively), and their resulting vertical gradient across the tropopause.

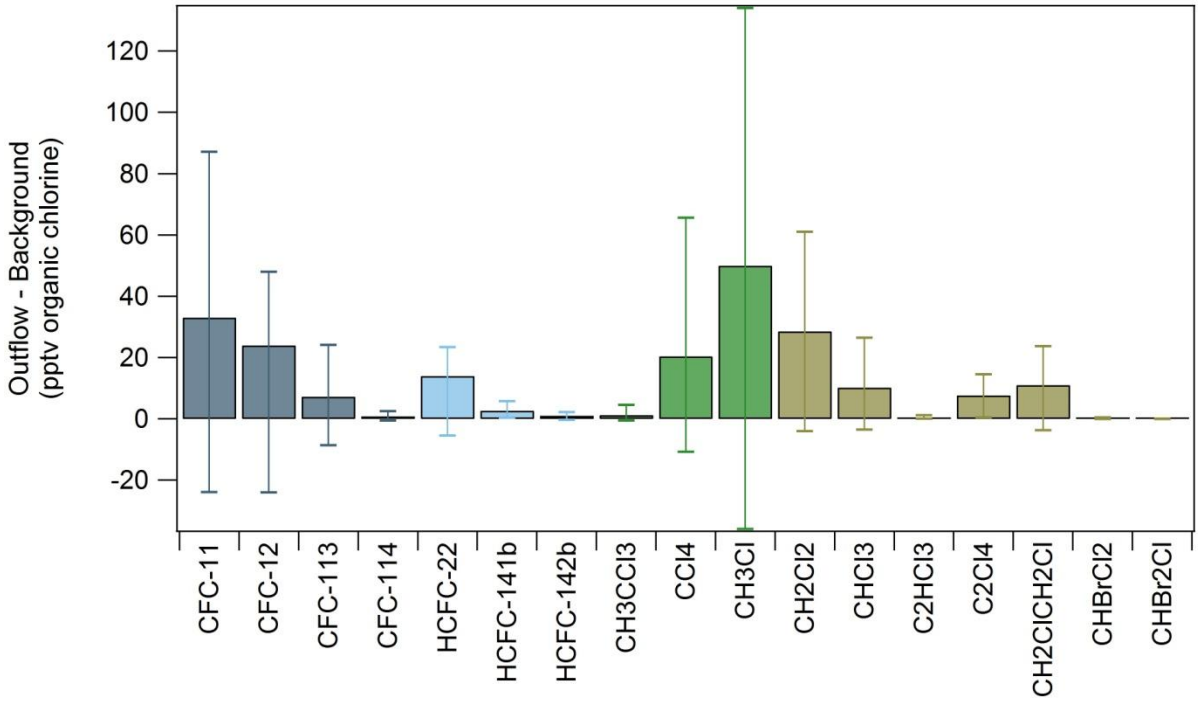

Figure 5.3. The average enhancement of organic chlorine (outflow – background) in overshooting tops for different halocarbon species. CFCs are colored gray, HCFCs are light blue, LLHC are green, and VSLH are colored brown. Error bars are asymmetric and represent the maximum and minimum enhancement for each species. Halons contribute a negligible amount to the total organic chlorine enhancement, and have been omitted for clarity.

Because the Outflow-LS dataset is small (N=5), these calculations cannot be further broken down to examine trends on a regional or flight-by-flight basis while remaining statistically significant.

5.2.2. The Effects of Deep Convection on Organic Chlorine in the UT

Using equations 5.1-5.6, mixing ratios of total organic chlorine and organic chlorine contributions from different halocarbon classes were calculated for each sample in the Outflow-UT and Background-UT datasets. These calculated values are shown in Table 5.2, and are visually represented in Figure 5.4. In contrast to overshooting tops, convective outflow in the UT appears to have, on average, little effect on the total organic chlorine content of the UT. Of all the classes of halocarbons considered here, only organic chlorine from VSLH is, on average, modestly enhanced over background levels. However, mixing ratios of VSLH organic chlorine in

convective outflow have a large range (86 – 247 pptv), and background mixing ratios of VSLH organic chlorine have an even larger range (24 – 249 pptv), including a maximum that is higher than the maximum value measured in convective outflow. This result is unexpected, as VSLH are not predicted to have a large presence in the background UT due to their relatively short lifetimes and the long transport time (around one month) required to reach the UT in the absence of deep convection (Apel et al., 2012; Bechara et al., 2010). The lack of significant enhancement in total organic chlorine and the high variability in total organic chlorine in both convective outflow and the background UT suggest the presence of some highly-varying factor that affects organic chlorine mixing ratios in convective outflow and/or organic chlorine mixing ratios in the background UT. It is possible that this variability is derived from geographic location: Surface sources of chlorinated halocarbons – which are primarily anthropogenic – tend to be unevenly distributed geographically, which would result in a noticeable geographic distribution in organic chlorine mixing ratios in convective outflow, as well. In order to investigate this theory, convective outflow samples and background UT samples were binned based on their geographic location, which allowed direct comparison between co-located outflow and background samples. Another possible source of variability is temporal variation: large day-to-day variations in either the organic chlorine content of convective outflow or the organic chlorine content of the UT background (likely via long-range transport) would result in a wide range of measured enhancements, and a relatively modest average enhancement. Both of these sources of variability (spatial and temporal) are investigated in the remainder of this section.

Table 5.2. Calculated values for total organic chlorine, and the organic chlorine contribution from different classes of halocarbons in the Outflow-UT and Background-UT datasets, where SI samples have been removed from both datasets. All values listed have units of pptv. The average outflow enhancements over background were calculated by subtracting the average value from the Background-UT dataset from the average value from the Outflow-UT dataset. The maximum enhancement was calculated by subtracting the minimum value from the Background-UT dataset from the maximum value from the Outflow-UT dataset (i.e. Outflow-UT max – Background-UT min), and the minimum enhancement was calculated by subtracting the maximum value from the Background-UT dataset from the minimum value from the Outflow-UT dataset (i.e. Outflow-UT min – Background-UT max).

		Total organic chlorine	CFCs	HCFCs	Halons	LLHCs	VSLH
Outflow-UT	Average	3860	2354	318	4.3	1059	167
	max	4407	2415	344	4.5	1607	247
	min	3754	2281	246	3.9	976	86
	St. dev.	56	22	9	0.1	45	17
Background-UT	Average	3840	2354	310	4.3	1047	124
	max	4406	2509	335	4.5	1520	249
	min	3647	2280	291	4	949	24
	St. dev.	90	22	8	0.1	57	33
Outflow enhancement over background	Average	20	0	8	0	12	43
	max	760	135	53	0.5	658	223
	min	--655	-228	-89	-0.6	-544	-163
	St.dev	146	44	17	0.2	102	50

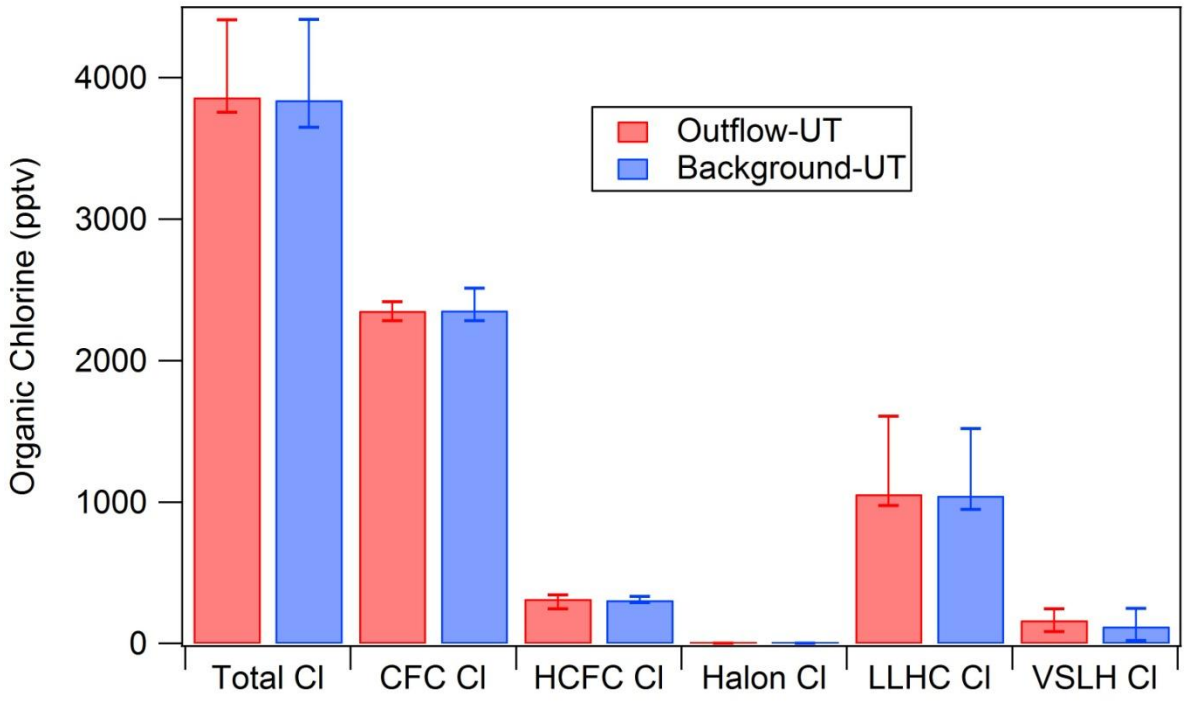

Figure 5.4. A visual representation of the average, maximum, and minimum values of organic chlorine from different classes of halocarbons. Error bars are asymmetric and cover the range of calculated values (i.e. error bars represent the max and min values shown in Table 5.2).

To determine the impact of spatial variability on the overall variability seen in Figure 5.4, samples from the Outflow-UT and Background-UT datasets were binned into 2° x 2° boxes. For each box, the average mixing ratio of total organic chlorine was calculated, and boxes containing fewer than three samples were discarded. The resulting boxes are shown in Figure 5.5. In general, there does not appear to be a significant trend in organic chlorine mixing ratios in either the convective outflow or background UT. That is, high and low values appear to be scattered, particularly in the background UT where the highest and lowest average mixing ratios appear. Using these boxes, the average enhancement in total organic chlorine from convective outflow in a given box was calculated by subtracting the background UT average from the convective outflow average in a given box. If a given box did not have average values for both convective outflow and UT background, this enhancement was not calculated. The resulting boxes are shown in Figure 5.6. These enhancements also appear to be scattered and have no discernible geographic trend. However, it is apparent that the magnitude of the enhancement generally follows the amount of organic chlorine in the background UT. That is, the amount of organic chlorine in the background UT is driving the enhancement due to convection, rather than the convection itself.

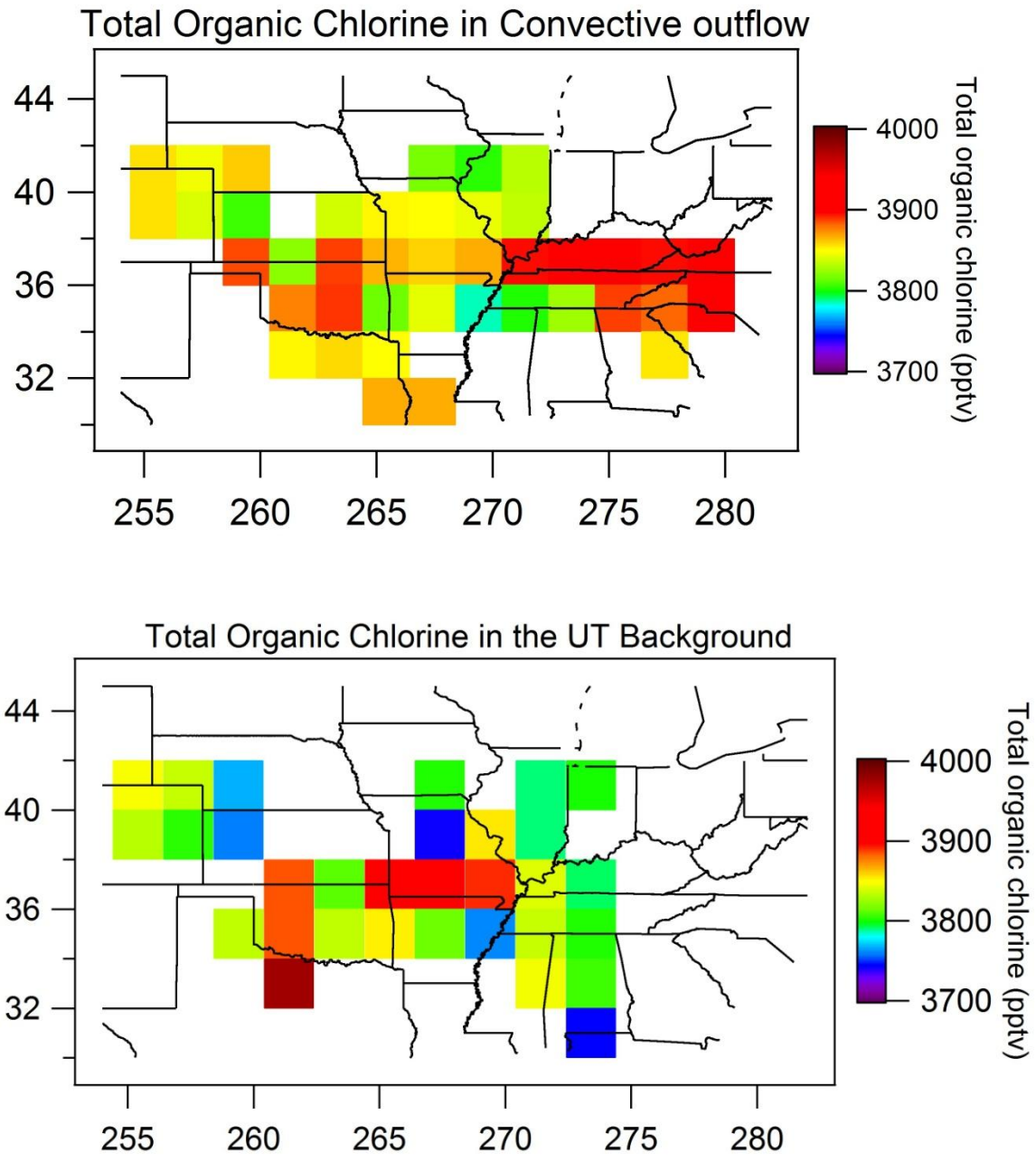

Figure 5.5. Geographic distribution of organic chlorine in convective outflow (top) and in the UT background (bottom) during DC3. Samples were binned into 2° x 2° boxes, and the average value of each box was calculated. Boxes where fewer than three samples were collected are not shown.

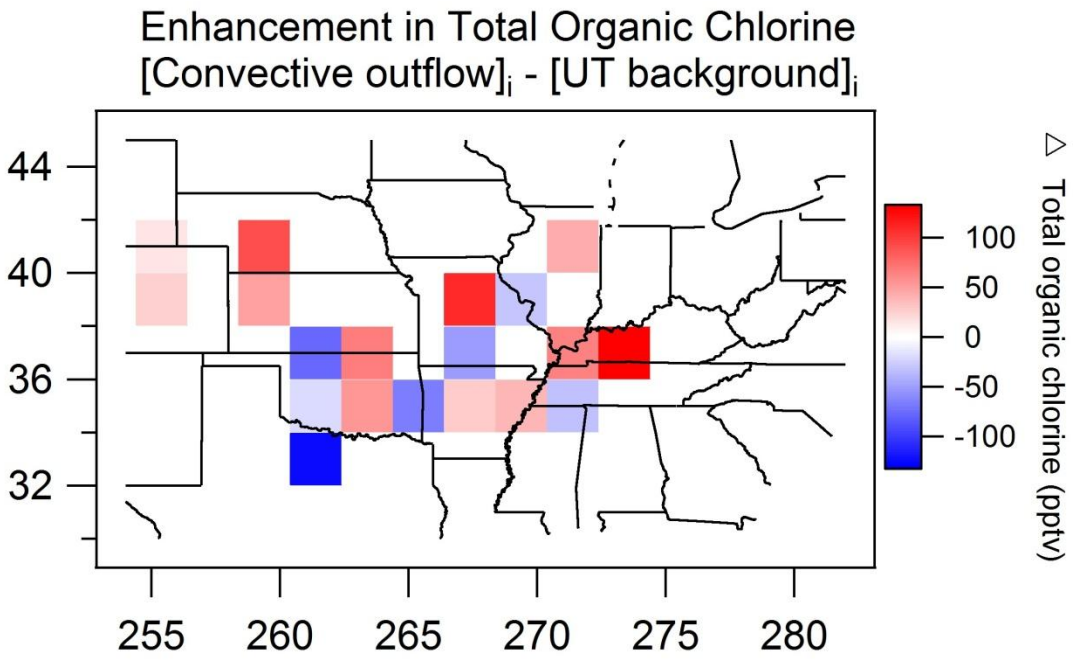

Figure 5.6. Geographic distribution of the enhancement in organic chlorine in convective outflow relative to the UT background. Samples were binned into 2° x 2° boxes, and the average value of each box was calculated.

To check this hypothesis, least squared regressions were made between co-located Outflow-UT boxes and enhancement boxes (i.e. the boxes in the top panel of Figure 5.5 vs. co-located boxes from figure 5.6.), and the Background-UT boxes and co-located enhancement boxes (i.e. the boxes in the bottom panel of Figure 5.5 vs. co-located boxes in figure 5.6.). These linear regressions are presented in Figure 5.7 along with r^2 values for each fit. The r^2 value for the Background-UT fit is 0.75, which indicates a fairly high degree of correlation, while the r^2 value for the Outflow-UT fit is 0.16, which indicates no statistical correlation. Indeed, this result suggests that the degree to which convection affects the total organic chlorine content of the regional UT is a function of the composition of the regional background UT, rather than the composition of convective outflow itself. The Durbin-Watson test was used to determine if the Background-UT fit showed autocorrelation (i.e. a serial correlation between the residuals of adjacent observations) (Durbin and Watson, 1950). The Durbin-Watson statistic (*d*) was

calculated using equation 5.7, where x represents the number of observations (in this case, the number of points shown in Figure 5.7), and e_x represents the residual associated with observation x. Essentially, the Durbin-Watson test calculates the ratio of the sum of the squares of lag_{x-1} residuals to the sum of the squares of residuals:

$$d = \frac{\sum_{x_2}^{x}(e_x - e_{x-1})^2}{\sum_{x_1}^{x} e_x^2} \tag{5.7}$$

Values of d always lie in the range 0-4, where a value of $d = 2$ indicates no autocorrelation, $d < 1$ indicates substantial positive autocorrelation, and $d > 3$ indicates substantial negative autocorrelation. For the Background-UT fit shown in Figure 5.7, a value of $d = 2.15$ was calculated, indicating no significant autocorrelation. The Durbin-Watson test was not applied to the Outflow-UT fit, as the degree of correlation was statistically significant.

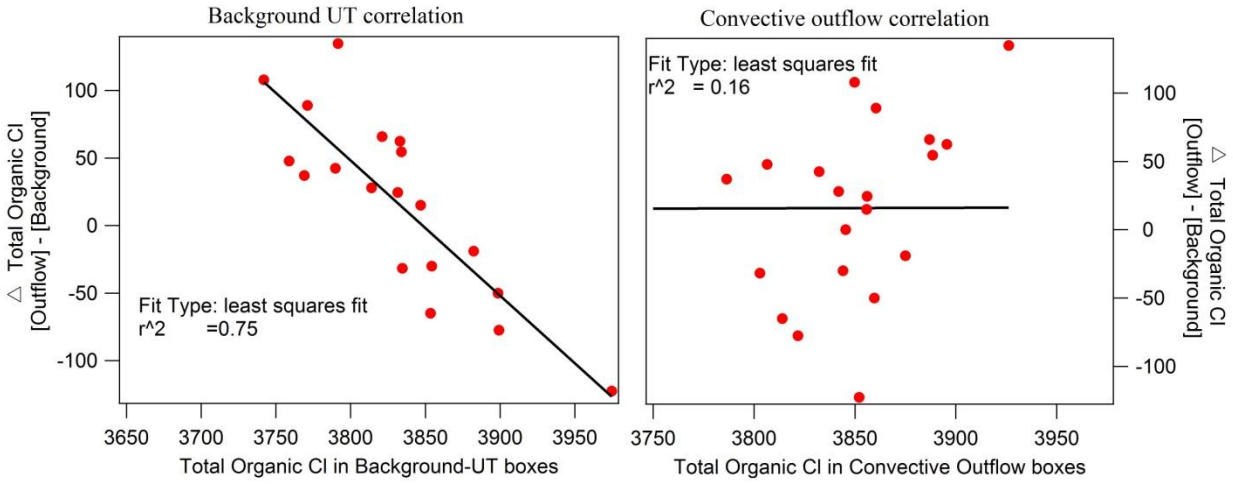

Figure 5.7. Correlations between the total organic chlorine boxes presented in figure 5.5 and the outflow enhancement boxes presented in figure 5.6.

Since VSLH were expected to be the class of halocarbon that is most affected by convection, similar correlations were made for VSLH organic chlorine enhancements, and are shown in Figure 5.8. Indeed, VSLH organic chlorine enhancements in convective outflow are

strongly correlated with the amount of VSLH organic chlorine in the UT background ($r^2 = 0.91$) and show no statistical correlation with the amount of VSLH organic chlorine in convective outflow ($r^2 = 0.20$). These results necessitate a further understanding of the factors that drive the variation in the organic chlorine content and the VSLH organic chlorine content of the background UT. The Durbin-Watson test for autocorrelation (equation 5.7) was applied to the Background-UT fit for VSLH (i.e. the left panel of Figure 5.8), and yielded a value of $d = 2.09$, indicating no significant autocorrelation. This test was not applied to the Outflow-UT fit (i.e. the right panel of Figure 5.8) because the degree of correlation was not statistically significant.

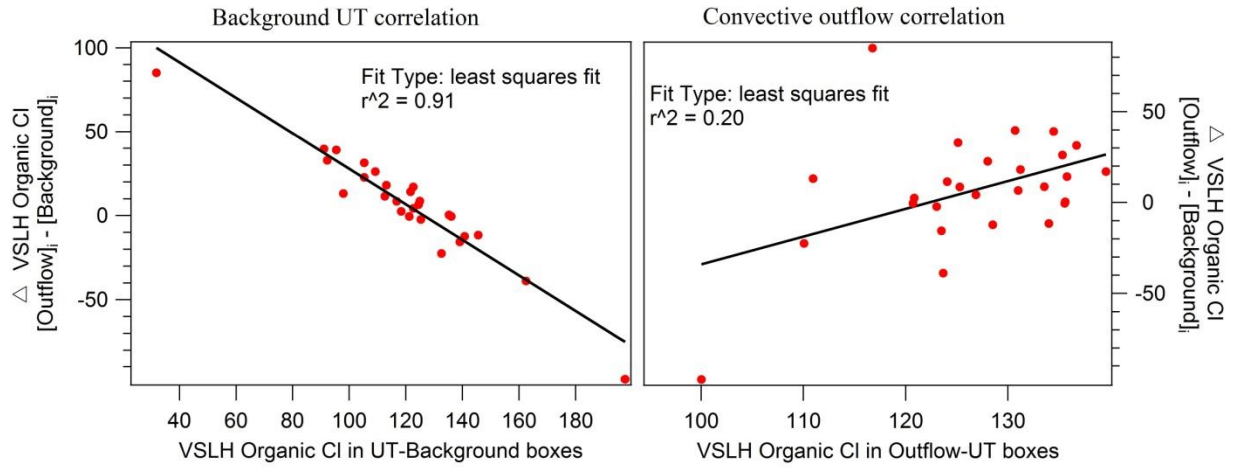

Figure 5.8. Correlations between VSLH organic chlorine in UT background boxes and outflow enhancements (left panel) and between VSLH organic chlorine in convective outflow boxes and outflow enhancement boxes (right panel).

Because the effects of deep convection on the organic chlorine content of the local UT are strongly dependent on the amount of organic chlorine in the background UT, the process(es) that drive the variation in organic chlorine mixing ratios in the background UT must be understood. To investigate this, temporal trends of organic chlorine in convective outflow and in the background UT were evaluated. The average mixing ratio of organic chlorine in the Outflow-UT and Background-UT datasets was calculated for each research flight. The average values (± 1σ)

for total organic chlorine, LLHC organic chlorine, and VSLH organic chlorine are shown in Figure 5.9. Next, the average enhancement from convective outflow (that is, Outflow-UT – Background-UT) for each flight was calculated for total organic chlorine (Figure 5.10), LLHC organic chlorine (Figure 5.11) and VSLH organic chlorine (Figure 5.12). In these figures, a negative enhancement represents a flight in which organic chlorine mixing ratios encountered in the background UT were higher than those in convective outflow.

In Figure 5.9 it is apparent that there is a greater day-to-day variability in background UT organic chlorine mixing ratios than in convective outflow. There also appear to be trends in background UT organic chlorine values: For example, background UT mixing ratios of total organic chlorine reached a local minimum during research flight 12, but then increased during each flight until it peaked during research flight 16. Conversely, VSLH organic chlorine reached a local maximum during research flight 2, and then began decreasing until reaching a local minimum during research flight 6. During both of these events (the build-up during research flights 12-16 and the drop-down during research flights 2-6), organic chlorine mixing ratios in convective outflow stayed relatively stable. These trends are also apparent in Figure 5.10 - 5.12, where enhancements in organic chlorine from convective outflow (relative to the UT background) also reach a local maximum during research flight 6 (when UT background mixing ratios of organic chlorine reached a local minimum), and reach a local minimum during research flight 16 (when UT background mixing ratios reached a local maximum). Of particular interest are research flights 2 and 16, where LLHC organic chlorine and VSLH organic chlorine mixing ratios are significantly higher in the UT background than in convective outflow.

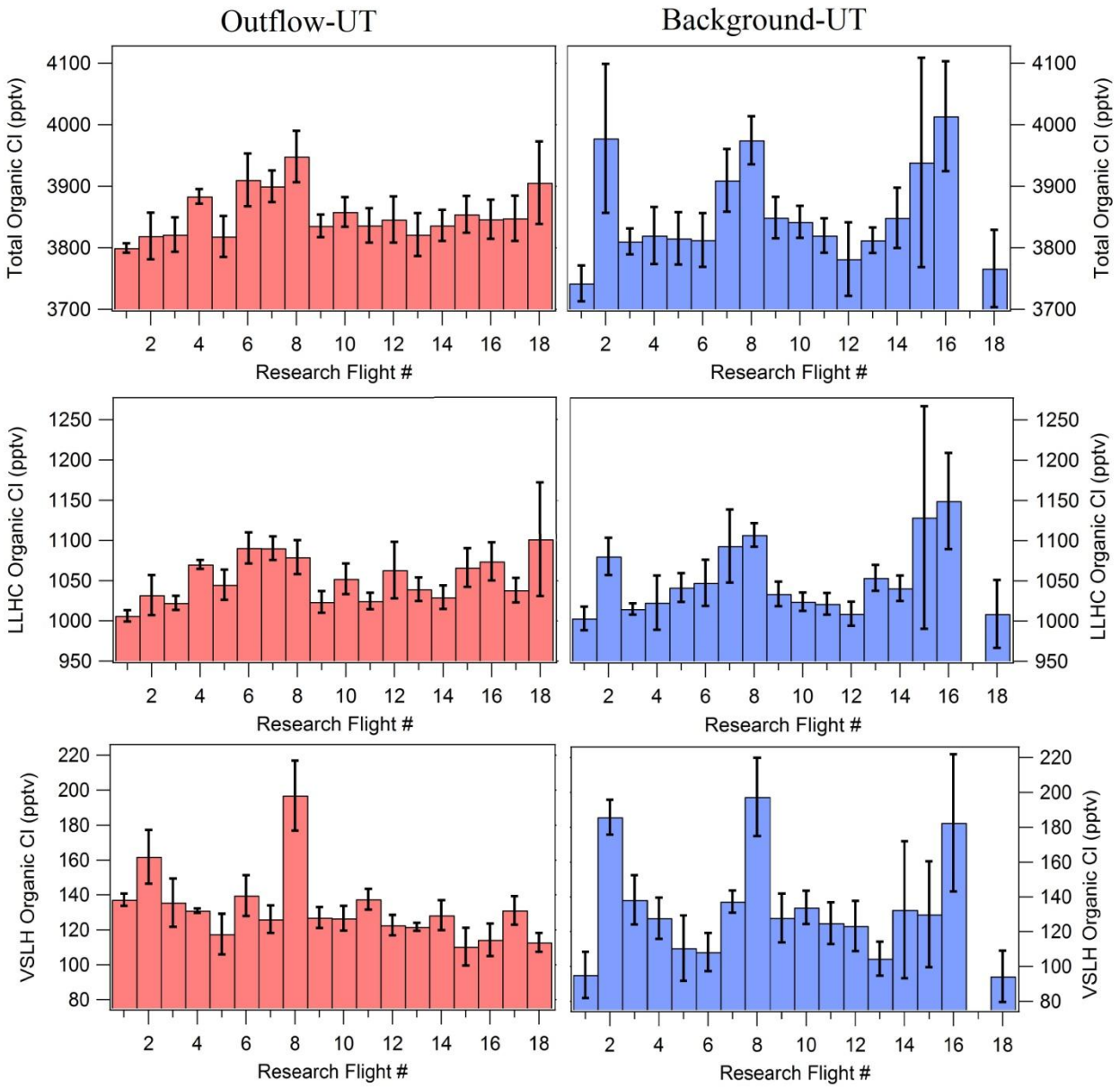

Figure 5.9. The average mixing ratios of total organic chlorine (top panels), LLHC organic chlorine (middle panels), and VSLH organic chlorine (bottom panels) for each research flight from the Outflow-UT (left side) and Background-UT (right side) datasets. Error bars represent ±1σ. Note: no Background-UT samples were collected during research flight 17.

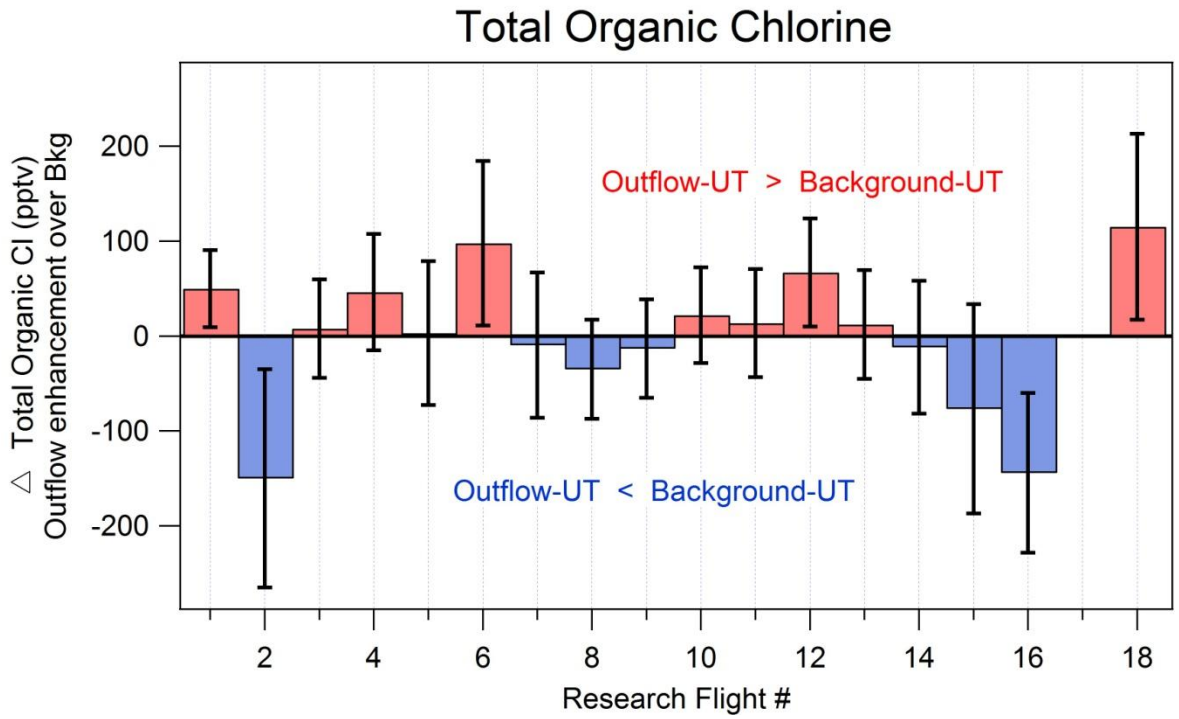

Figure 5.10. The average (±1σ) enhancement in total organic chlorine in convective outflow relative to the UT background for each research flight. Note: no background samples were collected during research flight 17, so the enhancement was not calculated.

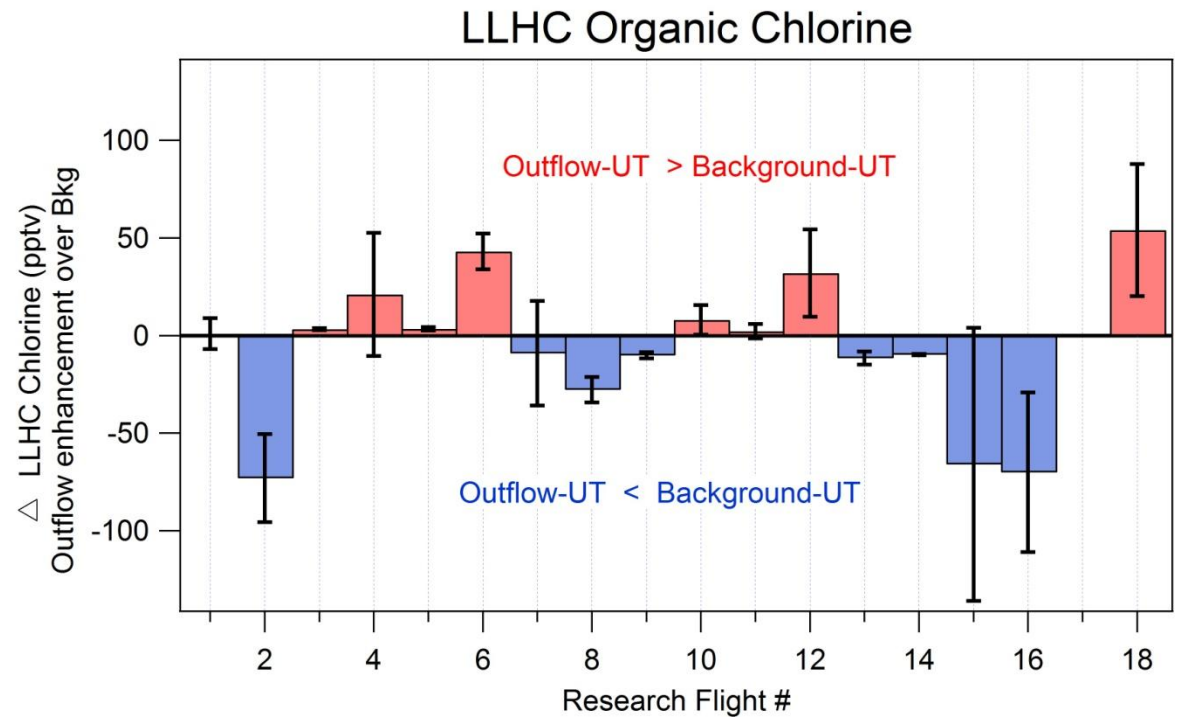

Figure 5.11. The average (±1σ) enhancement in LLHC organic chlorine in convective outflow relative to the UT background for each research flight. Note: no background samples were collected during research flight 17, so the enhancement was not calculated.

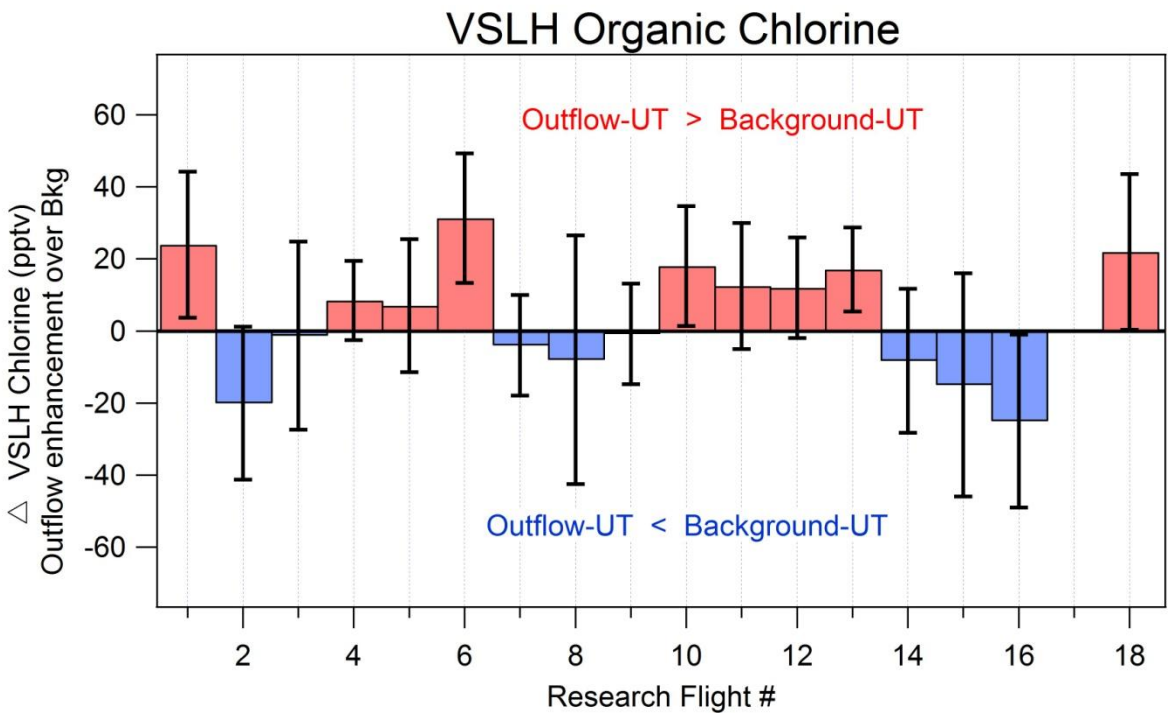

Figure 5.12. The average (±1σ) enhancement in VSLH organic chlorine in convective outflow relative to the UT background for each research flight. Note: no background samples were collected during research flight 17, so the enhancement was not calculated.

The presence of these build-up and drop-down events suggests that a slow, large-scale process such as long-range transport is affecting background UT mixing ratios of organic chlorine. To investigate this hypothesis, back trajectory analyses of the background UT during several research flights were run. Back trajectory analyses were performed using the Global Data Assimilation System (GDAS) meteorological data supplied within the NOAA HYSPLIT lagrangian particle trajectory model. Model runs were initiated using a matrix of 111 initial locations at an initial altitude of 10 km, covering the UT over the entire DC3 study region. Back trajectory analyses were carried out for 168 hours (7 days) for research flights of interest. While the HYSPLIT model does not accurately represent small-scale local convection, it does accurately depict large-scale flow and long-range transport. Back trajectory analyses were carried out for research flights 1, 2, 6, 8, 12, and 16. These flights were chosen because they represent a range of organic chlorine enhancements and cover much of the variability in

background UT mixing ratios of total organic chlorine, LLHC organic chlorine, and VSLH organic chlorine. Depictions of these back trajectories are available in the Appendix of this section. In general, research flights 2, 8, and 16 (flights with blue bars in Figure 5.10, which represent a flight in which higher organic chlorine mixing ratios were observed in the background UT than in convective outflow) showed a strong influence from Eastern Asia, while research flights 1, 6, and 12 (flights with red bars in Figure 5.10, which represent a flight in which higher organic chlorine mixing ratios were observed in convective outflow than in the background UT) showed a strong influence from the central Pacific Ocean and a minor influence from East Asia.

The results obtained from these back trajectories are consistent with the calculated mixing ratios of total organic chlorine, LLHC organic chlorine, and VSLH organic chlorine in the UT background. The presence of airmasses originating from East Asia in the UT background over the central US on some days would imply higher mixing ratios of chlorinated halocarbons during those days, since many chlorinated halocarbons have strong anthropogenic sources and are often most heavily-used in East Asia. On the other hand, since few chlorinated halocarbons have strong oceanic sources, the presence of airmasses originating from the central Pacific on some days would imply relatively low levels of chlorinated halocarbons in the background UT during those days.

Further analysis of the chemical composition of the background UT was used to confirm the presence of airmasses originating from East Asia and airmasses originating from the central Pacific. Research flights in which organic chlorine in the background UT was enhanced over organic chlorine in convective outflow (i.e. research flights 2, 8, 15, and 16 – the suspected "East

Asian Influence" flights) were binned together, and research flights in which organic chlorine in convective outflow was enhanced over organic chlorine in the background UT (i.e. research flights 1, 4, 6, 10, 12, and 18 – the suspected "Oceanic Influence" flights) were binned together. The average, standard deviation, maximum, and minimum values for these bins were calculated and are presented in Table 5.3.

Table 5.3. Compiled averages from the Background-UT dataset for selected research flights. All mixing ratios have units of pptv unless otherwise noted.

	Research flights 1, 4, 6, 10, 12, 18 (Suspected Oceanic Influence)				**Research flights 2, 8, 15, 16 (Suspected East Asian Influence)**			
	avg	**st. dev**	**max**	**min**	**avg**	**st. dev**	**max**	**min**
CO (ppbv)	89	16	130	63	167	22	188	94
PAN	93	59	218	24	264	111	601	109
HCHO (ppbv)	111	88	313	26	163	109	427	82
Methyl Nitrate	2.30	1.42	7.27	0.76	1.76	0.44	2.68	0.94
$CHBr_3$	0.38	0.20	0.82	0.02	0.30	0.12	0.48	0.02
HCFC-22	240	7	255	227	248	5	262	240
HCFC-141b	22.3	1.1	24.4	19.5	23.4	1.6	26.9	21.2
HCFC-142b	22.2	0.6	23.5	20.8	22.7	0.6	23.9	21.6
CH_3Cl	641	35	730	573	737	111	1137	626
CH_3CCl_3	5.8	0.2	6.3	5.1	5.7	0.2	6.2	5.4
CCl_4	91	2	94	84	92	2	98	89
CH_2Cl_2	30	6	39	17	45	11	67	28
$CHCl_3$	8.6	1.1	10.5	6.8	11.3	2.5	16.1	7.1
C_2Cl_4	1.76	0.46	2.77	0.95	2.59	0.74	3.75	1.13
C_2HCl_3	0.08	0.09	0.29	LOD	0.11	0.09	0.33	LOD
CH_2ClCH_2Cl	9.5	3.5	17.8	2.7	17.5	7.5	31.7	2.9
$CHBrCl_2$	0.15	0.03	0.21	0.07	0.14	0.03	0.20	0.08
$CHBr_2Cl$	0.08	0.03	0.16	0.02	0.59	0.14	0.80	0.21

In Table 5.3, mixing ratios of HCFCs, LLHC, and VSLH are presented, while CFCs and halons were omitted due to their lack of variability. In general, the suspected "East Asian-

influenced" flights featured higher mixing ratios of most chlorinated halocarbons than the suspected "oceanic-influenced" flights. HCFCs were modestly higher in these flights (HCFC-22 higher by ~3%, HCFC-141b and HCFC-142b higher by ~5% and ~3%, respectively), which suggests an East Asian influence, as the most significant global source of HCFCs is China. Of the LLHCs, only mixing ratios of CH_3Cl were significantly higher in the "East Asian-influenced" flights than the "oceanic-influenced" flights (~15%). Mixing ratios of many chlorinated VSLH were also higher in the "East Asian-influenced" flights, including CH_2Cl_2 (higher by ~50%), $CHCl_3$ (higher by ~30%), C_2Cl_4 (higher by ~50%), and CH_2ClCH_2Cl (higher by ~85%). These chlorinated VSLH all have anthropogenic sources (many of which are produced by coal burning), which provides further evidence that the background UT sampled during some research flights was affected by long-range transport from East Asia. Additional anthropogenic tracers, including CO, peroxy acetyl nitrate (PAN), and HCHO were included in this analysis. Mixing ratios of these tracers were also significantly higher in the suspected "East Asian-influenced" flights. Mixing ratios of CO, which is primarily produced during combustion, were higher by ~90%, while mixing ratios of PAN and HCHO, which are tracers of photochemical oxidation (furthermore, PAN is only produced in the presence of NO_x), were higher by ~180% and ~50%, respectively. Tracers of oceanic influence, such as $CHBr_3$ and methyl nitrate, had lower mixing ratios in the suspected "East Asian-influenced" flights than in the suspected "Oceanic-influence" flights, but not by a statistically significant amount. Given the evidence at hand, it is clear that research flights with high background UT mixing ratios of organic chlorine were affected, to varying degrees, by long-range transport of airmasses from East Asia. Meanwhile, other research flights were affected, to varying degrees, by long-range transport of airmasses from the central Pacific and had lower mixing ratios of organic chlorine.

Linear least squares regressions were made between the average total organic chlorine enhancement for each flight (as shown in Figure 5.10) and the mixing ratio of organic chlorine in convective outflow in the UT and in the background UT for each flight, and are shown in Figure 5.13. In general, fits with organic chlorine in convective outflow show no statistical correlation, while fits with organic chlorine in the background UT show modest correlations. The Durbin-Watson test was performed for each regression had an r^2 value greater than 0.30, and no evidence of autocorrelation was found. The sum of VSLH organic chlorine and LLHC organic chlorine in the background UT (bottom panel of Figure 5.13) yields a high degree of correlation ($r^2 = 0.74$) with the convective outflow enhancement (nearly as high as the degree of correlation between convective outflow enhancement and total organic chlorine in the background UT, where $r^2 = 0.76$), meaning that, on a flight-by-flight basis, nearly all of the variation in organic chlorine enhancements from convective outflow are due to these two classes of halocarbon.

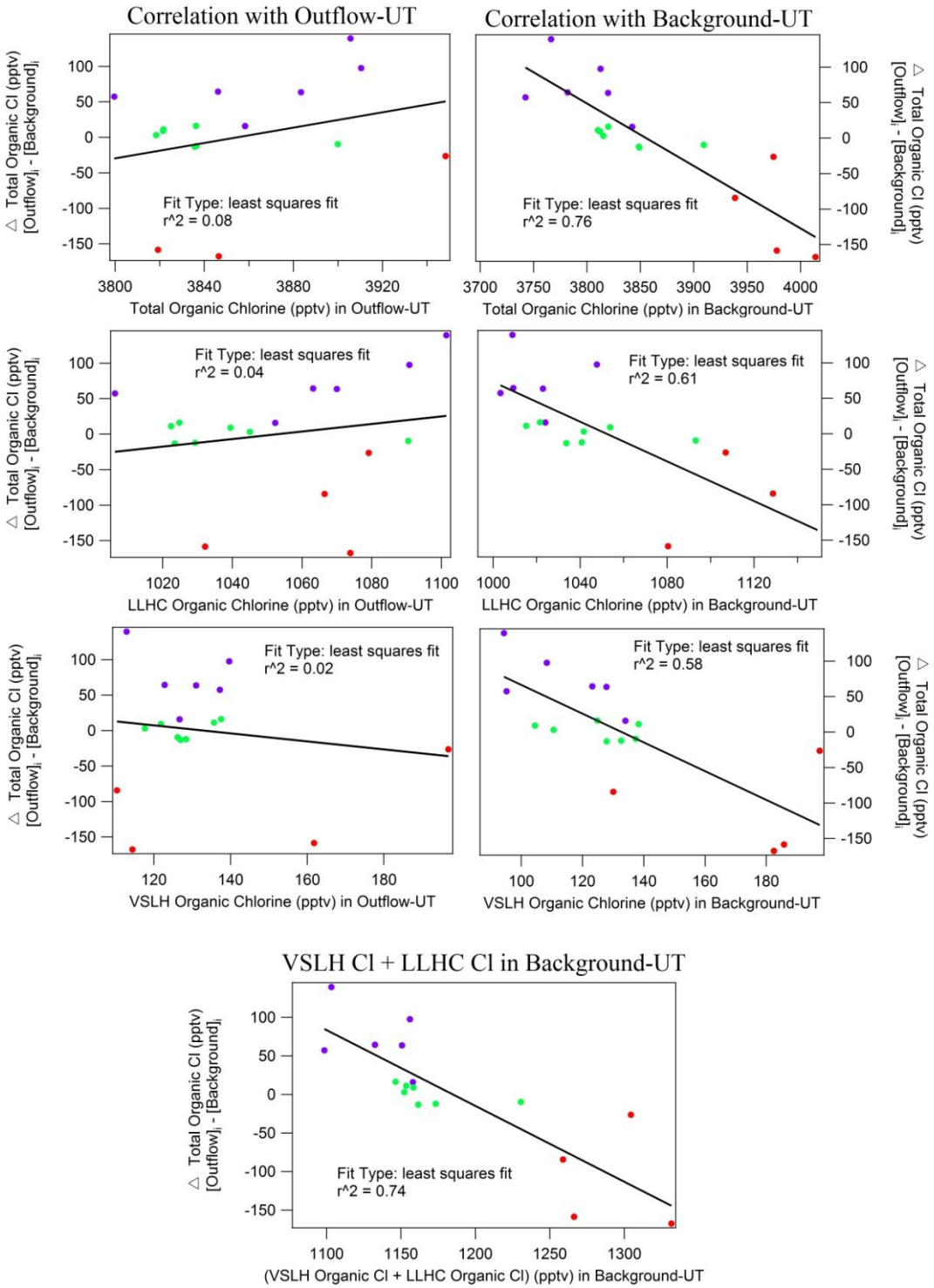

Figure 5.13. Correlations between the average total organic chlorine enhancement in convective outflow from each flight (i.e. the average mixing ratio of organic chlorine in the convective outflow of flight *i* minus the average mixing ratio of organic chlorine in the background UT of flight *i*) and the organic chlorine contribution from different halocarbon species. Panels on the left show correlations between enhancements and organic chlorine in convective outflow, while panels on the right shown correlations between enhancements and organic chlorine in the background UT. The bottom panel shows the correlation between the outflow enhancement in organic chlorine and the sum of organic chlorine from VSLH and LLHC. All graphs are color-coded as follows: purple points represent "oceanic-influenced" flights, red points represent "East Asian-influenced" flights, and green points represent flights where the background UT was likely influenced by both regions.

The results presented in this section indicate that deep convection over the central US can affect the organic chlorine content of the UT on a regional scale. However, the sign and magnitude of this effect are highly dependent on the organic chlorine content of the background UT rather than on the organic chlorine content of the convective outflow itself. During flights where the UT background was strongly-influenced by relatively clean air from the central Pacific, deep convection enhanced the local mixing ratio of organic chlorine in the UT. The largest enhancement in total organic chlorine from deep convection that was observed during any DC3 flight was 115 ± 98 pptv, which occurred during research flight 18. During this flight organic chlorine from LLHC was enhanced by 34 ± 22 pptv over the local UT background, while organic chlorine from VSLH was enhanced by 22 ± 21pptv over the local UT background. On the other hand, when the UT background was strongly-influenced by the long-range transport of polluted air from East Asia, deep convection actually lowered the local mixing ratio of organic chlorine in the UT. During research flight 2, mixing ratios of total organic chlorine in the background UT were 150 ± 115 pptv higher than those in convective outflow. During this flight, mixing ratios of organic chlorine from LLHC and VSLH were also higher in the background UT than in convective outflow (LLHC organic chlorine was higher by 73 ± 23 pptv and VSLH organic chlorine was higher by 24 ± 20 pptv).

5.3. Organic Bromine in the UT/LS

As described in Chapter 1, atomic bromine catalytically destroys O_3 about 60 times more efficiently than atomic chlorine (Molina and Rowland, 1974; Montzka et al., 2010; Stolarski and Cicerone, 1974). Of the classes of halocarbon discussed in Chapter 1, only halons, LLHC and

VSLH contribute to the organic bromine content of an airmass. Halons have purely anthropogenic sources, while brominated LLHC and VSLH tend to have strong biogenic sources (primarily oceanic) and small anthropogenic sources (Montzka et al., 2010). Because DC3 focused on continental convection rather than marine convection and the convective outflow sampled during DC3 showed anthropogenic influence (see Chapter 3), we expect the deep convection sampled during DC3 to provide a modest enhancement in mixing ratios of organic bromine in the UT/LS. Of all of the classes of halocarbon considered here, UT/LS mixing ratios of brominated LLHC and VSLH are expected to be most affected by the presence of convection because of their short lifetimes. Unlike the diverse group of chlorinated LLHC considered in section 5.2, only one brominated LLHC, CH_3Br, was measured during DC3. It should be noted that, of all of the LLHC considered in this dissertation, CH_3Br has the shortest atmospheric lifetime (~ 8 months) and falls only just above the six-month lifetime cutoff used to differentiate LLHC from VSLH. Thus, while the definitions of LLHC and VSLH used in the literature would consider CH_3Br a LLHC, its vertical distribution in the atmosphere more closely resembles that of a VSLH than a very-long-lived halocarbon (Montzka et al., 2010).To be consistent with the literature, CH_3Br is considered a LLHC in this work. This section will be partitioned into two subsections that focus on the effects of convection on mixing ratios of organic bromine in the UT and LS, respectively.

5.3.1. The Effects of Deep Convection on the Organic Bromine in the LS

Using equations 5.1-5.6, mixing ratios of total organic bromine and organic bromine contributions from different halocarbon classes were calculated for each sample in the Outflow-LS and Background-LS dataset. These calculated values are shown in Table 5.4, and are visually represented in Figure 5.14. Mixing ratios of total organic bromine in the Outflow-LS dataset are

higher than those of the Background-LS dataset by an average of 2.8 ± 3.2 pptv (± 1σ). Of all the classes of halocarbon considered here, VSLH (VSLH organic bromine enhanced by 1.3 ± 1.9 pptv) contribute the most to this enhancement over the background LS, while both halons and LLHC contribute less to the total organic bromine enhancement (organic bromine from both halons and LLHC were enhanced by 0.8 ± 1.2 pptv in outflow). Because the standard deviations are quite large (larger than the average enhancement in all cases), the range of enhancements should also be considered. The maximum enhancement for a given species (i.e. total bromine, bromine from halons, etc.) was calculated by subtracting the minimum value from the Background-LS dataset from the maximum value from the Outflow-LS dataset, and is shown in Figure 5.15. The minimum and maximum enhancements were using the method described in section 5.2.1. The large ranges of enhancements presented here may further suggest some limitations of the filtering process described in Chapter 3. Because both the Outflow-LS and Background-LS datasets are quite small (N=5 and N=11, respectively), this cannot be remedied by creating a new tracer for convection above the tropopause.

Table 5.4. Calculated values for total organic chlorine, and the organic chlorine contribution from different classes of halocarbons in the Outflow-UT and Background-UT datasets, where SI samples have been removed from both datasets. All values listed have units of pptv. The average outflow enhancements over background were calculated by subtracting the average value from the Background-UT dataset from the average value from the Outflow-UT dataset. The maximum enhancement was calculated by subtracting the minimum value from the Background-UT dataset from the maximum value from the Outflow-UT dataset (i.e. Outflow-UT max – Background-UT min), and the minimum enhancement was calculated by subtracting the maximum value from the Background-UT dataset from the minimum value from the Outflow-UT dataset (i.e. Outflow-UT min – Background-UT max).

		Total organic bromine	**Halons**	**LLHCs**	**VSLH**
Outflow-LS	Average	19.1	8.4	8.4	2.2
	max	22.1	9.3	9.0	3.9
	min	16.5	7.6	7.6	0.7
	St. dev.	2.7	0.8	0.6	1.5
Background-LS	Average	16.1	7.6	7.6	0.9
	max	16.8	7.9	8.4	1.6
	min	14.2	6.6	6.6	0.6
	St. dev.	0.5	0.4	0.6	0.4
Outflow enhancement over background	Average	2.8	0.8	0.8	1.3
	max	7.9	2.7	2.4	3.3
	min	-0.3	-0.3	-1.2	-0.9
	St.dev	3.2	1.2	1.2	1.9

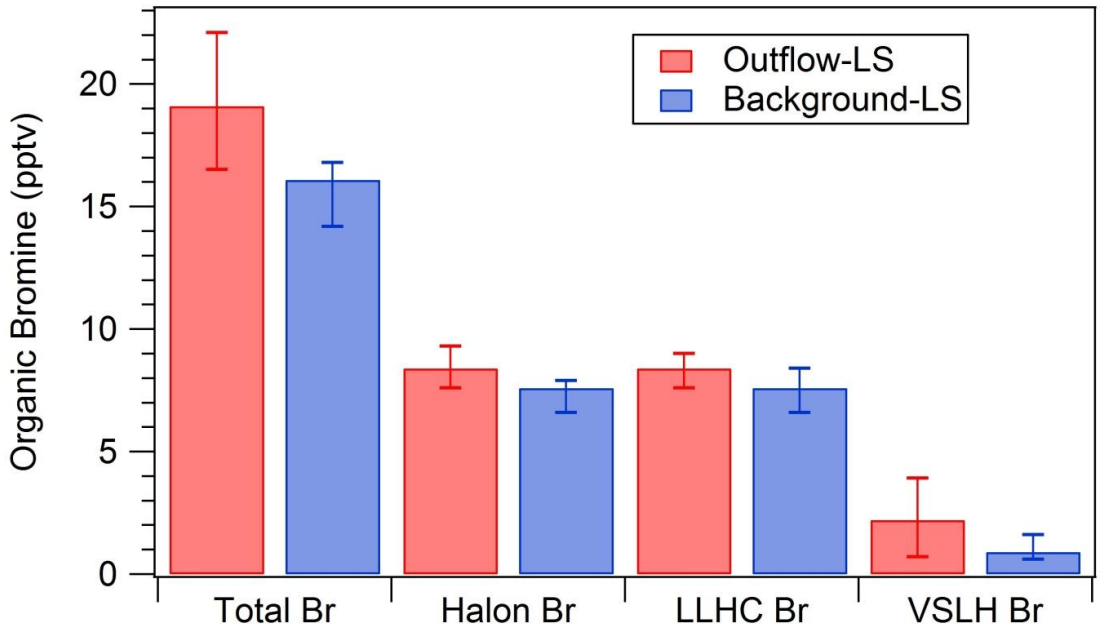

Figure 5.14. A visual representation of the average, maximum, and minimum values of organic bromine from different classes of halocarbons. Error bars are asymmetric and cover the range of calculated values (i.e. error bars represent the max and min values shown in Table 5.4).

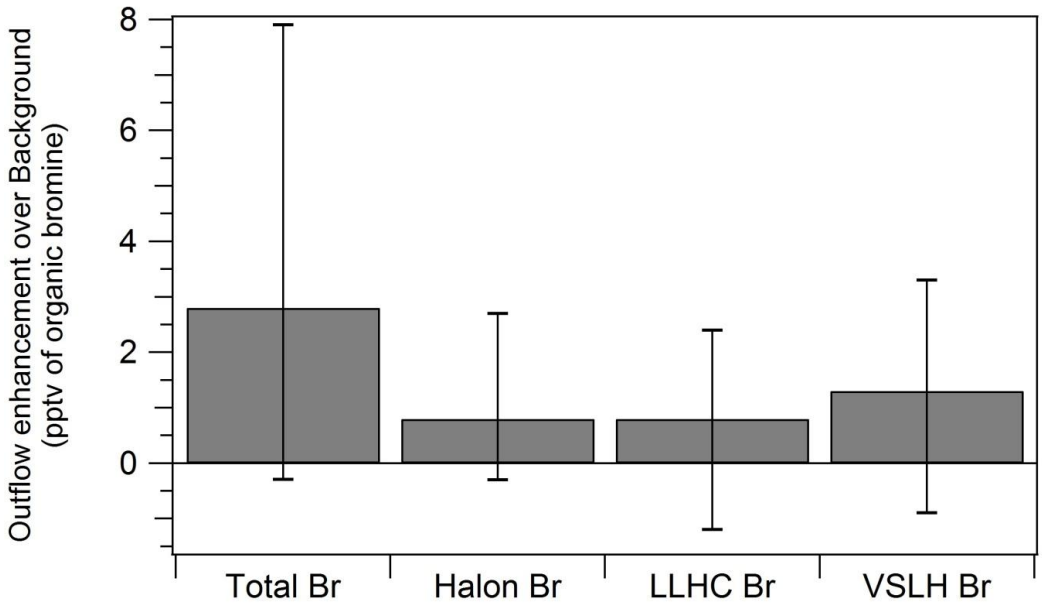

Figure 5.15. A visual representation of the average enhancement of organic chlorine in the Outflow-LS dataset relative to the Background-LS dataset. Error bars are asymmetric and represent the calculated range of enhancements (i.e. the min and max enhancements calculated in Figure 5.14).

Previous airborne studies of the tropical UT, such as PEM-West A and B, TC4, Pre-AVE, and CR-AVE, estimate the amount of organic bromine from VSLH entering the stratosphere to be 2.7 pptv (range 1.4 – 4.6 pptv) (Laube et al., 2008; Law and Sturges, 2006; Montzka et al., 2010; Schauffler et al., 1999). Additional estimates of the organic bromine contribution from VSLH in the stratosphere were obtained using ground- and space-based vertical profile measurements of BrO and subtracting the modeled BrO contributions from halons and LLHC (Hendrick et al., 2008; McLinden et al., 2010; Salawitch et al., 2010; Sinnhuber et al., 2005; Theys et al., 2007). These studies estimate ~ 6 pptv (range 0-11 pptv) of bromine in the stratosphere originated from VSLH. All of these studies are higher than the 0.9 pptv (range 0.6 – 1.6 pptv) of VSLH organic bromine measured in the LS during DC3. As discussed in section 5.2.1, the lower mixing ratio of VSLH organic bromine measured in the background LS during DC3 was likely a result of the midlatitude location of the study, and the associated dilution of TTL air with air from the middle stratosphere as it moves poleward towards the midlatitudes.

In Figure 5.16, the average organic bromine enhancement in overshooting tops (enhancement relative to the background LS) from individual halocarbons is shown. H-1211 and H-1301, which each contain one bromine atom, contributed an average of 0.20 and 0.53 pptv of organic bromine to the average enhancement, while H-2402 was enhanced by a negligible amount. The LLHC CH_3Br contributed an average of 0.82 pptv of organic bromine to the average enhancement. Of the brominated VSLH, CH_2Br_2 and $CHBr_3$ were the most enhanced in convective outflow (enhancements of 0.3 and 0.25 pptv, respectively), and contributed averages of 0.6 and 0.75 pptv of organic bromine to the enhancement.

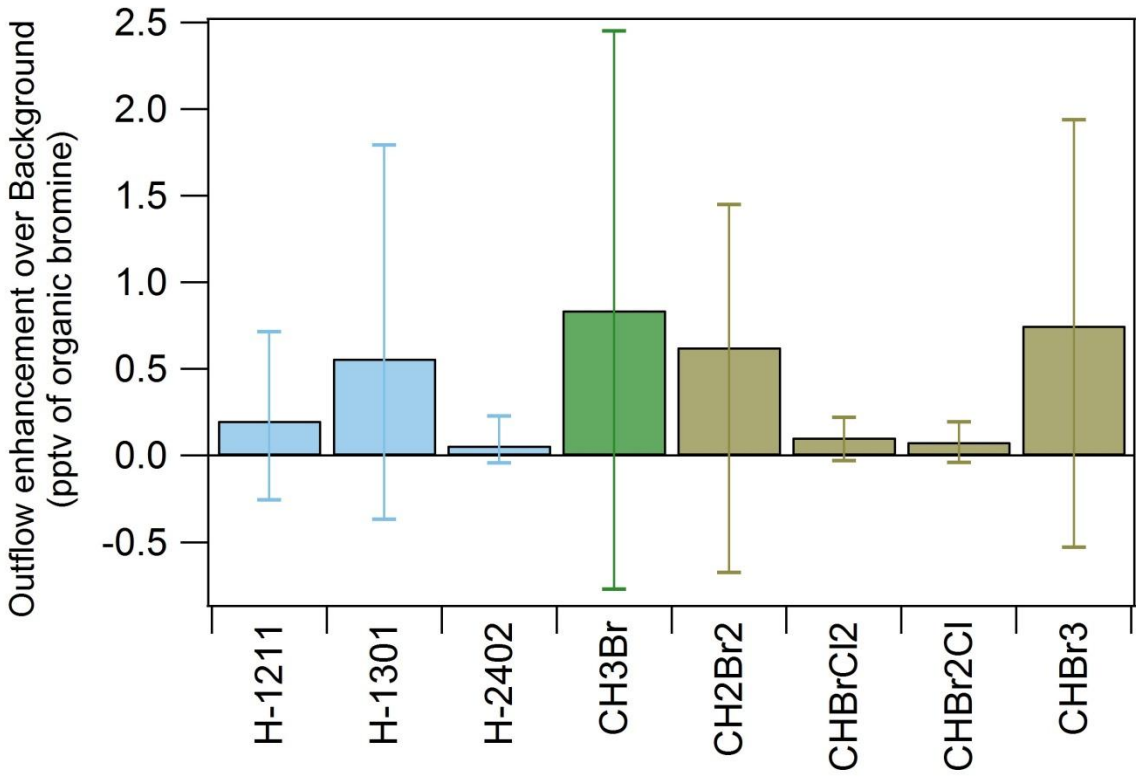

Figure 5.16. The average enhancement of organic bromine (outflow – background) in overshooting tops for different halocarbon species. Halons are colored cyan, LLHCs (CH_3Br) are green, and VSLH are colored tan. Error bars are asymmetric and represent the maximum and minimum enhancement for each species.

5.3.2. The Effects of Deep Convection on Organic Bromine in the UT

Using equations 5.1-5.6, mixing ratios of total organic bromine and organic bromine contributions from different halocarbon classes were calculated for each sample in the Outflow-UT and Background-UT datasets. These calculated values are shown in Table 5.5. In contrast to organic chlorine, which had, on average, a negligible enhancement in convective outflow relative to the background UT, organic bromine was, on average, modestly enhanced in convective outflow relative to the background UT – although the associated uncertainty for this enhancement is quite large (relative standard deviation of 220%). Of all the classes of halocarbons considered here, only organic bromine from VSLH was, on average, modestly

enhanced over background levels – although the associated uncertainty for this enhancement is also quite large (relative standard deviation of 180%). Just as in section 5.2.2, geographic variability in the organic bromine content of convective outflow or the organic bromine content of the background UT could be driving the variability in the organic bromine enhancement noted here. Even though DC3 focused on continental convection, the surface of the south and central US is often influenced by warm, moist air from the Gulf of Mexico. In fact, this warm, moist air is the driving force behind the genesis of much of the convection over the region (Barth et al., 2014). Thus, it is possible that regions close to the Gulf of Mexico (such as Alabama or Oklahoma) may have higher mixing ratios of organic bromine than regions far from the Gulf of Mexico (such as Colorado), and a detectable geographic trend in mixing ratios of organic bromine will be observed. To investigate this, convective outflow samples and background UT samples were binned based on their geographic location, which allowed direct comparison between co-located outflow and background samples. Another possible source of variability is temporal variation. In section 5.2.2 it was noted that the organic chlorine content of the background UT was highly variable and was influenced by long-range transport of air from East Asia and the central Pacific. In this section we will also investigate the effects of long-range transport on the organic bromine content of the background UT, and how this affects the magnitude of enhancement in organic bromine from convective outflow.

Table 5.5. Calculated values for total organic chlorine, and the organic chlorine contribution from different classes of halocarbons in the Outflow-UT and Background-UT datasets, where SI samples have been removed from both datasets. All values listed have units of pptv. The average outflow enhancements over background were calculated by subtracting the average value from the Background-UT dataset from the average value from the Outflow-UT dataset. The maximum enhancement was calculated by subtracting the minimum value from the Background-UT dataset from the maximum value from the Outflow-UT dataset (i.e. Outflow-UT max – Background-UT min), and the minimum enhancement was calculated by subtracting the maximum value from the Background-UT dataset from the minimum value from the Outflow-UT dataset (i.e. Outflow-UT min – Background-UT max).

		Total organic bromine	**Halons**	**LLHCs**	**VSLH**
Outflow-UT	Average	22.5	8.4	9.2	4.8
	max	81.0	9.6	66.6	15.3
	min	18.1	7.9	7.6	1.0
	St. dev.	4.0	0.2	2.9	2.5
Background-UT	Average	19.9	8.5	8.8	2.6
	max	28.4	9.0	14.9	11.2
	min	15.6	7.5	7.2	0.2
	St. dev.	1.8	0.2	0.8	1.5
Outflow enhancement over background (ppt)	Average	2.6	-0.1	0.4	2.2
	max	65.4	2.1	59.4	15.1
	min	-10.3	-1.1	-7.3	-10.2
	St.dev	5.8	0.4	3.7	4.0

To determine the impact of spatial variability on the overall variability in organic bromine enhancements from convective outflow, samples from the Outflow-UT dataset were binned into boxes based on their geographic area, as described in section 5.2.2. These boxes are shown in Figure 5.17. For the convective outflow boxes (top panel of Figure 5.17), there appears to be relatively high organic bromine mixing ratios over the great plains and lower mixing ratios towards the south and east. For the background UT boxes, the opposite is true, and the highest mixing ratios were observed near the Gulf States. However, the range of values for the background UT boxes is smaller than the range of values for the convective outflow boxes. Using these boxes, the enhancement in total organic bromine from convective outflow in a given box was calculated, as described in section 5.2.2. This is shown in Figure 5.18. These enhancements are generally positive (that is, there was more organic bromine in the convective outflow samples in each box than the background UT samples) and have no discernible

geographic trend. However, it is apparent that the magnitude of the enhancement generally follows the amount of organic bromine in the convective outflow, rather than the UT background as was the case for organic chlorine.

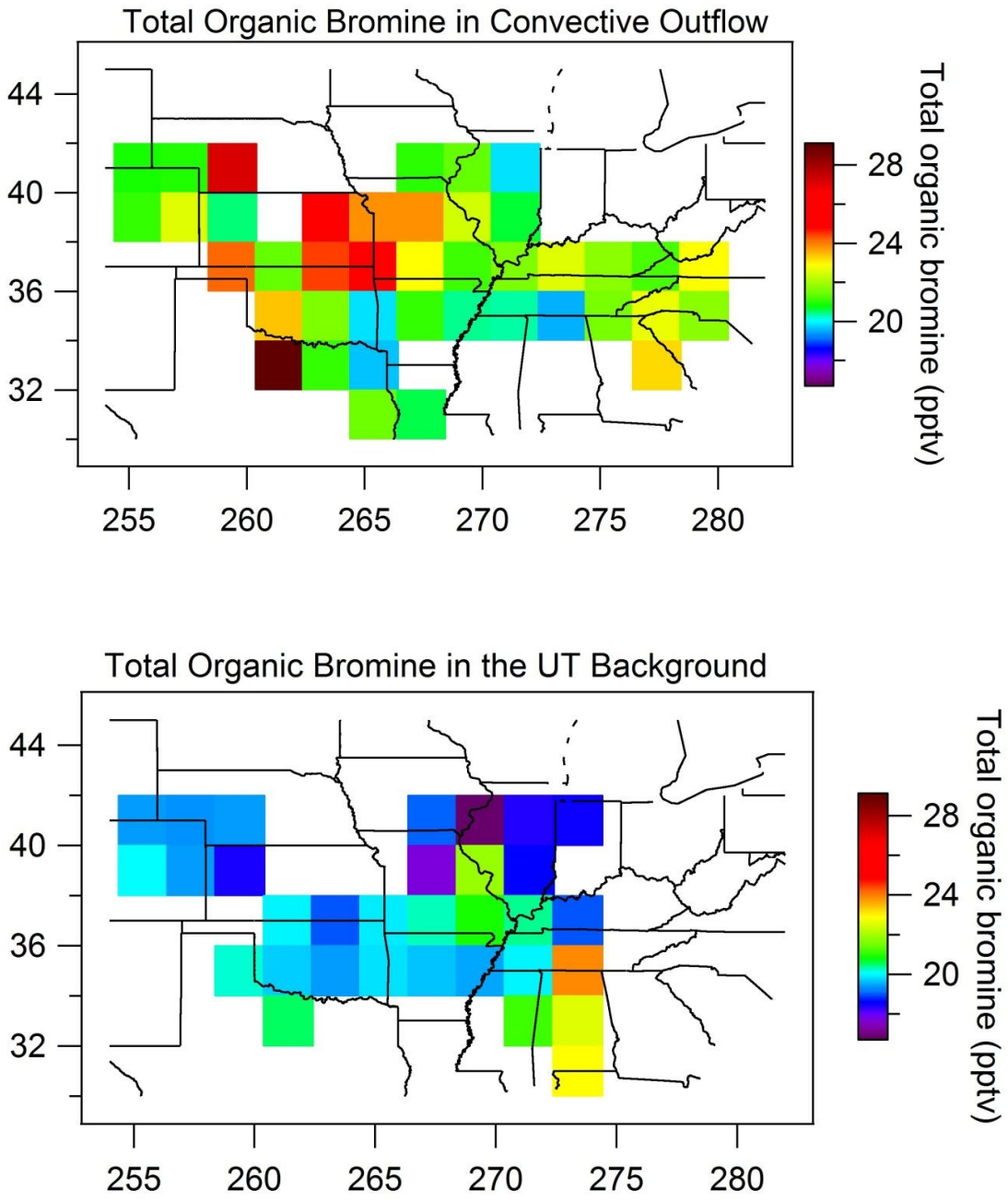

Figure 5.17. Geographic distribution of organic bromine in convective outflow (top) and in the UT background (bottom) during DC3. Samples were binned into 2° x 2° boxes, and the average value of each box was calculated. Boxes where fewer than three samples were collected are not shown.

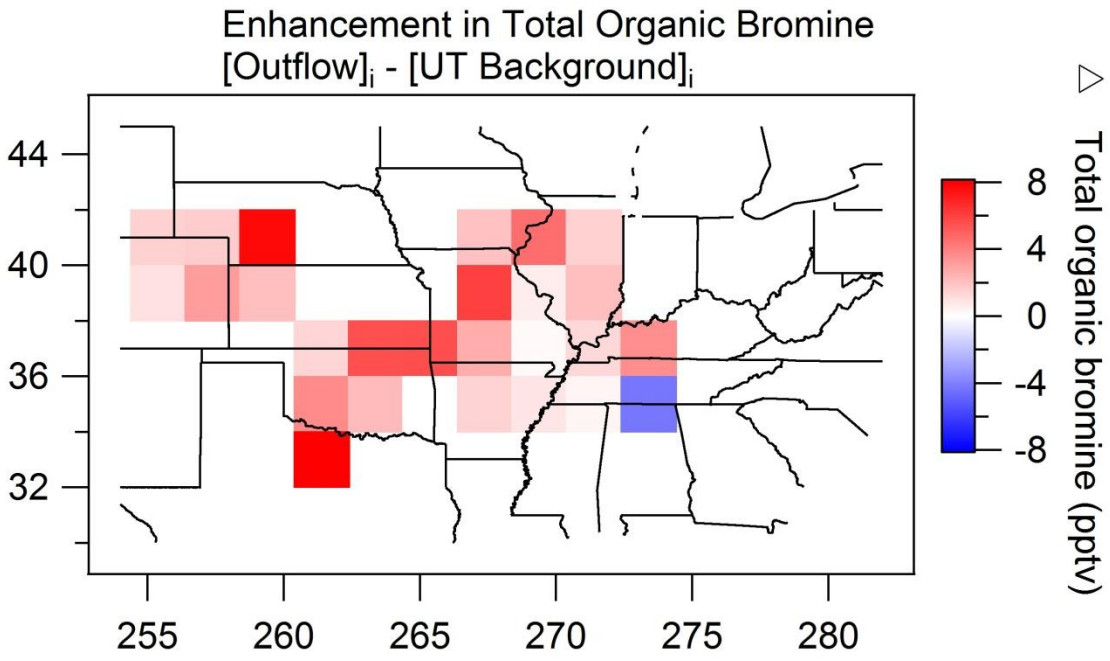

Figure 5.18. Geographic distribution of the enhancement in organic bromine in convective outflow relative to the UT background. Samples were binned into 2° x 2° boxes, and the average value of each box was calculated.

Least squares regressions were made to determine if the magnitudes of the enhancements in organic bromine in convective outflow were correlated with organic bromine mixing ratios in the background UT or with organic bromine mixing ratios in convective outflow. These regressions were made using the same methods described in section 5.2.2, and are presented in Figure 5.19 along with r^2 values for each fit. The r^2 value for the background UT fit is 0.25, which indicates no statistical correlation, while the r^2 value for the convective outflow fit is 0.77, which indicates a fairly high statistical correlation. Indeed, these results suggest that the degree to which convection affects the total organic bromine content of the regional UT is a function of the composition of the convective outflow in the region, rather than the composition of the regional background UT as was the case for organic chlorine. The Durbin-Watson test (equation 5.7) was used to determine if the convective outflow fit (right panel of Figure 5.19) showed

autocorrelation. A Durbin-Watson statistic d=1.96 was calculated, and suggested no autocorrelation. The Durbin-Watson test was not applied to the background UT fit, as the degree of correlation was not statistically significant.

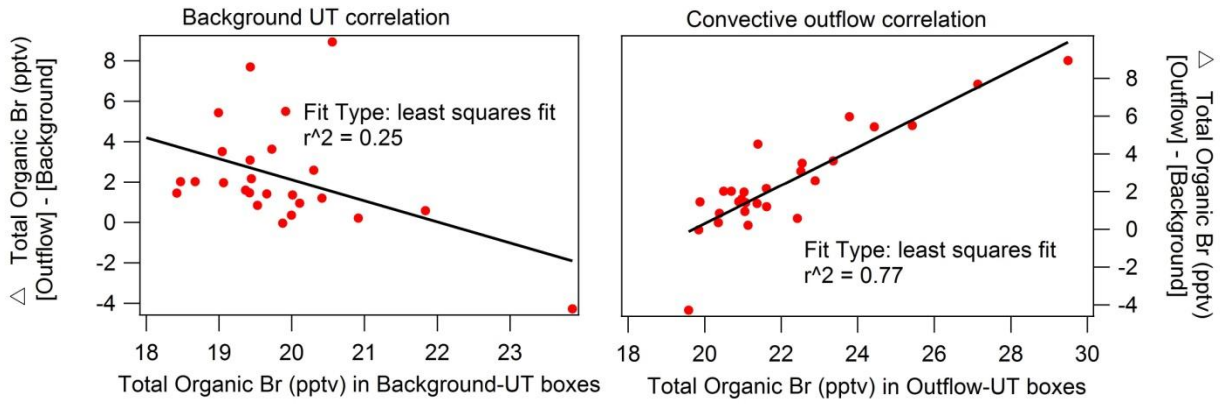

Figure 5.19. Correlations between the total organic bromine boxes presented in figure 5.16 and the outflow enhancement boxes presented in figure 5.18.

Since VSLH were expected to be the class of halocarbon that is most affected by convection, similar correlations were made for VSLH organic bromine enhancements, and are shown in Figure 5.20. Indeed, VSLH organic bromine enhancements were correlated with the amount of VSLH organic bromine in the convective outflow of the region (r^2 = 0.74) and showed no statistical correlation with the amount of VSLH organic bromine in the regional background UT (r^2 = 0.03). The Durbin-Watson test for autocorrelation (equation 5.7) was applied to the convective outflow fit for VSLH (i.e. the right panel of Figure 5.20), and yielded a value of d = 2.10, indicating no significant autocorrelation. This test was not applied to the background UT fit (i.e. the left panel of Figure 5.20) because the degree of correlation was not statistically significant.

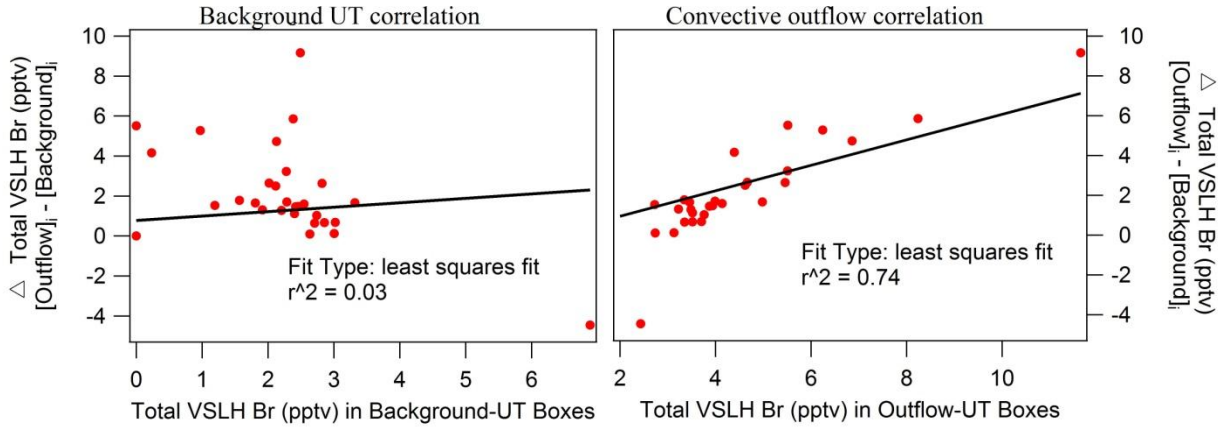

Figure 5.20. Correlations between VSLH organic bromine in UT background boxes and outflow enhancements (left panel) and between VSLH organic bromine in convective outflow boxes and outflow enhancement boxes (right panel).

In contrast to organic chlorine, the degree to which convection affects the organic bromine content of the regional UT is a function of the organic bromine content of the convective outflow, and not the organic bromine content of the regional UT background. While organic bromine in the background UT showed modest spatial variability, it shows very little temporal variability. Figure 5.21 shows the average (± 1σ) mixing ratios of total organic bromine, LLHC organic bromine, and VSLH organic bromine in the convective outflow and background UT for each flight. While the convective outflow shows some temporal variability, especially for total organic bromine and VSLH organic bromine, the background UT shows very little temporal variability except for research flight 13. During research flight 13, the DC-8 flew south towards the Gulf of Mexico and may have encountered outflow from recent marine convection. Because the boundary over the Gulf of Mexico would not contain appreciable mixing ratios of the hydrocarbons used to detect convective outflow over the DC3 study region (see Chapter 3), this marine convective outflow may not have been detected by our filters, and thus would have been incorrectly flagged as a background UT sample. This may explain the high mixing ratios of the LLHC CH_3Br - which has a strong oceanic source - seen in the background UT during research

flight 13. Because of this potential outlier, some correlations and calculations in the following paragraphs are performed twice: both including research flight 13 and excluding research flight 13. Because of the small variability in the total organic bromine content of the background UT (19.8 ± 0.7 pptv of organic bromine if research flight 13 is included, 19.7 ± 0.5 pptv of organic bromine if research flight 13 is excluded) and the lack of build-up and drop-down events that were observed for organic chlorine, it is apparent that mixing ratios of organic bromine in the background UT over the DC3 study region are not significantly affected by long-range transport of air from East Asia or the Central Pacific region.

Linear least squares regressions were made between the average total organic bromine enhancement for each flight and the mixing ratio of organic bromine in convective outflow and in the background UT for each flight, and are shown in Figure 5.22. In general, fits with organic bromine in convective outflow show some degree of statistical correlation, while fits with organic bromine in the background UT show no statistical correlation. LLHC organic bromine has a low degree of correlation with the organic bromine enhancement ($r^2 = 0.10$) that increases slightly to 0.11 if data from research flight 13 is removed. VSLH organic bromine has a strong correlation with the organic bromine enhancement ($r^2 = 0.84$) that increased to 0.86 if data from research flight 13 are removed. The Durbin-Watson test was performed for each regression had an r^2 value greater than 0.30, and no evidence of autocorrelation was found. Because VSLH show a strong correlation with the total organic bromine enhancement and other brominated species show weak or no correlation, brominated VSLH are the primary drivers behind the enhancement in UT mixing ratios of organic bromine due to convection. Because brominated VSLH are primarily emitted by oceans, this suggests that the degree to which oceanic air from the Gulf of Mexico affects the surface of the DC3 study area (and hence, the convective outflow

that would be produced over that area) determines the degree to which convective outflow affects the organic bromine content of the regional UT.

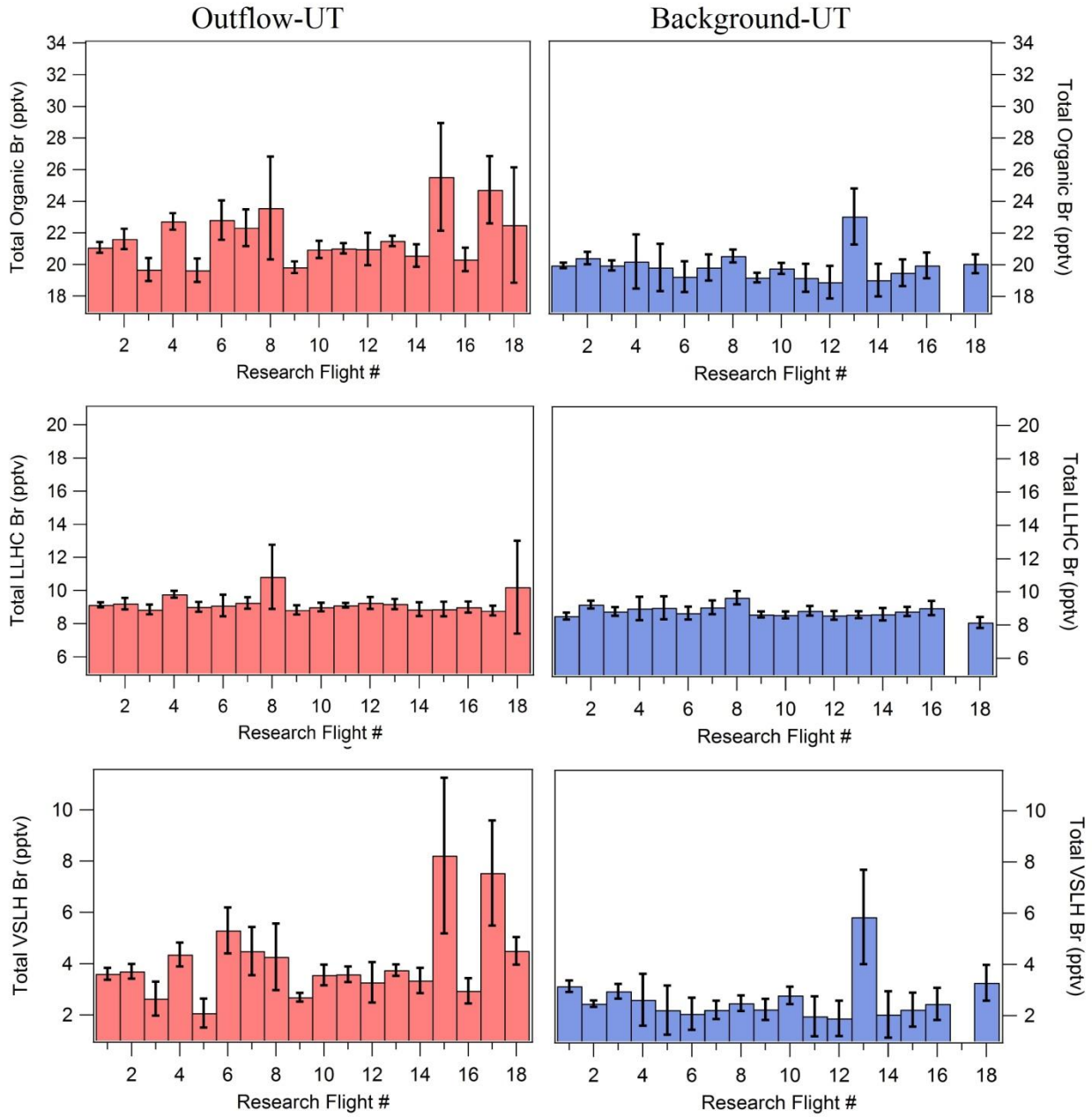

Figure 5.21. The average values of total organic bromine (top panels), LLHC organic bromine (middle panels), and VSLH organic bromine (bottom panels) for each research flight from the Outflow-UT (left side) and Background-UT (right side) datasets. Error bars represent ±1σ. Note: no Background-UT samples were collected during research flight 17.Halons have been excluded for clarity.

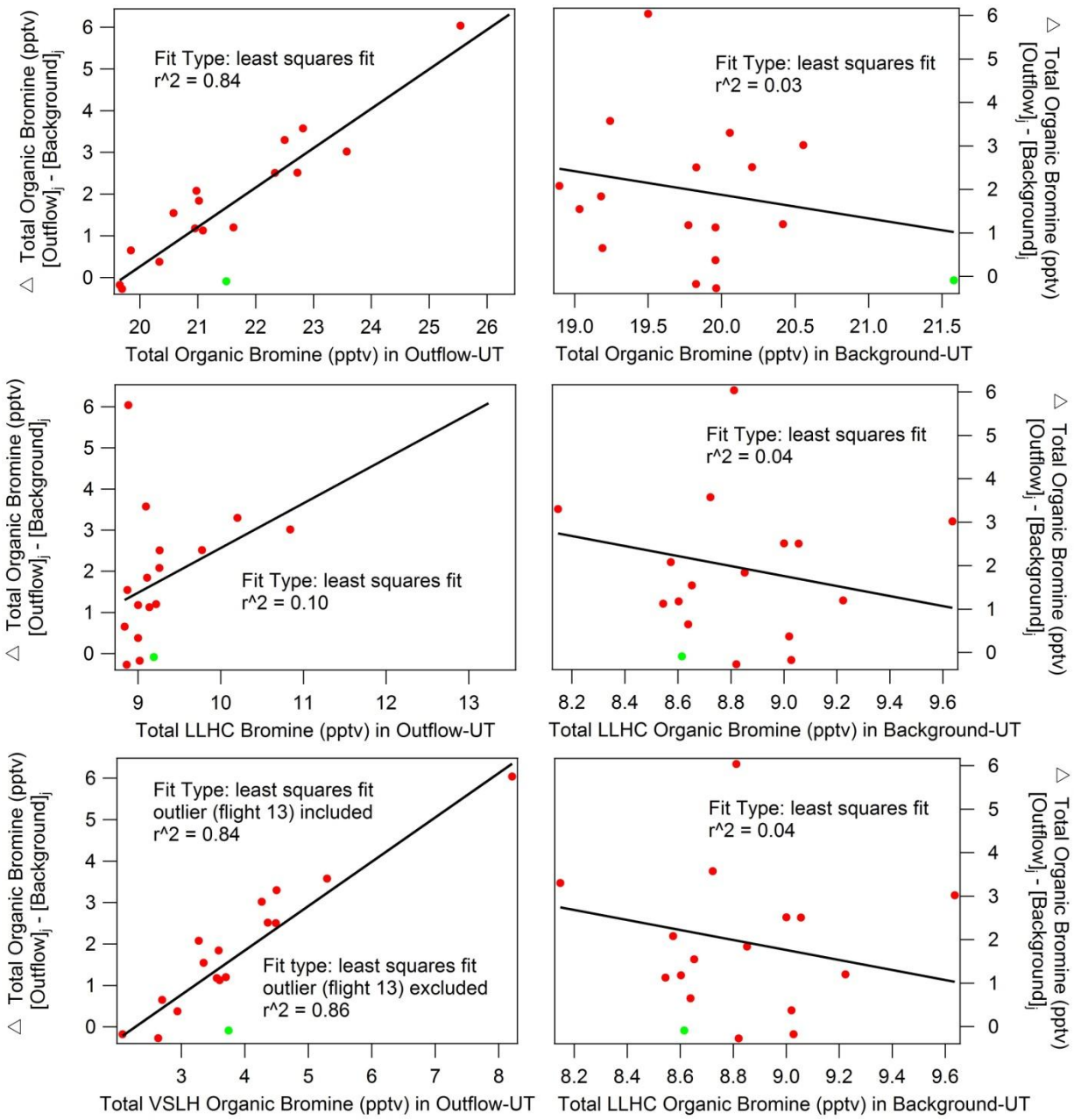

Figure 5.22. Correlations between the average total organic bromine enhancement in convective outflow from each flight (i.e. the average mixing ratio of organic chlorine in the convective outflow of flight *j* minus the average mixing ratio of organic chlorine in the background UT of flight *j*) and the organic bromine contribution from different halocarbon species. Panels on the left show correlations between enhancements and organic bromine in convective outflow, while panels on the right show correlations between enhancements and organic bromine in the background UT. In all graphs, the average value from research flight 13 is highlighted in green. Unless otherwise noted, this value was included in determining the r^2 value for each correlation.

5.4. Conclusions

In this section, the effects of convection on mixing ratios of organic chlorine and organic bromine were investigated. Because the tropopause acts as a fairly strong barrier to mixing between the troposphere and stratosphere, convective outflow that was sampled above the tropopause was considered separately from convective outflow that was sampled in the UT.

Deep convection that penetrates above the tropopause was found to increase the organic halogen loading of the regional LS by a considerable amount. The total organic chlorine mixing ratio in overshooting tops was higher than that of the background LS by an average of 217 ± 179 pptv (± 1σ), with VSLH (enhanced by 76 ± 42 pptv), LLHCs (enhanced by 65 ± 69 pptv), and CFCs (enhanced by 56 ± 78 pptv) contributing the most to this enhancement over the background LS mixing ratios. The atmospherically-abundant refrigerants CFC-11, CFC-12, and HCFC-22 were enhanced in overshooting tops by an average of 11 pptv, 12 pptv, and 14 pptv respectively (contributing 33 pptv, 24 pptv, and 14 pptv of organic chlorine to the total enhancement in overshooting tops). The long-lived, atmospherically-abundant species CCl_4 was enhanced by 5 pptv in overshooting tops, contributing 20 pptv of organic chlorine to the total enhancement in overshooting tops). Long-lived species with low tropospheric abundances were also enhanced in overshooting tops, but contributed a much smaller amount to the total organic chlorine enhancement in overshooting tops. Of the shorter-lived halocarbons, CH_3Cl and CH_2Cl_2 produced large enhancements in organic chlorine in overshooting tops: CH_3Cl was enhanced by 50 pptv, while CH_2Cl_2 was enhanced by 14.5 pptv in overshooting tops (contributing 50 and 29 pptv of organic chlorine to the total enhancement in overshooting tops). The total organic bromine mixing ratio in overshooting tops was higher than that of the background LS by an average of 2.8 ± 3.2 pptv (± 1σ), with VSLH (enhanced by 1.3 ± 1.9 pptv) contributing the most

to this enhancement, and halons and LLHC contributing less to this enhancement (organic bromine from both halons and LLHC were enhanced by 0.8 ± 1.2 pptv in overshooting tops). H-1211 and H-1301, which each contain one bromine atom, contributed an average of 0.20 and 0.53 pptv of organic bromine to the average organic bromine enhancement in overshooting tops, and the LLHC CH_3Br contributed an average of 0.82 pptv of organic bromine. Of the brominated VSLH, CH_2Br_2 and $CHBr_3$ were the most enhanced in convective outflow (enhancements of 0.3 and 0.25 pptv, respectively), and contributed averages of 0.6 and 0.75 pptv of organic bromine to the organic bromine enhancement in overshooting tops.

In overshooting tops, VSLH contribute an additional 76 pptv of organic chlorine and 1.3 pptv of organic bromine to the organic halogen loading of the regional LS. For organic chlorine, this represents 2.2% of the total organic chlorine in the LS. For organic bromine, this represents 8.1% of the total organic bromine in the LS. If we include the LLHCs CH_3Cl and CH_3Br, which have atmospheric lifetimes of less than one year, these numbers increase to 126 pptv (3.7%) for organic chlorine and 2.1 pptv (13.2%) for organic bromine. These numbers may have a great importance. The ODP of a given substance is measured relative to that of CFC-11. Because these compounds have atmospheric lifetimes that are much shorter than CFC-11, they have disproportionately small ODPs. However, the O_3-depleting effects of these short-lived halocarbons are non-linear with respect to CFC-11, and are maximized when considering shorter time scales (i.e. less than one year). In effect, introducing a pulse of VSLH into the LS will result in a loss of O_3 in a relatively small area – in this case the midlatitude LS, while introducing a pulse of a long-lived halocarbon such as CFC-11 will result in O_3 loss that is spread throughout the stratosphere and focused on the mid and upper stratosphere. Because the GWP of O_3 is altitude-dependant and maximized near the tropopause (see Chapter 1), halogenated VSLH that

are injected into the LS by convection may play a disproportionately large role in controlling the radiative effects of the region.

In the UT, the effects of convection on organic halogen mixing ratios were more complicated. On average, organic chlorine mixing ratios in convective outflow in the UT were similar to those in the background UT. When the enhancement in organic chlorine (i.e. organic chlorine in outflow – organic chlorine in the background UT) was examined spatially, there was a strong correlation between the enhancement in organic chlorine and the mixing ratio of organic chlorine in the regional background UT. When examined on a flight-by-flight basis, the mixing ratio of organic chlorine in the background UT appeared to have a temporal trend, which manifested itself as a temporal trend in the average enhancement in organic chlorine in convective outflow. Using modeled back trajectories and examining the chemical composition of the background UT, it was found that outflow from East Asia and from the central Pacific affected the background UT over the DC3 study region. During days when the Background UT was influenced by East Asian outflow, local convection actually had a lower mixing ratio of organic chlorine than the local background UT by up to 150 ± 115 pptv (VSLH organic chorine was lower by up to 24 ± 20 pptv, and LLHC organic chlorine was lower by 73 ± 23 pptv). During days when the Background UT was influenced by clean air originating from the central Pacific, local convection had a higher mixing ratio of organic chlorine than the local background UT by up to 115 ± 98 pptv (VSLH organic chlorine was higher by up to 22 ± 21 pptv. And LLHC organic chlorine was higher by up to 34 ± 22 pptv).

For organic bromine in the UT, the opposite was observed: convective outflow had, on average, higher mixing ratios of organic bromine than the background UT (higher by an average of 2.2 ± 5.8 pptv). When examined both spatially and temporally, there was a strong correlation

between organic bromine in convective outflow and the enhancement in organic bromine in convective outflow (i.e. organic bromine in convective outflow – organic bromine in the background UT). Of all the classes of halocarbon considered here, brominated VSLH had the strongest correlation with this enhancement. The background UT showed very little variation from day-to-day, indicating that organic bromine mixing ratios in the background UT were not affected by long-range transport processes in the same way that organic chlorine mixing ratios were. When organic bromine enhancements in convective outflow were calculated on a flight-by-flight basis, organic bromine mixing ratios in convective outflow were higher than those in the background UT by an average of 1.7 ± 1.6 pptv (range -0.3 to 6.0 pptv), VSLH organic bromine was higher by an average of 1.3 ± 1.5 pptv (range -0.3 to 6.0 pptv), and LLHC organic bromine was higher by an average of 0.5 ± 0.5 pptv (range -0.1 to 2.0 pptv).

In general, the effects of convection on organic halogens in the UT are as follows: when a deep convective storm occurs over the DC3 study region, a relatively constant amount of organic chlorine is injected into a background with highly-variable organic chlorine mixing ratios. These background organic chlorine mixing ratios are affected by long–range transport, and can have organic chlorine mixing ratios higher than that of convective outflow. On the other hand, variable amounts of organic bromine are injected into a background that has a relatively-constant mixing ratio of organic bromine. The amount of organic bromine contained in convective outflow depends on the degree to which air at the surface is affected by oceanic outflow from the Gulf of Mexico.

The results presented in this chapter highlight the wide range of variables one must account for to successfully model the effects of halogens on the chemistry of the UT/LS: 1) The location of the convective outflow relative to the local tropopause height, 2) the impact of long-

range transport on the composition of the regional UT, and 3) variations in the geographic location and strength of halocarbon sources at the surface. In order to understand these results in the context of a global climate, global models that incorporate detailed chemical and climate schemes would need to be used. The results presented here can be used to help provide missing pieces of data regarding the effects of deep convection on the organic halogen (particularly VSLH) budget of the UT/LS, and can be used to constrain global chemistry/climate models that incorporate convection and O_3-halogen chemistry into their calculated UT/LS outputs.

5.5 References

Apel, E. C., Olson, J. R., Crawford, J. H., Hornbrook, R. S., Hills, a. J., Cantrell, C. a., Emmons, L. K., Knapp, D. J., Hall, S., Mauldin III, R. L., Weinheimer, a. J., Fried, a., Blake, D. R., Crounse, J. D., Clair, J. M. St., Wennberg, P. O., Diskin, G. S., Fuelberg, H. E., Wisthaler, a., Mikoviny, T., Brune, W. and Riemer, D. D.: Impact of the deep convection of isoprene and other reactive trace species on radicals and ozone in the upper troposphere, Atmos. Chem. Phys., 12(2), 1135–1150, doi:10.5194/acp-12-1135-2012, 2012.

Barth, M. C., Cantrell, C. a., Brune, W. H., Rutledge, S. a., Crawford, J. H., Huntrieser, H., Carey, L. D., MacGorman, D., Weisman, M., Pickering, K. E., Bruning, E., Anderson, B., Apel, E., Biggerstaff, M., Campos, T., Campuzano-Jost, P., Cohen, R., Crounse, J., Day, D. a., Diskin, G., Flocke, F., Fried, A., Garland, C., Heikes, B., Honomichl, S., Hornbrook, R., Huey, L. G., Jimenez, J. L., Lang, T., Lichtenstern, M., Mikoviny, T., Nault, B., O'Sullivan, D., Pan, L. L., Peischl, J., Pollack, I., Richter, D., Riemer, D., Ryerson, T., Schlager, H., Clair, J. St., Walega, J., Weibring, P., Weinheimer, A., Wennberg, P., Wisthaler, A., Wooldridge, P. J. and Ziegler, C.: The Deep Convective Clouds and Chemistry (DC3) Field Campaign, Bull. Am. Meteorol. Soc., 1412, doi:10.1175/BAMS-D-13-00290.1, 2014.

Bechara, J., Borbon, a., Jambert, C., Colomb, a. and Perros, P. E.: Evidence of the impact of deep convection on reactive Volatile Organic Compounds in the upper tropical troposphere during the AMMA experiment in West Africa, Atmos. Chem. Phys., 10(21), 10321–10334, doi:10.5194/acp-10-10321-2010, 2010.

Durbin, J. and Watson, S. G.: Testing for Serial Correlation in Least Squares Regression: I, Biometrika, 37(3), 409–428, 1950.

Hendrick, F., Johnston, P. V., De Mazière, M., Fayt, C., Hermans, C., Kreher, K., Theys, N., Thomas, a. and Van Roozendael, M.: One-decade trend analysis of stratospheric BrO over Harestua (60°N) and Lauder (45°S) reveals a decline, Geophys. Res. Lett., 35(14), 1–5, doi:10.1029/2008GL034154, 2008.

Hossaini, R., Chipperfield, M. P., Montzka, S. a, Rap, a, Dhomse, S. and Feng, W.: Efficiency of short-lived halogens at influencing climate through depletion of stratospheric ozone, Nat. Geosci., 8(February), 1–5, doi:10.1038/NGEO2363, 2015.

Laube, J. C., Engel, a., Bönisch, H., Möbius, T., Worton, D. R., Sturges, W. T., Grunow, K. and Schmidt, U.: Contribution of very short-lived organic substances to stratospheric chlorine and bromine in the tropics – a case study, Atmos. Chem. Phys. Discuss., 8(3), 8491–8515, doi:10.5194/acpd-8-8491-2008, 2008.

Law, K. S. and Sturges, W. T.: Halogenated Very Short-Lived Substances, in Scientific Assesment of Ozone Depletion: 2006, World Meteorological Organization, Geneva, Switzerland., 2006.

McLinden, C. a., Haley, C. S., Lloyd, N. D., Hendrick, F., Rozanov, a., Sinnhuber, B. M., Goutail, F., Degenstein, D. a., Llewellyn, E. J., Sioris, C. E., Van Roozendael, M., Pommereau, J. P., Lotz, W. and Burrows, J. P.: Odin/OSIRIS observations of stratospheric BrO: Retrieval methodology, climatology, and inferred Bry, J. Geophys. Res. Atmos., 115(15), 1–19, doi:10.1029/2009JD012488, 2010.

Molina, M. J. and Rowland, F. S.: Stratospheric sink for chlorofluoromethanes: chlorine atom-catalysed destruction of ozone, Nature, 249, 1974.

Montzka, S. A., Reimann, S., Engel, A., Kruger, K., O'Doherty, S. and Sturges, W. T.: Ozone Depleting Substances (ODSs) and Related Chemicals, in Scientific Assesment of Ozone Depletion: 2010, World Meteorological Organization, Geneva, Switzerland., 2010.

Saiz-Lopez, a., Lamarque, J. F., Kinnison, D. E., Tilmes, S., Ordóñez, C., Orlando, J. J., Conley, a. J., Plane, J. M. C., Mahajan, a. S., Sousa Santos, G., Atlas, E. L., Blake, D. R., Sander, S. P., Schauffler, S., Thompson, a. M. and Brasseur, G.: Estimating the climate significance of halogen-driven ozone loss in the tropical marine troposphere, Atmos. Chem. Phys., 12, 3939–3949, doi:10.5194/acp-12-3939-2012, 2012.

Salawitch, R. J., Canty, T., Kurosu, T., Chance, K., Liang, Q., Da Silva, a., Pawson, S., Nielsen, J. E., Rodriguez, J. M., Bhartia, P. K., Liu, X., Huey, L. G., Liao, J., Stickel, R. E., Tanner, D. J., Dibb, J. E., Simpson, W. R., Donohoue, D., Weinheimer, a., Flocke, F., Knapp, D., Montzka, D., Neuman, J. a., Nowak, J. B., Ryerson, T. B., Oltmans, S., Blake, D. R., Atlas, E. L., Kinnison, D. E., Tilmes, S., Pan, L. L., Hendrick, F., Van Roozendael, M., Kreher, K., Johnston, P. V., Gao, R. S., Johnson, B., Bui, T. P., Chen, G., Pierce, R. B., Crawford, J. H. and Jacob, D. J.: A new interpretation of total column BrO during Arctic spring, Geophys. Res. Lett., 37(21), 1–9, doi:10.1029/2010GL043798, 2010.

Schauffler, S. M., Atlas, E. L., Flocke, F., Lueb, R. A., Stroud, V. and Travnicek, W.: Distributions of brominated organic compounds in the troposphere and lower stratosphere chlorine, J. Geophs. Res., 104, 1999.

Sinnhuber, B. M., Rozanov, a., Sheode, N., Afe, O. T., Richter, a., Sinnhuber, M., Wittrock, F., Burrows, J. P., Stiller, G. P., von Clarmann, T. and Linden, a.: Global observations of stratospheric bromine monoxide from SCIAMACHY, Geophys. Res. Lett., 32(20), 1–5, doi:10.1029/2005GL023839, 2005.

Stolarski, R. S. and Cicerone, R. J.: Stratospheric chlorine - Possible sink for ozone, Can. J. Chem., 52(8), 1610–1615, doi:10.1139/v74-233, 1974.

Theys, N., Van Roozendael, M., Hendrick, F., Fayt, C., Hermans, C., Baray, J.-L., Goutail, F., Pommereau, J.-P. and De Mazière, M.: Retrieval of stratospheric and tropospheric BrO columns from multi-axis DOAS measurements at Reunion Island (21° S, 56° E), Atmos. Chem. Phys. Discuss., 7(3), 8261–8308, doi:10.5194/acpd-7-8261-2007, 2007.

5.6 Appendix

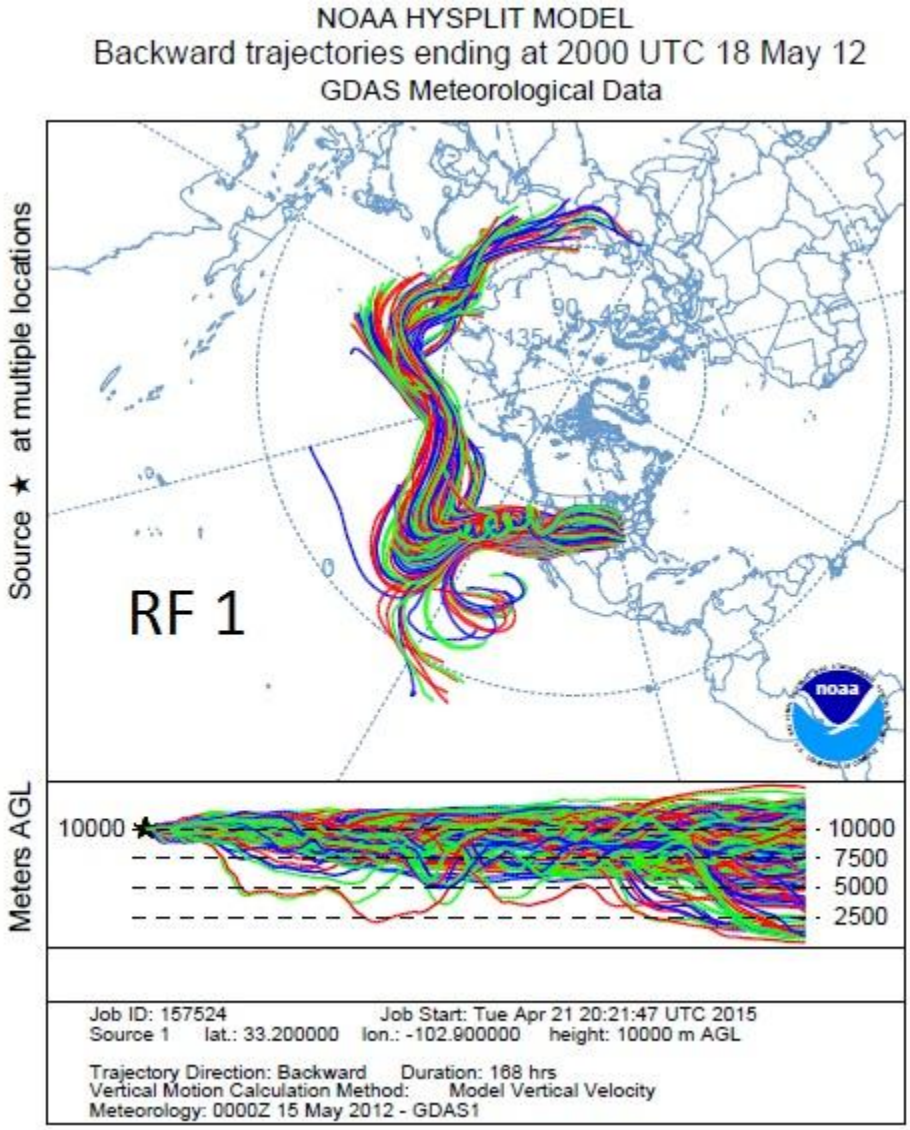
NOAA HYSPLIT MODEL
Backward trajectories ending at 2000 UTC 18 May 12
GDAS Meteorological Data
Source ★ at multiple locations
RF 1
noaa
Meters AGL
10000
10000
7500
5000
2500
Job ID: 157524 Job Start: Tue Apr 21 20:21:47 UTC 2015
Source 1 lat.: 33.200000 lon.: -102.900000 height: 10000 m AGL
Trajectory Direction: Backward Duration: 168 hrs
Vertical Motion Calculation Method: Model Vertical Velocity
Meteorology: 0000Z 15 May 2012 - GDAS1

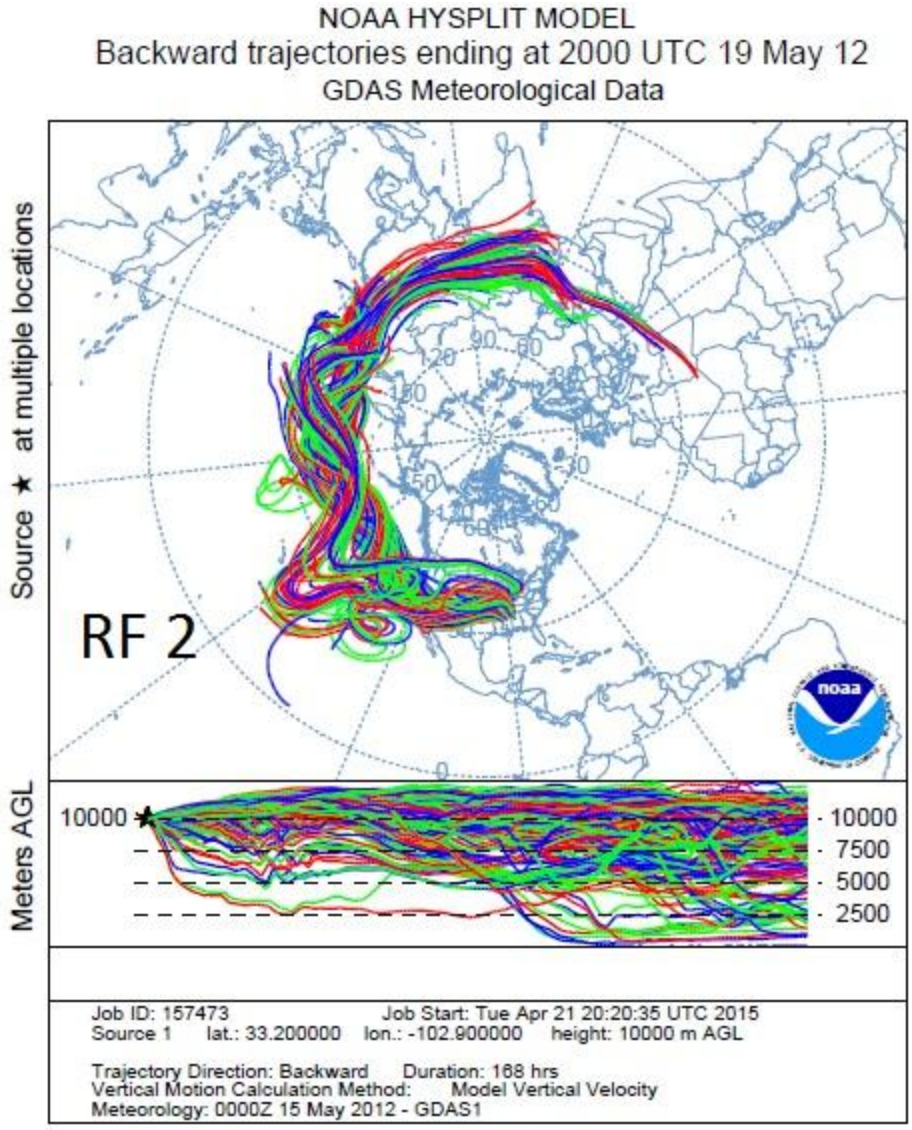
NOAA HYSPLIT MODEL
Backward trajectories ending at 2000 UTC 19 May 12
GDAS Meteorological Data
Source ★ at multiple locations
RF 2
noaa
Meters AGL
10000
10000
7500
5000
2500
Job ID: 157473 Job Start: Tue Apr 21 20:20:35 UTC 2015
Source 1 lat.: 33.200000 lon.: -102.900000 height: 10000 m AGL
Trajectory Direction: Backward Duration: 168 hrs
Vertical Motion Calculation Method: Model Vertical Velocity
Meteorology: 0000Z 15 May 2012 - GDAS1

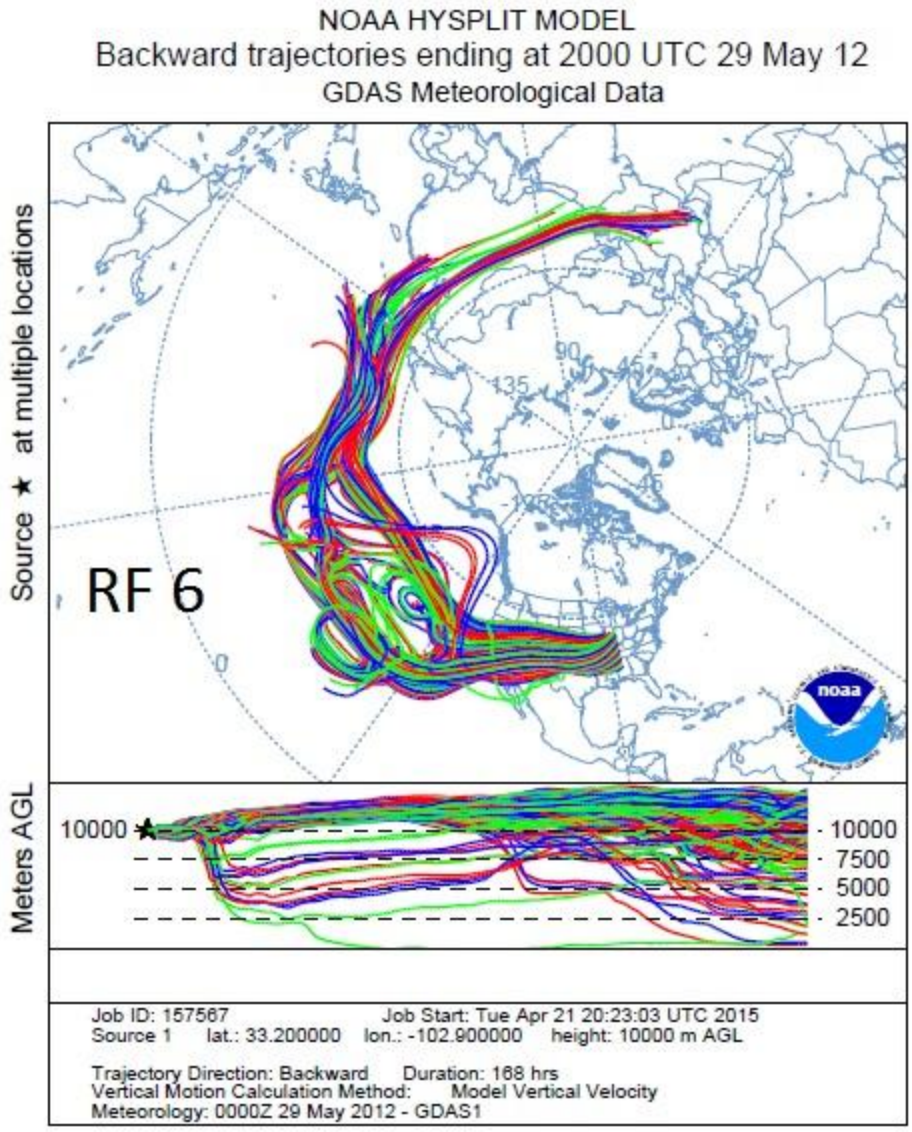
NOAA HYSPLIT MODEL
Backward trajectories ending at 2000 UTC 29 May 12
GDAS Meteorological Data
Source ★ at multiple locations
RF 6
90
135
0
noaa
Meters AGL
10000
10000
7500
5000
2500
Job ID: 157567 Job Start: Tue Apr 21 20:23:03 UTC 2015
Source 1 lat.: 33.200000 lon.: -102.900000 height: 10000 m AGL
Trajectory Direction: Backward Duration: 168 hrs
Vertical Motion Calculation Method: Model Vertical Velocity
Meteorology: 0000Z 29 May 2012 - GDAS1

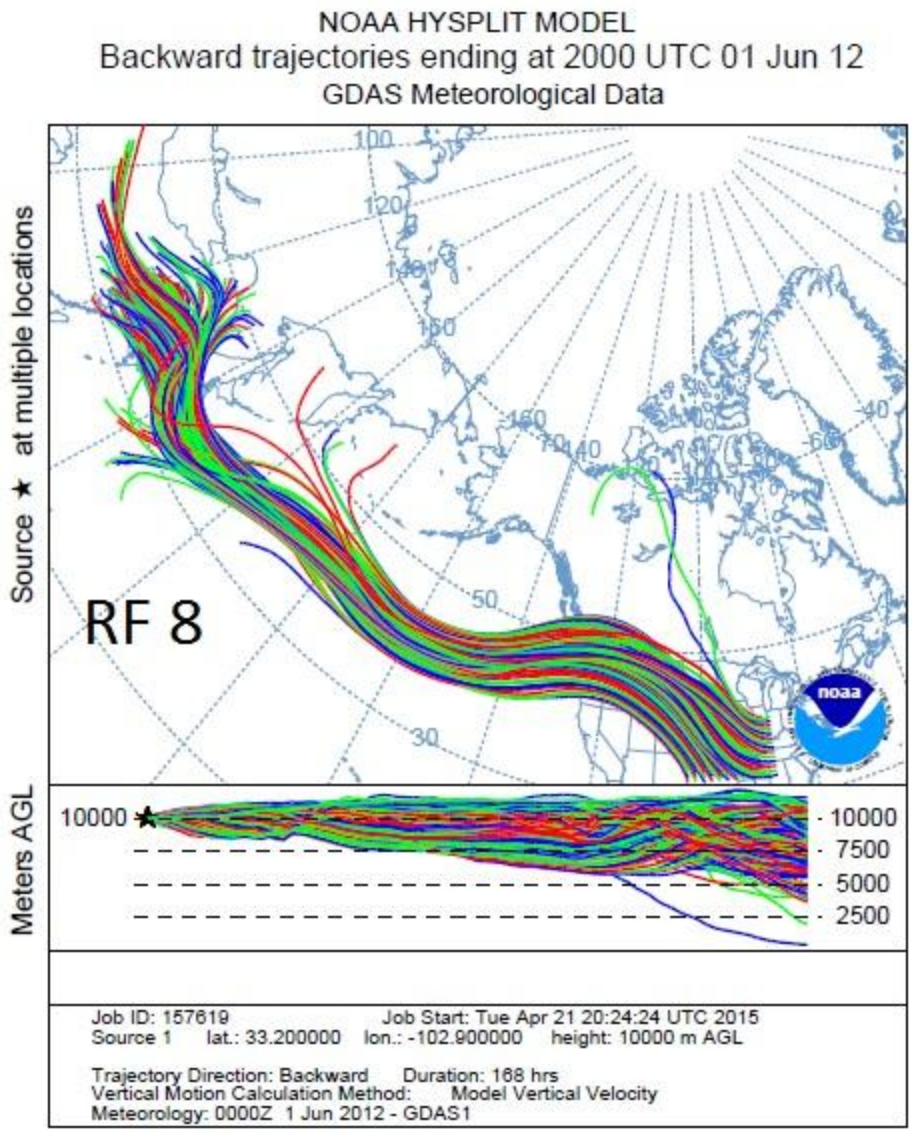
NOAA HYSPLIT MODEL
Backward trajectories ending at 2000 UTC 01 Jun 12
GDAS Meteorological Data
Source ★ at multiple locations
RF 8
Meters AGL
10000
10000
7500
5000
2500
Job ID: 157619 Job Start: Tue Apr 21 20:24:24 UTC 2015
Source 1 lat.: 33.200000 lon.: -102.900000 height: 10000 m AGL
Trajectory Direction: Backward Duration: 168 hrs
Vertical Motion Calculation Method: Model Vertical Velocity
Meteorology: 0000Z 1 Jun 2012 - GDAS1

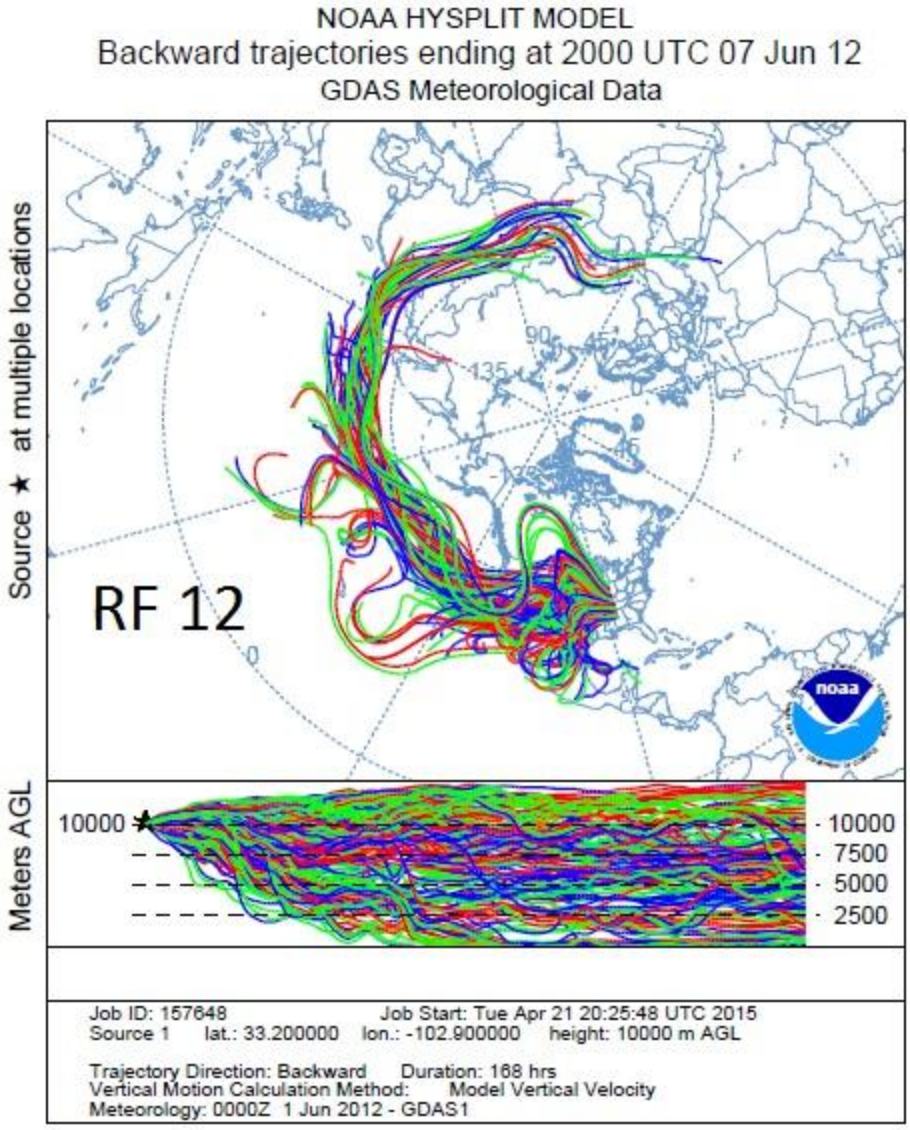
NOAA HYSPLIT MODEL
Backward trajectories ending at 2000 UTC 07 Jun 12
GDAS Meteorological Data
Source ★ at multiple locations
RF 12
90
135
0
noaa
Meters AGL
10000
10000
7500
5000
2500
Job ID: 157648 Job Start: Tue Apr 21 20:25:48 UTC 2015
Source 1 lat.: 33.200000 lon.: -102.900000 height: 10000 m AGL
Trajectory Direction: Backward Duration: 168 hrs
Vertical Motion Calculation Method: Model Vertical Velocity
Meteorology: 0000Z 1 Jun 2012 - GDAS1

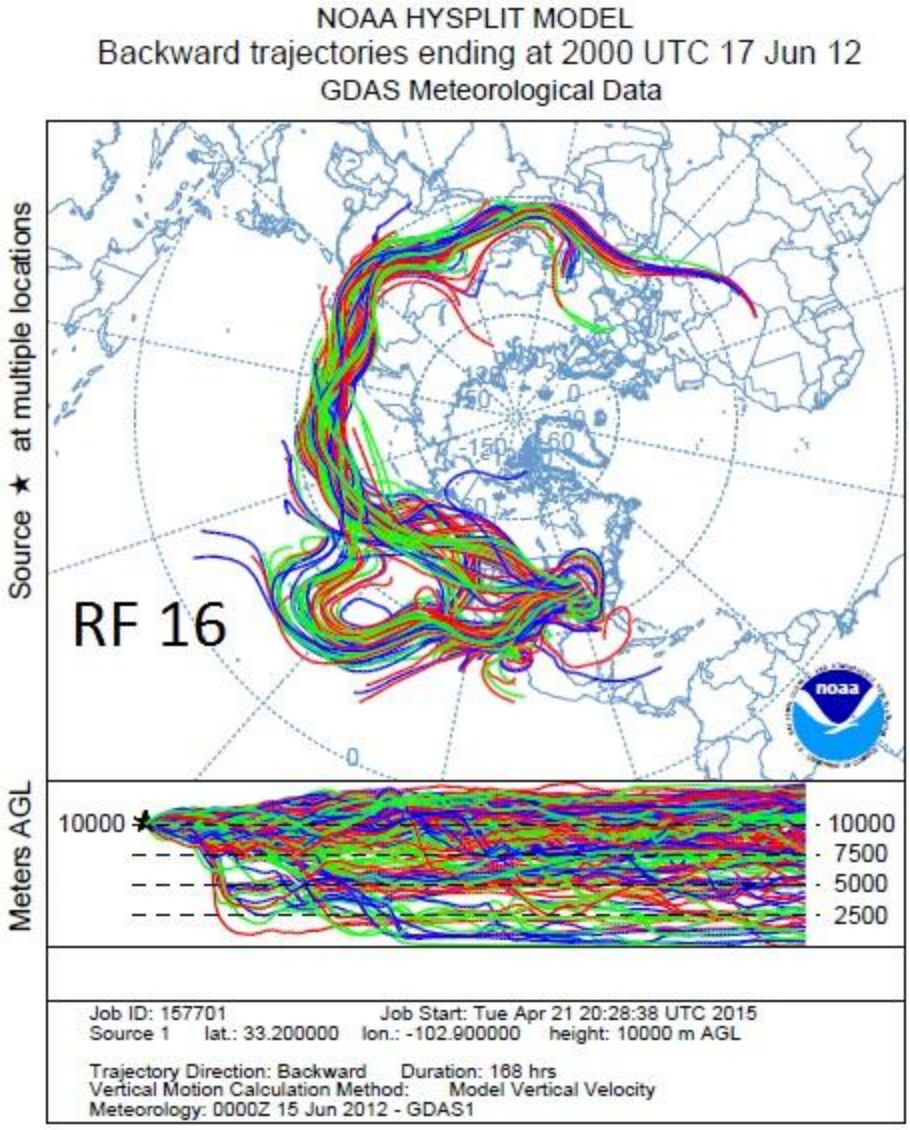
NOAA HYSPLIT MODEL
Backward trajectories ending at 2000 UTC 17 Jun 12
GDAS Meteorological Data
Source ★ at multiple locations
RF 16
Meters AGL
10000
10000
7500
5000
2500
Job ID: 157701 Job Start: Tue Apr 21 20:28:38 UTC 2015
Source 1 lat.: 33.200000 lon.: -102.900000 height: 10000 m AGL
Trajectory Direction: Backward Duration: 168 hrs
Vertical Motion Calculation Method: Model Vertical Velocity
Meteorology: 0000Z 15 Jun 2012 - GDAS1